Carbon nanotubes as a material for functional inks.

Graddage, Neil

Swansea University
Prifysgol Abertawe

Carbon Nanotubes as a Material for Functional Inks

Neil Graddage

A thesis submitted for the degree
of Doctor of Philosophy

2012

Abstract

Carbon nanotubes (CNTs) have been proposed as a material for use in printed electronics for a number of years. The potential to exploit the unique electrical and mechanical properties of these structures on the macro-scale is appealing; however there are a number of hurdles to overcome. Printing allows the deposition of CNT networks, the properties of which are governed by the CNT type and network density. The formulation of a suitable ink and deposition of a film with specific properties is challenging, and the work described in this thesis is concentrated on two specific areas, CNT ink development and CNT based device production.

The CNT ink was developed by identifying key ink and dried film parameters for characterisation and assessing the effect of several major variables, namely the resin material, resin concentration, processing temperature, CNT concentration, CNT functionality and processing energy. A suitable research ink was developed and optimised using *N*-methyl-2-pyrrolidone as the solvent and polyvinyl alcohol as the resin at a concentration ratio of 1:1 with the CNT content. The effects of CNT concentration, CNT functionality and processing energy are shown to be interdependent. This is among the first reported studies to investigate the dependence of these factors upon a CNT ink for roll-to-roll processing.

This ink system was then used in the production of CNT based thin film transistor (TFT) devices using flexography. Initially the concept was proven using MWCNTs. The design was then refined and devices were produced using SWCNTs at varying network densities. It was seen that the printing of CNT based devices using flexography is feasible, though careful control of the CNT network density is required to achieve suitable device performance. This is the first reported production of TFTs using flexography, and the first reported use of flexography to deposit CNTs.

DECLARATION

This work has not previously been accepted in substance for any degree and is not being concurrently submitted in candidature for any degree.

Signed ..... (candidate)

Date 31/1/13

STATEMENT 1

This thesis is the result of my own investigations, except where otherwise stated. Where correction services have been used, the extent and nature of the correction is clearly marked in a footnote(s).

Other sources are acknowledged by footnotes giving explicit references. A bibliography is appended.

Signed ..... (candidate)

Date 31/1/13

STATEMENT 2

I hereby give consent for my thesis, if accepted, to be available for photocopying and for inter-library loan, and for the title and summary to be made available to outside organisations.

Signed ..... (candidate)

Date 31/1/13

Acknowledgements

Firstly my thanks must be given to my supervisors Prof. David Gethin and Prof. Tim Claypole. Without the opportunity they gave me and their support and guidance throughout this project it would not have been possible.

The support of Haydale Ltd., especially Ian Walters and Martin Williams has been crucial. Their donation of materials, as well as time and expertise was essential.

Within the WCPC all staff have assisted without hesitation throughout this project. I have learnt more from the combined experience and knowledge of the people within this centre than I could have possibly imagined. Although I am eternally grateful to all, special thanks must be given. The assistance of Dr. Davide Deganello was vital at many stages of this work, his enthusiasm for research could never be underestimated. Essential help was also provided by Dr. Chris Phillips who never seemed to mind my constant disruption of his valuable time. The contribution of Mrs. Christine Hammett must also be recognised, her organisational skills and ability to handle bureaucracy I could never hope to match.

For someone who doesn't drink coffee, morning coffee trips became a surprisingly regular habit. Accompanying me were a a group of people who have always been there to cheer me on when results went well and commiserate when they (often!) did not. These especially include Dr. John Cherry, Dr. David Beynon, (now a Dr.) Chris Chapman and (at time of writing soon to be a Dr.) William Beer. Special thanks must go to Martyn Cherrington, who in our time sharing coffee breaks, an office and a house has never failed to support with discussions and beer.

Finally, the most invaluable support was provided through the highs and lows of this project by my parents and girlfriend, Samantha. Their patience has been often tested, however they have not judged me for it!

Contents

List of Figures

Part I

Thesis Introduction

Chapter 1

Introduction

The recent evolution of printing from its characteristic method of mass production of literature to a process for the potential volume fabrication of novel electronic devices has been a rapid one. This evolutionary process is far from complete, with materials development being one of the major challenges towards the wide-spread commercialisation of printed electronic products. New materials must be developed to provide functionality whilst being constrained by numerous requirements. Materials must be solution processable in a form suitable for rapid printing technologies. Attention must be paid to the applications, for many materials may be incompatible with others that are required during the fabrication of multilayer structured devices. Finally these materials must be affordable and supplies must be reliable, a hurdle which hinders many promising technologies.

One material being considered for use in printed electronics is carbon nanotubes (CNTs). However the formulation and printing of a functional ink containing CNTs is not a trivial task. This research was structured in such a way that the obstacles to successful ink formulation could be identified and overcome along the path to the creation of functional CNT based printed devices.

To this end, the objectives of this research were to:

- explore the potential for formulating a CNT based ink by studying potential resins, solvents and formulation techniques,
- optimise this ink by improvement of CNT dispersion, with emphasis on mixing and CNT modification, and
- develop a CNT based TFT manufactured entirely using processes that can be scaled for high speed, roll to roll printing techniques.

This chapter introduces the concepts underpinning this work. Many of these concepts will be expanded on further in the literature reviews in chapter 2 and chapter 7.

1.1 Printing

1.1.1 The Printing Process

Manufacturing using the printing process has been developed over hundreds of years. The first printing press in the volume manufacturing sense is believed to have been manufactured around 1440 by Johannes Gutenberg. This early technology is thought to have increased productivity by almost two orders of magnitude. Modern presses such as Manroland's Lithoman range can print onto over 900m of substrate per minute[16].

Conventional electronic device production is a relatively lengthy batch process. The fabrication of integrated circuits typically requires multiple lithographic steps and will create devices on limited substrates. The appeal for the use of printing as a manufacturing process for electronics are numerous. The capital cost compared to a comparable output lithographic fabrication facility is significantly lower. The ability to print onto flexible substrates and the potential for high speed roll to roll production enables the low cost fabrication of novel devices that could disrupt established markets. However it is not envisaged that printed electronics will replace conventional silicon fabrication. The resolution limitations of printing techniques compared to optical and electron beam lithography means that printed electronic device performance is unlikely to rival that of conventional electronic devices. However the two industries are likely to coexist, with the aforementioned advantages of printed electronics ideal for novel devices with modest performance requirements. The combination of conventional electronics with printed electronics is also a subject of much interest, with the appeal of flexible devices with the performance afforded by current silicon technologies obvious.

A number of printing techniques are available to achieve these goals, each with their own advantages and limitations. The basic mechanisms of these processes are well understood and information is available from a number of sources[16–18]. In the field of printed electronics research a number of processes have proven popular, these are flexography, gravure, screen and inkjet. These techniques will be discussed at various points throughout this work, and a summary of each method is provided below.

1.1.1.1 Flexography

The flexographic printing process is commonly used for packaging and newspaper printing and is becoming increasingly popular for the printing of functional inks. In brief it involves an image being replicated in relief on a polymer plate to which a metered volume of ink is applied. The plate is then brought into contact with a substrate and the image is transferred. This is shown schematically in Figure 1.1.1.

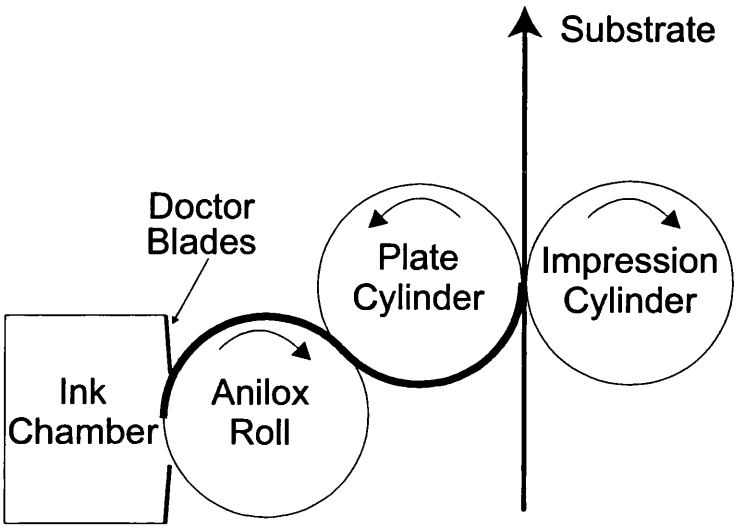

Figure 1.1.1: Graphical representation of the flexographic printing process.

The combination of the ink chamber, doctor blades and anilox roll is referred to as the inking system. In this segment of the press the ink is metered from an ink reservoir and transferred onto the printing plate. A number of aspects can govern the metering of the ink depending on the press setup used. In the illustrated system the ink reservoir is brought into contact with an anilox roll. The ink chamber is a closed system, which reduces solvent evaporation during printing. This is essential for controlling ink viscosity in solvent based ink systems and is beneficial from a health and safety perspective in a production environment. The anilox roll is a chrome or ceramic cylinder that is engraved with a uniform cell structure which the ink is drawn into and later released from. The layout, size and shape of the cells are the crucial factors in determining the ink transfer to the image cylinder, and should be optimised for the type of image to be printed. For functional inks high anilox volume may be preferred to increase the amount of ink deposited and improve conductance for current carrying tracks, however this will have a negative effect on the resolution of the final

print meaning finer details will not be possible. To avoid excess ink build-up on the anilox roll it is 'wiped' with a sharp blade placed in contact with the surface of the cylinder. The schematic illustrated shows a chambered doctor blade system, as used in most modern flexographic presses. The upper blade acts to both enclose the ink in the reservoir and wipe the cylinder, whilst the lower blade is often known as the containment blade which serves to enclose the ink reservoir. Doctor blade angles may or may not be fixed, with angles of $30 - 60^o$ to the tangent of the cylinder commonly used.

Once the anilox has been inked it is brought into contact with the image master plate, which is adhered to a cylinder by means of compressible adhesive tape. The compressibility of the tape will affect the final image, for solid areas such as those commonly used in printed electronics a harder tape is preferred due to improved plate contact. For finer features a softer tape is preferred as it reduces plate deformation at substrate contact. The ink is transferred onto only the relief sections of the plate, and is metered by the volume of the anilox cells and the engagement pressure between the anilox and plate. The image master is then brought into contact with the substrate, depositing the ink. The higher the substrate-to-plate pressure the more spreading of the printed features occurs.

Flexography can print a range of ink rheologies, with optimal dynamic viscosities in the liquid range of 0.05 to 1.5 Pa.s. Higher viscosity inks will decrease print quality at higher speeds due to poor filling of the anilox cells, but will often result in less spreading of the printed form after deposition. Closed ink chambers, such as the one shown in Figure 1.1.1 allow the practical use of lower viscosity inks. Ink film thicknesses of up to 1μm are typical in flexographic printing. Some solvent based inks may be incompatible with the polymer image master used, various polymers are available to minimise this effect.

In summary, the advantages of the flexographic process are

- the reproduction of a continuous, uniform image in any direction,
- high speed roll-to-roll capability of the technique,
- closed ink chambers reduce solvent evaporation during printing,
- large range of printable ink types and rheological characteristics, and
- large range of printable substrates.

Nevertheless flexography has limitations, such as

- potential ink incompatibility with the polymer plate, and
- image resolution cannot match that of other technologies such as gravure.

1.1.1.2 Gravure

Gravure (or rotogravure) is a similar printing process to flexography, however in this case the image is reproduced on a gravure cylinder roll. The image is replicated as a series of engraved cells similar to that of the cells on an anilox roll in flexography, known as intaglio. This results in the image carrier also acting as the ink metering system. The shape and depth of the cells controls the deposition coverage. Digital engraving technologies allow the cell properties to be varied across the cylinder, allowing high image master resolution, however the use of raster imagery will result in non uniform features, for example line edges.

As illustrated in Figure 1.1.2 the gravure cylinder is immersed in an ink bath, and any excess ink is removed by a similar doctor blade system to that described for flexography. The gravure cylinder is then brought into contact with the substrate, and the image transferred via a combination of printing pressure and adhesive forces between the substrate and ink. Gravure cylinders are costly to produce compared to flexographic plates but are more resilient to aggressive solvents sometimes found in functional inks and more suited to longer duration print runs. Gravure inks tend to be lower viscosity than flexographic inks, with dynamic viscosities in the range 0.05 to 0.5Pa.s.

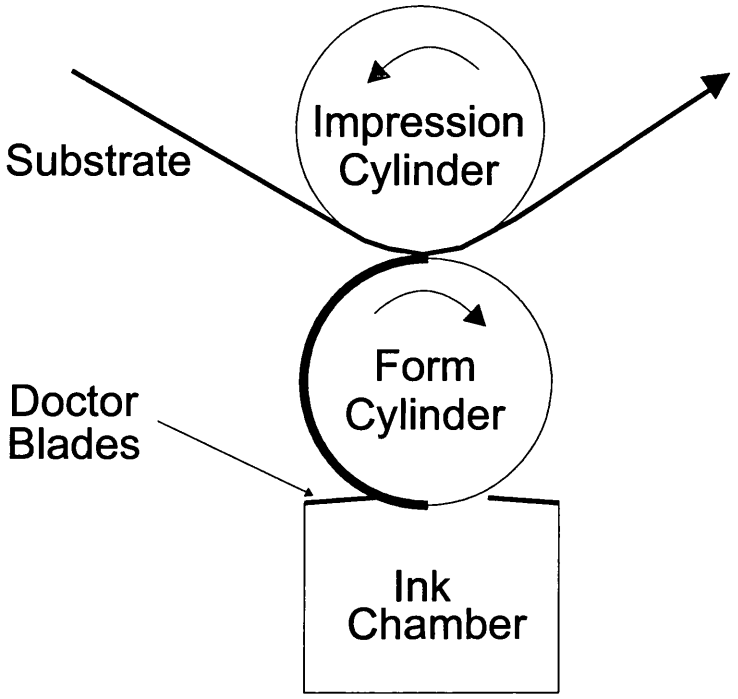

Figure 1.1.2: Schematic of an example gravure printing system.

In summary, the advantages of the gravure process are

- the high speed roll-to-roll capability of the technique,
- tolerance of aggressive ink contents,
- hard wearing image master allows high speed long duration print runs, and
- high resolution prints,

Nevertheless gravure has limitations, such as

- expense of gravure cylinder production, and
- cannot produce continuous uniform features in all print directions.

1.1.1.3 Screen Printing

Screen printing is a common printing process used for a wide variety of applications, including packaging, textiles, printed circuit boards and printed sensors. It involves the displacement of the ink through a stencil screen. The screen consists of a woven mesh (usually polyester or stainless steel) under tension coated with non image areas covered with a photopolymer emulsion.

To print, ink is deposited upon the screen and a substrate is brought into close proximity with the underside of the screen. The ink is drawn across the screen in a wave like fashion by a polymer blade known as a squeegee. This causes ink to flow through the exposed areas of the screen and deposit onto the substrate due to hydrodynamic pressure. The volume of ink deposited is defined by the thickness of the screen. This process is illustrated in Figure 1.1.3. Screen printing systems are capable of printing onto a wide variety of substrates and it is possible to print in a rotary fashion allowing for continuous roll-to-roll production.

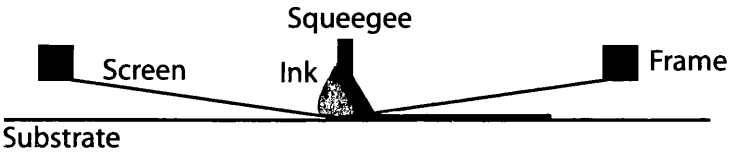

Figure 1.1.3: Schematic of an example screen printing system.

Screen inks tend to have higher dynamic viscosities than other printing inks (usually between 1 to 100Pa.s), but the inks tend to be more specialised with respect to the application with the process being capable of printing a large range of ink rheologies. The rheological properties of the ink are the dominant factor in the resulting print quality and thickness. The inks need to thin under the shear of the squeegee but quickly recover to avoid excess ink being drawn through the mesh at snap off. The application must also be taken into account as fast recovery times can lead to inhomogeneous solid areas but cause poorer resolution when printing dot features for raster imaging.

In summary, the advantages of the screen printing process are

- wide variety of substrate material and shapes,
- large printed film thickness ideal for some printed electronic applications,
- wide range of printable rheologies, and
- roll-to-roll capability at medium speed (relative to alternative technologies).

Nevertheless screen printing has limitations, such as

- potential ink incompatibility with the screen,
- cannot produce continuous uniform features in all print directions, and
- feature uniformity dependent on mesh and ink parameters.

1.1.1.4 Inkjet

The term inkjet encompasses a number of non-contact printing technologies. Inkjet systems create a print by propelling discrete droplets of ink onto a substrate. There are a number of methods of achieving this, however the most popular is piezoelectric drop on demand inkjet. As shown in Figure 1.1.4, the ink is held in a chamber where part of the containing wall is constructed from a piezoelectric ceramic. The application of an electric signal to this ceramic causes it to deform inward to the chamber, forcing a droplet outwards from the nozzle. Droplet size is governed by the amplitude of the applied deformation and the diameter of the nozzle, with overlapping drops required to form continuous structures. Minimum droplet sizes for a commercial 10pL printhead are 40μm[19].

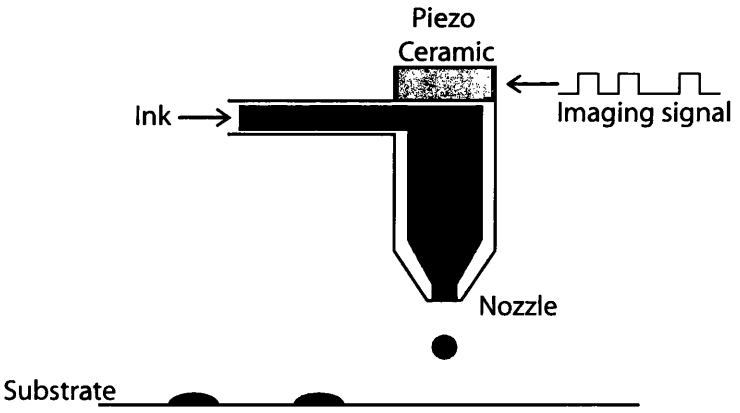

Figure 1.1.4: Schematic of an example piezoelectric drop on demand inkjet system.

Inkjet technologies tend to have similar ink requirements, with low viscosities and surface tensions required for stable drop formation. Viscosities should be of the order of 0.01Pa.s at operating temperatures with surface tensions of approximately 30mN/m[19]. These requirements vary between different printing systems, but all systems have low tolerance of deviation from the ideal specifications of ink properties. Particulates within the ink solutions must also be tightly controlled to avoid clogging of the nozzle. Common guidance is to limit particulate sizes to 1% of the nozzle diameter.

In summary, the advantages of the inkjet process are

- accurate droplet formation and deposition can provide relatively high resolution digital raster printing,
- ability to print low viscosity solutions,

- scalable process, from low cost desktop systems to large volume manufacturing,
- the large range of printable substrates,
- no image master required, lower cost for small batch production.

Nevertheless inkjet has limitations, such as

- limited range of printable rheologies and surface tensions,
- slow printing speed,
- nozzle diameter limits particulate size in solutions,
- limited printable layer thickness, and
- raster imaging cannot produce continuous uniform features due to droplet shape.

1.1.1.5 Printing Method Comparison

Table 1.1.1 provides a summary of the key aspects of the printing methods described above.

	Flexography	Rotogravure	Screen Printing	Inkjet
Representative Maximum Resolution	High (40-50μm)	Very high (<20μm)	Medium (50-100μm)	Variable (20-50μm)
Deposit Dry Thickness	Variable (<0.1-4μm)	Variable (<0.1-5μm)	Thick (1-20μm)	Very thin (<0.5μm)
Capital Cost	Medium	High	Low	Low
Manufacturing Speed (Graphics)	High (300m/min)	Very high (1km/min)	Slow (<100m/min, 20sheets/min)	Very slow (<10m/min)
Economic Run Length	Medium-large	Large	Small-medium	Very small
Ink Viscosity	Medium-low (0.05-1.5Pa.s)	Medium-low (0.05-0.5Pa.s)	High (1-100Pa.s)	Very low (<0.02Pa.s)
Ink Surface Tension	Depends on substrate but below 38mN/m is ideal for most films.[17]			Limited (ideally 28-33mN/m)[19]
Max % of Ink Cured on Substrate	40%	30%	90%	5%
Ink Formulation	Flexible	Flexible	Flexible	Constraints (particle size)
R2R/Sheet-Fed	R2R	R2R	Sheet-fed	Sheet-fed
Application	Large area, large volume production	Large area, large volume production	Large area, medium-small volume production	Small area, small volume production

Table 1.1.1: Comparison of printing methods discussed in this thesis. All data is reproduced with permission from a preprint chapter of 'Organic Light-Emitting Diodes (OLEDs): Materials, Devices and Applications' unless otherwise stated.[20]

1.1.2 Inks

The choice of printing process will influence the choice of ink composition, and both factors must be tailored for the application. A generalised approach for printed application development is outlined in Figure 1.1.5. This shows that the ink composition is usually decided by the choice of application and print method. The physical properties of the ink, both wet and dry, will then define the quality of the final product. This process flow is further complicated if the functional component of this ink required for a particular application is non standard with respect to behaviour in solution

compared to conventional pigments. For example carbon nanotubes tend to require low concentrations and are insoluble, resulting in low viscosity and poor stability without addition of undesirable additives. Material requirements will often introduce constraints to the ink properties which will define a particular process.

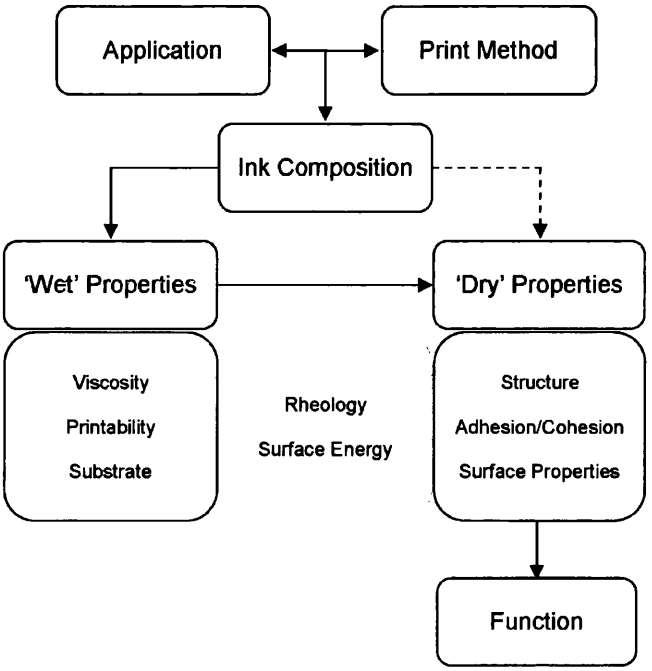

Figure 1.1.5: Flowchart illustrating approach for printed application development. Image reproduced from 'Printed Organic and Molecular Electronics' [1]

1.1.2.1 Requirements

The printing process requires an ink to be transported from a reservoir, through an inking system and deposited on a substrate to which it must adhere. To this end the ink properties must be tailored to the printing process. Basic printing process requirements including viscosities and surface tensions were discussed in section 1.1. It must be remembered that non-Newtonian materials (which most inks are) display a dependence of viscosity upon applied shear. The rate of change due to shear and recovery time is essential to the final print quality. The drying characteristics of the ink must also be determined, for high volume production a fast rate of drying is essential.

1.1.2.2 Structure

An ink is a substance (usually fluid or paste) which is deposited on a substrate during the printing process. In traditional graphics printing the purpose of this ink is to colour the substrate with the aim of creating an image or text. In functional printing such as printed electronics the aim is to add functionality to the substrate. A basic ink consists of three components

- functional compound,
- carrier substance, and
- vehicle.

The functional compound adds the functionality to the ink. In the case of graphics inks this will be a pigment or dye, used to colour the ink. For functional inks this will depend on the application, but some common compounds will be silver for printing conductive features, enzymes for bioprinting and semiconducting polymers for electronic components. The carrier substance will usually be oils or solvents (or combinations) selected for the application. Choice of solvents depends on solubility of the functional compound and vehicle, required viscosity and required drying characteristics. Common solvents used for printing inks are isopropanol, ethyl acetate and toluene. Solvent use is tightly controlled in production environments due to health and safety and environmental concerns, and many solvents including toluene are under strict usage limitations. The vehicle (often referred to as resin or binder) is used to adhere the material to the substrate and minimise functional compound agglomeration. Choice of binder depends on the solubility, required adhesion, required flexibility and substrate used. Some common binders are polyamide or nitrocellulose based.

Solvent based inks are not unique, other systems include water based and radiation (UV, electron beam) cured inks. Water based inks are increasing in popularity due to health and safety and environmental concerns due to their low toxicity. However, print quality of water based systems is usually poorer than that of solvent based alternatives due to the additives required to improve printability. UV curing inks are common in the graphics industry due to the speed of curing and the removal of solvent release in the printing process. However radiation curing inks are often unsuitable for functional printing due to the residual ink constituents impeding functional particle contact in the final film.

Various additives are often used in the formulation of a printing ink to improve various aspects of the ink behaviour, including surfactants for increasing the stability of the pigments and/or altering the surface tension of the ink. With respect to graphics inks the addition of additives is common at high percentages of the pigment base, however for functional inks this is not desirable as the surfactants will often remain in the printed film which can impede functionality. Further explanation of surfactant behaviour is given in section 3.3.2.1.

1.1.2.3 Manufacture

Once the basic constituents of the ink have been defined they must be mixed together to produce a homogeneous, stable dispersion or solution. A solution is defined as a stable single phase homogeneous mixture. Commonly in a printing ink the resin base is a solution. A dispersion (or suspension) is where solid particles are mixed in a solvent but are significantly large and thermodynamically unstable, meaning that they will tend to settle over time. Usually the pigment in a printing ink is in a suspension in the resin base. A number of methods are available to perform this, of which a combination may be used to produce the desired outcome. It may also be necessary during the mixing process to reduce the mean particle size of the functional compound, both aims can often be accomplished in tandem by use of high shear mixing processes. The choice of method depends chiefly on the rheological properties of the material and the durability of the particulates involved.

The most intuitive methods are hydrodynamic in nature and are based on the stirring of the material. This can be achieved mechanically by the use of disc dispersers or magnetic stirrers. The act of stirring applies a rotational shear force to the liquid, inducing a vortex flow. The usually turbulent nature of the induced vortex flows results in the random distribution of the particulate throughout the liquid. These methods are ideally suited to dispersing soluble particulates in solution, but have minimal deagglomeration capability.

Mechanical milling methods such as triple roll milling and bead milling are often preferred where particulates require deagglomeration. These methods apply direct shear to the particulate, which may damage the structure of some nanostructures affecting their properties. Triple roll milling applies the shear at a nip contact between rollers. The shear forces applied during the nip contacts serve to break down particle agglomerations and wet them within the liquid vehicle. Bead milling involves the mill base being flowed through a rotating drum containing ceramic beads. High

impact velocity collisions between the beads and mill base cause the breaking down of agglomerations and wetting of the particulates.

Vibration of the particulate within the fluid can also be used as a method of dispersing particles to make inks and coatings. This can be done at a low frequency, using manual or mechanical shaking. However, low frequency vibrations will not deagglomerate particulates. Higher frequency vibrations can be introduced by the use of ultrasonic generators. These are used in two forms, either indirectly in an ultrasonic bath or directly by the use of an ultrasonic probe. Bath methods tend to apply a lower amplitude of vibration due to the dampening effect of the additional fluids. Probe methods apply a higher vibration amplitude by immersing the vibrating probe tip directly into the sample. These methods can cause significant particle deagglomeration by the forces created when cavitation bubbles formed by the sonication collapse. It must be noted that structural damage may occur on the nanoscale as a result of these vibrations[21]. These methods are more suited to lower viscosity solutions, as vibrations tend to be dampened by the slower relaxation times of higher viscosity fluids.[22]

Literature discussing CNT dispersion formation is summarised in section 2.2.1 and discussion of technique choice and method for this work is provided in section 3.2.

1.1.3 Substrates

The choice of substrate is initially determined by the final application of the printed product. The choice of substrate will influence the printing process for deposition and hence the ink characteristics, and this influence also reciprocates. Solid substrates such as Si wafers or glass are not suited to direct gravure printing for example, whereas drying inks that require high processing temperatures on thin polymer films may prove problematic.

Substrate roughness, porosity and surface energy are just some of the critical factors that determine the final print quality and functionality. Substrates are often modified by the addition of coatings or by treatment to alter the surface energy to improve the printability. For example paper tends to be a rough substrate with high porosity, resulting in poor definition of features and high absorbance of ink compounds making low quality paper unsuitable for printed electronics applications. However high quality coated papers will have lower surface roughness and absorbance and can be exposed to high temperatures without damage, which may be advantageous for particular applications.

Flexible polymer films such as polyethylene terephthalate (PET) or polypropylene (PP) are common choices for printed electronics. Surface roughness tends to be lower than coated paper, and surface energies can be easily modified by techniques such as corona treatment or UV radiation exposure. Absorbance tends to be minimal, but solvent compatibility must be assessed before use.

Many printing methods are also suitable for printing onto solid, rigid substrates such as silicon or glass. These substrates will have no porosity and roughness can be carefully controlled during manufacture. However rigidity may be a limiting factor with respect to final application.

1.1.4 Drying

The homogeneity of a printed film is not only dependent on the behaviour of the ink during the deposition process but during the subsequent treatment of the wet film afterwards. The method of drying the printed film depends on the type of ink deposited. For solvent based inks heat must be applied to evaporate the solvent leaving the functional material and binder on the substrate. The higher the boiling point of the solvent used the higher the temperature that must be applied during the drying process, however care must be taken not to damage the substrate. If drying is performed in line with the printing in a roll-to-roll environment then thermal distortion of the substrate must be avoided, as this will lead to registration issues when overprinting and potentially web failure within the press. The rate of solvent evaporation can also be increased by increasing the flow of air across the substrate. Care must be taken not to deform the printed structure via shear applied from air flow.

During solvent evaporation there tends to be a liquid flow in the drying system towards the edge as evaporating liquid is replaced by liquid from the interior. This can result in preferential deposition of particulates at the edge of a drying feature, an effect known as the 'coffee ring' effect. Rapid drying of the printed features will minimise this effect.

As previously discussed, commonly graphics inks are cured using a UV light based system which will avoid any transport effects entirely and allow for high deposition speeds. The inks are formulated to contain a photo-initiator which when exposed to UV radiation cross link, solidifying the printed feature. This is rarely suitable for printed electronic components due to the fact that no ink components are removed from the system, impeding particle contact between the functional particles.

1.2 Carbon Nanotubes

> **nanotube** *n.* a structure consisting of one or more sheets of carbon atoms rolled up in the form of a cylinder, two or more concentric cylinders, or a cylindrical scroll; a buckytube; (also) any analogous tubular molecule composed of atoms other than carbon.*

Carbon is the fourth most abundant element in the universe and is non-metallic and tetravalent. However it can exist in several allotropic forms, each of which displays significantly different properties. For example, if the carbon atoms are arranged in a diamond lattice then diamond can be formed, which is usually an excellent electrical insulator, the hardest bulk material known to man and chemically inert. Another allotrope of carbon is graphite, where the carbon atoms are arranged in hexagonal lattice planar sheets which are stacked to form a 3d structure. Graphite is conductive along the planar direction, very brittle and not as chemically inert as diamond.

Carbon based structures have long been common constituents in printing inks. Carbon black, or amorphous carbon, was one of the first pigments used for black graphics inks and has gained usage in conductive inks for printed electronic applications where high conductivities are not required. Graphite has also been commonly used as a pigment for graphics printing.

The high dependence of electrical and physical properties upon the structural form has led to much research towards isolation of further carbon allotropes, or fullerenes. All fullerenes appear commonly in nature, for example carbon soot contains many different carbon structures, however deliberate manufacture of specific fullerenes has proved to be elusive. Many theoretical studies examined the properties of these structures, but the first fullerene to be practically manufactured and isolated was C_{60} (buckminsterfullerene) in 1985 by Smalley et al. at Rice University. This work led to the award of the Nobel Prize in Chemistry "for their discovery of fullerenes" to Robert F. Curl Jr., Sir Harold Kroto and Richard E. Smalley. Buckminsterfullerene is often treated as a one dimensional structure and correctly doped was shown to have superconducting properties, though in isolation it tends to be an insulator or semiconductor depending on the packing structure.

Research into fullerene isolation continued with many other structures theoretically predicted. The next major fullerene to spark the interest of the scientific

*"**nanotube** *n.*" OED Online. November 2008. Oxford University Press. 26 Nov. 2008 <http://dictionary.oed.com/cgi/entry/00320940>.

community was CNTs. Although imaged as far back as 1952, the first major paper detailing CNT manufacture with high resolution imagery was published by Iijima *et al.*[4] in 1991. This paper ignited scientific interest in the field of CNTs, an interest already sparked by the aforementioned isolation of buckminsterfullerene. Due to the high aspect ratio of the nanotubes they are treated as two dimensional structures, which provides unique physical and electrical properties of CNTs resulting in a myriad of potential applications that led to a boom in nanotechnology research. It is the potential for CNTs in semiconducting and conducting applications that has led to the research described in this thesis.

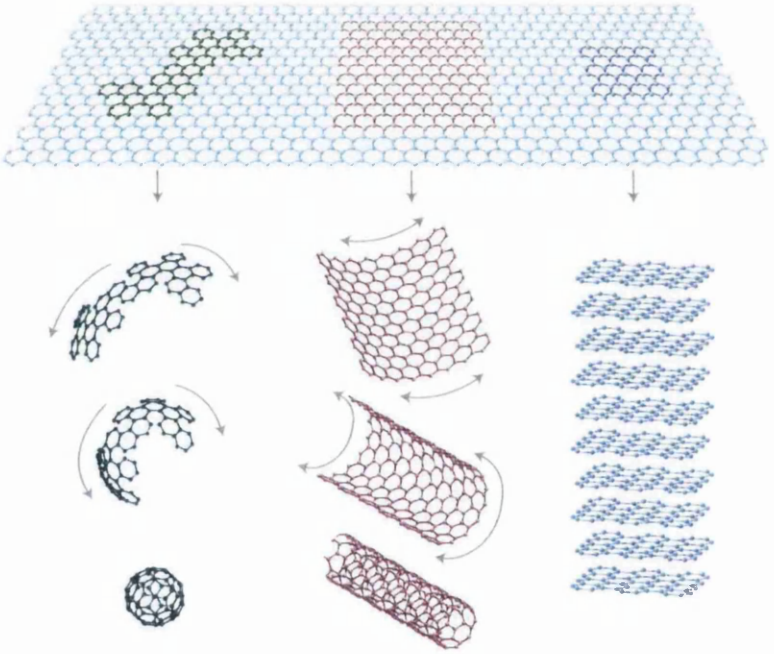

Figure 1.2.1: Projection of buckminsterfullerene, CNTs and graphite from a single graphene sheet. Image reproduced from 'Graphene: Status and Prospects' [2]

It must be noted that this was not the end of the fullerene search. It had long been observed that individual planar sheets of graphite were the building block of all the fullerenes previously mentioned, as illustrated in Figure 1.2.1. It was assumed that these single sheets were thermodynamically unstable and could not exist in isolation. However research by Novoselov *et al.*[23] in 2004 showed the first reliable manufacturing method for production of these planar sheets, or graphene as it is now commonly known. Graphene has exhibited unique electrical properties and has further fuelled the nanotechnology research field, especially with the award of the No-

bel Prize in Physics "for ground-breaking experiments regarding the two-dimensional material graphene" to Andre Geim and Konstantin Novoselov.

The basic properties of CNTs are well understood and information is available from a number of sources[24;25] However CNTs are still a highly active research field, and developments in relevant topics are expanded upon in the literature reviews in chapters 2 and 7.

1.2.1 CNT Synthesis

In the hunt for the isolation of specific fullerenes a number of production techniques have been developed.

1.2.1.1 Carbon Arc Discharge

This was the first method published that could reliably produce macroscopic amounts of CNTs, and is based upon the techniques pioneered by Iijima *et al.*. It involves placing two graphite electrodes a small distance (~mm) apart and applying a large current (~100A) across them whilst in vacuum. By using suitable metal catalysts and temperatures CNTs are formed in the condensates of the plasma from the electrical discharge. The CNT yield tends to be around 30% using this technique and CNT lengths are usually smaller in size compared to that produced by alternative techniques. However, it is a reliable and cheap production technique and is in common usage in research environments.

1.2.1.2 Laser Ablation

Developed in 1995 at Rice University, laser ablation uses a laser focused on a graphite target in a high temperature and pressure environment. This causes the target to vaporise and quickly condense onto the walls of the pressure vessel. By using different catalyst particles (typically cobalt and nickel) high yield and high quality CNT products can be formed. The diameter of the tubes formed can be controlled by the reaction temperature. The typical size of CNTs formed using this method is 10-20nm in diameter and 100μm long. The high CNT yield and quality of this method makes it ideal for scientific samples, however the equipment is expensive to purchase and run.

1.2.1.3 Chemical Vapour Deposition

This is the preferred method for large volume production. A suitable substrate is prepared by deposition of catalyst particles (again commonly cobalt or nickel) and is heated to 600-700^oC. The substrate is them exposed to a hydrocarbon gas (methane, ethanol, etc.) and as the gas decomposes at the edge of the catalyst particles, nanotubes are formed. This process gives a high yield of CNTs and has already been scaled up to produce nanotubes in industrial volumes. However the quality of the nanotubes is poor compared to laser ablation, with most containing many defects.

1.2.2 CNT Physical Structure

As illustrated in Figure 1.2.1 CNTs can be visualised as sheets of graphene rolled into a cylindrical form. This cylinder is usually capped at both ends by a half buckyball structure. The carbon atoms in the hexagonal lattice are in the sp^2 hybridised state, meaning that each atom is covalently bonded to another three carbon atoms, with a bond distance of 0.142nm. The valence shell configuration of carbon is $2s^2 2p^2$, meaning that four electrons are available for covalent bonding. This means that one electron is not used for bonding, and this electron is de-localised across the graphene plane, contributing to the charge transport and providing van der Waals bonding between adjacent planes.

Still following the visualisation of CNTs as rolled sheets of graphene, it can be seen that the sheet can be rolled at varying angles to form a seamless cylinder. This results in three structural types of CNTs, 'zigzag' and 'armchair' which are the only possible perfectly symmetrical structures and 'chiral', which is when the structure is arranged in a helix-like fashion around the central axis of the cylinder. These structures are specified by a vector notation in which the vector joins two points on a graphene plane which when rolled so that the two points are in contact forms a CNT. This is known as the chiral vector (C) and is illustrated in Figure 1.2.2. C is denoted in terms of integer multiples of the unit cell base vectors of the lattice (in this case a_1 and a_2) such that $C = na_1 + ma_2$ where $n \geq m$. It can be shown that $m = 0$ for all zigzag CNTs and $n = m$ for all armchair CNTs, with all other vectors denoting a chiral CNT. These structures partially define the electrical properties of the CNTs, as described in section 1.2.4.

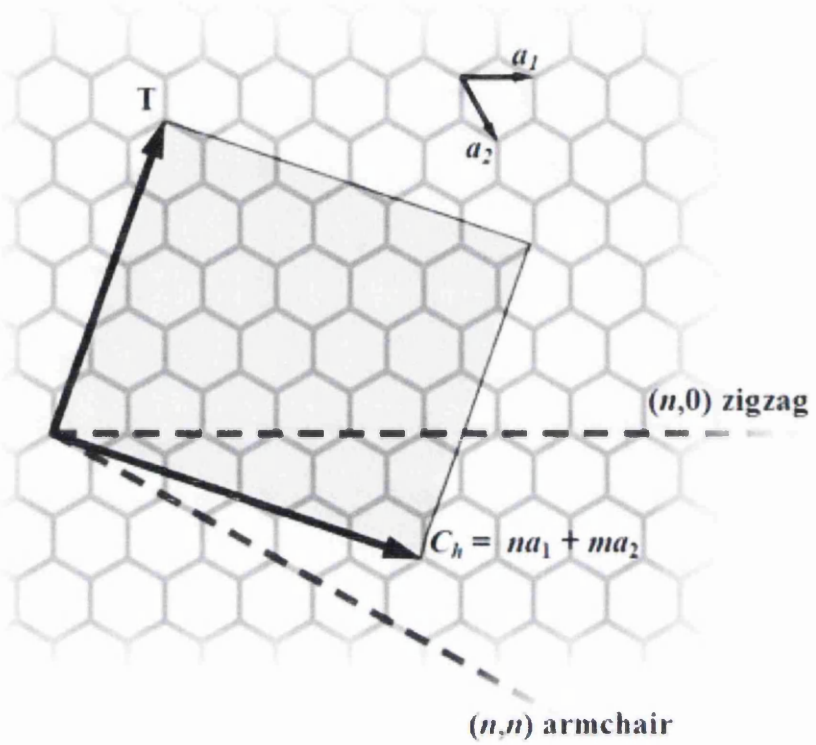

Figure 1.2.2: Chiral vector (C) projected onto hexagonal lattice. a_1 and $a_2$are the unit vectors of the lattice, and T is the CNT axis. Image sourced from Wikimedia Commons.

It must be noted that a perfect hexagonal structure throughout the entire CNT lattice is rare. Defects include pentagons and heptagons disrupting the hexagonal lattice and atomic vacancies. These defects affect the CNT shape and electronic and physical properties. The effect of these defects is discussed further in section 2.1.1.

CNTs are not solely found in this single walled (SWCNT) form. It is also common to find CNTs with evidence of a multiple wall structure (MWCNT). The exact nature of this structure was initially unknown, with the dominant options either multiple SWCNTs nested inside each other in a 'russian doll' fashion or a single graphene sheet wrapped around itself multiple times in a 'wrapping paper' fashion. TEM and chemical analysis indicated that the 'russian doll' structure is the correct option. These MWCNTs tend to have more defects within the structure than SWCNTs, including layers traversing the internal core of the tube resulting in closed compartments. The individual tubes are bonded by weak (relative to the carbon-carbon covalent bonds in the tube lattice) van der Waals bonds and show little stacking symmetry compared to graphite.

1.2.3 CNT Mechanical Properties

Theoretical analysis and experimental measurement has shown that the Young's modulus of single walled carbon nanotubes can be as high as 1TPa. This compares favourably with steel, for which the Young's modulus is given to be around 200GPa, depending on the grade. Combined with a measured tensile strength of as high as 63GPa (c.f. around 0.4GPa for A36 steel) the potential for CNTs as a reinforcing filler for composite applications is considered high.

CNTs have been observed to show remarkable capability to deform due to external stress without any major structural change. Ripples and kinks in the CNT structure develop when the tube is placed under compression or bending, as seen in Figure 1.2.3. When this stress is released the tube has been seen to relax to its original form as the stress does not exceed the elastic limit. It must also be noted that the wall separation between the CNTs remains constant, with no discontinuities present. This would not be the case if defects linking layers exist, which will reduce the elastic limit of the MWCNT.

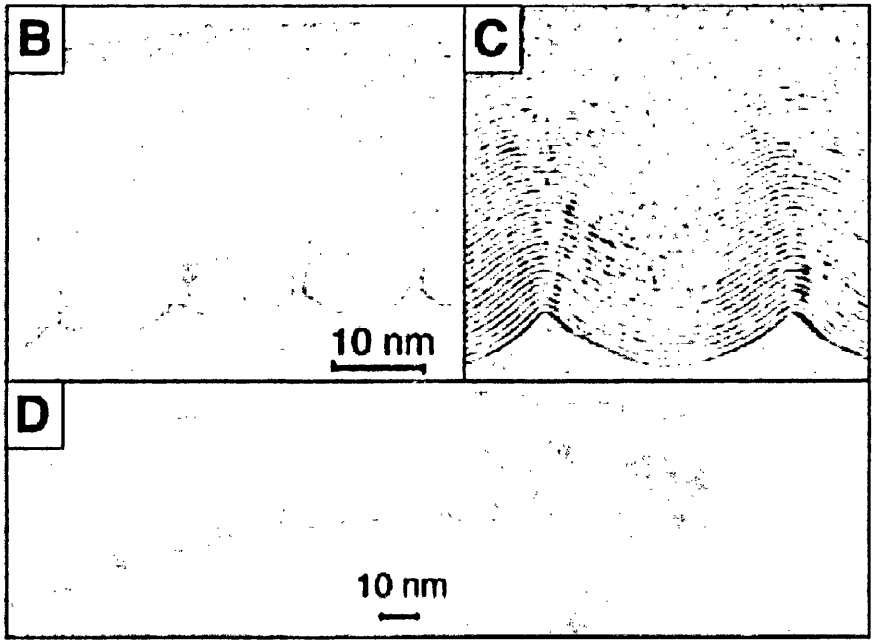

Figure 1.2.3: TEM images showing 'wavelike distortions' of the structure of MWCNTs bent with a radius of curvature of approximately 400nm. Image reproduced from 'Electrostatic Deflections and Electromechanical Resonances of Carbon Nanotubes' [3].

1.2.4 CNT Electronic Properties

As previously discussed, the electronic properties of CNTs are dependent on the chiral angle of the tube. This results in two distinct electronic groups of CNTs, metallic and semiconducting. It was predicted and experimentally proven that metallic conduction occurs when the chiral vector components n and m conform to the equation

$$n - m = 3q \tag{1.2.1}$$

where q is an integer value. This results in all armchair CNTs being metallic, as well as a proportion of zigzag and chiral. This equation also implies that if CNTs are produced with random chiral vectors statistically two thirds will be semiconducting and one third metallic. These properties are retained by the individual layers in MWCNTs, resulting in a hybrid structure known as a semi-metal (or zero bandgap semiconductor). However it must be noted that physical deformation of the CNT structure such as bending will affect the covalent bonding structure, resulting in the situation where non-armchair tubes become metallic, though armchair tubes are not affected.

Due to the one dimensional nature of carbon nanotubes there are a limited number of allowed electron states. The band gap introduced when equation 1.2.1 is not true results in the semiconducting behaviour of these tubes. Due to the discrete electron states the transport in metallic SWCNTs can be assumed to be ballistic, meaning that the resistance is independent of length. This assume no impurities or defects in the CNT structure.

Transport characteristics of semiconducting tubes are said to be diffusive rather than ballistic and they tend to show p-type behaviour, meaning that the dominant charge carriers are positive (holes). The mobility of these CNTs, meaning the ability for the movement of charge carriers to be influenced by an external electric field, is reported to be very high, with values of over $20000 cm^2 V^{-1} s^{-1}$ reported[24], higher than that of Si based field effect transistors. Further discussion on the semiconducting properties of CNTs is provided in section 7.2.2.

1.2.5 CNT Network Properties

CNTs can be arranged randomly into a planar macroscopic structure by random growth or solution deposition, such as in the image shown in Figure 1.2.4. In this case conduction occurs across a percolating network of tubes. If only metallic SWCNTs are present in the network then the network will have metallic properties, likewise for

a network of semiconducting CNTs the macroscopic properties will be semiconducting in nature. However for a structure containing random chirality CNTs the structure will tend to act as a semi-metal.

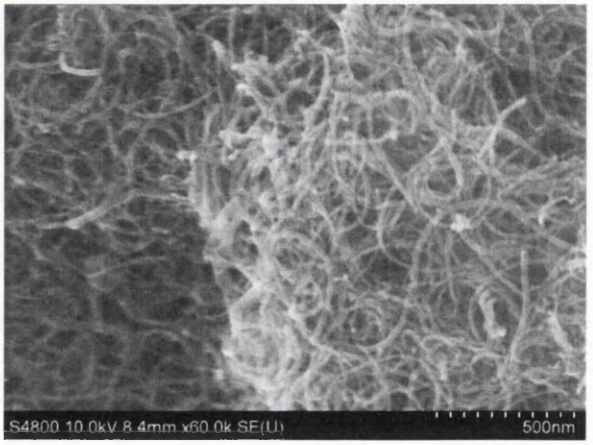

Figure 1.2.4: SEM image showing a random deposit of MWCNTs indicative of a conducting CNT network of a density significantly above the metallic percolation threshold.

If the density of the CNT network is carefully controlled then a random chirality network can be made to show semiconducting properties. This works by reducing the concentration of CNTs so that no electrical percolation is possible through the metallic tubes alone. However if the density is too low then no percolation will also occur along the semiconducting tubes. The specific density of CNTs where metallic percolation occurs is known as the percolation threshold.

1.3 Closure, Objectives and Thesis Layout

This chapter has given a brief overview of various printing and CNT concepts that are applicable to the work discussed in this thesis.

The purpose of this work is to study the potential for use of carbon nanotubes within a functional ink system. The work has attempted to follow the approach outlined in section 1.1.2 by initially focussing on the ink formulation. Initial work to determine ink constituents and manufacturing techniques is described, with the effect upon wet and dry properties of each variable assessed. Once a base ink formulation is decided upon the work focusses on the modification of the CNT structures to avoid the use of surfactants when possible. The effect of modification (or functionalisation) of the CNTs on the wet and dry properties of a printed film are assessed with the

aim of observing how changes to the nano-scale structure of the CNTs affects the macro-scale properties of a CNT network.. Finally the work focusses upon a possible final function of the CNT inks, in this case the use in a fully flexographically printed thin film transistor. Proof of concept device production and the further refinement of structure and ink is presented.

The thesis is set out in the following format:

- Part I - Thesis Introduction
  - Chapter 1: Introduction. This chapter provides a broad introduction to the topics of printing, ink formulation and carbon nanotubes and discusses the motivation for the work.
- Part II - CNT Ink Formulation
  - Chapter 2: Introduction and Literature Review. This chapter discusses developments in CNT ink formulation and deposition and expands on many of the details described in the thesis introduction.
  - Chapter 3: Experimental Techniques and Equipment. This chapter outlines the theory underpinning the parameters being measured and the measurement techniques utilised to investigate the properties of both the fluid ink and the deposited dry film.
  - Chapter 4: Initial Ink Formulation Determination. This chapter discusses the preliminary work used to decide the ink formulation and production method.
  - Chapter 5: Critical Mixing Energy, CNT Concentration and Functionalisation. This chapter discusses the investigation into the use of CNT functionalisation to obtain improved dispersion, and the effect this has on agitation energy required to create the dispersion.
  - Chapter 6: CNT Ink Formulation - Conclusions. This chapter discusses the results from the previous two chapters and discusses the consequences of the results in the context of printed electronic applications.
- Part III - Flexographically Printed CNT Based TFT Structures
  - Chapter 7: Introduction and Literature Review. This chapter discusses developments in CNT transistors and mass production of transistor structures by printing technologies.

- Chapter 8: Experimental Techniques and Equipment. This chapter outlines the theory underpinning the parameters being measured and the measurement techniques utilised to characterise the printed transistor structures.
- Chapter 9: Proof of Concept - MWCNT Based Field Effect Devices. This chapter describes the design and production of the initial TFT structures utilising MWCNTs as the semiconducting layer.
- Chapter 10: Flexographically Printed SWCNT Based Field Effect Devices. This chapter describes the design and production of TFT structures using SWCNTs as the semiconducting layer.
- Chapter 11: Flexographically Printed CNT Based TFT Structures - Conclusions. This chapter discusses the results from the previous two chapters and discusses the consequences of the results in the context of CNT TFT production.

- Part IV - Thesis Conclusions
  - Chapter 12: Conclusions and Further Work. This chapter discusses the overall conclusions and impact of the thesis and identifies avenues for further research.

Part II

CNT Ink Formulation

Chapter 2

Introduction and Literature Review

Since their isolation in 1991 the study of CNTs has increased dramatically, and this trend shows little sign of abating. Initial research focused on the properties of individual nanotubes and studied the effects of chirality upon the electrical properties. As production methods improved the study of the properties of multiple CNTs in a mesh structure became popular, as this was seen a likely route for industrial scale exploitation of the unique properties of CNTs described in section 1.2. These mesh structures could be produced in a variety of ways, dry deposition, in-situ growth or solution processing. The solution processing route naturally leads to the use of printing methods for deposition, and provides the basis of the academic interest for the work described in this thesis. As understanding and popularity of these solution processing methods increased so did the application driven research, leading towards demonstration of a number of devices exploiting the unique mechanical and electrical properties of CNTs in various fields. The potential for ballistic conductance in metallic CNTs along with the semiconducting nature of other chirality tubes allow applications in printed digital electronics, photovoltaics and more. Also the use of solution processed CNTs was of great interest to the composite research community as it provided a suitable route to the use of CNTs as fillers in composites to exploit their mechanical strength as well as the electrical properties.

This chapter will focus on the key developments in the timeline described above, concentrating on work related to the printing and coating of CNT solutions. This literature review alongside the concepts presented in the introduction (chapter 1) will outline the motivation and scientific basis for the work presented in this thesis.

2.1 CNT Properties

A basic outline of the properties of CNTs is provided in section 1.2. This section will discuss these properties in more depth, highlighting the literature that describes properties relevant to the functionality of CNT inks.

2.1.1 Individual CNTs

2.1.1.1 Electronic Properties

As previously stated, Iijima[4] is widely regarded as the first person to successfully isolate and image CNTs. These tubes were produced using an arc discharge method and all imaged tubes were MWCNTs of varying diameter, as shown in Figure 2.1.1. The structure of the tubes as a number of distinct cylinders placed inside one another was proposed, and the potential orientations of the hexagonal lattice when rolled was discussed.

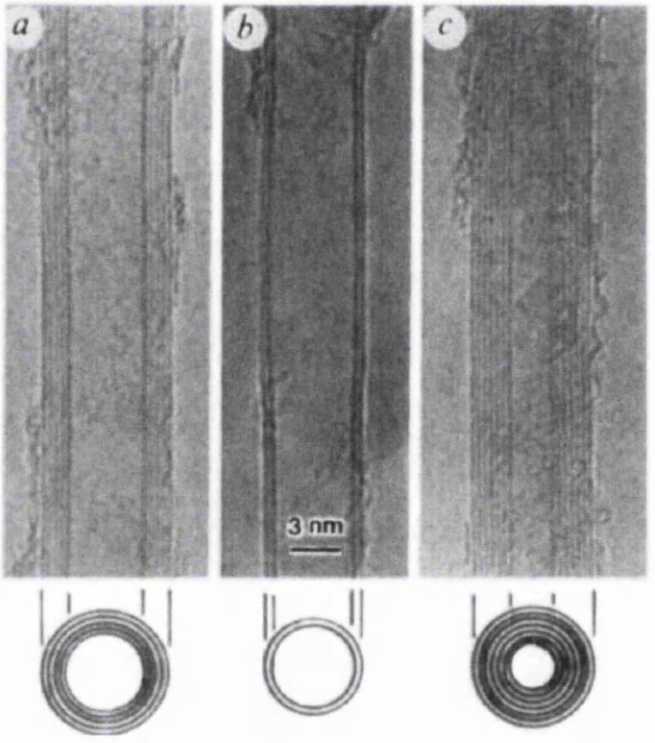

Figure 2.1.1: The first TEM image of MWCNTs, with illustration of proposed structure. Image reproduced from 'Helical microtubules of graphitic carbon'. [4]

The properties of the lattice when rolled into a tubular structure was further

studied by Saito *et al.*[5] who proposed the notation of the chiral vector previously described in section 1.2.2. By considering the SWCNTs as strictly one dimensional structures they calculated the density of states for various chiral vectors and noted that "the calculated electronic structure can be either metallic or semiconducting depending on the fibre diameter and on the chiral angle, though there is no difference in the local chemical bonding between the carbon atoms, and no doping impurities are present."[5]. Two example density of states are shown in Figure 2.1.2. Note the zero states at zero energy in Figure 2.1.2a, indicating the tube is semiconducting in nature. The finite state in Figure 2.1.2b indicates a metallic behaviour. They also calculated that given a random distribution of chiral vectors, two thirds will result in a semiconducting behaviour and one third will result in metallic behaviour. This realisation of the fundamental electrical properties of CNTs was key to sparking the explosion of research into these fullerenes.

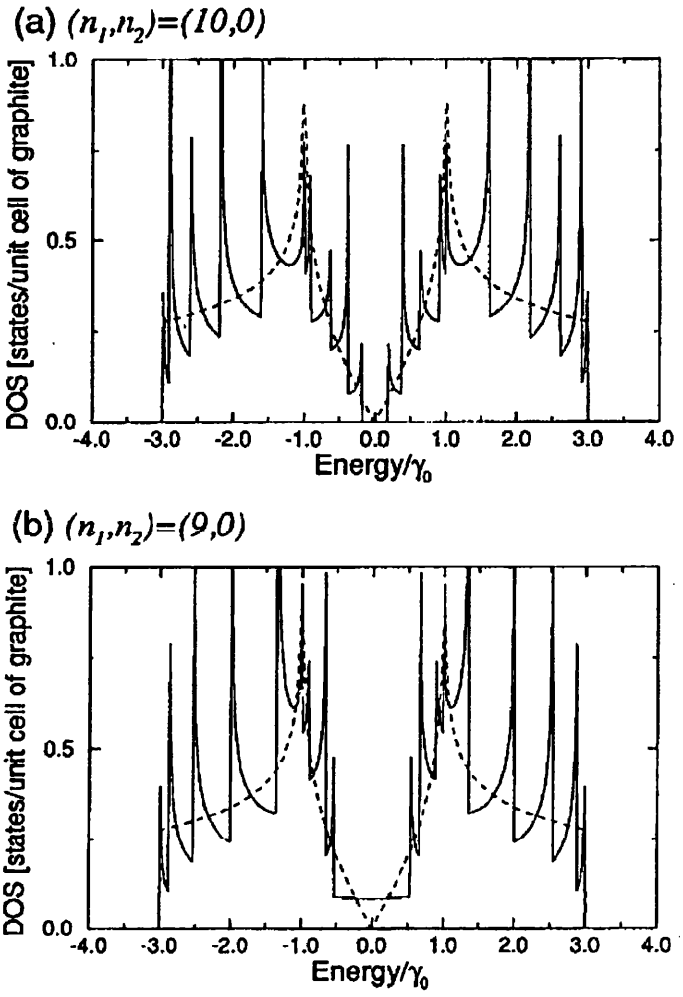

Figure 2.1.2: Density of stated of two zigzag CNTs. (a) shows a semiconducting tube, (b) a metallic. Image reproduced from "Electronic structure of chiral graphene tubules"[5].

The same research group went on to further discuss the physics of carbon nanotubes[26], including studying the electronic behaviour of MWCNTs. They found that any interlayer interactions between the individual tubes in a MWCNT structure did not perturb the electronic behaviour of the tubes. Thus they found that the tubes retained their behaviour and as a result metallic tubes stacked within each other resulted in net metallic behaviour, similarly for semiconducting chiralities. They then proposed that MWCNTs containing semiconducting and metallic properties could be used as metal-insulator structures. However it must be noted that the outer shell of a MWCNT will tend to dominate the transport properties, as predicted by Delaney *et al.*[27].

It has also been observed that conduction in pristine metallic tubes is ballistic in nature, meaning that the mean free path of the charge carriers is greater that the tube length. This was observed experimentally over partial sections of SWCNTs [28], with the lack of ballistic conductivity over the entire length blamed on defects. The absence of backward scattering in the pristine tube structure is key to ballistic transport, and this was further summarised theoretically by Ando [29], who clarified that the absence of backscattering in metallic tubes allows the wave function of the charge carriers to be extended to the whole nanotube.

Research has also focussed on the current carrying capacity of CNTs, essential to understanding the potential for CNTs in integrated circuits. Wei *et al.* [30] performed studies on MWCNTs and saw that individual tubes were capable of carrying current densities of up to 10^{10}A/cm^2 in normal atmospheric conditions without adverse effect, which is comparable to traditional interconnect structures such as copper. Theoretical studies clarified these high values and showed that the limit is dependent on tube diameter [31].

2.1.1.2 Mechanical properties

The remarkable properties that have kept CNTs in the research spotlight for so long are not confined to the electronic structure. The bond structure and dimensionality of CNTs also give rise to remarkable mechanical properties. In section 1.2.3 the headline figures for tensile strength and Young's modulus were introduced. It must be noted that these figures are dependent on a number of tube properties, especially tube diameter. This results in MWCNTs often having favourable mechanical properties over SWCNTs, especially concerning tube stiffness. A number of studies have confirmed this, including Hernández *et al.* [32] who theoretically predicted the dependence of the Young's modulus upon tube diameter, giving favourable comparisons with reported values in the literature at the time.

Determining these properties experimentally is difficult, and most reported results have been obtained by two main avenues of research. One common method is to study the vibrations of isolated tubes using a TEM, such as the work done by Krishnan *et al.* [33]. In this work they studied suitable isolated SWCNTs on a TEM grid, and measured vibrations at room temperature. This could then be compared to a clamped cantilever and the Young's modulus subsequently calculated for a number of samples. An average value of 1.25TPa was obtained. An alternative method, employed initially by Yu *et al.* [34] involves studying the properties of macroscopic ropes and deriving the

individual tube properties from the results. In this case a mean Young's modulus of 1TPa was derived.

2.1.1.3 Physical properties

The physical properties of CNTs are also of interest with regards to printed electronics applications. The powder density of CNT powder is crucial for future ink production, however values are variable depending on production method, post production treatment, CNT quality and CNT type. Rinzler *et al.*[35], when describing the powder produced by their initial laser ablation technique described in section 1.2.1.2, quote a density of 5mg/cm^3 for the raw powder. However purification and other treatments can change this value by orders of magnitude, so they clarify that density cannot be used as a constant for CNT classification. One article by Collins *et al.*[36] quotes CNT powder density as 1.33 to 1.4 g/cm^3 but do not state the source of this value.

Another physical property crucial to potential applications of CNTs is the specific surface area of CNT powders. The potential for CNTs in catalytic applications such as in dye sensitised solar cells and the need for a simple and quick quantification of CNT powder quality has led to much research in understanding the specific surface area of CNT powders. Due to the nanostructure of CNTs the surface areas of macroscopic quantities is expected to be large. Peigney *et al.*[37] calculated the theoretical surface areas for a range of CNT structures. Surface areas of approximately 1300m^2/g were predicted for SWCNTs whilst MWCNTs containing 20 walls were predicted to show surface areas of the order of 100m^2/g. These values correlated well with various experimentally derived values reported in the literature.

2.1.2 Functionalisation of CNTs

Due to the chemical stability and high van der Waals forces observed between carbon nanotubes their use in macro scale devices is limited. A common method for processing powders for device production is via solution techniques, however obtaining stable dispersions at high concentrations is impossible with pristine CNTs. The use of solution processing techniques for CNT deposition is discussed in sections 2.2 and 2.3, but to realise these techniques in volume some modification of the CNT is usually required, the effects of which are also discussed in the aforementioned sections.

Sun *et al.*[38] define functionalisation as *'the chemical modification and solubilization of carbon nanotubes'* and review the two functionalisation types available. One type is called non-covalent where molecules are adsorbed onto the CNT surface without

altering the structure of the tube. An example of this is the use of surfactants (see section 1.1.2.2) for CNT dispersal. The alternative type is covalent, where molecules are bonded directly to the CNT structure. Due to the hexagonal lattice structure of CNTs molecules can only bond at the end caps where pentagonal structures exist or at defect sites. The choice of molecule will usually depend on the application, and the key for ink formulation is to reduce CNT agglomeration and solublise the tubes. It was also noted that defunctionalisation is possible by thermal or chemical methods.

Balasubramanian *et al.*[39] reviewed methods for covalent functionalisation. They noted that the reactivity of pristine CNTs (and hence the susceptibility to functionalisation) is highest at the end caps, with the sidewalls increasing in reactivity as CNT diameter reduces due to increased strain on the bonds with higher sidewall curvature. One method for covalent functionalisation is acid refluxing. For example sonication in concentrated nitric and sulphuric acid adds oxygen containing groups to the CNT surface, effectively oxidising them. It was observed that this reduced the attractive forces between tubes, reducing the energy required to deagglomerate the CNT powder. Solubility in aqueous solutions and organic solvents is also improved. Further functional groups can often attach to the oxygen groups to suit the application. To attach specific groups directly to the sidewall other methods may be required. Other common methods discussed for covalent functionalisation are electrochemical and photochemical in nature.

Electrochemical functionalisation involves a CNT electrode being immersed in a solution containing a suitable reagent. If a constant current (or voltage) is applied across the electrode electron transfer occurs between the CNTs and the reagent solution. This can cause a polymer to coat the tubes, and the functionality type is determined by the reagent used. This is a popular method due to the degree of functionality control and the scalability of the process.

Photochemical functionalisation involved illuminating the CNTs by UV radiation whilst exposing them to specific atmospheres. The technique is still in its infancy, however promising results have been seen including selective functionalisation of metallic CNTs, potentially allowing chirality separation (as discussed further in section 2.1.4).

One method which was not mentioned in Balasubramanian's review was that of plasma functionalisation. Felten *et al.*[40] saw that MWCNTs can be functionalised by exposure to plasma formed in specific atmospheres. They saw that using oxygen atmospheres within their plasma reactor various oxygen containing groups (carboxyl, hydroxyl and carbonyl) were added covalently to the surface of the CNTs. Also

using ammonia atmospheres introduced amine, nitrile and amide groups to the CNT shell. The degree of functionality was controllable by tuning of the exposure time, gas pressure, power applied and the sample position within the plasma. They noted that this method is scalable and produces no waste, thus is a promising candidate for industrial scale functionalisation.

Chen *et al.*[41] used plasma functionalisation to oxidise CNTs with similar results seen. They observed a CNT solubility and solution stability in water, which is not possible with pristine CNTs. However SEM images showed significant damage to the CNT surface, though the tube form remained.

This damage to the CNT structure was investigated further by Shoda *et al.*[42] who investigated fluorination of MWCNTs in plasma by use of a tetrafluoromethane atmosphere within the reactor. It was seen that the functionalisation only occurred to the outer layer of the MWCNT, however TEM images showed an increase in observable defects including the destruction of individual layers. The degree of defects observed was directly proportional to reactor power, and they concluded that care must be taken to balance the functionality required whilst maintaining the CNT structure.

Tseng *et al.*[43] applied plasma functionalisation to reinforcement of epoxy composites. By choosing a compatible functionality they saw that the CNTs would become covalently integrated into the epoxy matrix through the covalent functional groups. This resulted in significant improvement in the composite properties, including an 85% increase in tensile strength compared to non functionalised CNTs.

2.1.3 CNT Network Properties

The concept of CNTs being arranged in a network structure and the macroscopic properties that result was introduced in section 1.2.5. This section will discuss these properties in more depth, reviewing the relevant literature.

The electrical properties of randomly orientated CNT networks have been extensively studied. Kim *et al.*[44] studied the temperature dependence of the DC conductivity of SWCNT sheets produced by arc discharge methods. They observed that the conductive properties of the network became non-ohmic below 15K. This means that the current does not depend linearly upon the voltage, as predicted by Ohm's Law. This behaviour was unexpected due to the fact that metallic CNTs do not display this behaviour independently, summarising that it must be a property of the tube-tube contact. This conclusion was reinforced by a good agreement of the practical data with a model that included fluctuation induced tunnelling at the tube contacts.

The study of the origin of this non-ohmic behaviour was continued by Kaiser *et al.*[45] who showed that the resistance of the SWCNT networks is dominated by barriers consisting of non-metallic defects, whether that be tube defects or tube-tube contact points. They noted that there was a discrepancy in the understanding of the dependency between conductivity and temperature, wherein the conductivity increases to a maximum before decreasing at lower temperatures. This suggests that metallic and non-metallic tube segments are in series, meaning that the resistances accumulate in a summation. Assuming that the resistance of non-metallic barriers will dominate at low temperatures but decrease as temperature increases, and that metallic segments show a linear positive dependence on temperature as expected then the behaviour can be accounted for. This theory was further tested by analysis of the frequency dependence of the CNT network resistance. At increasing frequencies the contribution of the barrier resistance should decrease due to the spatial movement of the carriers decreasing. This means that as frequency increases the conductivity should increase, until the conductivity in the metallic portions is inhibited, as predicted by the Drude model of electrical conduction. This dependence was experimentally observed and modelled, with good agreement seen.

Research also focused on the CNT density dependency of the network properties. Hu *et al.*[46] formed varying density networks and studied the 2D percolation behaviour. They found that the behaviour of the network could be described by percolation theory using a model of conductive rods. This predicted that the conductivity was proportional to the density (N), with a critical density (N_c) that needs to be achieved before the network becomes percolating. The predicted dependence was

$$\sigma \propto (N - N_c)^{\alpha} \tag{2.1.1}$$

where α is a dimensionality constant for which, in the two dimensional case, $\alpha = 1.33$ and in the three dimensional case $\alpha = 1.9$. The best fit for their data was $\alpha = 1.5$, which is attributed to the range of densities they performed their measurements over. They summarised that further understanding of this percolation behaviour will be critical to the development of CNT networks.

Bekyarova *et al.*[47] studied the effect of varying CNT type (SWCNT as produced, purified and functionalised) upon the percolation behaviour of sprayed CNT films. By repeated overspraying they found a critical thickness above which conductivity rapidly increased, and below which non ohmic behaviours was observed similar to that described by Kim[44] and Kaiser[45]. The effect of CNT functionalisation (in this case

octadecylamine and poly(m-aminobenzene sulfonic acid)) was to increase the percolation threshold due to the increased tunnelling barriers, meaning that the functionality was effectively reducing the concentration of conducting pathways. Calculated values of α confirmed that near the percolation threshold the network behaves as a two dimensional percolating system, as predicted by Hu [46].

One of the leading research groups in the field of nanoparticle percolation is the 'Chemical Physics of Low-Dimensional Nanostructures' group in Trinity College (Dublin, Ireland) led by Prof. Coleman. A number of papers have been released from this group in the field of carbon nanotube networks, including one by Lyons *et al.* [48] which studied the relationship between DC conductivity and film morphology. They emphasised that macro scale CNT networks consist of networks of CNT bundles rather than individual CNTs. By comparing the density of the CNT powder and the CNT films created an estimate of the porosity of the films was made and a resulting CNT junction density calculated. This was found to be linearly proportional to the film conductivity. By calculating an interjunction resistance in the range of 70kΩ to 3.5MΩ they suggested that ITO performance (90% transmission at 550nm at sheet resistivities of less than 90$\Omega/\square$) should be possible if high quality, defect free metallic CNTs are used. It was also shown that their model agrees with percolation theory near the percolation threshold, reinforcing the view that percolation theory is only valid near this point.

A later paper from the Coleman group by Pereira *et al.* [49] calculated upper bounds of the conductivity achievable in CNT networks assuming ideal contact between pristine CNTs. This estimation showed a dependency of the maximum conductivity upon volume fraction, tube length and tube diameter. By comparing the calculated conductivities with experimentally derived values they saw that limited improvement was achievable. Films of 6×10^5S/m were produced against a theoretical maximum (in this case) of 9×10^6S/m, indicating that the further improvement in CNT films will be limited due to the experimental impossibility of many of the assumptions made in the upper limit calculations. This implied a shift in viewpoint within the research group about the potential for CNT films.

A further paper was released from the same group by Nirmalraj *et al.* [6] that studied the effect of CNT type upon junction resistance. It was seen that acid treated (functionalised) CNTs displayed significantly lower junction resistances compared to pristine and thermally annealed tubes. This was measured by the use of conductive AFM techniques, as illustrated in Figure 2.1.3. The c-AFM images (Figure 2.1.3 (a) and (d)) allowed localised resistance measurements to be made (graphs (b) and (e),

illustrated in (c) and (f) respectively). It was suggested that this may be due to increased availability of charge carriers in the acid treated tubes. Increasing bundle size was also seen to result in an increase in junction resistance, highlighting the need for efficient deagglomeration of the CNT bundles during processing. The linear relationship between junction resistance and macroscopic film conductivity was also observed experimentally.

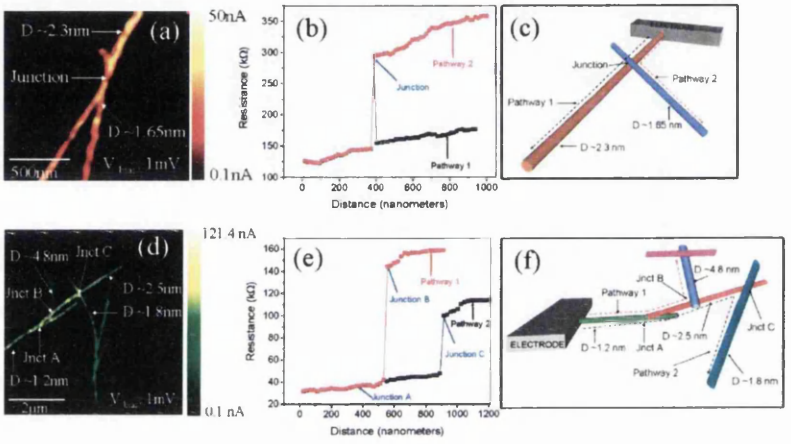

Figure 2.1.3: Conductive AFM image on low density acid treated CNT networks showing junction resistances. Reproduced from 'Electrical Connectivity in Single-Walled Carbon Nanotube Networks'[6].

CNTs are not the only nanostructure proposed for use in ITO replacement. The Coleman group, in a paper authored by De *et al.*[50] modelled the relationship between transmittance and sheet resistivity for various nanostructures including CNTs, graphene flakes, Ag nanowires and Ag flakes. They found that low diameter and low thickness structures are optimal for the application, and suggested Ag nanowires were the most promising candidate for ITO replacement, confirming the shift in viewpoint from the results of Lyons *et al.*[48].

However, the peak performance of CNT films may be improved by the addition of conductive polymers as a further component in CNT dispersions, as studied by Kyrylyuk *et al.*[51] (amongst others[52]). The addition of conductive fillers to the CNT matrix was modelled and it was observed that this addition had the effect of lowering the percolation threshold. The model compared favourably with experimental data, with a percolation threshold of 0.4wt% seen for a SWCNT-polystyrene multicomponent dispersion. However further understanding of the optimal particle morphology and transport between the two components of the dispersion is required to exploit the work fully.

2.1.4 Separation of Chiralities

As discussed in sections 1.2.4 and 2.1.1.1, the electrical properties of CNTs are predominantly governed by their chirality, with two thirds of randomly produced CNTs being semiconducting in nature and the remaining third metallic. Significant research effort has been spent on discovering a way to separate these chiralities, either by selective growth or post production separation. At the time of writing no selective growth mechanisms have been shown to be viable on a significant scale, whilst a number of post production separation techniques have been developed and commercialised to a limited degree.

Initial post production techniques were prompted by the need to improve CNT-FET efficiency (see chapter 7 for further discussion on CNT FETs). This required the destruction of metallic CNTs in a percolating network, and was performed by applying high enough currents to induce electrical breakdown [7]. As mentioned in section 2.1.1.1, it has been shown that CNTs can withstand high current densities, meaning that this technique requires high currents to be applied over significant timescales, as seen in Figure 2.1.4.

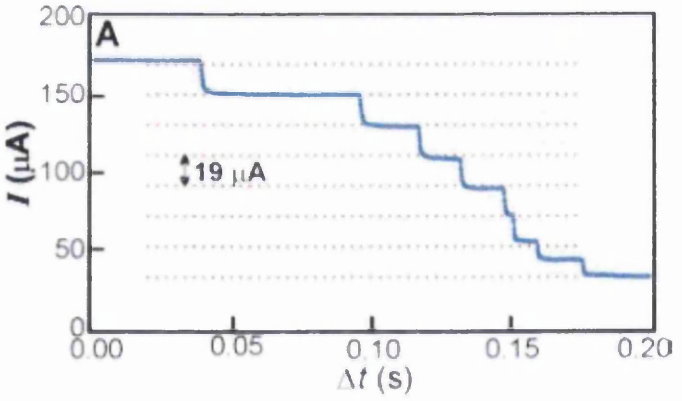

Figure 2.1.4: The breakdown of a MWCNT during constant voltage application can be seen in discrete steps as individual shells are destroyed. Reproduced from 'Engineering Carbon Nanotubes and Nanotube Circuits Using Electrical Breakdown' [7].

Alternative techniques have focussed on non destructive solutions. Krupke *et al.*[53] used a dielectrophoresis technique to separate chiralities in solution. SWCNTs were dispersed in a stabilised D_2O solution and deposited onto an electrode. An AC generator operating at a frequency of 10MHz and peak-to-peak voltage of 10V was applied and it was observed that due to the different relative dielectric constants of the metallic and semiconducting CNTs the metallic CNTs were drawn to the electrode

whilst the semiconducting tubes remained in suspension. This method only works if the CNTs are in pristine dispersions with no bundles, and was only proven on $10\mu l$ droplets, though it is claimed the method is scalable. Another technique discussed by Campidelli *et al.*[54] was selective functionalisation of CNT chiralities. Various methods to achieve this were introduced, including using selected molecules that preferentially bond to particular CNT types, and allowing the non-functionalised tubes to precipitate out of solution. The most promising method in terms of commercial potential appears to be based upon density gradient centrifugation. Chen *et al.*[55] found that after addition of bromine to a surfactant stabilised aqueous solution of deagglomerated CNTs the surfactant is selectively destabilised. After centrifugation the supernatant was shown to contain an enhanced proportion of semiconducting tubes. The selective use of surfactants is key to this technique, and the work was furthered by Arnold *et al.*[56] who achieved purities of 97% when using density gradient centrifugation. The method appears scalable with yields of 2.3% reported, which could provide gram quantities of sorted CNTs using a standard industrial scale centrifuge. This method is currently being commercialised by nanointegris (http://www.nanointegris.com/), but at the time of writing costs are still prohibitive for many applications.

It must be noted that progress has been made in the field of selective growth. Recently, Sundaram *et al.*[57] found that under certain growth conditions, CNTs produced using their proprietary CNT fibre spinning technique were predominantly metallic in nature.

2.2 CNT Solutions

Two methods are available for the production of CNT networks as described above. Either the CNTs can be grown in-situ, or they can be deposited onto a substrate from an initial powder production. Deposition usually occurs via solution techniques for ease of processing. To produce a stable dispersion of CNTs for solution deposition is not a trivial matter, and this section outlines the relevant literature in this field.

The definition of a suspension and solution (or dispersion) was discussed in section 1.1.2.3. It must be noted that confusion sometimes seems apparent in the literature with respect to the terminology used for CNT solutions. In all cases the terminology used will be taken from the source material.

2.2.1 Solution Production

To obtain a dispersion of CNTs from a standard powder product a suitable solvent must be chosen and the CNTs mixed using a suitable technique. CNT powders tend to consist of large bundled agglomerations often tens or hundreds of micrometers in diameter which need to be broken down to obtain suitable dispersions. An example SEM image of typical agglomerations in a commercial SWCNT product is shown in Figure 2.2.1. Care must be taken during this deagglomeration and mixing, as incorrect choice of solvent or mixing technique may damage the CNTs. Many mixing techniques were outlined in section 1.1.2.3 and are discussed in detail in section 3.2.1.

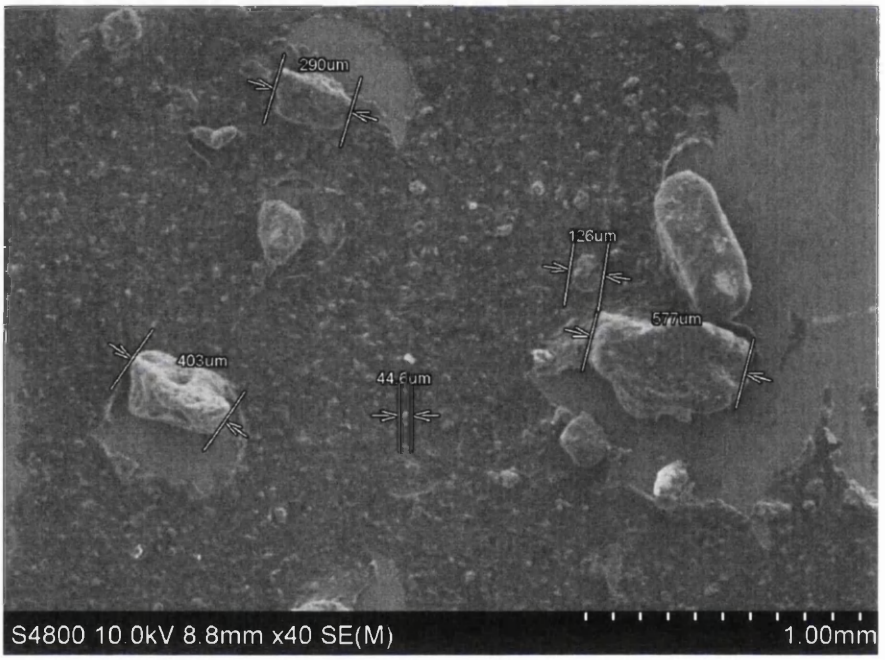

Figure 2.2.1: SEM image highlighting typical agglomeration sizes in an untreated commercial SWCNT powder.

Lu *et al.*[58] studied the use of sonication for CNT powders in methylene chloride (DCM, CH_2Cl_2). Samples were tip sonicated for various timescales at a power of 17W. After sonication a number of defects including buckling, bending and dislocations were directly observed using high resolution transmission electron microscopy and indirectly using Raman spectroscopy. It was shown that the magnitude of defect observance was directly proportional to the sonication time.

Due to their high chemical stability carbon nanotubes are insoluble in most solvents, including water. DCM has shown promise as a solvent for carbon nanotubes, but is highly volatile, making it unsuitable for many applications. Further

development in the field was required to identify alternative solvents. Ausman *et al.*[59] studied a variety of solvents with the aim of reducing agglomeration and obtaining pristine, stable solutions of CNTs at high density. They used uv-vis spectroscopy to characterise their dispersions after bath sonication, with higher absorbance indicating increased CNT content in the dispersion. They found two solvents showed promise, n-methyl-2-pyrrolidone (NMP, C_5H_9NO) and dimethylformamide (DMF, C_3H_7NO). Both showed similarities in various chemical parameters, but a solvent specification for CNT solubility was unable to be concluded.

This work was furthered by Bhar *et al.*[60] who studied a wider range of solvents specifically for small diameter tubes (which tend to be more reactive). Again, uv-vis spectroscopy was used to quantify the solution quality, and they were able to calibrate this against the physical mass of CNTs remaining in the dispersions after centrifugation and filtering. The results are shown in Table 2.2.1. The results for NMP and DMF seen by Ausman *et al.*[59] were verified by this study, with several superior candidates in terms of solubility identified. It must be noted that many of these chemicals show less than ideal properties with regards to health and safety aspects when studying this literature from a potential ink manufacturing point of view. The key similarity between the solvents identified as suitable for CNT dispersions was high polarity.

Solvent	mg L^{-1}
1,2-Dichlorobenzene	95
Chloroform	31
1-Methylnaphthalene	25
1-Bromo-2-methylnaphthalene	23
N-Methylpyrrolidinone	10
Dimethylformamide	7.2
Tetrahydrofuran	4.9
1,2-Dimethylbenzene	4.7
Pyridine	4.3
Carbon disulfide	2.6
1,3,5-Trimethylbenzene	2.3
Acetone	—[b]
1,3-Dimethylbenzene	—[b]
1,4-Dimethylbenzene	—[b]
Ethanol	—[b]
Toluene	—[b]

[a] The sonicator bath water temperature rose to *ca.* 35 °C over the course of 1 h. [b] Solubility in these solvents was < 1 mg L^{-1}

Table 2.2.1: Table showing room temperature solubility of SWNCTs in various solvents. Reproduced directly from 'Dissolution of small diameter single-wall carbon nanotubes in organic solvents '[60] .

To disperse CNTs in solvents that do not typically show high CNT solubility some type of chemical modification or functionalisation is required, as discussed in section 2.1.2. The addition of surfactants is a common route to improve solution stability in the ink making process. Islam *et al.*[61] attempted to solubilise SWCNTs in water by use of various surfactants. Atomic force microscopy (AFM) of dried deposits was used to quantify the dispersion quality. Bath sonication was used for mixing and mass fractions of stable, isolated CNT solutions as high as 20mg/ml were obtained. The surfactant that showed the most promise was NaDDBS-HiPCO, with the optimal CNT:surfactant ratio being between 1:5 and 1:10. As mentioned in section 1.1.2.2, surfactants are not ideal for printed electronic applications, but may be a 'necessary evil'. It was noted that the surfactant could be removed at temperatures over $180\,^{o}C$, however this would be unsuitable for most plastic film printing substrates. Paper could be used as a substrate at that temperature, but films are often preferred due to lower surface roughness.

With a number of suitable solvents identified, Hilding *et al.*[9] studied the effects of various mixing techniques upon the CNT dispersion (the fundamentals of these mixing techniques are described in section 3.2.1). Verifying the aforementioned work of Lu

et al.[58], sonication was seen to shorten SWCNTs and remove shells from MWCNTs. The common usage of probe sonication for CNT deagglomeration was noted, and it was summarised that the damage was done by bubble formation and implosion during cavitation at the tip. Tube length decreases of 40% were seen between probe sonication times of 5 and 20 minutes. In comparison, bath sonication was seen to show a decrease of 60% between 5 and 20 minute sonication times. It was noted that probe sonication caused significant tube shortening during the first 5 minutes of sonication, resulting in the smaller percentage decrease between 5 and 20 minute sonication times as the tube lengths tended to reach the same minimum for both methods. It was also observed that poor dispersions for composite applications gave extrudates that would not draw down homogeneously. The sonication energy required for MWCNT dispersion for composite applications was empirically modelled and the results are shown in Figure 2.2.2. Ball or Bead milling was also examined as a method for mixing CNTs, however destructive results were seen with significant amounts of amorphous carbon observed post processing, indicating complete break down of the CNT structure. It was noted that ball milling had been investigated for a number of alternative CNT applications, including CNT production from graphite, with limited results. Also intercalation of CNTs with various compounds (Li, K, Rb and Cs) was performed by ball milling for battery applications. Promising intercalation results were seen but care had to be taken not to apply excessive energy to the system which would result in the aforementioned CNT destruction. Finally the use of grinding or rubbing techniques was assessed. Hand grinding using mortar and pestle was used, and conclusions can also apply to techniques such as triple roll milling. Significant agglomeration reduction occurred, with minor length reduction of individual tubes observed. CNT defects were observed, but the data appears inconclusive to the cause.

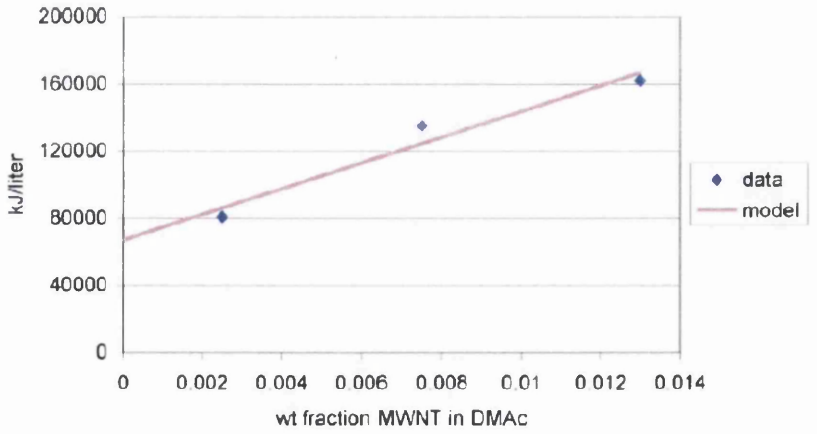

Figure 2.2.2: Sonication energy required for dispersal of MWCNTs in DMAc. Reported energy densities are high in comparison to scoping experiments and Garg *et al.*[8], suggesting that the y axis may be actually in units of J/litre. Image reproduced from 'Dispersion of Carbon Nanotubes in Liquids'[9].

In the same article the use of functionalisation to change the interaction between the CNT and surroundings was discussed, aiming for increased solubility. By using acid treatment the CNT powder is purified, removing catalyst particles and unwanted carbon residue. Oxidation occurs to the CNTs and shortening of the tubes is apparent, probably caused by the tubes being cut at defect sites. The strength of SWCNTs is usually degraded by approximately 15% using this oxidation method. They conclude that acid treatment is as destructive as ball milling to the CNT structure.

A number of surfactants were also utilized to non-covalently functionalise the CNTs. Suitable surfactants found were SDS and Triton X-100. Polyvinyl alcohol (PVA) was also tested, but was not seen as an efficient stabiliser. Issues removing the surfactant post processing were noted, reducing the effectiveness of the CNTs in most applications.

Sonication is the dominant tool for mixing of CNT dispersions due to the speed and repeatability of probe equipment, despite the increase in CNT defects it causes. Park *et al.*[62] used sonication to disperse CNTs in water, with similar results to previous work[9] with respect to size reduction in relation to sonication power. The addition of surfactant to the system was shown to increase the size reduction effect of the sonication. The percolation threshold was measured in the resulting composites at around 0.75wt% of CNTs.

When a solution of CNTs is obtained, they are often not stable with respect to time. Flocculation, or reagglomeration, has been observed to occur in short times-

cales, therefore optimisation of the dispersion to improve stability is often required. Measurement of this reagglomeration and settling was performed by Lee *et al.*[63] who studied the stability of pristine and functionalised (oxidised using acid treatment) MWCNTs in various solvents. The stability was assessed by measurement of the backscattering of monochromatic light, among other methods. Solutions were obtained by probe sonication for 15min at a concentration of 0.01wt% CNTs. Significant aggregation was observed in timescales of approximately 2 hours. Functionalisation was observed to increase the stability of the dispersions, with certain dispersions showing perfect stability over 24 hours, and visually stable over timescales of months.

The Coleman group, mentioned in section 2.1.3, has also studied CNT dispersal. Bergin *et al.* have published a number of articles studying suitable CNT solvents and their properties. One article[64] identified two solvents, structurally similar to NMP, cyclohexylpyrrolidone (CHP, $C_{10}H_{17}NO$) and 1-benzyl-2-pyrrolidinone (NBenP, $C_{11}H_{13}NO$) showed high CNT dispersability up to 0.33wt%. Both are less toxic than NMP but higher in unit cost, a key consideration for commercial ink manufacture. A further article[65] started to look at the potential for pristine, spontaneous dissolution of SWNCTs without functionalisation. They studied the enthalpy of the mixing process to find suitable solvents and compared to experimental data. They showed that 0.001wt% SWCNTs dispersed without mixing in NMP, compared to 0.35% in superacids such as chlorosulfonic acid. They concluded that a solvent can be shown to be suitable for CNTs when the surface energy is similar to the surface energy of graphitic surfaces. This work was continued by comparing the maximum stable concentrations achievable in various solvents. A summary of some of the solvents is shown in Table 2.2.2. The limited use of many solvent parameters to predict CNT solubility was discussed and suggested that further understanding of the interactions at the CNT-solvent interface is required.

Solvent	C_{max}(mg/ml)
CHP	3.5
DMPU	0.65
NBP	0.279
NBenP	0.18
NMP	0.116

Table 2.2.2: Table showing maximum stable concentration (C_{max}) of SWCNTs in various solvents. Data reproduced from 'Multicomponent Solubility Parameters for Single-Walled Carbon Nanotube–Solvent Mixtures'[64].

Once a stable solution of CNTs is obtained, the effect of ambient conditions on long term stability must be considered, especially when looking at ink applications. Sun *et al.*[66] (also from the Coleman group) studied the degradation of NMP-CNT dispersions when exposed to varying storage temperatures and humidity. Due to the reported hygroscopic nature of NMP, water uptake can result if not stored correctly. The uptake of water was seen to significantly accelerate sedimentation at high concentrations, however the effect was negligible below 10% H_2O concentration. Solutions were found to be stable with respect to temperature within the range of $\pm 40^{o}C$. Outside this range sedimentation was accelerated.

The effect of CNT functionalisation has also been examined within the Coleman group. Amiran *et al.*[67] obtained commercial functionalised SWCNTs (functionalised with PABS, PEG and ODA) and dispersed them in various solvents. They found that optimal solvents had solubility parameters close to that of the functional groups, indicating that functionalities are the dominant factor rather than pristine CNT solubility. Concentration dependent aggregation was minimised by the functionalisation, with stable dispersions of 4.4mg/ml observed. All samples were sonicated using a mixture of probe and bath sonication, with 5 minute exposure to a probe (750W. 40% amplitude, 60kHz, sample cooled in ice bath), followed by bath sonication for 1 hour and then finally tip sonicated for a further 5 minutes (same settings). Remaining aggregations were then removed by centrifuge.

It must be noted that much of the research towards CNT solubility also applies to alternative fullerenes. In a recent review, Coleman[68] demonstrated that many of the lessons learnt from the CNT research can be used in the field of graphene dispersions.

2.2.2 Rheological Properties

The concept, theory and measurement of rheology is discussed in detail in section 3.3.1. Much research has been done on the rheological properties of CNT dispersions, especially in the polymer composites field where careful control of the rheology is key to efficient production. There are many overlaps with composite production and ink formulation, especially in the rheology of polymer/CNT mixtures. Also, Green[69] calls rheology a 'promising' candidate for characterisation of CNT dispersions.

Pötschke *et al.*[70] studied the effect of CNT content upon the rheological behaviour of MWCNT polycarbonate compression moulded composites at temperatures of 170 to $280^{o}C$. They saw that a significant change in the rheological behaviour occurred at a CNT content of 5 to 0.5wt% depending on temperature. The rate of increase in viscosity increased significantly above these critical values of CNT concentration.

The electrical percolation threshold was observed to be 1wt% in this system. This strong temperature dependence is attributed to interaction between the CNT and polymer networks.

A similar study but with functionalised CNTs was performed by Sung *et al.*[71] who used CNTs oxidised by acid treatment in hydrogen peroxide. The correlation between a rheological and electrical percolation threshold was observed. The oxidation of the CNTs resulted in a reduction in the percolation threshold and a reduction in the viscosity of the system.

The quality of the dispersion has also been seen to have a significant effect upon the rheological properties of the composite, indicating that the rheological properties of a CNT solution may be a viable indicator for the dispersion quality. Song *et al.*[10] studied the effect of CNT dispersion quality upon the rheological behaviour of an epoxy nanocomposite resin. They used two mixing methods, one was a combination of pre-sonication in a solvent before further sonication and shear mixing into the epoxy resin, which was observed to provide higher quality dispersions that the alternative method which was sonication directly into the resin. It was seen that increasing CNT loading increased the complex viscosity magnitude (or dynamic viscosity), with the rate of change of the viscosity increase smaller for well dispersed CNTs, as shown in Figure 2.2.3. Poorly dispersed CNTs also showed a higher degree of non-Newtonian behaviour. The tensile strength of the hardened composites were seen to increase with higher CNT loading if the CNTs were well dispersed. However, if the CNTs were poorly dispersed, a decrease in the tensile strength was observed highlighting the importance of dispersion quality upon application performance.

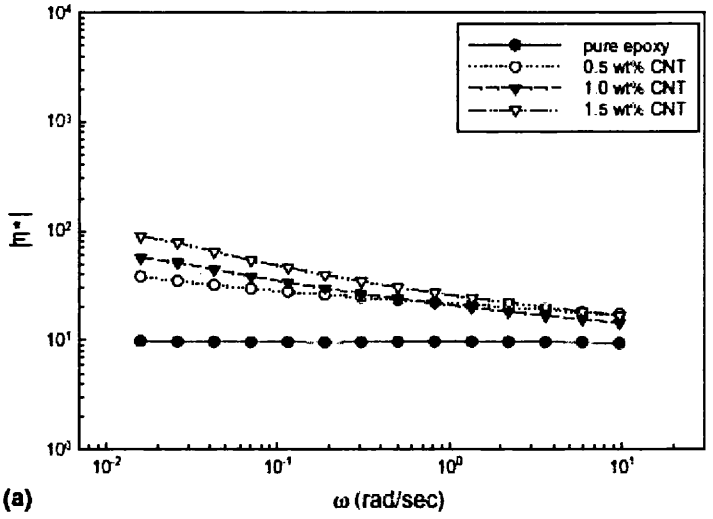

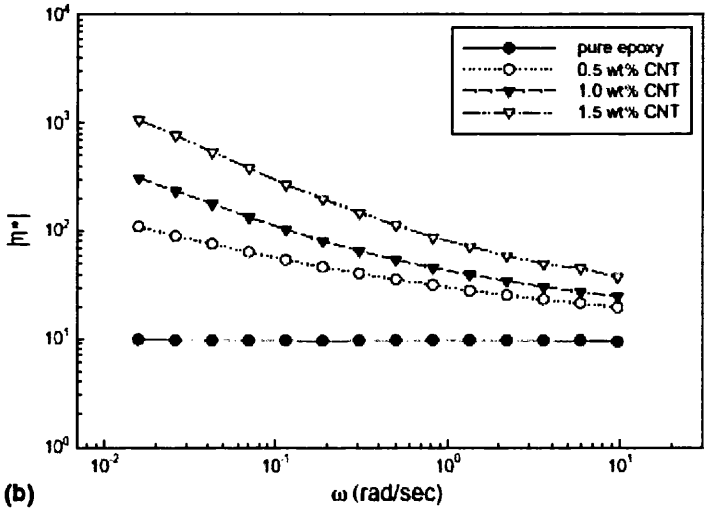

Figure 2.2.3: Magnitudes of complex viscosity of epoxy composites with varying CNT loadings. (a) shows well dispersed CNTs, (b) is poorly dispersed. Image reproduced from 'Influence of dispersion states of carbon nanotubes on physical properties of epoxy nanocomposites'[10].

This increase in viscosity for poorly dispersed CNTs can be explained by an increase in the volume fraction of CNTs within the solution. Work on the effect of particle size distribution upon the viscosity of suspensions was performed by Barthelmes *et al.*[72] who showed that an increase in volume fraction of solids within a solution increases the viscosity of the solution. Though the work was not specifically concerning CNTs the same principles can be applied. When aggregated into bundles void spaces are created, thus increasing the volume fraction in the dispersion

compared to a deagglomerated dispersion, for the same weight fraction. As a result deaggomeration will reduce the volume fraction, and therefore reduce the viscosity.

This use of viscosity to characterise the dispersion quality has been investigated by a number of groups. Cotiuga *et al.*[11] studied the viscosity change during mixing of a stabilised aqueous solution of SWCNTs. A CNT dispersion was compared theoretically to a rigid rod polymer system (a technique also proposed by Green *et al.*[73]), with a model derived as such. The model predicted a viscosity that is strongly dependent upon rod length and diameter, and therefore it was suggested that viscosity could be used to predict dispersion state. During sonication it was experimentally observed that the solution viscosity increases with time to a maximum, after which it decreases in an exponential fashion, as shown in Figure 2.2.4. This behaviour can be explained as the exfoliation of individual tubes from bundles increasing the viscosity until the sonication starts to damage the CNTs by cutting them at the defect sites (as discussed in section 2.2.1), resulting in a viscosity decrease. The behaviour is similar for both bath and probe sonication techniques, with the lower applied energy of the bath resulting in a lower viscosity peak due to fewer exfoliated CNTs. The use of this technique for CNT solution characterisation was also supported by Grady[74].

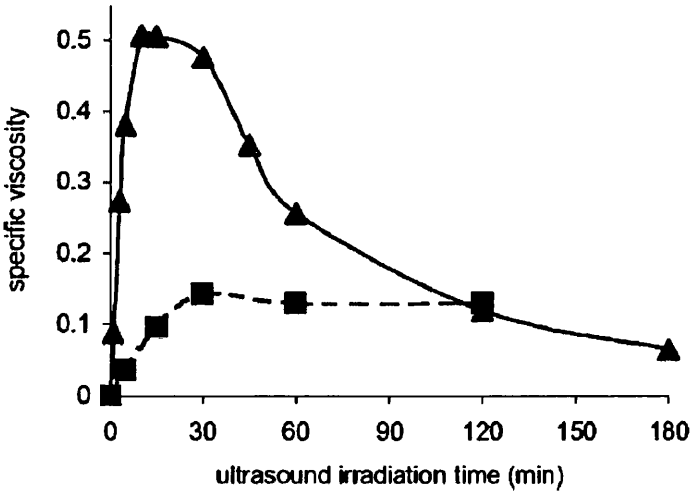

Figure 2.2.4: Effect of sonication time upon specific viscosity for a stabilised SWCNT aqueous solution. Ultrasonic bath mixing is represented by squares, ultrasonic probe by triangles. Graph reproduced from 'Block-Copolymer-Assisted Solubilization of Carbon Nanotubes and Exfoliation Monitoring Through Viscosity'[11].

Garg *et al.*[8] performed a similar experiment with MWCNTs and saw analogous results. Optimal sonication parameters for 1wt% MWCNTs in an aqueous Gum

Arabic solution was sonicated for 40 minutes using a 130W, 20 kHz ultrasonicator resulting in a specific energy applied of 113J/g. Sonication was performed in 5 minute periods punctuated by 5 minute periods of magnetic stirring to improve dispersion homogeneity.

Huang *et al.*[12] studied the rheological properties of MWCNTs dispersed in a viscous polymer solution. Shear mixing was used, with energies applied below the amount predicted to damage individual CNT structures. A critical time was seen for which the dispersion had to be mixed before the rheology became consistent and reproducible. Below this time CNT solutions were observed to be inhomogeneous and often showed erratic rheological behaviour. CNT concentration was also seen to be a factor in the rheological properties, with a 'mechanical percolation' threshold observed below which solution stability is high and viscosity dependence upon the CNT concentration is linear. Above this threshold it appears an elastic network forms and the dependence of viscosity upon CNT concentration becomes non-linear, as shown in Figure 2.2.5.

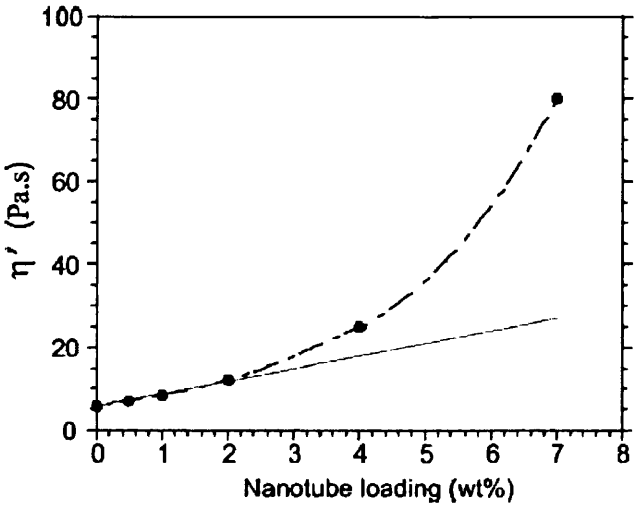

Figure 2.2.5: Real component of complex viscosity of dispersed CNT suspensions at varying concentration. Note the linear dependence at low concentrations (illustrated by the solid line) and the non linear dependence at higher concentrations (dashed line). Graph reproduced from 'Dispersion rheology of carbon nanotubes in a polymer matrix'[12].

Pegal *et al.*[75] saw that the dispersion behaviour of MWCNTs was highly variable, with similar CNT types from different suppliers showing significant changes in percolation threshold. Even samples from the same supplier showed variations. The

agglomeration strength of the CNTs is cited as the most important property with respect to dispersion behaviour. They also showed that sonication type showed no effect upon sedimentation behaviour, comparing two hours of low power sonication with five minutes of high power. Secondary agglomeration was observed after mixing, with prolonged mixing having no effect upon the rate of reagglomeration.

2.3 CNT Printing for Conductive Films

Once a suitable CNT dispersion is obtained it must be deposited in a suitable manner onto a substrate for printed electronics applications. A number of methods to achieve this have been studied, the choice of which is often dependent on the application. All printing methods discussed are outlined in section 1.1.1.

2.3.1 Coating - Dip, Spin, Spray

For proof of concept device fabrication of transparent conductive coatings over large areas dip, spin or spray coating is commonly used due to the low equipment cost required. Dip and spray coating are scalable to roll-to-roll technologies, however spin coating is not.

Schindler *et al.*[76] used spray coating to deposit a surfactant stabilised SWCNT aqueous coating onto heated substrates (glass and varieties of plastic). Solutions were produced by probe (24kHz) sonication, followed by bath sonication (39kHz) and high speed (40000g) centrifugation for one hour. After spray coating the CNTs were immobilised by spin coating a polyimide layer above. Sheet resistivities of $400\Omega/\square$ were observed at 80% transmittance. It was shown that the polyimide layer increases sheet resistivity by approximately 10%. The lower the surface roughness of the substrate the lower the sheet resistance due to improved percolation through the CNT network. They also note poor homogeneity of the resistance of the films over large areas.

Song *et al.*[77] used a combination of dip and spray coating methods to deposit thin films of SWCNTs onto flexible substrates. SWCNTs were dispersed in DCE at 0.1mg/ml by bath sonication and centrifugation. Substrates were dipped (in an argon atmosphere to avoid moisture absorption) for 2 seconds between 100 and 400 times. After 100 cycles sheet resistivities of $1300\Omega/\square$ were observed at 88% transmittance. After one layer of spray coating in addition to the 100 dip cycles sheet resistivity was reduced to $340\Omega/\square$ at 80% light transmittance. It was concluded that the spray coating improved the film homogeneity as it was observed through sheet

resistivity measurements that dip coating appears to introduce CNT alignment in the dip direction.

Kim *et al.*[78] used spray or spin coating for producing SWCNT films for use in organic solar cells. SWCNTs were dispersed in DCA by mild sonication and centrifugation at an initial concentration of 0.001wt%. Aqueous solutions were also produced by the same method using SDS or SDBS as the surfactant (surfactant to CNT ratio was approximately 10:1). Spray coated films were seen to be rougher than spin coated, though spin coating required several hundred repetitions to build up a film over 20nm thick. All films were deposited on coated glass and were treated by thermal and acid treatments to remove impurities such as surfactants and to oxidise the CNTs. Average reported sheet resistivities for the spray coated samples was $62.5\Omega/\square$ at 62.5% transmittance and $128\Omega/\square$ at 90% transmittance for the spin coated samples. Organic photovoltaic cells with efficiencies similar to that of ITO were reported using the DCE and SDS stabilised solutions.

Rahy *et al.*[79] studied the coating of SWCNTs onto flexible substrates. SWCNTs were dispersed in methanol using probe and bath sonication, then diluted further with methanol and constantly agitated using bath sonication during a dip coating process. PET (UV treated) and PEN substrates were dipped for varying timescales to control the layer thickness and dried under ambient conditions. Optimal results were seen using purified SWCNTs with sheet resistivities as low as $110\Omega/\square$ at 88% transmittance observed. CNT films were seen to retain their electrical properties under bending angles of over 90^o compared to a maximum of 30^o for ITO films. The PEN substrate was seen to be superior to PET which is attributed to the fact that it is more hydrophobic and has lower surface roughness.

The aforementioned Coleman group has also studied the deposition of CNT solutions on flexible substrates[80], targeting a transmittance of at least 90% for potential ITO replacement applications. Samples were dispersed in an SDS solution using a combination of probe (750W, 20%, 60kHz) and bath sonication before centrifugation and dilution to 0.1 to 0.2 mg/ml. Samples were then spray coated onto a heated PET substrate before rinsing to partially remove surfactant. Some samples were acid treated to remove surfactant and dope the CNTs, this was seen to result in a 70% drop in resistivity. For films with a transmission of 90% sheet resistivities of below $400\Omega/\square$ were observed.

2.3.2 Flexography

To the best knowledge of the author, no literature has been published concerning the printing of CNT based solutions using flexography.

2.3.3 Gravure

The Noh group, based in Sunchon National University, have been working towards the goal of direct printing of CNT based solutions using gravure [81;82]. Initial work discussed the printing of CNT based TFT devices using gravure for all layers except the CNT active layer, which was printed using inkjet techniques. Further discussion of this device structure and performance is in section 7.2.2.2. This work has been advanced by combining roll-to-roll (continuous) and roll-to-plate (batch) gravure techniques. Roll to plate techniques involve the image to be printed being engraved on a flat plate, with the substrate being wound around a cylinder which is brought into contact with the plate. CNT inks were printed using the roll-to-plate process, but without explanation as to why. This may be due to the low viscosity reported for their CNT solution resulting in the inability to use roll-to-roll ink chambers.

The use of gravure to print CNT based inks is also covered in US patents [83;84].

2.3.4 Screen

The deposition of CNTs by screen printing can provide a thicker deposit than other techniques. This lends itself to particular applications, including field emission devices and for printed sensors.

Li *et al.* [85] formulated a CNT screen printing paste by shear mixing CVD grown MWCNTs at concentrations of 10, 5 and 3wt% with ethylcellulose and terpineol. This formed what the authors described as a 'slurry', which was printed using a $350\mu m$ mesh, indicating that large agglomerations were present. The prints were then sintered at temperatures up to $400°C$ to remove organic residue. Field emission devices were produced and it was observed that there is an optimal CNT concentration for the application, which in this case was approximately 5wt%.

Lee *et al.* [86] discussed the issue of field emission luminosity being limited by CNT bundles and lack of protruding CNTs. A similar ink formulation was used as Li *et al.* [85] replacing the shear mixing with a triple roll mill, which was found to reduce agglomerations and improve homogeneity. The CNT layer surface was found to be controllable by use of controlled atmosphere high temperature sintering. By using a combination of nitrogen and air atmospheres during sintering steps at up to $430°C$ an

increase in CNTs protruding from the layer surface were observed under SEM. This resulted in reduced turn on voltage and improved emission uniformity.

Choi *et al.*[87] also produced CNT based field emitters via a pseudo screen printing technique. Inks consisted of SWCNTs dispersed in isopropanol and a nitrocellulose binder which was removed after printing by heat treatment.

The use of carbon electrodes is well established for screen printed biosensors. Wang *et al.*[88] discuss the potential increase in electrode performance with respect to sensitivity and stability by use of CNTs. An ink was formulated using MWCNTS (hand ground to reduce agglomeration size), isophorone, PVC, DBE-4, and DBE-5 mixed via an unspecified technique until observed to be homogeneous. Screen printing was performed manually, and samples were dried for one hour at $150°C$. In comparison to similarly prepared carbon electrochemical sensors the CNT electrodes showed an improvement in sensitivity to various analytes with an increased signal-to-noise ratio. The resistance of the CNT lines was 2400Ω compared to 220Ω for a commercial carbon ink.

The use of screen printing to print CNT based inks is also covered in US patents[83;84].

2.3.5 Inkjet

Inkjet has been the most popular method for patterned deposition of CNTs due to the low cost and availability of the printing equipment. The first inkjet printed CNTs were reported by Fan *et al.*[89] MWCNTs were acid treated and dispersed in water via sonication and centrifugation. Although acid treated CNTs should disperse in water to a degree, a dispersant named S27000 was used, presumably to also lower the surface tension of the solution for inkjet printing (a requirement discussed in section 1.1.1.4),. Prints were made on paper, and an exponential behaviour was observed for the surface resistance with number of overprints. The nozzle diameter reportedly used was $1\mu m$, meaning that the CNTs must have been of short length and agglomerated in bundles of no more than approximately 100nm for successful printing, indicating the acid treatment had a severe shortening effect. The same group have advanced this work by printing onto plastic film and removing the CNT layer from the substrate[90]. A MWCNT solution was prepared using the same method as described above and printed using the same printer. The CNT film could be exfoliated from the substrate by electrochemical means, and was stable. A similar proportionality of sheet resistivity to number of printed layers was observed to the previously mentioned work,

indicating that it is a property of the CNT film and that substrate interactions were not a major factor in this case. The lowest sheet resistance reported was 12M$\Omega/\square$.

Sheet resistivities as low as 1k$\Omega/\square$ at 70% transmission were reported by use of carboxyl functionalised SWCNTs in thin PEDOT:PSS films deposited by inkjet [52]. The PEDOT:PSS and SWCNT were dispersed in water and ethanol at an approximate ratio of 24:1 PEDOT:PSS to CNT. It was noted that above a critical film thickness the PEDOT:PSS forms a percolating network around the CNTs resulting in the CNTs becoming insignificant with respect to conductivity.

Denneulin *et al.* [91] performed similar experiments investigating the use of SWCNTs in PEDOT:PSS solutions. Functionalisation of the CNTs was seen to have a significant effect, with commercial carboxylic acid (COOH) and polyethylene glycol (PEG) functionalised SWCNTs compared to MWCNTs. Functionalised CNTs showed improved film homogeneity and improved sheet resistivity, with addition of MWCNTs reducing the sheet resistivity. Lowest sheet resistivity reported was 225$\Omega/\square$ with an equal ratio of SWCNT-PEG to PEDOT:PSS. Transmission was not reported. Functionalisation was shown to be preferable to the use of surfactants with respect to dispersion quality and film properties.

One issue with printing low solid content inks on plastic films is spreading and inhomogeneous films after drying. A method to avoid these issues was proposed by Kumar *et al.* [92] who printed onto a porous stamp then transferred the prints onto a plastic film. Sheet resistivities of 500$\Omega/\square$ were observed after 40 prints, transmission was not reported.

Inkjet has also been used to deposit catalyst particles for selective CNT growth using CVD techniques [93], although unsuitable for flexible electronics it could provide an alternative to some lithography steps in certain applications.

The use of inkjet to print CNT based inks is also covered in US patents [83;84].

Inkjet is commonly used for printing of CNT based TFT structures. Further discussion of developments in this field is given in section 7.2.2.2.

2.4 Concluding Remarks

This chapter has discussed the key developments published in the field of CNT solution processing. The electronic, mechanical and physical properties show a potential for CNT use in printed electronics. The metallic and semiconducting behaviour of different tube chiralities provide a range of possible applications, from transparent conductive films to transistor devices. CNTs can also be modified to optimise their

properties for the proposed application. This has been seen to be key for solution processing and techniques are available to perform this functionalisation on an industrial scale.

The formation of random mesh networks of CNTs allows the exploitation of the unique properties in macro scale devices. The network structure coupled with the strength and flexibility of CNTs provides a durable thin film, ideal for printed electronics. The electrical properties of the random networks is dominated by the tube defects and the contact resistance at tube-tube junctions. Conduction through the network can be modelled by percolation theory under suitable conditions and it has been shown that CNTs show promise for transparent conductor applications. This could be enhanced by forming networks consisting of only metallic behaviour tubes, which is possible but on an industrial scale costs are prohibitive at this time.

Solution processing is a promising method for the production of these random networks, however the solubility of CNTs is poor with agglomeration into large bundles difficult to overcome. Careful choice of solvent and functionality has been shown to be the key to overcoming these issues whilst avoiding the use of surfactants which can negatively impact the properties of the printed films. To produce these solutions a number of mixing techniques are available, however sonication is the most popular. Care must be taken however as excess sonication can result in substantial structural damage to individual CNTs. This can be monitored indirectly by observing the rheological properties of the solution, as seen in composites research which has a number of overlaps with ink formulation.

Once a suitable ink is formulated traditional printing techniques can be used for deposition. Inkjet is the most popular choice for this application, as there are a number of issues when printing low solid content solutions using a high speed roll-to-roll method such as gravure. To the best of the author's knowledge flexography has not been reported as a method for CNT deposition.

A number of areas for further research are apparent from this literature review. Firstly, although a significant amount of work is reported that studies the optimal dispersion of CNTs in solvents and composites, little discussion has been made with regards ink formulation specifically. Work has been reported formulating inks for screen printing, but the formulation has not been the focus of the work. This is especially true for inks formulated for use in high speed, roll-to-roll techniques. Work has been reported using gravure for CNT deposition, however this used CNT dispersions in only a solvent and modification to the deposition technique was required. Investigation into formulation of a suitable ink will therefore be novel work.

Secondly a number of methods have been reported to facilitate CNT dispersal, from functionalisation to sonication optimisation. However the effect of these upon the resulting ink and film properties is less well understood. Improvement in the understanding of how modification of the CNT structure affects the properties of macro-scale CNT networks is crucial to future printed electronics applications.

Following this literature review a practical understanding of the dispersion of CNTs was required and to this end a number of scoping experiments were performed, the details of which are not included in this thesis. These experiments were primarily to provide the author with experience of handling CNTs, but also provided a background understanding of practical parameter settings and material selections for use in further study. Exploratory experiments were performed to test the effects of CNT concentration and type, with various characterisation methods and parameters used. These experiments, along with data taken from the literature and invaluable discussions with numerous experienced people provided the basis for most of the initial parameters used for the further comprehensive experiments described in this thesis.

Chapter 3

Experimental Techniques and Equipment

3.1 Introduction

This chapter introduces the concepts, equipment and experimental methods utilised in the formulation and deposition of CNT based inks and the characterisation of both the wet ink and the printed film. To achieve this a number of challenges must be overcome, and the experimental methods and equipment described in this chapter have been carefully trialled in a number of preliminary scoping experiments.

A number of challenges and opportunities were identified in the literature review, and were summarised in section 2.4. The initial challenge to overcome to achieve the aims outlined in section 1.3 is the formulation and dispersion of the ink, for which methods and approaches are discussed and detailed in this chapter. Firstly a suitable ink formulation must be investigated, then further investigations can focus on the optimisation of the system.

To achieve this a number of characterisation parameters have been defined based on the traditional approach for printed application development illustrated in figure 1.1.5. After numerous scoping experiments discussed in section 2.4, methods for measurement of the wet and dry properties of the ink have been selected and are discussed and outlined in this chapter. Ink samples were prepared using ultrasonic probe techniques, and characterised in the wet form with respect to viscosity and surface tension. The ink was then deposited using bar coating, a common method used for small sample rapid deposition (as well as a scalable technique). The dried film was then characterised in terms of sheet resistivity, transparency and adhesion, in line with the previously mentioned development flow.

3.2 Ink Formulation Methods

3.2.1 Mixing, Dispersion and Formulation

3.2.1.1 Background

The basic components of an ink were described in section 1.1.2, however the integration of these solid and liquid components into an ink requires suitable mixing methods to be utilised. The act of mixing an ink is the formation of a fine particle dispersion from initially separate constituents, as introduced in section 1.1.2.3. This requires the random distribution and deagglomeration of the functional materials in a liquid vehicle. Classically, for graphics inks, the quality of a dispersion was often assessed visually from the final print. The homogeneity of the final dispersion is also critical to the electrical performance of functional inks, and if the dispersions appears to be optically inhomogeneous after deposition then it is usually the case that the electrical properties will be similarly inhomogeneous. The act of mixing does not imply the formation of a homogeneous dispersion, merely that the constituents are blended. It can be said that a dispersion is created when the functional material is fully wetted, with contaminants such as adsorbed air removed. This implies that a force must be applied to the material to deagglomerate and isolate individual particles so these become well dispersed throughout the liquid medium. A summary of common mixing techniques is provided in section 1.1.2.3.

3.2.1.2 Equipment

Due to the average viscosity profiles of the inks observed during preliminary scoping experiments, the need to deagglomerate the CNT bundles and the prevalence of the technique in literature (section 2.2.1) ultrasonic techniques were used for all sample preparation. A Bandelin Sonopuls 3100 ultrasonic homogeniser (as shown in Figure 3.2.1) was used due to the reproducibility of the probe configuration as this model probe can provide constant amplitude vibrations to the probe tip. The probe used a 3mm tip, which gave a maximum vibration amplitude of $235\,\mu m$ at 20kHz.

Figure 3.2.1: Bandelin Sonopuls 3100 ultrasonic homogeniser probe setup in the configuration described in section 3.2.1.3.

3.2.1.3 Method

All ink samples used N-Methyl-2-pyrrolidone (NMP) as the solvent due to the reported compatibility with CNTs (see section 2.2.1) and the high boiling point simplifying sample preparation due to minimal evaporation during mixing. To further simplify sample preparation a resin base was created by dissolving a fixed percentage of resin in NMP. This was mixed using a magnetic stirrer at a fixed RPM for a minimum of 24 hours.

For final ink preparation, firstly CNTs were measured to the required mass using a Sartorius Analytic calibrated 4 point mass balance. The balance is accurate to $\pm 0.1mg$, which is essential for accurate repeatability. The prepared resin base was then added so that the ratio between the mass of CNTs and resin was as specified. Further NMP was then added to dilute the CNT concentration to specification. The sample was then placed in a water bath and exposed to ultrasonic vibration. The probe was inserted to a depth of 10mm into the sample, which had a total depth of 20mm when stored in standard 30ml glass vials. The probe was run at 75% amplitude ($176.25\mu m$), with a pulse duration of 0.5 seconds applied in 1 second intervals. This setting was used to minimise excess cavitation around the probe tip. Applied energy was recorded as reported by the equipment. Samples were removed from the water bath and characterised immediately after mixing to minimise effects of reagglomeration and particle sedimentation. No surfactants or other additives were used within the inks described in this thesis which may otherwise reduce the agglomeration

effects because of the desire to avoid the reported detrimental effects on the printed film performance.

3.3 Ink Fluid Characterisation Methods

3.3.1 Rheology

3.3.1.1 Background

The rheological characteristics of an ink describe the flow and deformation of the fluid. The rheological properties of inks must be tuned to the particular printing process by which the ink is to be deposited. The behaviour of the ink under various stresses will affect the transfer of the ink from reservoir, through the distribution system and eventually onto the substrate, all areas where high shear is applied to the ink. The effect of this shear will usually alter the rheology of the ink throughout the printing process, which must also be considered when formulating the ink. The resistance of a fluid to flow (in a closed system) is defined as its viscosity (η, Pa.s), the measurement of which is called viscometry. Shear viscosity is further defined as the ratio of the shear stress applied to a system and the velocity gradient across the fluid. Viscometry is an established field, the concepts of which are described in numerous available literature[94–96], the relevant basics of which are outlined below.

Viscosity derives from the shear stresses between conceptual layers within a liquid that are parallel to an applied stress. The friction between these layers resists the shearing force. There is also an elastic component to the reactionary forces of the fluid to an applied shear. The combination of the viscous and elastic components can be described as the viscoelastic properties of a material. This is usually studied analytically and experimentally by the application of a rotational two plate model. In this system a fluid is placed in between two plates, as shown in Figure 3.3.1. A shear force is then applied by the upper plate surface. Assuming laminar flow within the sample and no slippage at the fluid-plate interface the resulting plate velocity can then be measured. The resulting shear rate and shear stress measurements can then be used to describe the viscosity profile of the fluid.

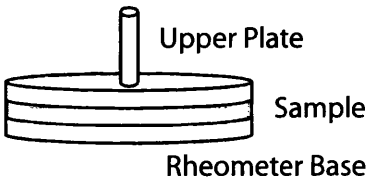

Figure 3.3.1: Diagram showing plate setup of typical shear rheometry equipment.

Fluids can be described as Newtonian or non-Newtonian. This describes the viscosity profile of the fluid with respect to the shear rate. If the shear stress versus the shear rate curve is linear and passes through the origin then the fluid can be described as Newtonian. An example of a Newtonian fluid is water. Any other behaviour is described as non-Newtonian, and this includes most polymer solutions, solid suspensions and high viscosity fluids. Non-Newtonian fluids can exhibit a number of dependencies of their viscosity when under an applied shear. Some will decrease in viscosity when a stress is applied, known as shear thinning. If the viscosity increases the behaviour is described as shear thickening. Most inks and coatings will display shear thinning behaviour. A steady shear rate constantly applied can also lead to changes in the viscosity of the sample. This is known as thixotropic behaviour if the viscosity decreases with the duration of the applied stress and rheopectic behaviour if the viscosity increases.

With respect to printing the key characteristics to quantify are the behaviour under shear and extension. During all printing processes the ink is subjected to high shear forces, with approximate shear rates during the multiple stages of a traditional coating operation ranging between 10^{-2} to $10^{5}s^{-1}$[96]. Viscometry tests must therefore cover the majority of this range of shear rates. Extensional rheology is also of interest as most printing processes have an extensional component acting upon the ink, for example after the printing nip contact in flexography or gravure. This is performed using an extensional rheometer, based on a similar schematic to the plate setup shown in Figure 3.3.1 but with an extensional force applied by moving the plates apart.

With respect to CNT based inks typical suspension rheology is expected. Literature relevant to the rheology of CNT suspensions was discussed in section 2.2.2. The viscosity of any solid particulate dispersion is controlled by the medium into which it is dispersed, which is known as the continuous phase. The viscosity behaviour of the suspension is directly proportional to the continuous phase. In almost all cases the addition of solid particles to a liquid medium will result in a net increase in viscosity.

This is caused by the particles disrupting the flow of continuous phase when under shear. This also results in a shear thinning effect being introduced, even if the continuous phase shows Newtonian behaviour. The shear thinning behaviour is caused by particle orientation parallel to the flow of the fluid as shear forces increase. The exact effect of the solid addition is defined by the volume concentration, agglomeration behaviour, size and shape of the particulate. Higher concentrations result in higher viscosities due to the increased flow disruption. Aggregating particles increase the shear thinning behaviour, with the shear forces resulting in a decrease in agglomerate size and therefore decreasing flow disruption. Reagglomerating particles will increase the viscosity, causing a time dependent (or thixotropic) effect. Also the degree of particle attraction (hence tendency to agglomerate) affects low shear viscosities. If particles are attractive then this will cause a higher increase in low shear viscosity than neutral particles due to flocculation, though repulsive forces between particles causes the highest low shear viscosity due to the inability of particles to align with shear flows. Particle shape defines the degree of flow disruption local to the particulate. Spherical particles show the least resistance to flow and therefore the lowest increase in viscosity. Rod like particles, such as CNTs, cause the largest diversion of streamlines within the flow, resulting in the largest increase in viscosity. The aspect ratio of the rod like particles affects the solution viscosity, with higher aspect ratios causing a higher viscosity increases at a given volume concentration.

3.3.1.2 Equipment

The device used to perform rheological characterisation is a Bohlin Gemini HR Nano rheometer, as shown in Figure 3.3.2. The instrument can apply a torque range of between 10nNm and 200mNm during controlled stress viscometry, at a torque resolution of $<$1nNm[97]. This allows the measurement of a wide range of sample rheologies utilising the same measurement setup, minimising experimental errors.

Figure 3.3.2: Photograph showing Bohlin Gemini HR Nano rheometer.

The rheometer was used in the cone and plate viscometry configuration. This configuration is similar in principle to that described above and shown in Figure 3.3.1. The fluid to be measured is placed on the lower plate (a flat, circular surface), and the upper plate (in this case a shallow cone) is then brought into contact with the upper surface of the fluid. The upper surface is conical in shape, with a shallow cone angle to equalise the shear forces being applied through the ink volume. This cone is then rotated to give varying rates of shear and the resulting shear stress is measured. This equipment cannot measure extensional flow.

3.3.1.3 Method

To measure the viscosity profile of the inks 1.5ml of the sample was pipetted onto the lower plate of the rheometer. This amount was calculated to be the volume of the required void between the plates of the rheometer. The plate was held at a constant 25^oC, which was approximately the same temperature as the environment where the samples were coated onto the substrate (see section 3.4) and the temperature in the

measurement area of the Fibro DAT 1100 (see section 3.3.2). The upper cone (5.5cm and 2^o angle, selected to maximise torque response) was then lowered onto the sample, and the equipment checked to ensure the sample filled the void between the plates without overlap onto the outer edges of the plates. The upper cone then was rotated such that a shear rate sweep between 0.01 and $1000 s^{-1}$ was applied. These values were selected to cover the reported range of shear rates expected in the printing process[96] and as preliminary trials showed that variation in sample viscosity could occur throughout this range. Although sample viscosity depends on the formulation, a single test was selected for all samples for comparative purposes. The rheometer recorded applied shear rate and shear strain.

Equipment and setup accuracy was tested using a viscosity standard silicone fluid supplied by Brookfield Engineering. The fluid was rated to $9.5 mPas \pm 1\%$, and average viscosity measured over three tests, with the equipment cleaned and reset after each test. The average viscosity within the shear rate range of 1 to $1000 s^{-1}$ was $9.5 mPas \pm$ 12%, however at low shear rates the viscosity was too low for accurate measurement. The same testing was repeated for a standard fluid rated to $49.4 mPas \pm 1\%$, with a average viscosity within the shear rate range of 0.1 to $1000 s^{-1}$ of $51.7 mPas \pm$ 4.5%. Errors could be reduced with optimised settings for the test fluids, however preliminary tests using CNT based inks implied that viscosities will be higher over the entire shear range than the standard fluids tested, hence the testing range used.

3.3.2 Surface Tension

3.3.2.1 Background

Surface tension (γ, mN/m) is a description of the cohesive forces acting between molecules at the surface of a liquid[98]. The attractive force between liquid molecules within a liquid is usually omnidirectional in nature, with a net force of zero. However, in the absence of any external force at the boundary of a liquid the net force will act inwards. It is this force that gives liquid drops their shape, which naturally tends to a sphere in the absence of external forces.

Surface tension is an important property of an ink. The printing process results in a liquid coming into contact with a solid. The interaction between the surface energy of the solid and the surface tension of the fluid determines the behaviour of the ink at this interface. This is known as wetting, and an ink is said to wet a substrate if the intermolecular forces at the liquid/solid interface are strong enough to overcome the surface tension and cause the liquid to spread. An ink is said to

dewet if the surface tension of the ink will overcome the interfacial forces and the ink will only partially spread, or in extreme cases not spread at all. This is illustrated in Figure 3.3.3. Surface tension is also critical before the deposition phase of the printing process. For example in flexography inks need to wet onto the polymer printing plate and in inkjet the surface tension must be tightly controlled to ensure accurate drop formation.

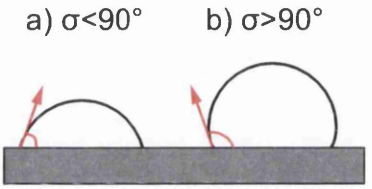

Figure 3.3.3: Illustration of substrate wetting. a) shows an example of good wetting, with contact angle (σ) below 90°. b) is an example of poor or partial wetting, with a contact angle higher than 90°.

The surface tension of an ink can be altered in a number of ways. The first is to dilute or replace existing solvents with a lower surface tension fluid that is compatible with the current ink formulation. For example the dilution of a water solution with 5% propan-2-ol will reduce the surface tension by approximately 45% [16]. This must be applied carefully so as not to affect the final printed film as solvent addition will alter the drying process. Another method for controlling the surface tension of the ink is the addition of additives such as surfactants. Surfactants, or surface active agents, act as dispersants, wetting agents or defoaming agents. Surfactants generally consist of a molecule that is constructed of a hydrophilic and a hydrophobic component. When acting as wetting agents these will tend to concentrate at an interfacial layer between the fluid and surroundings, lowering the interfacial tension. Common non-covalent functionalisation methods for CNTs use surfactants. Surfactants tend to remain in the printed film after the drying process is complete, making their use undesirable in functional inks as they can adversely affect the functionality of the product by impeding intermolecular contact.

There are a number of methods commonly used to measure the surface tension of a liquid including the Du Noüy ring and pendant drop shape. The pendant drop shape method is one of the most commonly used due to its convenience and simplicity. In this method a drop of fluid is extruded from a tube until the weight of the droplet

is approximately equal to the reciprocal force exerted by the surface tension at the tube nip. This causes the droplet to form a pendant shape instead of a spherical one that would be more energetically favourable without the external influence of the tube tip. The parameters d_s and d_e (as shown in Figure 3.3.4) can then be measured. The ratio of the dimensions d_s/d_e is related to a shape dependent quantity H, with the relationship initially calculated empirically but which has since been calculated numerically using the Young–Laplace equation. These values can then be substituted into

$$\gamma = \frac{\triangle \rho g d_e^2}{H} \tag{3.3.1}$$

where $\triangle\ \rho$ is the difference in density between the two fluids at the interface and g is acceleration due to gravity. It must be noted that accuracy is reduced compared to the Du Noüy ring method which directly measures the force at the interfacial boundary, but this is balanced by the speed of measurement and simplicity of the methodology.

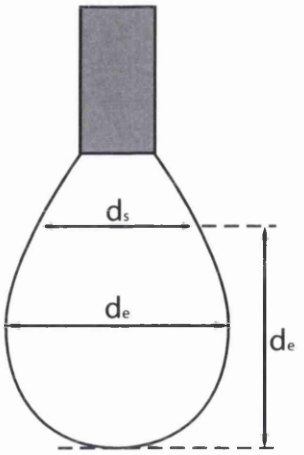

Figure 3.3.4: Illustration of pendent drop from a nip, showing relevant dimensions.

3.3.2.2 Equipment

The device used to perform surface tension characterisation is a Fibro DAT 1100 dynamic contact angle measurement system, as shown in Figure 3.3.5. This measures surface tension using the pendant drop shape method [99], with the external fluid being

air. The equipment consists of a grayscale camera, a suitable illuminated measurement space and an automatic pump device. The output from the camera is processed by proprietary software. The Fibro software contains lookup tables for calculation of the ratio $1/H$ from the drop dimensions and automatically calculates surface tension from the droplet image and provided fluid density. Once a drop is analysed it is discarded and another identical volume drop is pumped. A typical visual report of a surface tension measurement being taken is shown in Figure 3.3.6.

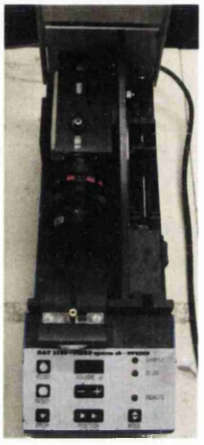

Figure 3.3.5: Photograph showing Fibro DAT 1100 equipment setup.

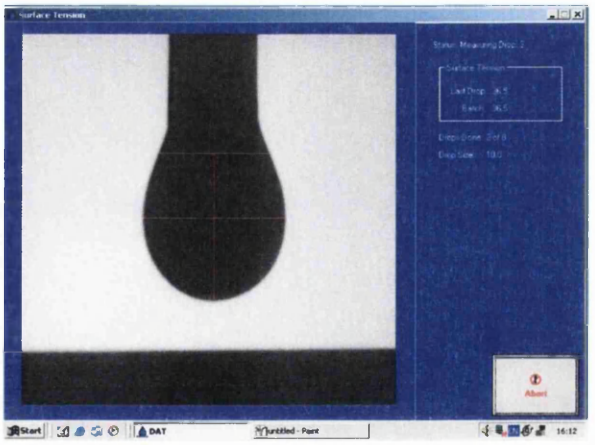

Figure 3.3.6: Typical surface tension measurement being taken using the Fibro DAT 1100 system.

3.3.2.3 Method

A sample volume of no less than 1ml was loaded into the system. Measurements were taken of $10\mu l$ droplets in sets of 8 drops. This was repeated 3 times so that a total of 24 measurements were recorded. Due to the higher viscosity of some samples the system was unable to reliably form the drops automatically. In these circumstances the drops were formed manually, which is reported in the results.

The accuracy of this test setup was assessed by repeated measurement of distilled water. The temperature within the sample volume was measured to be $22.5°C$ using a calibrated thermometer. At this temperature the surface tension of pure water is 72.4mN/m[100]. Measurements were repeated 20 times and an average value of 71.6 ± 0.3 was obtained.

3.4 Deposition

3.4.1 Meyer Bar Coating

3.4.1.1 Background

The inks were coated onto the substrate using the Meyer bar (or k bar) coating technique. This is a common roll-to-roll coating technique and requires the substrate to be brought into contact with a wire wound metering bar. The diameter of the winding wire specifies the void size between the wire to substrate contact points, as shown in Figure 3.4.1. Ink is applied in advance as the bar is moved across the substrate surface. The ink flow to the substrate is metered by the void size, and the ink relaxes to form a continuous film on the substrate. This method can be used to produce uniform films of a wide range of ink rheologies, with the key rheological property being the relaxation time. If this is too slow then the film will exhibit roughness of wavelength identical to the wire diameter. Particle size in the ink must be carefully controlled as clogging in the winding gaps will cause major print defects.

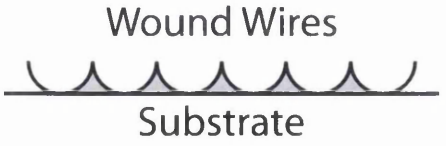

Figure 3.4.1: Schematic showing ink metering during bar coating. The grey shading signifies ink flow through the wire gaps.

3.4.1.2 Equipment

The bar coater used was a TMI K Control Coater, a photograph of which is shown in 3.4.2. Several metering bars were available, a selection of which are described in Table 3.4.1. Bar coating was selected due to the common use of the technique as a method of rapidly producing repeatable coated samples of controlled thickness. The technique is commonly used in industry for test sample production and has been reported in the literature as a suitable technique for solution deposition for functional device production[101]. Alternative available coating methods require significant setup and cleaning which would result in prohibitive time delays.

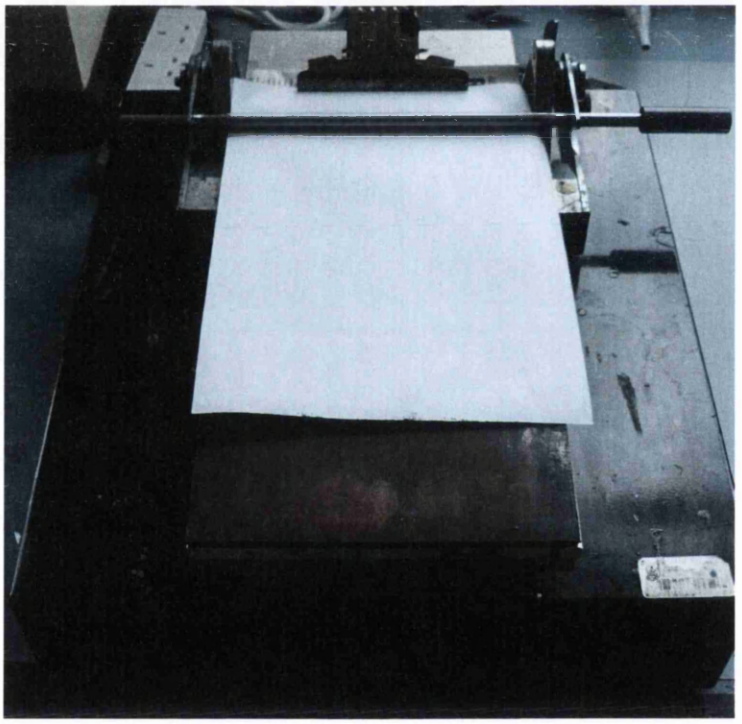

Figure 3.4.2: Photograph showing TMI K Control Coater setup.

Bar	Wire Diameter [mm]	Wet Film Thickness [μm]
US2	0.05	4.57
US4	0.1	9.14
US8	0.2	18.29
US16	0.41	36.58
US20	0.51	45.72

Table 3.4.1: Selection of available bar sizes, showing wire diameter of the winding and approximate wet film thickness after coating. Data courtesy of RD Specialities, inc..

3.4.1.3 Method

Samples were coated at an arbitrary bar speed of 3 and dried immediately after coating (see section 3.4.2). A US8 bar was used for all coatings, details of which are shown in Table 3.4.1. This diameter was verified using white light interferometry (WLI, for further details on this experimental technique see section 8.3.1). This measured the average wire diameter to be 0.201 ± 0.002mm. The US8 bar was selected as preliminary experiments showed that it gave a suitable thickness coating for all further experiments. Larger gauge bars caused problems with lower viscosity inks resulting in inhomogeneous films, and smaller gauge bars resulted in clogging issues if larger agglomerates are present. All inks were coated immediately after mixing onto DuPont Melinex ST504 $175\mu m$, a commercially available heat stabilised PET film coated with an adhesion promoter. This was selected due to the common usage of PET as a film for printed electronics, the adhesion promoter coating which gives a more suitable surface energy for ink wetting, the transparency of the film and the heat stabilisation improving sample production reliability.

3.4.2 Drying

3.4.2.1 Background

The wet films were dried using warm air impingement (convective) drying. The basic mechanisms of ink drying are described in section 1.1.4.

3.4.2.2 Equipment

Samples were dried using a generic desktop fan heater, chosen for experimental simplicity whilst providing suitable results. Impingement was required to dry the films within a suitable timescale.

3.4.2.3 Method

The heater outlet was placed 10.4cm from the sample. The average recorded temperature at the sample position was $64°C$ at an average air speed of 0.18m/s. Samples were exposed to the heater until visibly dry. Exposure times were dependent on the solvent content of the ink, average drying times were of the order of 30s. Sample inhomogeneity could be observed at macroscopic (mm to cm) scale if care was not taken during the drying process. Samples displaying excess inhomogeneity were discarded and repeated. When performing further characterisation areas of observable defects were avoided.

3.4.3 Example of Coated Sample

A scan of a representative sample is shown in Figure 3.4.3. An area of higher concentration is visible in an upwards direction in the centre of the sample, this is a result of inhomogeneity in the airflow during the drying process and is an area avoided in subsequent testing. Other areas avoided during subsequent testing were the edges of the substrate where higher concentrations can be observed and the upper area of the coating where witness marks caused by the initiation of the coating process are visible.

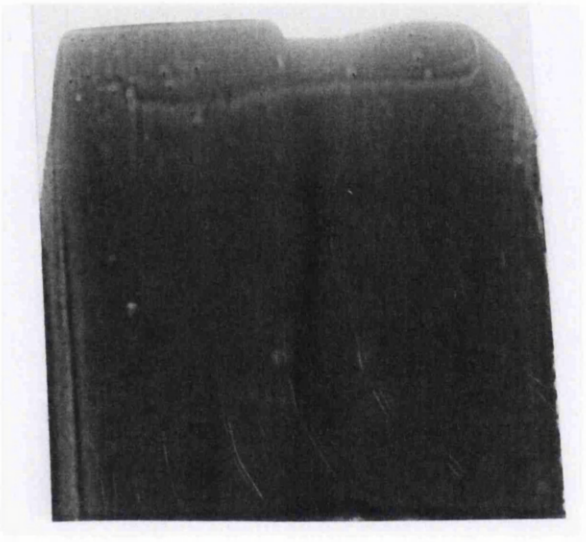

Figure 3.4.3: Optical scan of a representative coated sample. In this case CNT concentration was 2wt%.

3.5 Printed Film Testing

3.5.1 Adhesion

3.5.1.1 Background

The adhesion of a film describes the strength of the bonding between the dry ink film and the substrate. This can be measured and quantified in a number of ways, including pull-off tests (ISO 4624:2003) and cross-cut tests (ISO 2409:2007). Each of these involve the removal of adhered film using an adhesive tape. The pull-off test quantifies the adhesion of a layer by measuring the minimum tensile stress necessary to damage the film. The cross-cut tests does not give a quantifiable measure of adhesion, however it provides a qualitative description of the adhesion by classification of coating damage at the boundary of cross hatched pattern cuts in the film.

3.5.1.2 Equipment

Adhesion was tested using 'Scotch' brand adhesive tape for sample testing, an Epson V700 photo scanner for image capture and ImageJ software for image analysis. This method is a hybrid of the two ISO tests discussed above, designed for black, relatively inhomogeneous thin coatings.

3.5.1.3 Method

Scotch tape was applied to the samples in three areas, and applied with approximately equal pressure. The tape was then removed with care taken to maintain a consistent removal angle of 90° to the substrate. These tape samples were then mounted onto a consistent white substrate (Leneta Co. Form 150C standard test card) and digitised at 1200dpi. This image was processed using the ImageJ image analysis software, with the mean pixel grey value measured from representative areas of each test tape. The grey value is reported between 0 and 255 where 0 is black and 255 is white. This gives a representative value of the area coverage of CNTs removed from the film, which can be used in a comparative basis with other, identically performed, tests.

As this method gives an arbitrary scale of CNT removal no calibration was possible, however analysis was performed on bare tape samples to test the repeatability of the method. This gave an average value of the bare tape of 236.4 ± 3.12. This indicates a percentage error resulting from the materials used and measurement method of 1.3%. Any further deviation is due to the tape application and removal process or the sample quality.

3.5.2 Optical Transparency

3.5.2.1 Background

An optically transparent material is defined as one which allows visible light (wavelengths of 390 to 750nm) to pass through it. If a material allows complete optical light transmission through its structure it can be said to be optically transparent. If the reverse is true and all of the light is either reflected, absorbed or scattered then it is known as an opaque material. Partial transparency where light passes through diffusively is called translucency. Materials can transmit, absorb or reflect light over particular frequency ranges. The selective absorption of specific frequencies of visible light gives rise to the perception of colour. The degree of transparency is governed by the absorption and scattering of the light within the material. A material with a large number of defects or other scattering centres will scatter the light in random directions, impeding the light transmission through the material.

3.5.2.2 Equipment

Optical transmission was measured using a Vipdens 620 transmission densitometer, as shown in Figure 3.5.1. This unit uses a fluorescent light source with a colour temperature of $5000^{o}K$ and is designed for taking area saturation percentage measurements of transparent black and white documents [102]. This directly correlates with the transmission of CNT films, assuming that the CNTs absorb 100% of incident light. The CMOS sensor is illuminated through the sample film and the illumination level is compared to a zero percentage area coverage calibration. The unit then returns the surface coverage as a percentage.

Figure 3.5.1: Photograph showing Vipdens 620 transmission densitometer.

3.5.2.3 Method

Samples were measured at 5 random locations and a single location of the substrate was also measured. The average substrate transmission value (from all sample substrate measurements) was subtracted from each sample average measurement, giving results indicative of the CNT ink film alone.

The equipment was calibrated using the reference illumination before each use. Measurement repeatability can be seen from the 389 measurements taken of the PET substrate which showed a variability of $\pm 1\%$.

3.5.3 Sheet Resistivity

3.5.3.1 Background

The electrical conductivity of a material describes a material's ability to allow the flow of electrical current, taking into account geometric factors. A highly conductive material has many charge carriers available for transport and allows the flow of

electrical current through the material with minimal scattering of the charge carriers. Conductivity is usually represented by the symbol σ and is measured in units of Sm^{-1}. The inverse of the conductivity is the resistivity (ρ, $[\Omega m]$) of the material and is calculated using the expression

$$\rho = R\frac{A}{L} \tag{3.5.1}$$

where A is the cross sectional area of the sample and L is the length perpendicular to this area. However when measuring the resistivity of thin films where the thickness of the film is significantly smaller than the planar dimensions, the resistivity can be given in terms of sheet resistivity (ρ_s) as described by Smits[103]. The sheet resistivity of a sample is measured in ohms per square ($\Omega/\square$) and for rectangular samples is calculated using the expression

$$\rho_s = RC \tag{3.5.2}$$

where C is a constant defined by the geometric constraints of the sample shown in Figure 3.5.2, relevant values of which are given in Table 3.5.1.

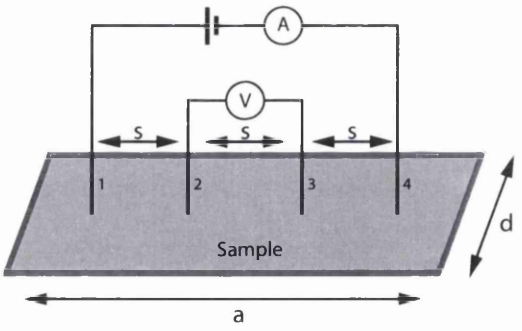

Figure 3.5.2: Schematic of four point probe experimental setup. a, d are sample dimensions, s is probe spacing, all measurements in m. Probes 1 and 4 are the source probes, 2 and 3 are the sense probes.

		a/d			
		1	2	3	≥4
s/d	1			0.9988	0.9994
	2		1.9454	1.9475	1.9475
	5	3.5098	3.5749	3.575	3.575
	10	4.2209	4.2357	4.2357	4.2357
	20	4.4516	4.553	4.4553	4.4553
	40	4.512	4.5129	4.5129	4.5129
	∞	4.5324	4.5324	4.5325	4.5324

Table 3.5.1: Correction factor (C) for calculating sheet resistances of varying rectangular sheet geometries, as calculated by Smits[103]

3.5.3.2 Equipment

Measurements were taken using a combination of a Signatone S-116O four point probe station for reproducible contact and an Keithley 2400 SourceMeter for measurement. This setup will measure resistances up to $200M\Omega$. Probes used were tungsten with a 5um tip, spaced linearly at 5mm intervals. An image of the equipment setup is shown in Figure 3.5.3. The claimed accuracy of the equipment is ±0.67% at the highest range of measurement (up to 200MΩ)[104]. Equipment accuracy was confirmed against a calibrated sample (ITO coated glass) prior to measurement. Although the expected resistances of CNT films is high enough that contact resistance should be negligible, the use of the four point technique is preferred for measurement of sheet resistivity using the method defined by Smits[103].

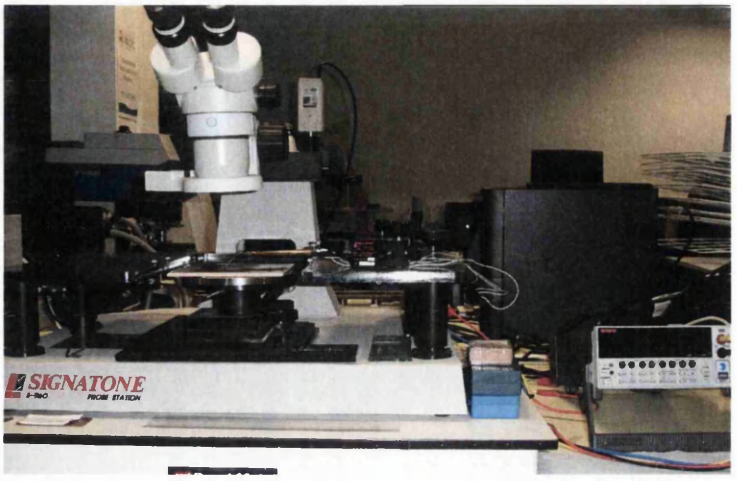

Figure 3.5.3: Photograph showing Keithley 2400 Sourcemeter plus Signatone S-116O probe station.

3.5.3.3 Method

Samples were measured at 5 random locations. The resistance was measured using the automatic four point resistance setting on the Keithley 2400, with a filter applied set to average every 30 readings. The sheet resistivity was calculated using equation 3.5.2 with a correction factor of 4.2357 selected due to sample geometry. The substrate is considered to have infinite resistance and hence does not contribute to the sample conductivity.

3.6 Concluding Remarks

This chapter has focused on the experimental techniques and equipment used to prepare, deposit and characterise the CNT ink samples. Inks will be prepared using sonication and shear mixing techniques. The liquid inks will be characterised in terms of their viscosity and surface tension. The inks will then be coated using a bar coating system onto a transparent PET substrate and dried. The final films will be characterised in terms of transparency and resistance, with selected samples also tested for adhesion. The following chapters detail the particular ink formulations tested, the justification for ink component selection and the characterisation results.

Chapter 4

Initial Ink Formulation Determination

4.1 Introduction

The aim of the work described in this chapter was to determine suitable initial ink constituents and manufacturing parameters for further ink formulation investigations. As stated in section 1.2.4, the unique electrical properties of CNTs outlined have the potential to enable disruptive technologies in the printed electronics sector. However, with the issues in creating and maintaining a suitable CNT dispersion well known (see section 2.2.1) there has been limited success in this field. At the outset of this research programme there was no academic work reported towards the formulation of a CNT ink suitable for roll-to-roll processing with technologies such as gravure or flexography. Limited work had been done towards formulation of screen printing pastes, however most work was focussed on inkjet where the 'ink' was merely a CNT dispersion, without binders. During this research programme some commercial inks were reported, however a systematic study of the use of CNTs as the functional pigment in a strict printing ink formulation has not been academically reported.

A large number of scoping experiments were performed (as reported in section 2.4) to determine key parameters for measurement settings and initial values for further investigations. These experiments highlighted the need for a more systematic study of particular variables in the ink formulation process. The variables altered in this chapter were the resin used within the ink formulation, the ratio between the weight concentration of resin and CNTs in the ink formulation and the temperature of the ink during ultrasonic agitation for dispersal. Preliminary studies had highlighted the choice and quantity of resin as crucial to the ink characteristics, both fluid and dry. Also it was seen that excess heat during mixing would result in solvent evaporation, and further investigations were required to optimise the mixing temperature due to

the reported temperature dependence of CNT dispersion stability. [66] These initial formulation trials were characterised by measuring the viscosity response to applied shear and surface tension of the ink solutions and the sheet resistance, optical transparency and adhesion of a coated film. These parameters were chosen as they are the key 'wet' and 'dry' properties to consider in the flow of printed application development, as discussed in section 1.1.2. The methods used to measure these characteristics are described in chapter 3.

The decision was made to maintain NMP as the only solvent used throughout these tests. The suitability of NMP for CNT dispersion has been proven in the literature[59], and compared to many other suitable alternatives it is less toxic and more cost effective (for further solvent discussion see section 2.4). The CNTs used in this section were Baytube® C150P, used without modification. Baytube® is the commercial tradename of MWCNTs produced by Bayer MaterialScience, which are produced by a CVD method (see section 1.2.1.3). Baytubes® were chosen due to their commercial availability at large volumes, bearing in mind the potential of producing large volume quantities of ink in the future. The use of commercially available MWCNTs increases the current industrial relevance of the work due to the reduced cost of CVD grown MWCNTs compared to SWCNTs (the cost difference being a factor of 10 at the time of writing*) making commercial use of MWCNTs more likely in the short term.

The target was to develop an ink formulation suitable for flexographic or gravure printing, due to the flexibility of these systems and similarity in basic requirements. As summarised in Table 1.1.1, this requires a viscosity within the optimal range of 0.05 to 1.5Pas and a surface tension low enough to allow wetting onto a variety of substrates and printing forms, preferably in the region of 30 to 40mN/m. For further details on flexography and gravure see section 1.1.1.

4.2 Resins

This section compares CNT inks formulated to contain one of four printing resins. Each sample was characterised as described above. The four resins chosen were a commercial polyamide (PA) based resin system, a commercial nitrocellulose (NC) based resin system, a commercial polyanaline (PLA, trade name Panipol®) based system and a polyvinyl alcohol (PVA) system. The PA and NC based systems were chosen due to their popularity in commercial ink manufacture. NC based resins

*Prices sourced from http://www.cheaptubes.com, June 2012.

have been reportedly used within screen printing CNT ink formulations [87]. The PAN system was chosen due its conducting nature, as used in Denneulin *et al.*[91], to aid the conductivity of the final film. The pure PVA based system was chosen due to the common usage of PVA as a binder and to reduce the complexity and unknown elements of the system inherent in the usage of commercial resin systems. PVA has also been shown to provide a weak stabilisation, or surfactant effect upon CNTs dispersions[9], potentially improving the CNT dispersability and stability.

4.2.1 Experimental Outline

All inks samples were made in 20g batches. CNT content was measured as a percentage of total mass and target was 2wt%, with a mass ratio of 1:1 between the resin and the CNTs. These parameter values were determined as suitable for preliminary trials as a result of initial scoping experiments. Inks were prepared using the method described in section 3.2.1.3. Resin bases in NMP were prepared before the addition of CNTs and further solvent to ensure resin solubility in the final ink, a common step in commercial ink manufacture. These bases were prepared at concentrations of 10% for the PA and PVA, 3.92% for the NC and the PAN system was supplied prepared as a 15% base. These percentages were chosen (in the case of PA, PVA and NC) to provide a suitable viscosity base for further sonication. Ink formulation quantities are given in Table 4.2.1.

Constituent	Target Mass [g]
CNT	0.4
NMP	19.2
Resin	0.4
Total Mass	20

Table 4.2.1: Target ink constituent mass for resin investigation.

Three ink samples of each resin system were tested, and all results averaged. Samples were prepared in advance but not mixed. All samples were mixed using an ultrasonic probe for 30 minutes, whilst suspended in a water bath set to approximately 5^oC to avoid evaporation, in line with the method outlined in section 3.2.1.3. The average energy applied to the system was 21.9kJ, as reported by the ultrasonic probe.

Immediately after mixing samples were removed from the water bath and three film samples of approximately 15cm x 10cm were coated (see section 3.4.1.3). After coating the film samples were dried and the viscosity of the ink sample measured (see section 3.3.1). Concurrently the ink surface tension was measured (see section 3.3.2)

and the ink density was measured using calibrated pipettes and a mass balance. Once the film samples were dried the resistance, transmission and adhesion of the coated film was measured using the methods outlined in sections 3.5.3.3, 3.5.2.3 and 3.5.1.3 respectively.

All experiments were performed as rapidly as possible after mixing to minimise effects due to reagglomeration of the CNTs. Typically all experiments would be complete within 10 minutes of the completion of the mixing process. As discussed in section 2.2.1, the reagglomeration of CNTs in dispersion occurs over short timescales (within 2 hours[63]) if surfactants or functionalisation are not used, therefore efficient characterisation methodology after mixing was required to minimise any resulting effects.

4.2.2 Characterisation Results and Discussion

4.2.2.1 Ink Viscosity

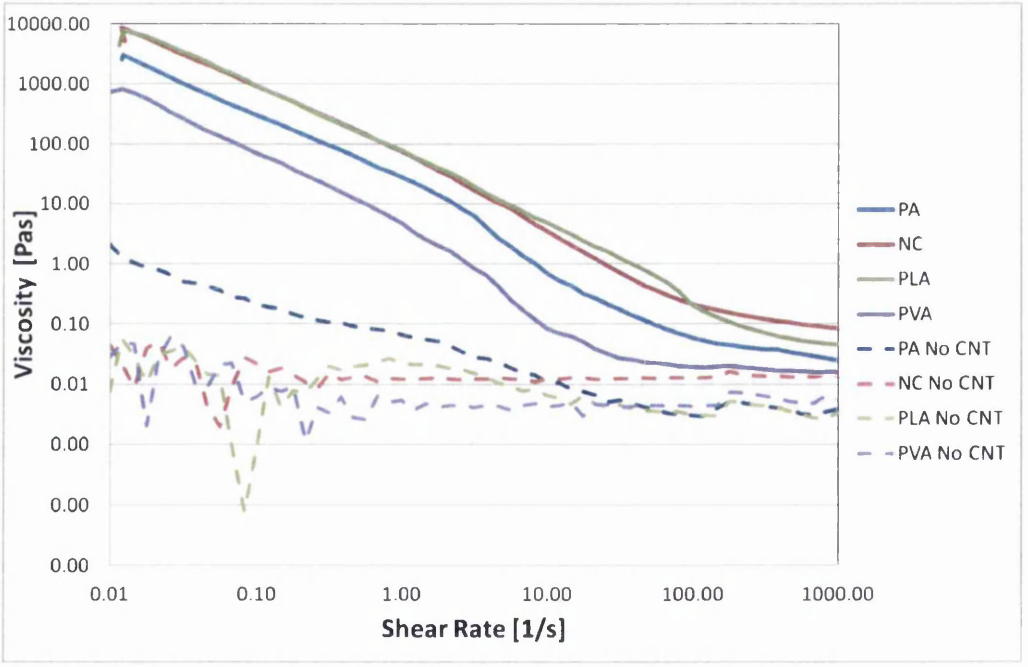

Figure 4.2.1: Average viscosity/shear-rate curves of samples containing PA, NC, PLA and PVA based resin systems, both with (solid lines) and without (dashed lines) CNTs.

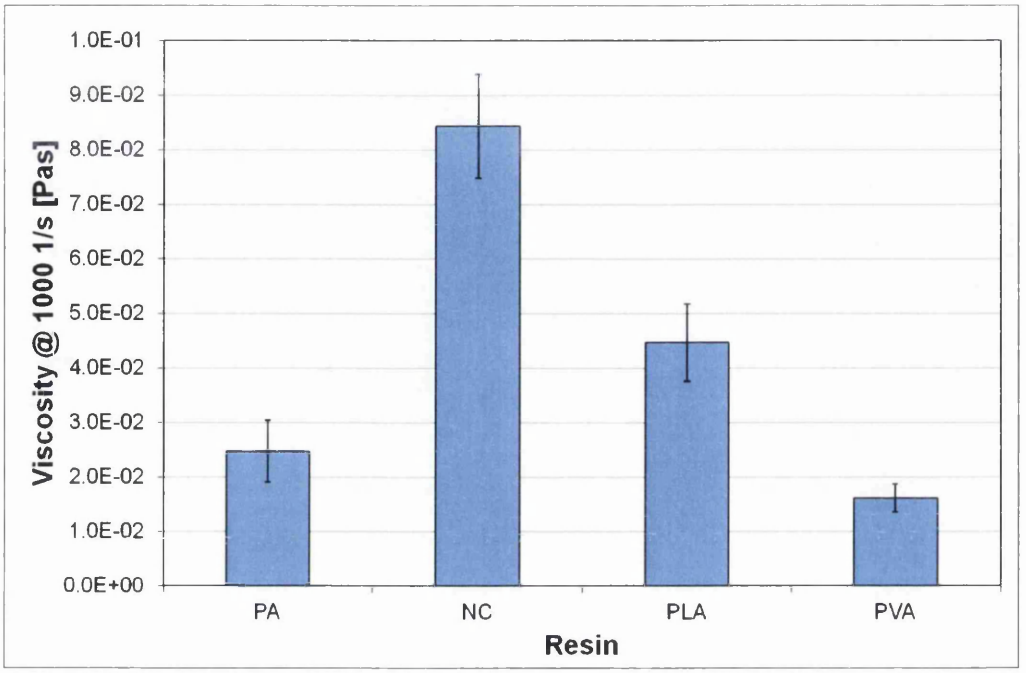

Figure 4.2.2: Average viscosity curves of samples containing PA, NC, PLA and PVA based resin systems in the final Newtonian regime at 1000 1/s. Error bars shown are ± one standard deviation.

As shown in Figure 4.2.1 all samples containing CNTs showed shear thinning behaviour, with a typical power law region seen during increasing shear rate until the viscosity curve plateaus to a minimum and tends towards a constant viscosity, or Newtonian, region. The final viscosities in the Newtonian region and their standard deviations are shown in Figure 4.2.2. This behaviour is typical of many non-Newtonian dispersions such as polymer solutions and particulate dispersions [95]. Shear thinning is due to the increase in the order of a system under shear, until a point at which the particles in the system are in a state at which minimum disruption is caused to the flow of the constant phase, which is where the final constant viscosity region occurs. Further discussion of this phenomena is provided in section 3.3.1.1. The PVA samples shows the lowest Newtonian viscosity, followed by the PA, then the PLA and NC. Observationally the PLA and NC based systems appeared inhomogeneous and poorly dispersed, this is supported by the inconsistency in viscosity observed in the non-Newtonian and Newtonian regions. This can also be observed by the higher standard deviation of the Newtonian regime viscosity shown in Figure 4.2.2. This may signify that insufficient energy was applied to the system, analogous

to the system being below the 'critical mixing time' proposed by Huang *et al.*[12]. It must be noted that the higher the viscosity of the fluid during mixing, the lower the power density applied to the system due to the higher viscosity increasing damping of the ultrasonic mixing through the fluid[22].

The addition of CNTs to the ink has a significant effect on the viscosity profile under shear. All systems initially showed weak shear thinning behaviour, with the PA based system showing the highest dependence upon shear. The addition of CNTs had the result of increasing the viscosity gradient with respect to shear of all the resin systems, and had differing effects upon the viscosities in the Newtonian regime, with the PVA system seeing the lowest increase in viscosity. This may be due to the reported weak stabiliser effect of PVA[9] resulting in a more homogeneous dispersion and hence lower viscosity change as a result of the more ordered system.

4.2.2.2 Ink Surface Tension

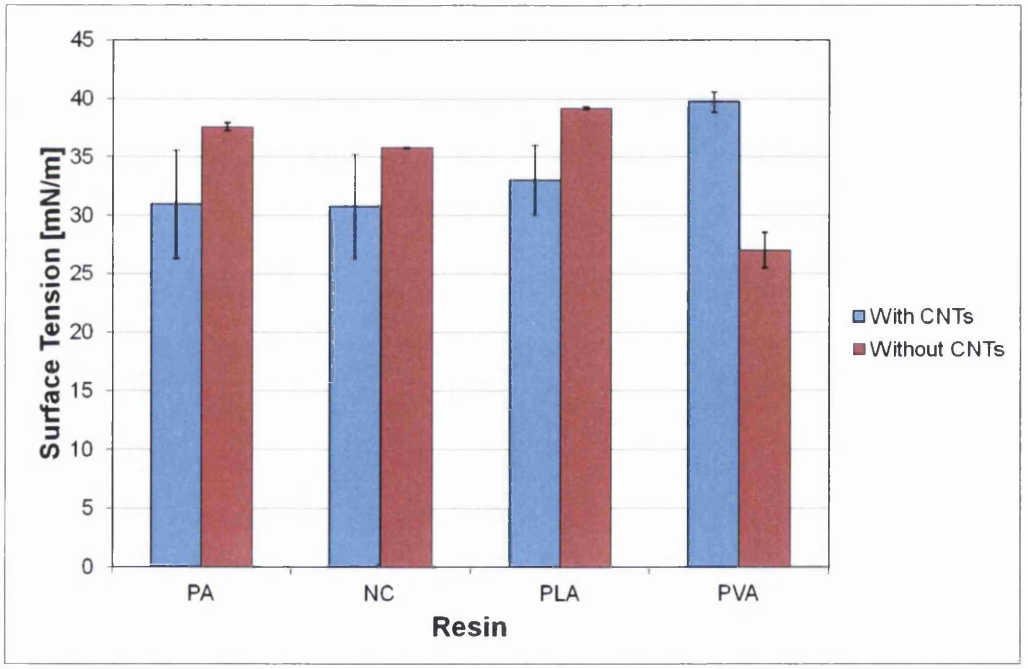

Figure 4.2.3: Average surface tensions of inks containing PA, NC, PLA and PVA based resin systems, both with and without CNTs. Error bars shown are ± one standard deviation.

The average surface tensions of inks containing PA, NC, PLA and PVA based resin systems are shown in Figure 4.2.3. The PVA system showed minimal effect upon the

surface tension of the NMP solvent used (40.79mN/m), whilst the PA, NC and PLA based systems showed a reduction in the surface tension. This implies a reduction in the intermolecular forces in these systems. It must be noted that the higher ink viscosity of the PA based system and the viscosity and observed inhomogeneity of the PLA and NC systems results in increased measurement uncertainty due to the reduced repeatability of the pipetting system. All systems except PVA showed a decrease in surface tension and an increase in measurement uncertainty after the addition of CNTs. This indicates that the PVA system results in CNT concentration in the bulk of the dispersion, indicative of the reported surfactant effects of PVA. This increase in surface tension is also observed in inorganic PVA suspensions by Liu *et al.*[105].

4.2.2.3 Printed Film Transparency

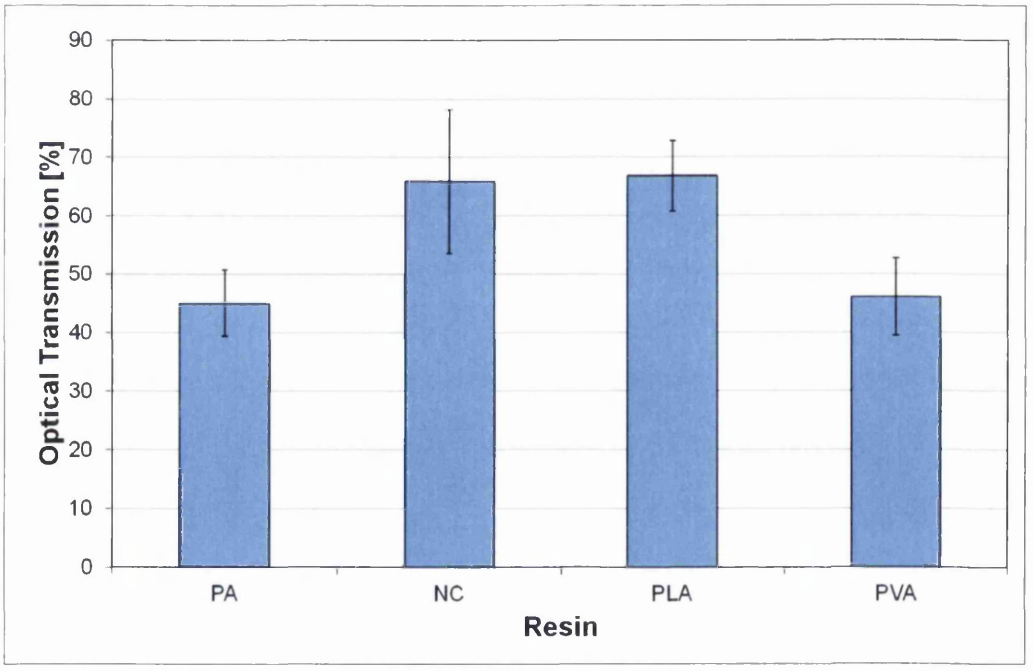

Figure 4.2.4: Average optical transmission of coated films containing PA, NC, PLA and PVA based resin systems. Error bars shown are ± one standard deviation.

Measurements of the optical transmission of the films were taken at 5 random points and the results averaged and normalised with respect to the substrate, the data from which is shown in Figure 4.2.4. The PA and PVA based films showed

a significant reduction in optical transmission compared to the NC and PLA based systems. This correlates with the indication of improved dispersability of the CNTs in these systems seen in the rheological results. It should be expected that the sheet resistivity should follow a similar trend if this is the case.

4.2.2.4 Printed Film Sheet Resistivity

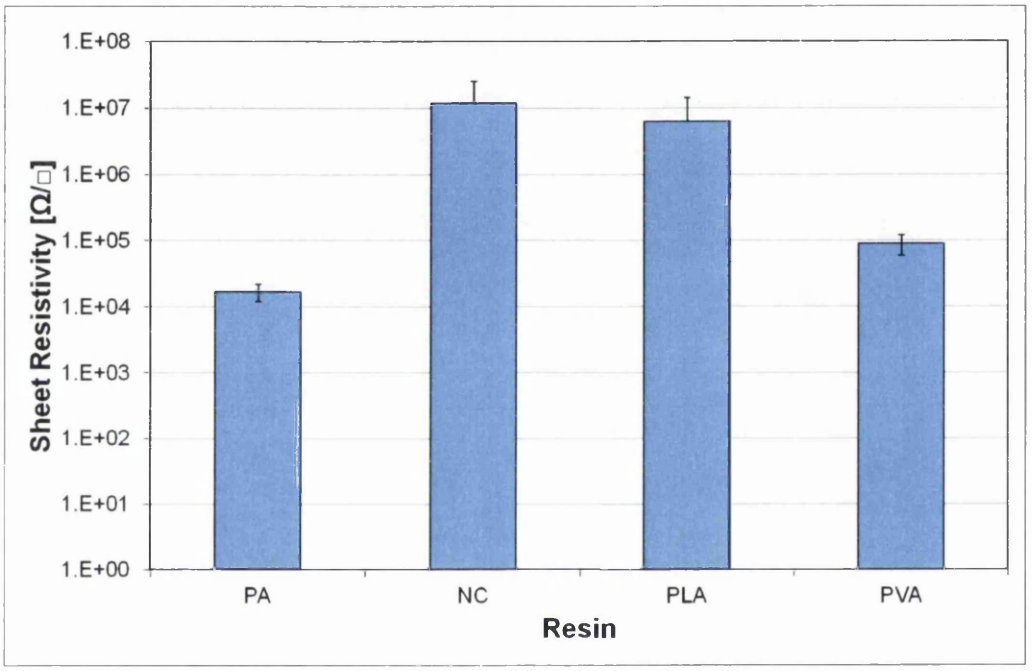

Figure 4.2.5: Average sheet resistivity of coated films containing PA, NC, PLA and PVA based resin systems. Error bars shown are ± one standard deviation. Error bars not displayed are due to the magnitude of the standard deviation being higher than the measured average. Deviation values are reported in Table 4.2.2.

Measurements of the sheet resistivity of the coated films were taken at 5 random points on 3 samples of each resin coating and the data averaged, the results of which are shown in Figure 4.2.5 and summarised in Table 4.2.2. The trend shown in the optical transmission (Figure 4.2.4) is followed as predicted, with the NC and PLA showing the highest average sheet resistivities. The inhomogeneity of the films is also emphasised by the extremely high standard deviation of the NC and PLA results. Resistivities are similar to those reported for MWCNT networks in available literature[90].

Resin	Sheet Resistivity [Ω/□]	St. Dev. [Ω/□]	St. Dev. As % Mean [%]
PA	1.68E+04	4.94E+03	29.3
NC	1.18E+07	1.36E+07	115.2
PLA	6.25E+06	7.96E+06	127.4
PVA	8.90E+04	2.99E+04	33.5

Table 4.2.2: Table summarising average sheet resistivity of coated films containing PA, NC, PLA and PVA based resin systems.

4.2.2.5 Printed Film Adhesion

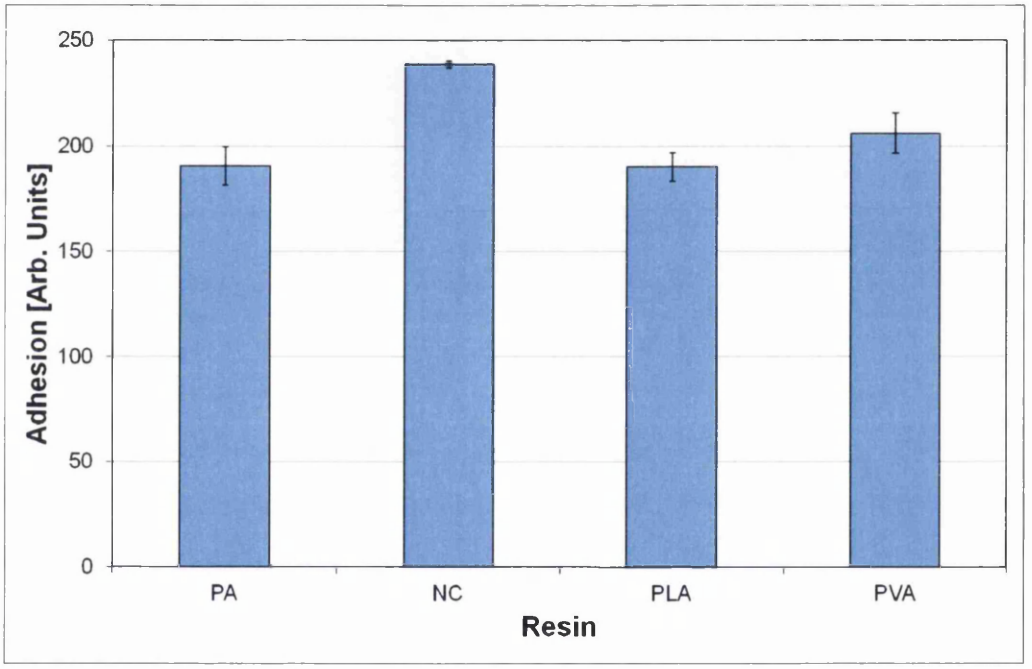

Figure 4.2.6: Measured adhesive strength of coated films containing PA, NC, PLA and PVA based resin systems. Higher adhesion values indicate fewer CNTs removed from the film during the tape test. Error bars shown are ± one standard deviation.

The adhesion test results are shown graphically in Figure 4.2.6 and are the average of three tests per printed sample (of which there are three per resin), each of an approximately $2cm^2$ patch. The NC and PVA resins result in increased binding strength of the CNT deposits to the film, with the high adhesion seen with the NC resin system correlating with the observed high resistance and viscosity relative to

the other systems tested. Adhesion strength required is dependent upon application. Rub resistance could be described as adequate for all samples, though the NC resin system showed significantly higher rub resistance than the others.

4.2.3 Collated Discussion of Results

Section 4.2 has discussed the properties of four common printing ink resin systems when used in a 2wt% MWCNT based functional ink in an NMP solvent. The performance is judged on the five key criteria; namely viscosity and surface tension of the ink and optical transmission, sheet resistivity and adhesion of coated films.

The PA based system showed a consistent viscosity trend with a final constant viscosity region that was below the ideal range for flexographic and gravure printing (see Table 1.1.1). Also surface tensions were suitable for all printing technologies. With regards to the final printed film the film was more homogeneous than the PLA and NC films, a fact demonstrated by the lower sheet resistivity and transmission observed. Adhesion was relatively poor compared to the alternative resins tested.

The NC based system showed a relatively high viscosity and poor homogeneity resulting in high transmission and high sheet resistivity. Surface tension was suitable for all printing technologies. Adhesion was higher than all alternative resins tested, indicating that the resin content could be lowered if improvement in other criteria is required.

The PLA based system showed comparable inhomogeneity to the NC system, with relatively high viscosity, high sheet resistivity and high transmission. Surface tension was suitable for all printing technologies. Adhesion was relatively poor compared to the alternative resins tested. It was originally hypothesised that a conducting polymer system would reduce net sheet resistivity, however this didn't prove to be the case. This may be due to large contact resistance between the CNT network and the conducting polymer matrix or insufficient conducting polymer within the print to have a significant effect.

The PVA based system showed the lowest viscosity of the tested resin systems, with a consistent trend visible. Again, surface tension was suitable for all printing technologies. The printed film was of comparable homogeneity to the PA based system, as indicated by the sheet resistivity and transmission data. Adhesion was higher than the PA based system, again indicating the potential for varying the CNT:resin ratio.

Of the four resins tested the PVA based system shows the most promise for further investigation. High adhesion indicates scope for reduction of CNT:resin ratio, which

would be expected to reduce sheet resistivity by reducing junction resistance and improve optical transmission by reducing film thickness. However, care must be taken to keep the viscosity within printable ranges. Surface tension is likely to remain within a printable range whilst the NMP solvent remains the primary ink constituent. PVA has also been reported to provide weak stabilisation[9], and the use of pristine PVA will simplify analysis compared to the use of commercial resin systems which will often include additives to improve performance. Subsequent testing should focus on optimisation of the CNT:PVA ratio.

4.3 PVA:CNT Concentration

This section compares CNT inks using a PVA based resin at three varying ratios of PVA:CNT mass. Ratios of 1:2, 1:1 and 1:0.5 were chosen. An increase in resin content is expected to increase ink viscosity and durability whilst adversely increasing sheet resistivity. Each sample was characterised using the same method used for the resin tests (see section 4.2.1), and in addition scanning electron microscope (SEM) images were taken to observe the effect of increasing resin content.

4.3.1 Experimental Outline

All inks samples were made in 20g batches. CNT content was measured as a percentage of total mass and target was 2wt%, with a mass ratios of 1:2, 1:1 and 1:0.5 chosen between the CNTs and the PVA. Inks were prepared using the method described in section 3.2. PVA bases in NMP were prepared at concentrations of 10%. Ink formulation quantities are given in Table 4.3.1. Three inks of each CNT:resin ratio were tested, and all results averaged. Data from the resin tests (section 4.2) was used for the 1:1 ratio to avoid repetition.

CNT:Resin Ratio	1:2	1:1	1:0.5
Constituent	Target Mass [g]		
CNT	0.4	0.4	0.4
NMP	18.8	19.2	19.4
PVA	0.8	0.4	0.2
Total Mass	20	20	20

Table 4.3.1: Target ink constituent mass for CNT:resin ratio investigation.

4.3.2 Characterisation Results and Discussion

4.3.2.1 Ink Viscosity

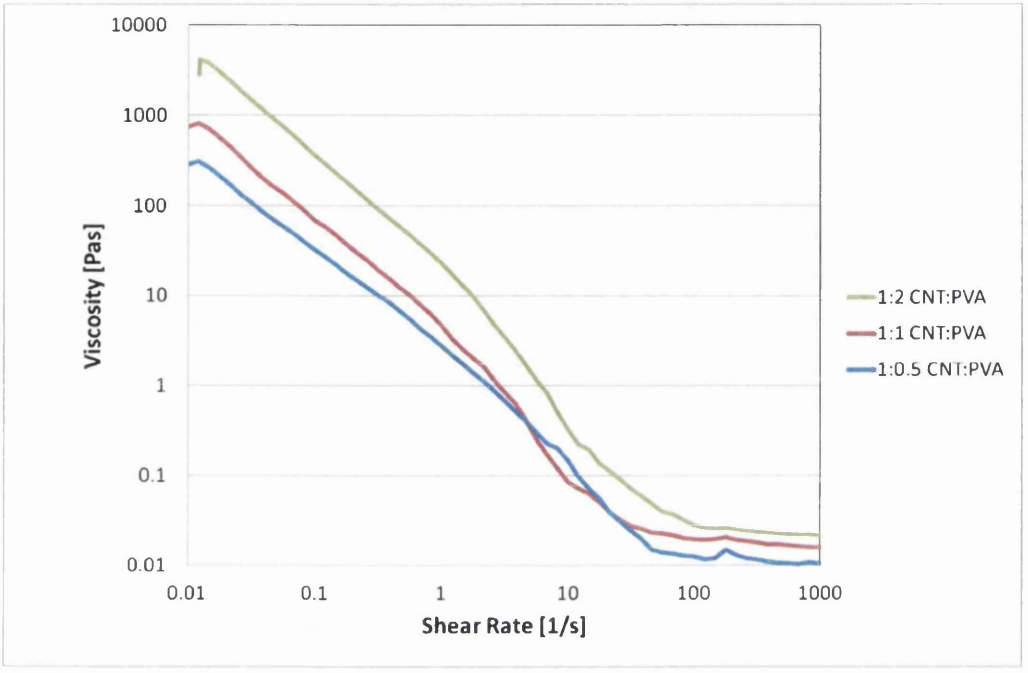

Figure 4.3.1: Average viscosity/shear-rate curves of samples containing 2% CNTs and a CNT:resin ratio of 1:2, 1:1 and 1:0.5.

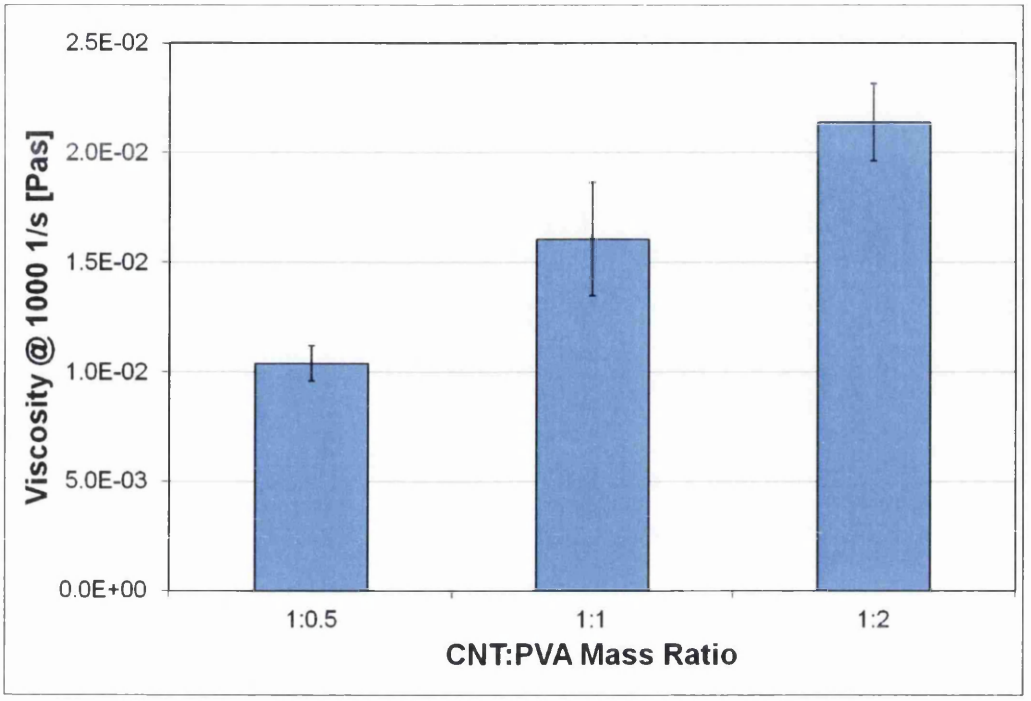

Figure 4.3.2: Average viscosity of samples in the final Newtonian regime (at 1000 1/s) containing 2% CNTs and a CNT:resin ratio of 1:2, 1:1 and 1:0.5. Error bars shown are ± one standard deviation.

Figure 4.3.1 shows the viscosity flow curves of the three ratios tested. All samples show the same shear thinning behaviour, with a convergence apparent between the 1:1 and 1:0.5 ratios observed. This could indicate that the increase in resin content has a stabilising effect on the CNTs, thus improving dispersion homogeneity and hence viscosity profile consistency. The final constant viscosity values show that the increase in resin content increases the viscosity of the ink, which is also illustrated in Figure 4.3.2.

4.3.2.2 Ink Surface Tension

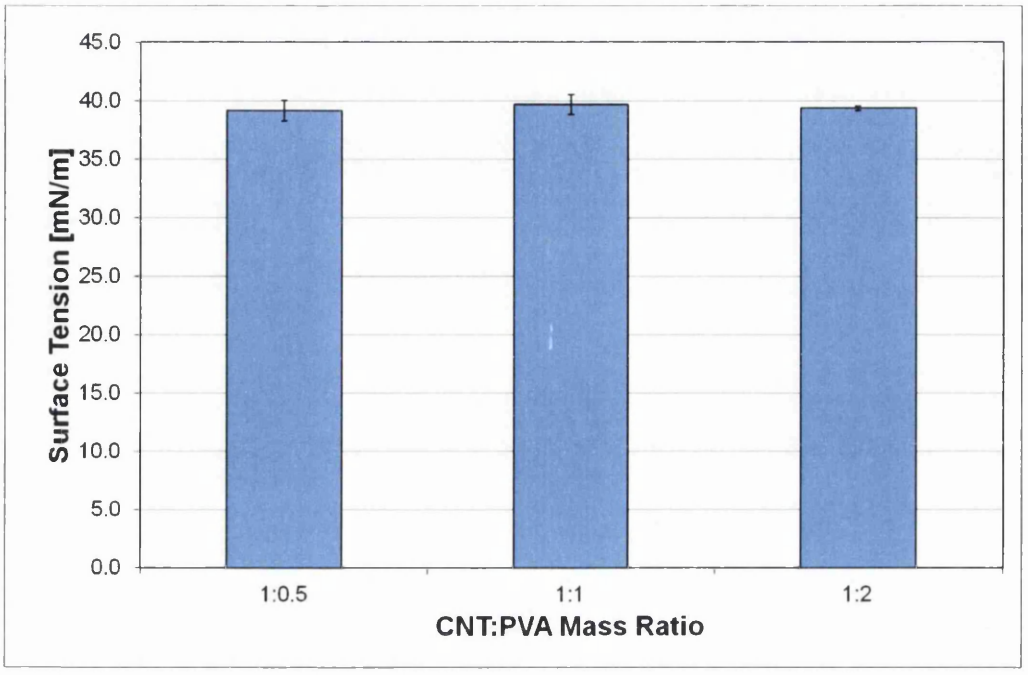

Figure 4.3.3: Average surface tensions of inks containing CNT:PVA mass ratios of 1:0.5, 1:1 and 1:2. Error bars shown are ± one standard deviation.

The average surface tensions of the inks are shown graphically in Figure 4.3.3. No significant change is seen between the three ratios, implying that the PVA has no significant effect on surface tension at the quantities tested and that it is still dominated by the NMP as suggested in section 4.2.2.2. However it must be noted that the consistency of the samples with the highest proportion of PVA (1:2 CNT:PVA) was significantly higher that the other samples implying improved sample consistency, possibly due to the reported weak stabilising effect of PVA on CNT dispersions.

4.3.2.3 Printed Film Transparency

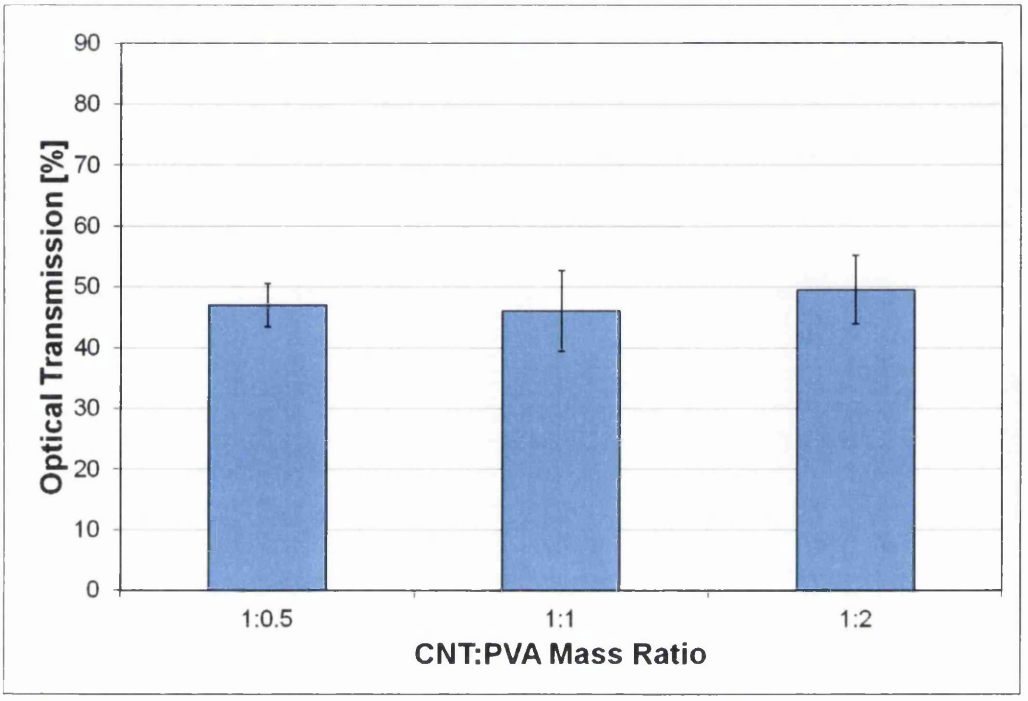

Figure 4.3.4: Average optical transmission of coated films containing CNT:PVA mass ratios of 1:0.5, 1:1 and 1:2. Error bars shown are ± one standard deviation.

Figure 4.3.4 shows the optical transmission data for the ratio tests. It was originally hypothesised that the increase in PVA content will have a stabilising effect, thus increasing sample homogeneity and transmission. However no significant change in transmission due to the PVA content of the ink is observed.

4.3.2.4 Printed Film Sheet Resistivity

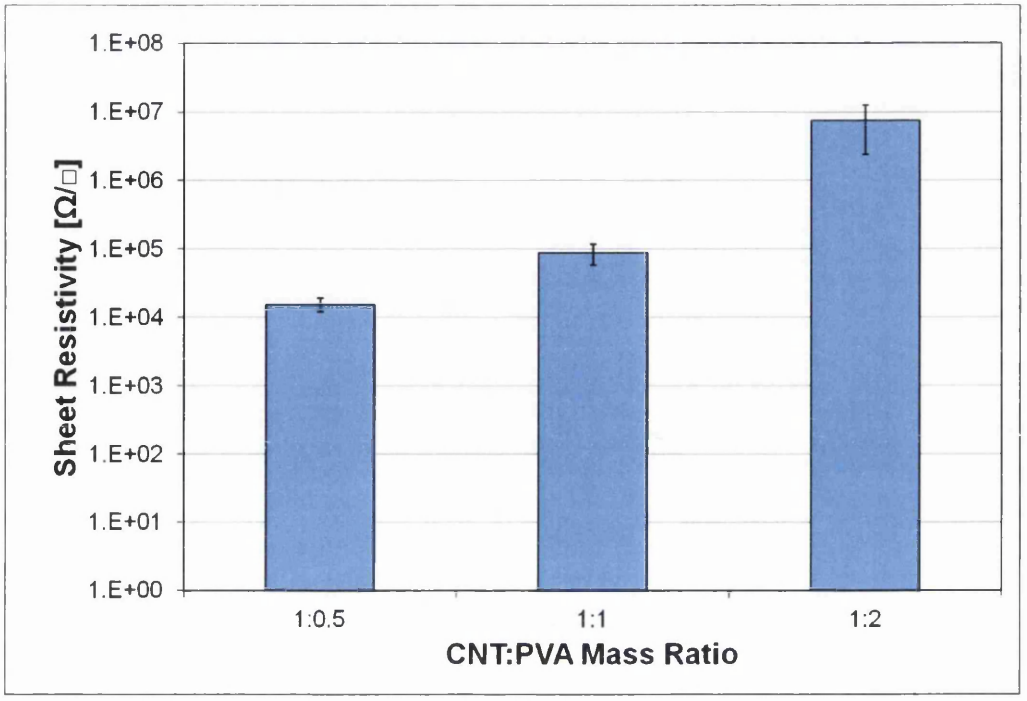

Figure 4.3.5: Average sheet resistivity of coated films containing CNT:PVA mass ratios of 1:0.5, 1:1 and 1:2. Error bars shown are ± one standard deviation.

Figure 4.3.5 shows the effect of the ratio upon the sheet resistivity of the coated films. This data is summarised in Table 4.3.2, including the standard deviation of the data. The increase in resin content has a significant effect upon the sheet resistivity of the film, with an increase in PVA concentration resulting in an increase in sheet resistivity. This is due to the insulating PVA hindering CNT contact throughout the percolating network, hence increasing the CNT junction resistance which is reported to be the dominant factor in network resistivity. The standard deviation of the data does not support the hypothesis that the increase in PVA content increases the homogeneity of the film.

CNT:PVA Ratio	Sheet Resistivity [Ω/□]	St. Dev. [Ω/□]	St. Dev. As % Mean [%]
1:0.5	1.55E+04	3.56E+03	23.0
1:1	8.90E+04	2.99E+04	33.5
1:2	7.41E+06	5.03E+06	67.9

Table 4.3.2: Table summarising average sheet resistivity of coated films containing CNT:PVA mass ratios of 1:0.5, 1:1 and 1:2.

4.3.2.5 Printed Film Adhesion

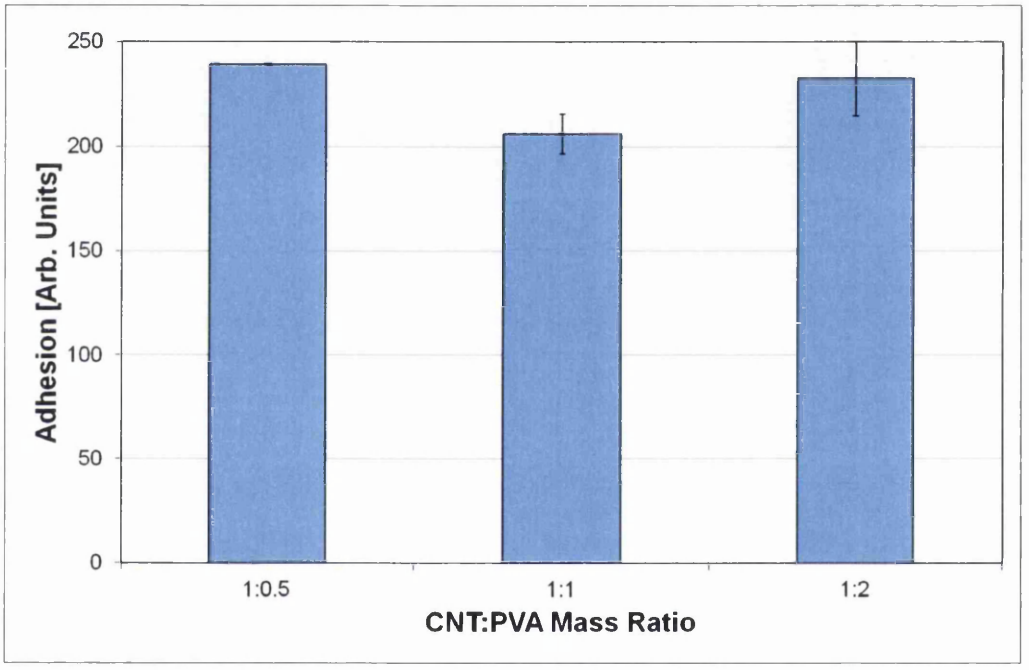

Figure 4.3.6: Measured adhesive strength of coated films containing CNT:resin ratios of 1:0.5, 1:1 and 1:2. Higher adhesion values indicate fewer CNTs removed from the film during the tape test. Error bars shown are ± one standard deviation.

Figure 4.3.6 shows the adhesion results for the ratio tests. It would be expected that the higher the resin content the higher the adhesion, however the results do not support this, and show no clear trend.

4.3.2.6 SEM Imagery

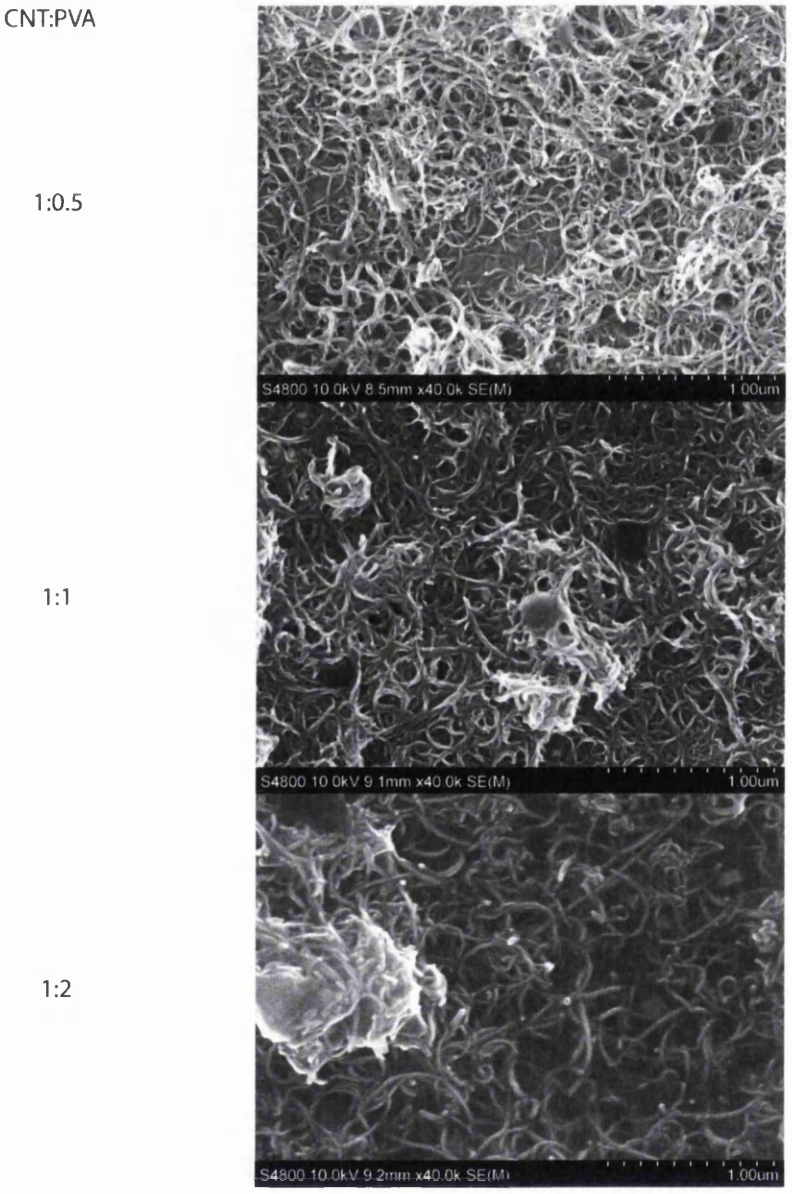

Figure 4.3.7: SEM images of varying CNT:PVA ratios obtained at 40000x magnification.

Figure 4.3.7 shows three representative SEM images taken of printed samples containing each resin ratio. The increase in PVA content has a noticeable effect, with many individual CNTs (approximately 20-30nm in diameter including PVA coating) visible at lower PVA concentrations. As the PVA content within the ink is increased, the

layer appears more coalesced, with the PVA coating many of the bundles of CNTs.

4.3.3 Collated Discussion of Results

Section 4.3 has discussed the properties of three resin concentrations when used for a 2wt% MWCNT based functional ink in an NMP solvent. The performance can now been judged on the five selected criteria; namely viscosity and surface tension of the ink and optical transmission, sheet resistivity and adhesion of coated films.

The ink samples containing a 1:0.5 ratio of CNT:PVA showed the lowest viscosity and a suitable surface tension for common printing techniques. The resulting coated films showed similar transparency to the alternative ratios tested but the lowest sheet resistivity by an order of magnitude. Individual CNTs were still visible in SEM images.

The ink samples containing a 1:1 ratio of CNT:PVA showed an intermediate viscosity and similar surface tension compared to the alternative ratios tested. The coated films again showed intermediate performance relative to the other ratios with respect to sheet resistivity and similar transmission.

Finally, the ink samples containing a 1:2 ratio of CNT:PVA showed the highest viscosity. Again, surface tension remained suitable for printing on a variety of substrates using most common techniques. Sheet resistivity was high in comparison to the alternative ratios and transmission was similar. The increase in sheet resistivity is due to the increased coating of CNTs with PVA, which is clearly visible in SEM images.

Of the three ratios investigated the optimal for further testing is the 1:1 CNT:PVA ratio. The resin content does not impede sheet resistivity to an unacceptable degree compared to the 1:2 ratio whilst the viscosity, crucial to print quality, is higher than the 1:0.5 ratio.

Further optimisation on this ink formulation can be achieved by investigation of the processing parameters. One key parameter that was arbitrarily defined for the prior tests was the temperature of the sample during sonication. Further tests must be performed to study the effect of the mixing temperature upon the PVA and CNT dispersions.

4.4 Temperature During Sonication

This section compares CNT inks using a PVA based resin at a 1:1 ratio of PVA:CNT mass but sonicated whilst immersed in a water bath at three different temperatures,

namely 5, 10 and 15^oC. CNT solutions have been shown to show instability outside a temperature of $\pm 40^oC$[66]. Localised heating during sonication can be high, so cooling of the sample will be essential to maintain sample temperatures below this value. Solvent evaporation should also be minimised during mixing, with NMP having a boiling point of 202^oC[100]. Each sample was characterised as described above, including measurement of mass loss during mixing. Adhesion testing was not performed on this sample set.

4.4.1 Experimental Outline

During probe sonication samples are immersed in a water bath to control ink temperature. The water bath is controlled by an analogue dial and the temperature recorded by a calibrated thermometer. Temperatures are stable to $\pm 0.5^oC$ over significant time scales. For the purposes of this experiment all temperatures chosen were below ambient temperature, with values of 5, 10 and 15^oC selected. These temperatures were selected to keep the sample temperature below 40^oC, with the minimum temperature achievable by the equipment being 5^oC.

All inks samples were made in 20g batches. CNT content was measured as a percentage of total mass and target was 2wt%, with a CNT:PVA mass ratio of 1:1. Inks were prepared using the method described in section 3.2. PVA bases in NMP were prepared at concentrations of 10%. Ink formulation quantities are given in Table 4.4.1. Three inks were mixed at each temperature, and all characterisation results averaged. Data from the resin tests (section 4.2) was used for the 5^oC to avoid repetition. Samples were also weighed before and after sonication to assess maximum sample temperatures as direct measurement during sonication was not feasible. Any reduction in mass post-sonication will be caused by solvent evaporation, implying localised temperatures above the boiling point of NMP.

Consituent	Target Mass [g]
CNT	0.4
NMP	19.2
PVA	0.4
Total Mass	20

Table 4.4.1: Target ink constituent mass for bath temperature investigation.

4.4.2 Characterisation Results and Discussion

4.4.2.1 Sample Mass Loss

Samples were weighed before and after sonication, the results of which are shown in Table 4.4.2. Samples were weighed using a Sartorius Analytic calibrated 4 point mass balance. Mass loss was seen to increase at higher mixing temperatures, however it can be concluded that at no time do the net sample temperatures exceed the boiling point of NMP.

Bath Temperature [^oC]	Average Mass Loss [g]
5	0.00
10	0.01
15	0.02

Table 4.4.2: Mass loss from samples sonicated whilst immersed in a water bath at temperatures of 5, 10 and 15^oC.

4.4.2.2 Ink Viscosity

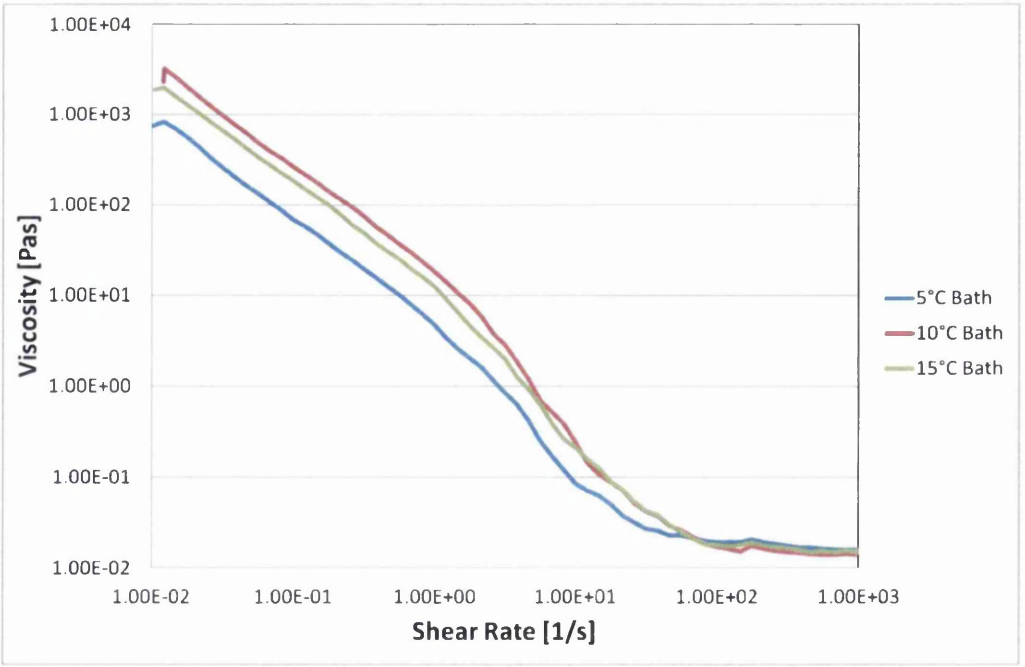

Figure 4.4.1: Average viscosity/shear-rate curves of samples mixed at 5, 10 and 15^oC.

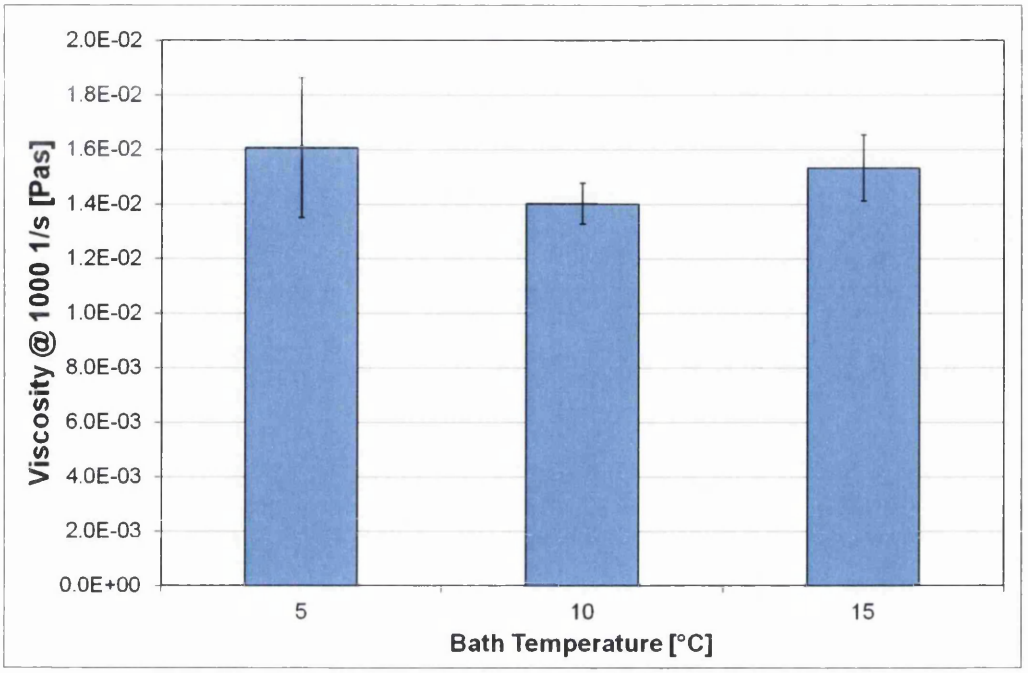

Figure 4.4.2: Average viscosity in the final Newtonian regime (at 1000 1/s) of samples mixed at 5, 10 and 15^oC. Error bars shown are $\pm$ one standard deviation.

Figure 4.4.1 shows the viscosity flow curves of the inks mixed at the three specified temperatures. For all three the final constant viscosity regime is of similar value, with the Newtonian regime graphically displayed in Figure 4.4.2. The variance observed does not correlate directly with temperature, and is not of significant magnitude.

4.4.2.3 Ink Surface Tension

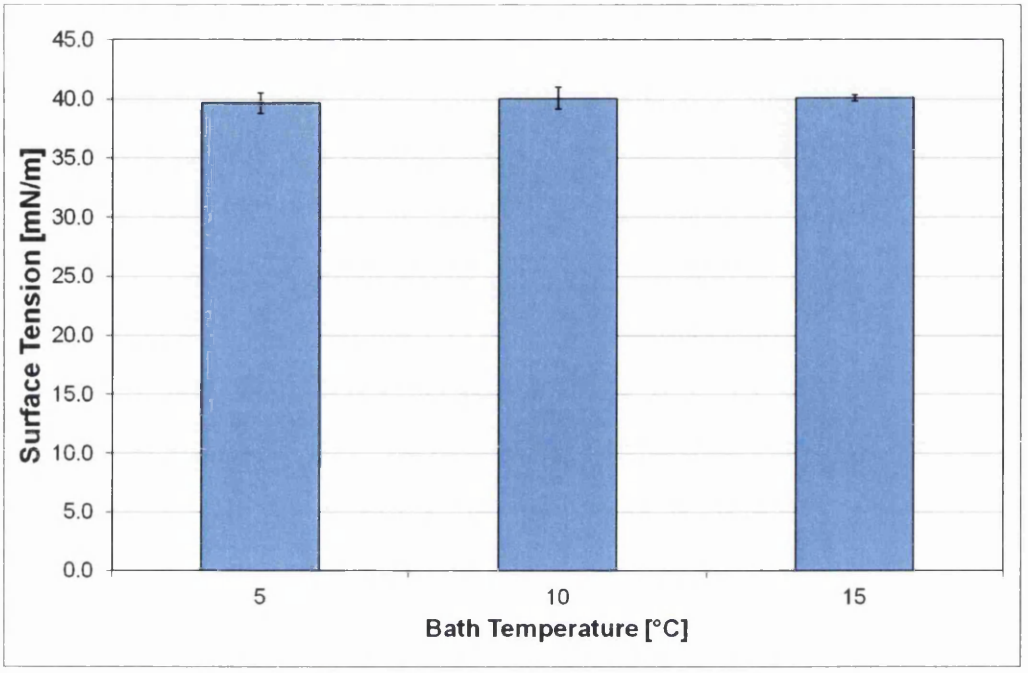

Figure 4.4.3: Average surface tensions of samples mixed at 5, 10 and 15^oC. Error bars shown are $\pm$ one standard deviation.

No dependence of surface tension upon bath temperature is observed in Figure 4.4.3.

4.4.2.4 Printed Film Transparency

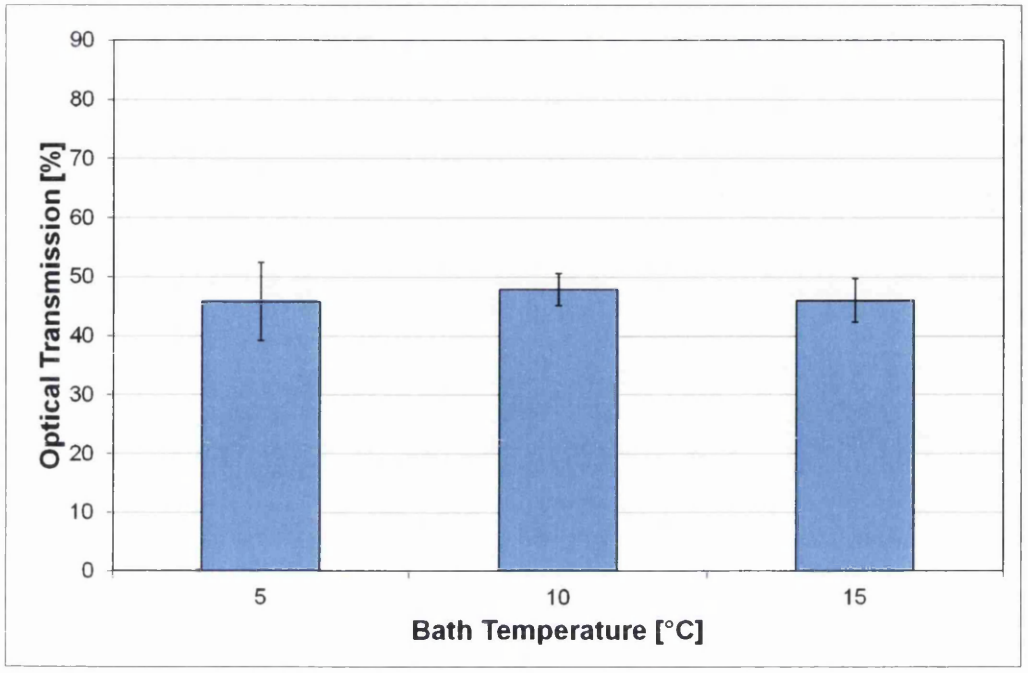

Figure 4.4.4: Average optical transmission of coated films mixed at 5, 10 and 15^oC. Error bars shown are $\pm$ one standard deviation.

Figure 4.4.4 shows that film transmission is independent of bath temperature during mixing.

4.4.2.5 Printed Film Sheet Resistivity

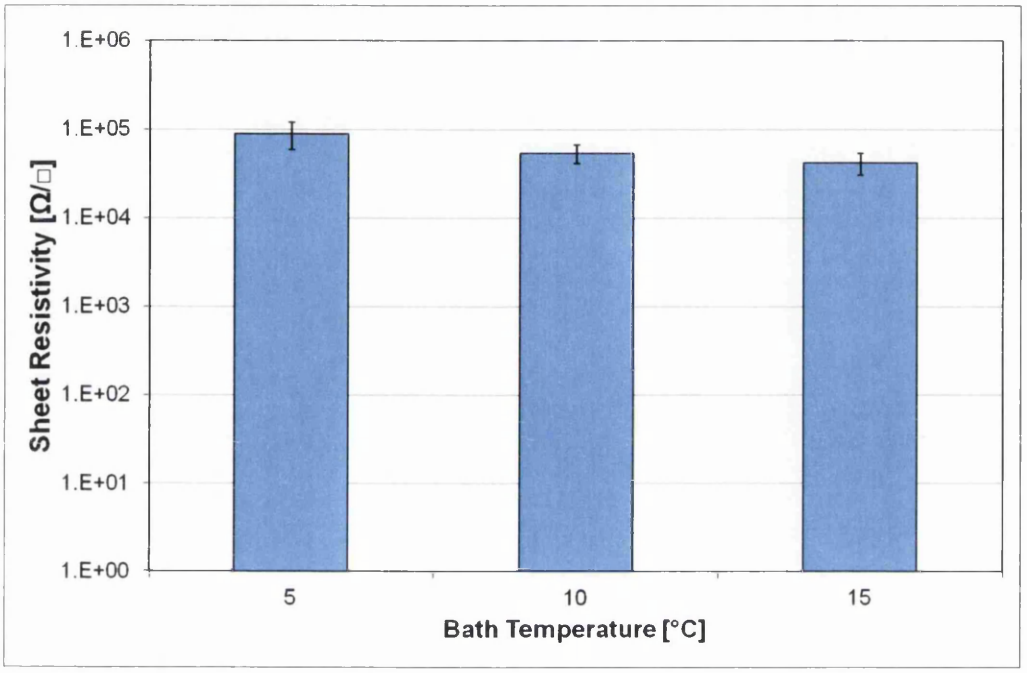

Figure 4.4.5: Average sheet resistivity of coated films mixed at 5, 10 and 15^oC. Error bars shown are $\pm$ one standard deviation.

The sheet resistivities of the coated films are shown graphically in Figure 4.4.5 and summarised in Table 4.4.3. The results show that sheet resistivity reduces at higher mixing temperatures. This may be due to to increased energy in the system at higher temperatures facilitating dispersion.

Bath Temp. [^oC]	Sheet Resistivity [$\Omega/\square$]	St. Dev. [$\Omega/\square$]	St. Dev. As % Mean [%]
5	8.90E+04	2.99E+04	33.5
10	5.42E+04	1.29E+04	23.9
15	4.22E+04	1.16E+04	27.5

Table 4.4.3: Table summarising average sheet resistivity of coated films mixed at 5, 10 and 15^oC.

4.4.3 Collated Discussion of Results

Temperature during mixing appears to have a negligible effect upon the ink and film properties within the range tested. Viscosity, surface tension and film transmission all show no clear dependence upon mixing temperature. Sheet resistivity does show a dependence, with an increasing temperature resulting in a decrease in sheet resistivity. This could be due to an improved network homogeneity, which would be caused by improved solubility with higher temperature. No significant mass loss was recorded at a 15^oC bath temperature implying that sample temperatures do not exceed the boiling point of NMP. Higher temperatures were not investigated due to the need to ensure net sample temperatures were kept within the stability limits reported by Sun *et al.*[66].

4.5 Conclusions

This chapter has described the effect of resin choice, resin content and sample temperature during mixing on several key properties of the CNT ink and coated film. The optimal formulation of a CNT ink should provide a well dispersed suspension of CNTs which will provide an efficient percolating network that is bound to the substrate upon printing. Ink properties should also be in line with the requirements for the selected printing process summarised in Table 1.1.1.

With respect to the choice of resin the results show that under the same processing conditions the resulting ink properties will vary. It is clear that the processing conditions would have to be optimised for each resin, with the PLA and NC systems showing inhomogeneity that is likely due to the mixing energy applied being below that which would be applied at a 'critical mixing time' for that system, as predicted by Huang *et al.*[12]. The PA system and PVA system showed improved dispersion homogeneity, especially with regard to the transmission and sheet resistivity results. A decrease in transmission, such as that seen in the PA and PVA systems compared to the NC and PLA, could be due to increased CNT agglomeration size in the poorer dispersions. A well dispersed network would inhibit light transmission throughout the printed film consistently, whereas large agglomerations would inhibit light transmission at particular points but allow increased transmission over the remainder of the film. This could potentially result in a net increase in light transmission over an area much larger than that of an individual CNT. The increase in individual agglomerations would also result in a higher and more variable sheet resistivity, which is clearly shown in Table 4.2.2. The resistance of all samples is comparable to that

observed in literature for MWCNT films[89;90], indicating that CNT content is above the theorised percolation threshold[46]. The PLA conducting polymer system was expected to improve the sample sheet resistivity, however this was not observed. This may be due to sub optimal dispersion parameters, however overall performance in other areas was not sufficient to warrant further investigation. Surface tension for all samples is similar to that of the NMP solvent which is suitable for deposition on most common substrates. PA, NC and PVA showed suitable adhesive properties at the 1:1 resin:CNT ratios used. PVA was selected as the resin for further ink investigations due to the improved solution quality compared to the NC and PLA. Although the PA system showed a higher quality of dispersion (in terms of sheet resistivity and transmission), the use of a single specified polymer as opposed to the commercial PA system should simplify further experimental conclusions. PVA has also been reported in literature as having a weak stabilisation effect[9].

The PVA:CNT ratio was tuned to optimise the ink and film properties. The resistance of CNT networks is dominated by barrier resistance, either at defect sites or contact resistance at junctions, as shown by Kaiser *et al.*[45] The use of MWNCTs increases the number of defect sites, which partially accounts for the high film resistances compared to reported values for SWCNT networks[76–79], but as stated above values were similar to that reported for MWCNT films without polymer binders. The resin will result in an increase in sheet resistivity[76], probably due to increased barrier resistance at junctions. It is expected therefore that a higher PVA content would increase sheet resistivity, which was observed in the results. All other characterisation parameters showed no conclusive dependency upon PVA content.

Sun *et al.*[66] stated that CNT suspensions in NMP are temperature sensitive, with a values between of $\pm 40^{o}C$ stated as optimal. Also, temperatures above $202^{o}C$ will result in evaporation of the NMP solvent[100]. The use of sonication imparts energy to a system which naturally leads to an increase in temperature throughout the system, plus localised heating will occur to a higher magnitude at the probe tip. Average mass loss during sonication was minimal for all temperatures tested, and sample temperatures were kept within the recommended range. The only significant effect upon the ink properties was upon the sheet resistance of the coated film. Higher temperatures resulted in a lower sheet resistivity. This may imply a better dispersion quality due to the increased energy in the sample during mixing resulting in an increase in suspension homogeneity. However this conclusion is not supported by the transmission results.

To conclude the results indicate that PVA shows promise as a resin for CNT based systems. The PVA content has a significant effect upon the properties of the ink, especially sheet resistivity, and therefore further inks should have a PVA:CNT ratio of 1:1 to optimise the balance between film durability and sheet resistivity. Finally the temperature during processing has a minimal effect upon the ink properties, however the sheet resistivity of the coated film is reduced at higher temperatures within the range measured.

Further processing experiments still need to be performed to assess the effect of ultrasonic mixing energy and CNT concentration and functionality upon the ink and film. These are discussed in the following chapter.

Chapter 5

Critical Mixing Energy, CNT Concentration and Functionalisation

5.1 Introduction

The previous chapter outlined the basic constituents and processing parameters for a CNT based functional ink for flexographic or gravure printing. However it was clear from initial scoping experiments that optimisation of any ink will require investigation into several further key parameters. These are investigated in this chapter, namely the concentration of CNTs in the ink, the agitation energy applied to the system during mixing and the effect of CNT functionalisation.

The CNT concentration within the inks was varied between 0.5, 1, 2 and 4wt%. The concept of a percolation threshold has been discussed by many (see section 2.1.3), where the CNT concentration must be above a certain threshold for conduction to occur between any two points in a network. According to available literature, 0.5 to 1wt% may be close to or below the bulk network percolation threshold, with 1wt% and beyond being above. Increasing CNT content should increase the viscosity of the ink (see section 2.2.2), with the effect upon the surface tension unknown. With respect to the coated film, an increase in CNT concentration should result in a decrease in sheet resistivity and a corresponding decrease in optical light transmission through the film. At higher CNT concentrations it should be expected that higher energies should be applied to the system to obtain a suitable dispersion. Scoping studies suggested that the CNT concentrations of over 8wt% become increasingly difficult to disperse and electrical performance shows limited improvement, hence the experiments described in this chapter will range up to 4wt%.

During probe sonication the total energy applied to the sample is reported by the probe. As described in the literature[8;9] the higher the energy applied to the

system the more dispersed the CNTs will become, but above a certain point the sonication will damage the CNT structures, introducing defects and shortening the CNTs. Dispersion quality has also been highlighted as important for application functionality[10]. Applied energy was varied by changing the time the samples were sonicated for, with all other processing parameters kept constant. The times selected were 5, 15 and 30 minutes. It is expected that the 'critical mixing time' predicted by Huang *et al.*[12] will have an analogous critical mixing energy which will be observed. Scoping experiments and the previous chapter showed that 30 minutes of mixing at the chosen settings described in section 3.2 were sufficient to obtain a suitable dispersion of a 2wt% unfunctionalised MWCNT ink. Hence further testing should investigate lower mixing times as minimisation of mixing energy has direct industrial applicability. Scoping experiments showed that the average reported energies applied to the sample after these mixing times at the chosen settings were 3.7, 11.0 and 21.9kJ respectively. It must be noted that higher energies were applied to higher viscosity fluids due to the feedback system used to apply constant amplitude vibrations (see section 3.2.1.2), the reported values are averages for all CNT concentrations tested. This results in specific energy densities being applied to 20g samples that is similar to the values suggested for CNT samples by Garg *et al.*[8] (and Hilding *et al.*[9] if the assumption of a mistake in Figure 2.2.2 is correct) discussed in section 2.2.1.

The effect of CNT functionalisation is described in section 2.1.2. Functionalised and control CNT samples were donated by Haydale Ltd. and were functionalised using a proprietary plasma based process, similar to that discussed in section 2.1.2. Samples provided were a control sample, which were Baytube® C150P without any post production treatment applied, Baytube® C150P that had been processed in an O_2 atmosphere and Baytube C150P that had been processed in an NH_3 atmosphere (hereby referred to by the notation of AsRec, O2 and NH3 respectively). All samples provided were from the same production batch of Baytubes® . These functionalities were chosen due to the commercial availability and for comparison with reported results. It is expected that the functionalised tubes will show a lower critical mixing energy due to the improved solubility[67]. The impact of the increased number of defects in the CNT structure will negatively impact the sheet resistivity of the coated films, however this may be offset by an improvement in film homogeneity due to the improved CNT solubility. The effect of the precise functionalisation chemistry is unknown, and may depend on a number of factors, not least the solvent and resin material used.

5.2 Functionalised CNT Characterisation

The functionalised CNTs used in this chapter were characterised using X-ray photoelectron spectroscopy (XPS). The XPS experiments and analysis were provided alongside the samples by Haydale Ltd.. The results are summarised in Table 5.2.1. The control sample (AsRec) XPS spectra showed that the MWCNTs were 96% carbon (CNTs and amorphous carbon structures), with 4% oxygen present. When O_2 treatment was applied the oxygen concentration increased to 20%. The NH_3 treatment showed the oxygen concentration had decreased to 3.8%, with 2.2% nitrogen present and evidence of N-H bonding. These percentages should be treated with care due to the inherent uncertainties in the quantitative analysis process; however effect of the functionalisation is clear. Any effect of functionalisation chemistry upon the ink properties may be masked by the large difference in elemental composition observed between the O2 and other samples.

Sample	Elemental Composition [%]		
	C	O	N
AsRec	96.0	4.0	-
O2	80.0	20.0	-
NH3	94.0	3.8	2.2

Table 5.2.1: Summary of XPS characterisation results showing degree of functionality of AsRec, O2 and NH3 CNT samples.

5.3 Experimental Overview

Samples were prepared in advance of mixing. As stated above, three variables were investigated, two of which were within the ink formulation. These were the CNT concentration (0.5, 1, 2 and 4wt%) and CNT functionality (AsRec, O2 and NH3 samples). These were based on the work described in the previous chapter and used a PVA resin at a 1:1 CNT:PVA ratio with NMP used as the solvent for reasons described previously. The third variable was mixing time (5, 15 and 30min). A summary of the ink formulations is given in Table 5.3.1.

Ink samples were characterised in terms of the viscosity profile at varying shear rates and surface tension, with printed films characterised in terms of film transparency and sheet resistivity, in line with the methods described in chapter 3.

Samples were sonicated at a bath temperature of 15^oC, as this was seen to be optimal in section 4.4. Immediately after mixing samples were removed from the

Constituent	Ink Target Mass [g]			
	0.5wt%	1wt%	2wt%	4wt%
CNT (AsRec, O2, NH3)	0.1	0.2	0.4	0.8
NMP	18.9	17.8	15.6	11.2
PVA	1	2	4	8
Total Mass	20	20	20	20

Table 5.3.1: Target ink constituent mass for CNT concentration and CNT type investigation. CNT samples tested are AsRec, O2 and NH3.

water bath and three film samples of approximately 15cm x 10cm were coated (see 3.4). After coating the film samples were dried and the viscosity of the ink sample measured (see section 3.3.1). Concurrently the ink surface tension was measured (see section 3.3.2) and the ink density was measured using calibrated pipettes and a mass balance. Once the film samples were dried the sheet resistivity, transmission and adhesion of the coated film was measured using the methods outlined in sections 3.5.3, 3.5.2 and 3.5.1 respectively. Three ink samples of each combination of CNT functionality, concentration and mixing time were tested, with all results averaged. As with previously described work all experiments were performed as rapidly as possible after mixing to minimise effects due to reagglomeration of the CNTs.

5.4 Results

The results for each characterisation parameter are presented below, in which the effect of ultrasonic mixing time,CNT functionality and CNT concentration are discussed in turn to highlight any observed trends in the data.

5.4.1 Newtonian Viscosity Magnitude

5.4.1.1 Effect of Ultrasonic Exposure Time With Varying CNT Functionality

Figures 5.4.1 to 5.4.4 show the Newtonian regime viscosities of the ink samples after varying ultrasonic probe exposure times and CNT functionality. Firstly it must be noted that no data is available for any AsRec samples after 5min mixing time due to agglomerations being too large for the rheometer plate gap resulting in unreliable results.

At 0.5wt% (Figure 5.4.1) there is no significant trend at 15min exposure. At 30min ultrasonic exposure the AsRec samples have a higher viscosity than the NH3 ink, with

the O2 sample in between but showing higher variability. Viscosity magnitude does not appear affected by mixing times at this lowest concentration.

At 1wt% concentration (Figure 5.4.2) there appears to be a maximum measured viscosity at 15min for the O2 and NH3 samples. This trend is continued for NH3 samples at 0.5, 2 and 4wt%.

At 2wt% concentration (Figure 5.4.3) the AsRec samples show high variability. NH3 samples show a higher magnitude viscosity than the O2 samples, with the trend with respect to mix time for the O2 samples showing an increase to a maximum at 30min, with the viscosity appearing to plateau at 15 and 30min. The O2 samples show the lowest viscosity magnitude at every mix time.

At 4wt% concentration (Figure 5.4.4) the NH3 inks show the highest viscosity at every mix time tested. AsRec and O2 samples show similar magnitude viscosities at the 15 and 30min mix times. The NH3 sample still shows the maximum viscosity at 15min trend described earlier, with the AsRec and O2 samples increasing in viscosity with mix time.

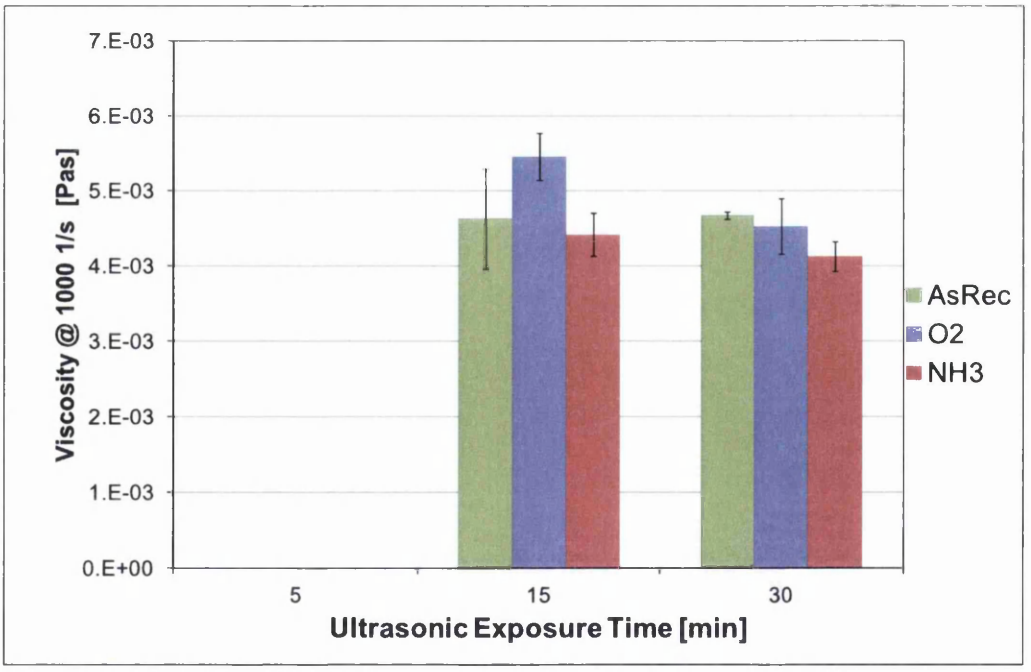

Figure 5.4.1: Viscosity of 0.5wt% MWCNT ink after different probe sonication exposure times. Control sample and functionalised CNTs are shown.

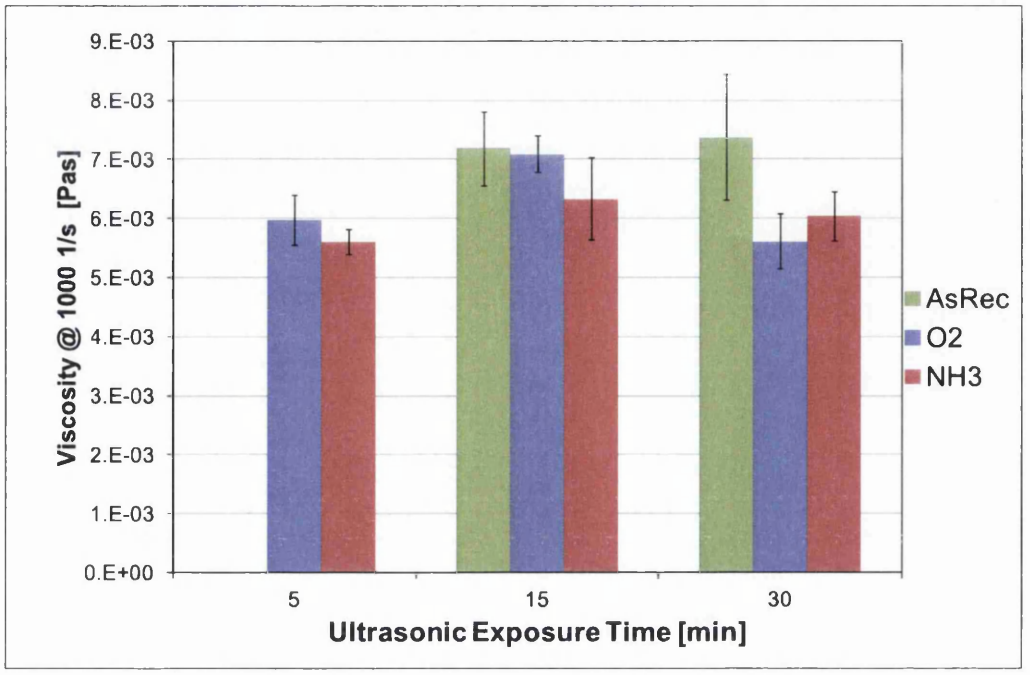

Figure 5.4.2: Viscosity of 1wt% MWCNT ink after different probe sonication exposure times. Control sample and functionalised CNTs are shown.

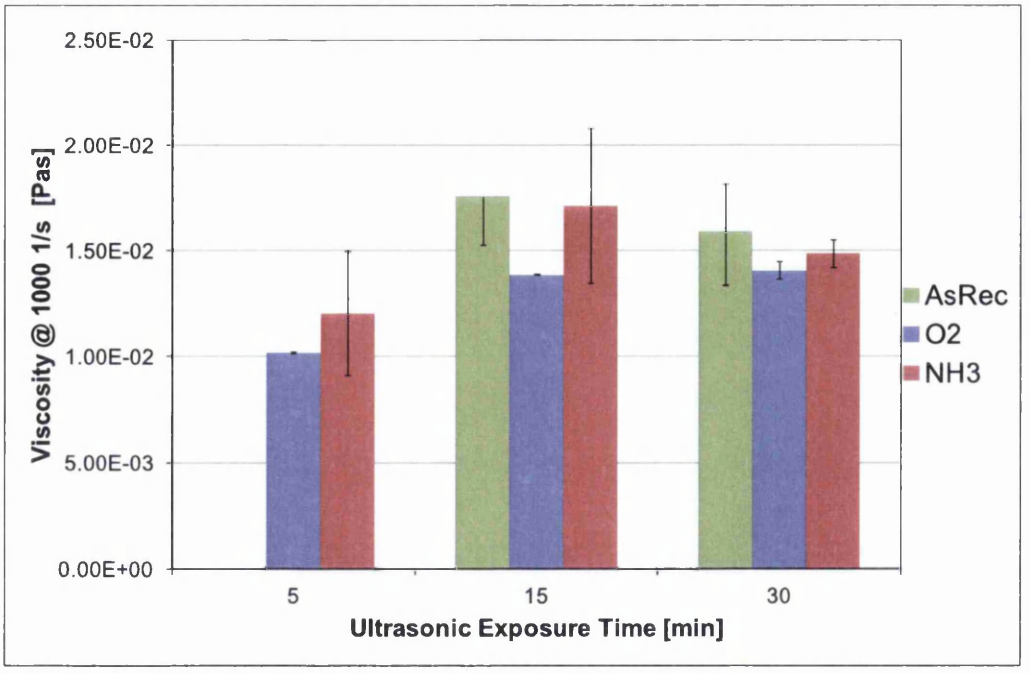

Figure 5.4.3: Viscosity of 2wt% MWCNT ink after different probe sonication exposure times. Control sample and functionalised CNTs are shown.

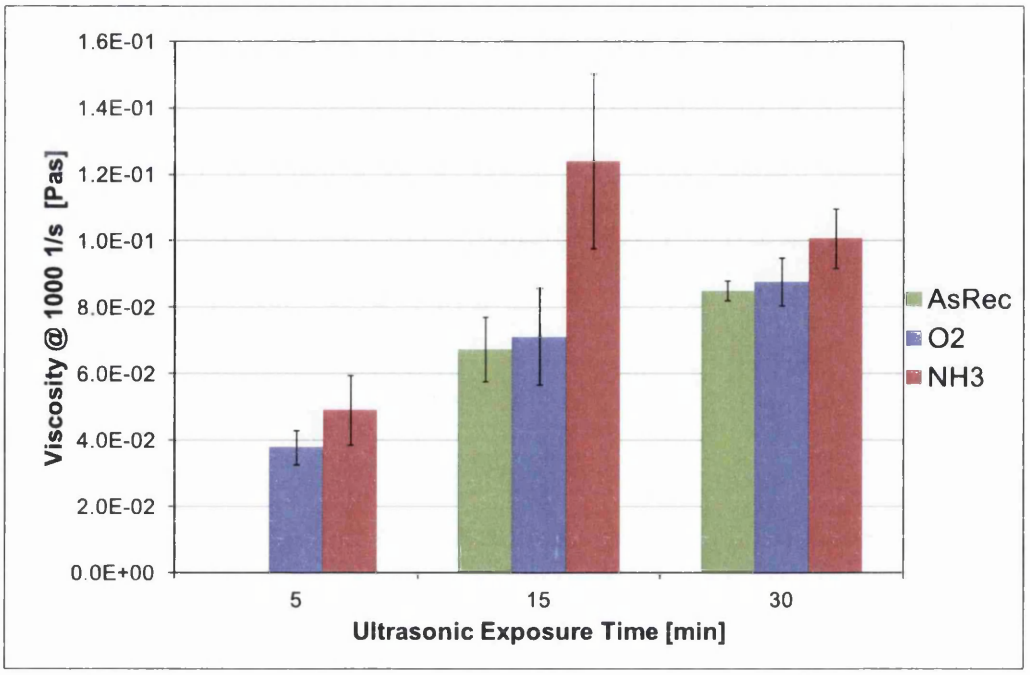

Figure 5.4.4: Viscosity of 4wt% MWCNT ink after different probe sonication exposure times. Control sample and functionalised CNTs are shown.

5.4.1.2 Effect of CNT Functionality at Varying Concentrations

Figures 5.4.5 to 5.4.7 show the Newtonian regime viscosities of the ink samples after varying CNT functionality and concentration.

After 5min ultrasonic mixing (Figure 5.4.5) it can be observed that the NH3 samples show similar viscosities to the O2 samples. Increasing CNT concentration results in a significant increase in viscosity. No results are available for the AsRec samples for reasons described above.

With further sonication, for 15min (Figure 5.4.6) it can be seen that at lower concentrations CNT functionality has little effect upon the viscosity. However at 4wt% the NH3 sample has a significantly higher viscosity. This trend is also seen after 30min sonication (Figure 5.4.7).

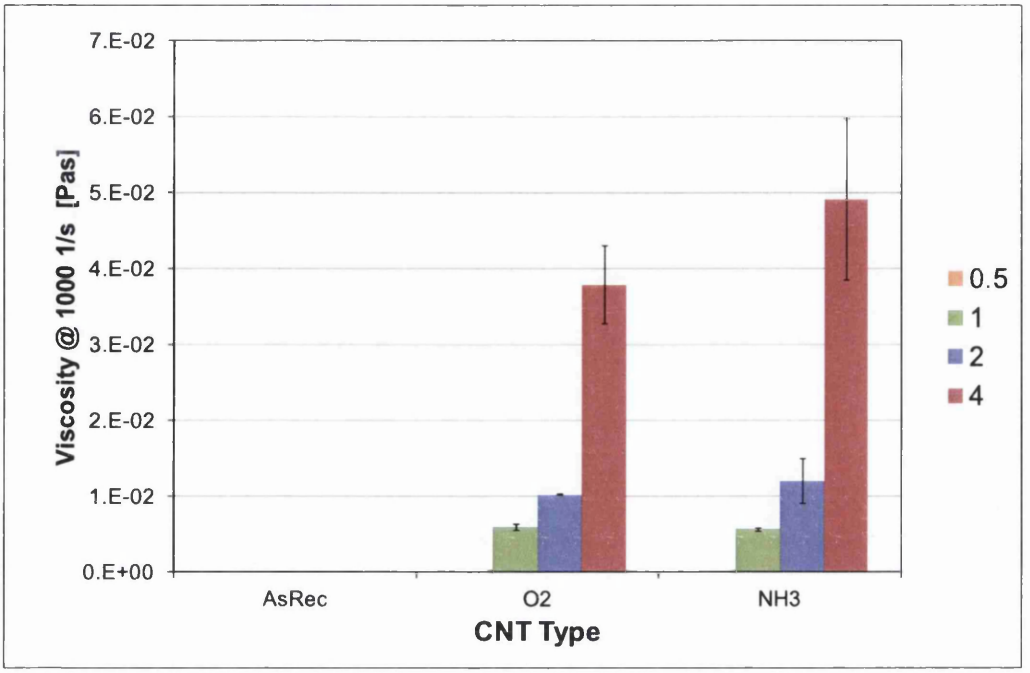

Figure 5.4.5: Viscosity of MWCNT ink after probe sonication for 5 minutes at varying CNT functionalities. CNT concentrations of 0.5, 1, 2 and 4wt% are shown.

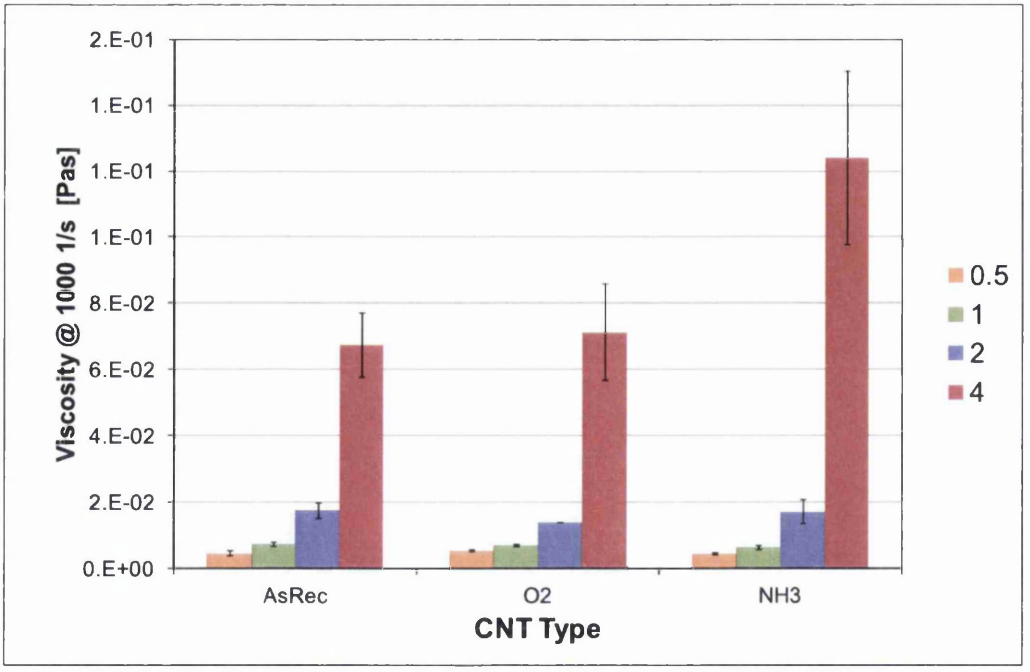

Figure 5.4.6: Viscosity of MWCNT ink after probe sonication for 15 minutes at varying CNT functionalities. CNT concentrations of 0.5, 1, 2 and 4wt% are shown.

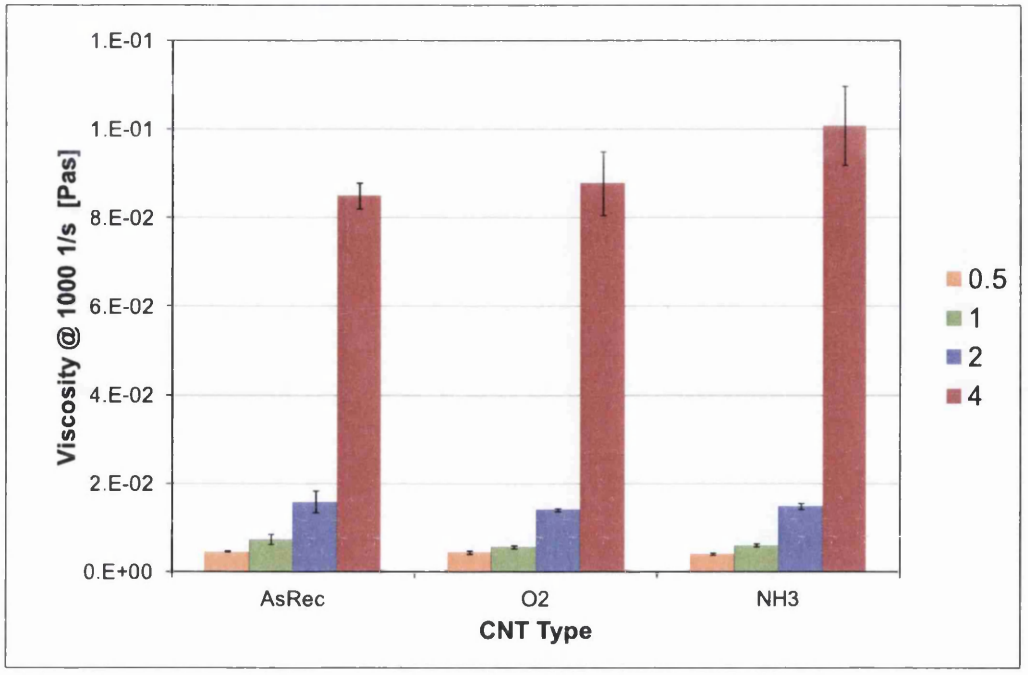

Figure 5.4.7: Viscosity of MWCNT ink after probe sonication for 30 minutes at varying CNT functionalities. CNT concentrations of 0.5, 1, 2 and 4wt% are shown.

5.4.1.3 Effect of CNT Concentration at Varying Ultrasonic Exposure Times

Figures 5.4.8 to 5.4.10 show the Newtonian regime viscosities of the ink samples after varying CNT concentration and functionality.

For the AsRec samples shown in Figure 5.4.8 it is clear that viscosity increases with CNT concentration, as observed in all samples. Viscosity magnitude does not have a significant dependence upon mixing time until concentrations reach 4wt% where 30min of mixing results in a higher viscosity than at 15min.

Similar trends are seen when the O2 CNT sample is used within the ink (Figure 5.4.9). At 0.5 and 1wt% the viscosities are of similar magnitude for all mixing times. However when concentrations increase to 2wt% the 15 and 30min samples show higher viscosity magnitudes, and this change in viscosity increases further at 4wt%. It also appears that at 4wt% concentration the 30min mixed sample shows higher viscosity than the 15min sample, however the data is not conclusive.

The NH3 CNT sample shows similar trends to the O2 sample (Figure 5.4.10), with viscosities independent of mixing time at low concentrations. At higher concentrations higher mixing times result in higher viscosities, with the 15min mixing time samples

appearing to show higher viscosities than the 30min mixing times. This the opposite of the O2 sample, however the data is not conclusive due to the high standard deviations.

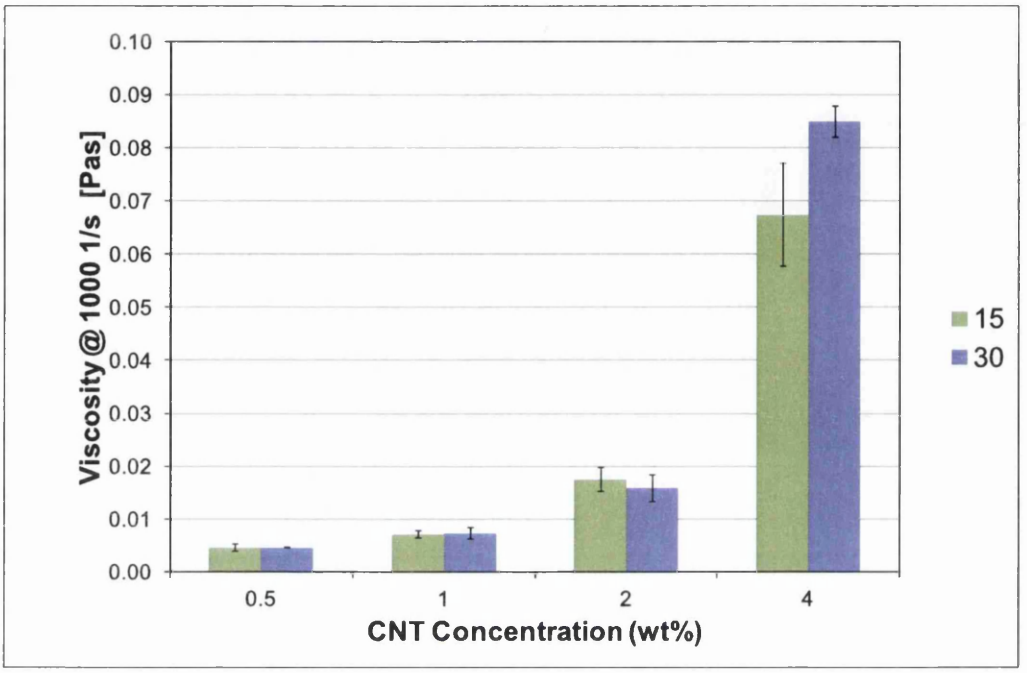

Figure 5.4.8: Viscosity of AsRec MWCNT ink at varying CNT concentrations. Samples exposed to probe sonication for 15 and 30 minutes are shown.

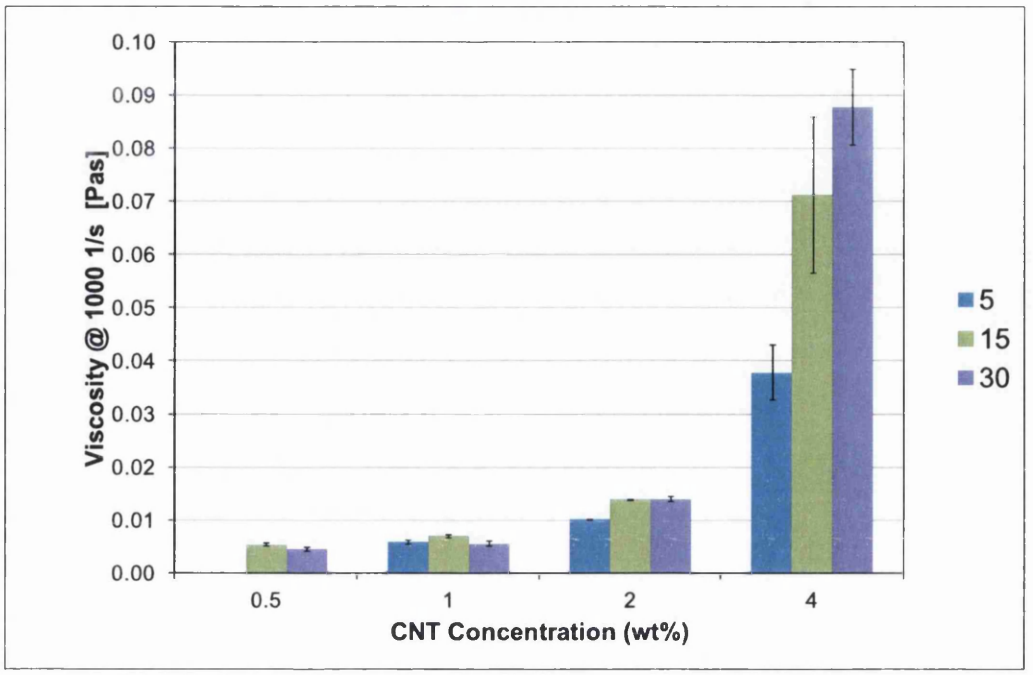

Figure 5.4.9: Viscosity of O2 MWCNT ink at varying CNT concentrations. Samples exposed to probe sonication for 5, 15 and 30 minutes are shown.

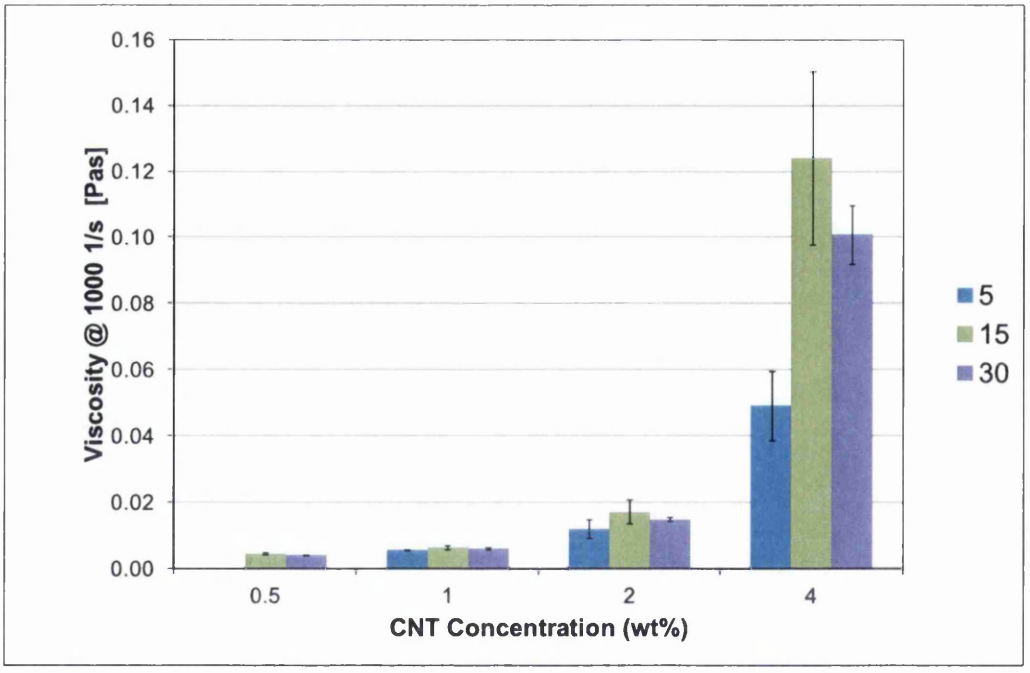

Figure 5.4.10: Viscosity of NH3 MWCNT ink at varying CNT concentrations. Samples exposed to probe sonication for 5, 15 and 30 minutes are shown.

5.4.1.4 Newtonian Viscosity Magnitude Discussion

Initial analysis focussed on the effect of ultrasonic exposure time upon the final Newtonian regime viscosity of the inks (section 5.4.1.1). Ultrasonic exposure time is not observed to have a significant effect on ink viscosity at low (0.5 and 1wt%) CNT concentrations. At 2wt% an increase in ultrasonic exposure time from 5 to 15min results in an increase in viscosity. Further sonication does not appear to significantly change viscosity. This is likely due to the increase in agglomeration breakdown due to the higher density of CNTs within the ink. This change in the behaviour of the ink over 2wt% correlates with the results seen by Pötschke *et al.*[70] who observed a significant rheological change in MWCNT composites at 2wt%, where the rate of increase in viscosity increased. At 4wt% the change in viscosity with mixing time is more pronounced, with viscosity magnitudes increasing from 15 to 30min mix times for the AsRec CNTs, but not significantly different for the O2 CNTs. This suggests the 'critical mixing time' proposed by Huang *et al.*[12] has been achieved for the O2 CNTs but not the AsRec, implying that the lack of functionalisation results in higher energies being required for dispersal. The NH3 CNTs also show a maximum viscosity implying that the 'critical mixing time' has been achieved, however it can also be noted that the viscosity after 30min mixing is lower than after 15min. This correlates with results seen by Cotiuga *et al.*[11] who saw a viscosity maximum with respect to sonication time and concluded that the decrease in viscosity was due to CNT damage caused by excessive sonication.

Further analysis focussed on the effect of CNT functionality upon the final Newtonian regime viscosity of the inks (section 5.4.1.2). For the AsRec CNT sample it was clear that 5min of sonication was not sufficient to give a homogeneous dispersion due to the large agglomerate sizes causing inconsistent results. This implies further that the AsRec CNT require higher mixing energies for dispersion. The rate of increase of viscosity with concentration appears higher for the NH3 samples than the AsRec and O2 CNTs. This non linear rate of viscosity increase at higher concentrations was also observed experimentally by Huang *et al.*[12] which is explained by the formation of an unstable elastic network and is indicative of a 'mechanical percolation threshold' being reached. This increase in the rate of change of viscosity observed in the NH3 CNT based ink samples may indicate a lower mechanical percolation threshold than the O2 or AsRec samples. This could be due to the decreased degree of functionalisation compared to the O2 sample (see Section 5.2), as excess functionalisation is known to cause tube shortening[41;42], resulting in an increase in the percolation threshold. This would also explain the observation that the NH3 sample based inks show the highest

viscosity magnitudes at higher CNT concentrations. This is because if the CNTs are longer the aspect ratio of the rod like structures is higher, which is known to result in higher viscosities[95].

Final analysis focussed on the effect of CNT concentration upon the final Newtonian regime viscosity of the inks (section 5.4.1.3). It was observed that viscosity increases proportionally to CNT concentration, an intuitive result that is common for particle suspensions[94–96]. The dependence upon a combination of CNT concentration and sonication time is further highlighted, with viscosity magnitudes tending to be similar with respect to mixing time until higher concentrations where significant differences are seen, especially at 4wt%, as previously discussed.

5.4.2 Ink Surface Tension

5.4.2.1 Effect of Ultrasonic Exposure Time With Varying CNT Functionality

Figures 5.4.11 to 5.4.14 show the surface tensions of the ink samples after varying ultrasonic probe exposure times and CNT functionality. At 0.5wt% CNT concentration (Figure 5.4.11) no clear dependence on sonication time or CNT functionality is visible. At 1wt% the surface tension measurements seem to stabilise with respect to CNT type at higher mixing times. This trend is not seen at higher concentrations of 2 and 4wt% (Figures 5.4.13 and 5.4.14 respectively), with no significant effect on the surface tension due to the variables tested visible.

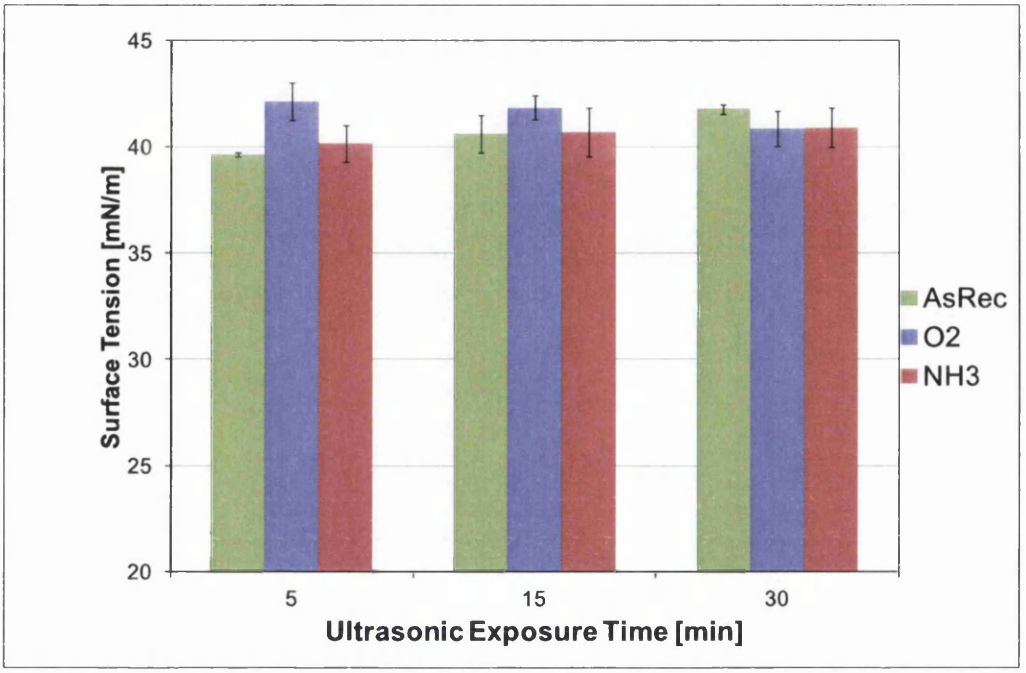

Figure 5.4.11: Surface tension of 0.5wt% MWCNT ink after different probe sonication exposure times. Control sample and functionalised CNTs are shown.

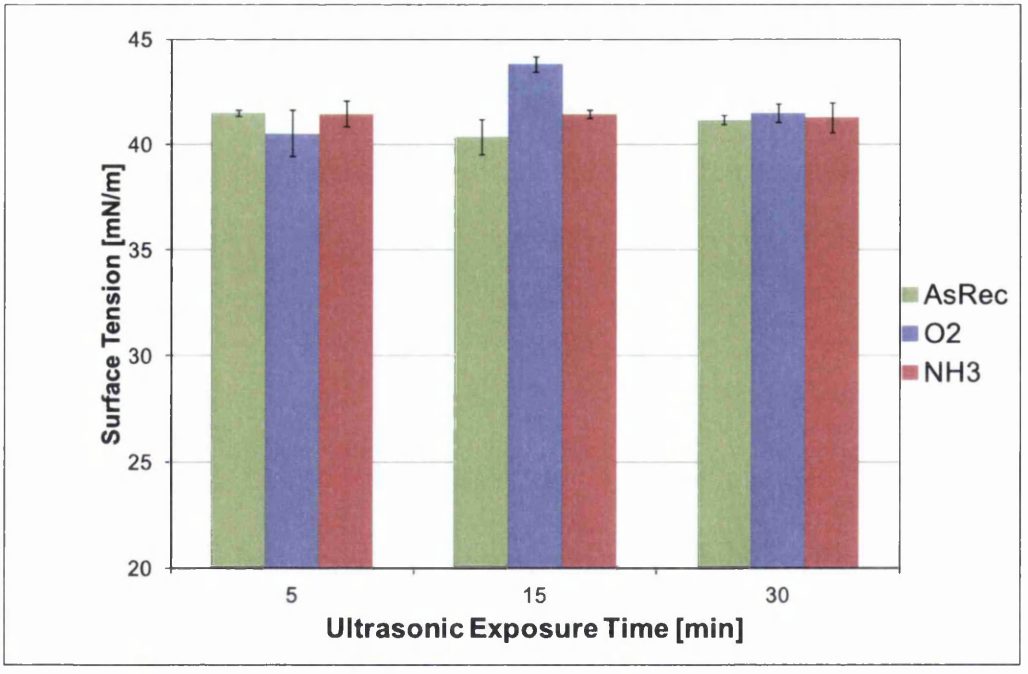

Figure 5.4.12: Surface tension of 1wt% MWCNT ink after different probe sonication exposure times. Control sample and functionalised CNTs are shown.

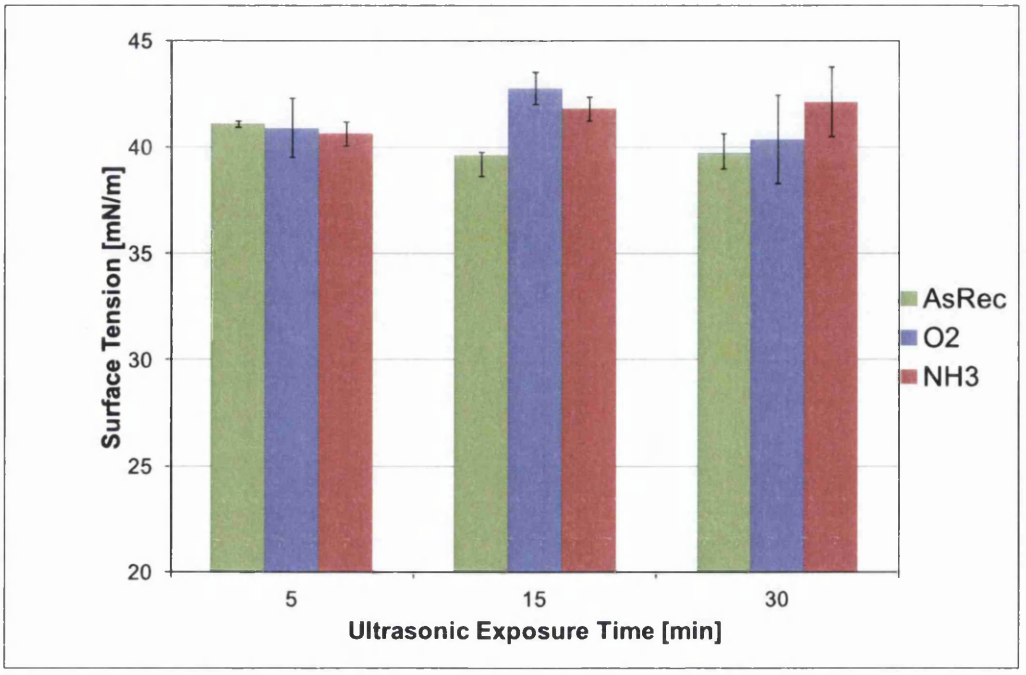

Figure 5.4.13: Surface tension of of 2wt% MWCNT ink after different probe sonication exposure times. Control sample and functionalised CNTs are shown.

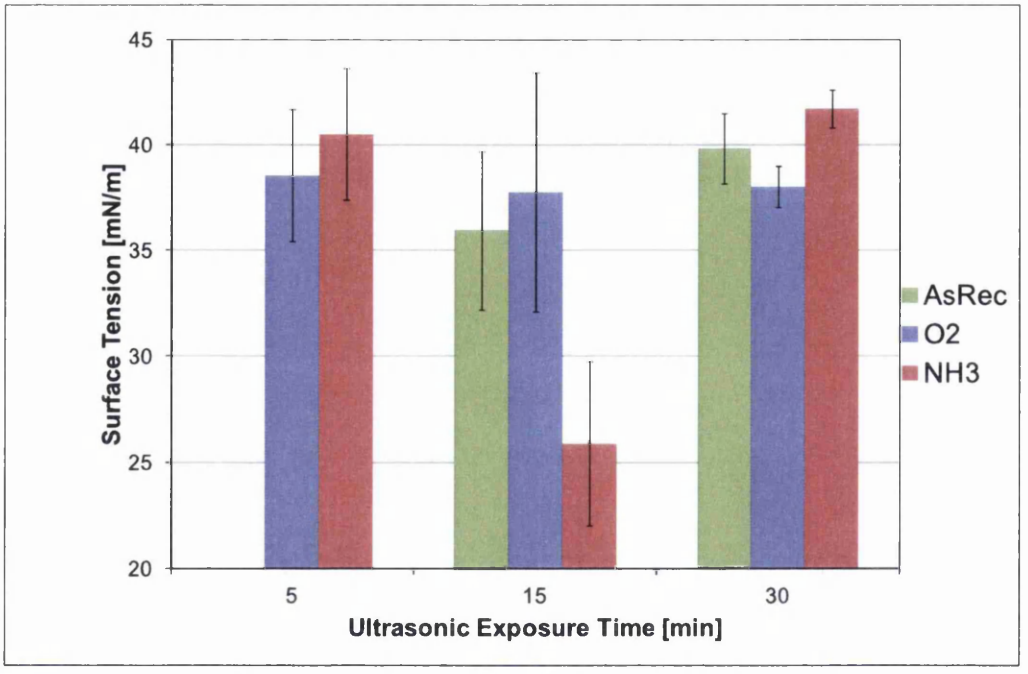

Figure 5.4.14: Surface tension of 4wt% MWCNT ink after different probe sonication exposure times. Control sample and functionalised CNTs are shown.

5.4.2.2 Effect of CNT Functionality at Varying Concentrations

Figures 5.4.15 to 5.4.17 show the surface tensions of the ink samples after varying CNT functionality and concentration. Still no significant dependence of the magnitude of the surface tension upon the tested variables is visible. After 5min of ultrasonic mixing (Figure 5.4.15) the standard deviation of the results from the highest concentration inks are higher than at lower concentrations, this trend is also visible after 15min mixing (Figure 5.4.16) but not after 30min (Figure 5.4.17). NH3 CNT samples appear to show a more stable surface tension magnitude irrespective of mixing time or concentration.

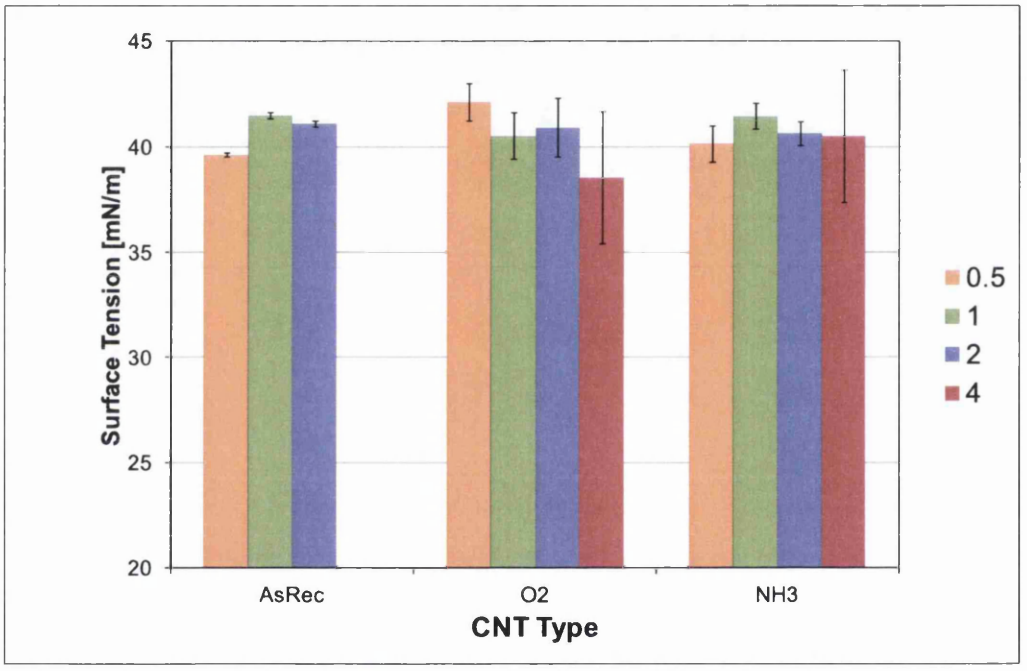

Figure 5.4.15: Surface tension of MWCNT ink after probe sonication for 5 minutes at varying CNT functionalities. CNT concentrations of 0.5, 1, 2 and 4wt% are shown.

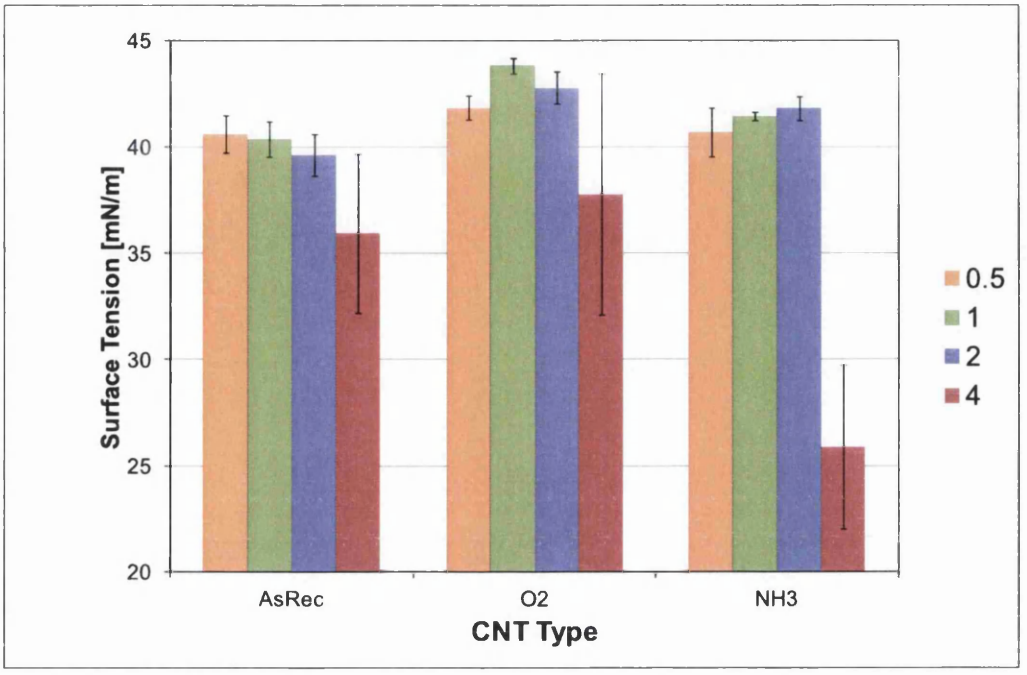

Figure 5.4.16: Surface tension of MWCNT ink after probe sonication for 15 minutes at varying CNT functionalities. CNT concentrations of 0.5, 1, 2 and 4wt% are shown.

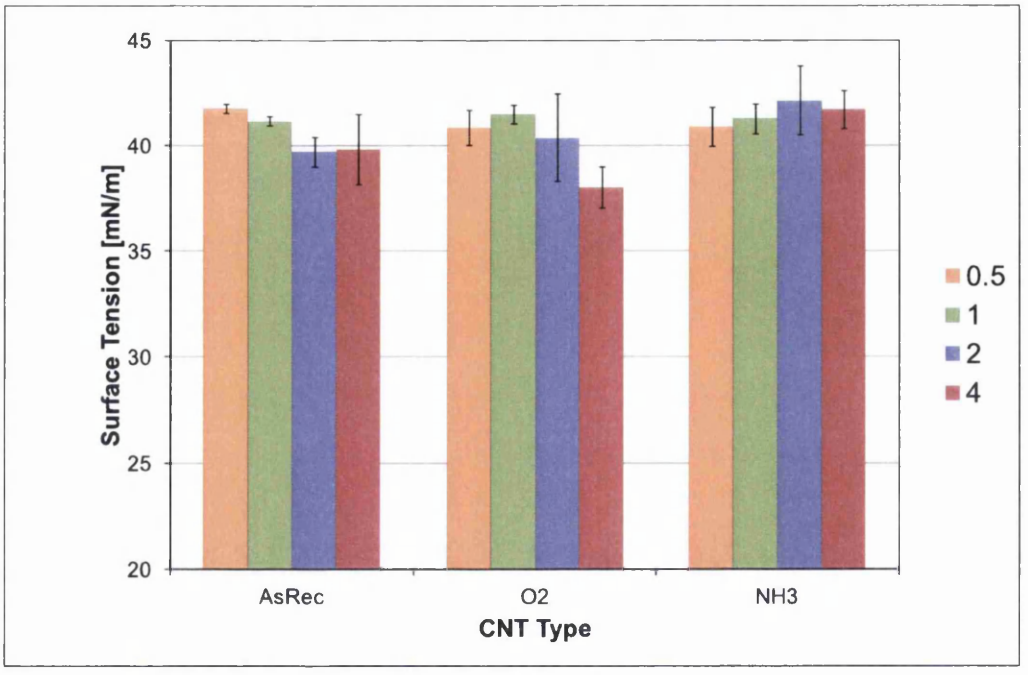

Figure 5.4.17: Surface tension of MWCNT ink after probe sonication for 30 minutes at varying CNT functionalities. CNT concentrations of 0.5, 1, 2 and 4wt% are shown.

5.4.2.3 Effect of CNT Concentration at Varying Ultrasonic Exposure Times

Figures 5.4.18 to 5.4.20 show the surface tensions of the ink samples after varying CNT concentration and functionality. No significant trends are visible in the graphs, however higher standard deviations at higher CNT concentrations are observed.

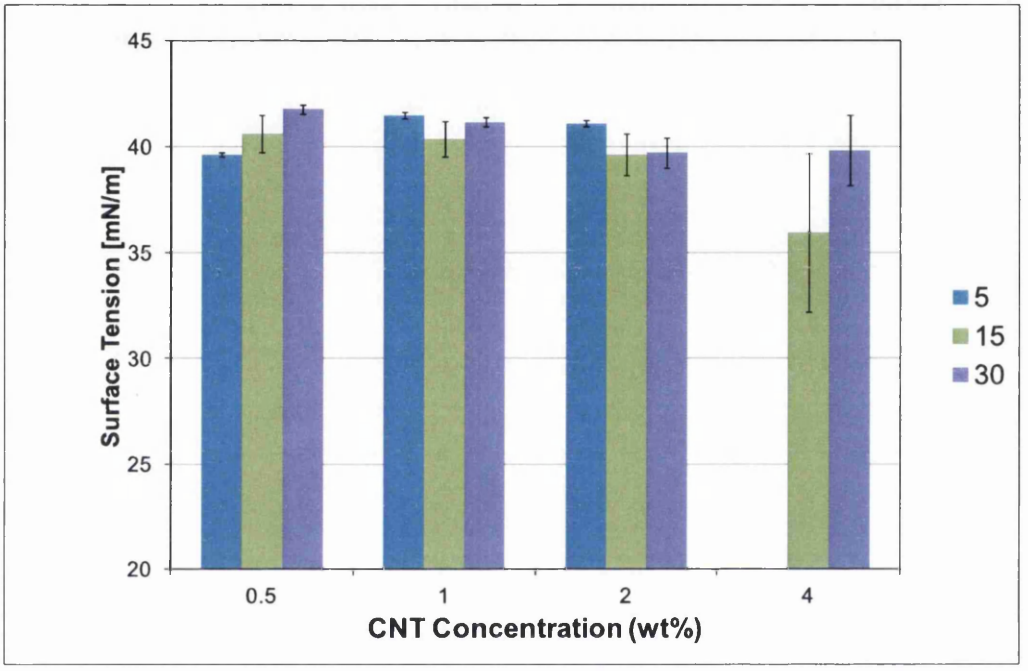

Figure 5.4.18: Surface tension of AsRec MWCNT ink at varying CNT concentrations. Samples exposed to probe sonication for 15 and 30 minutes are shown.

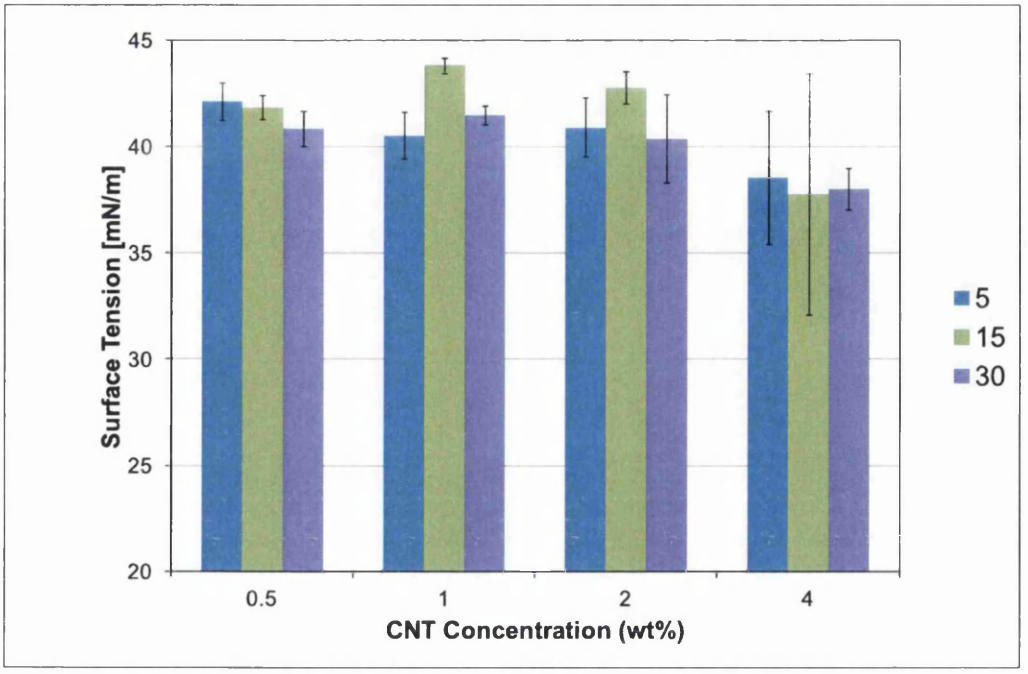

Figure 5.4.19: Surface tension of O2 MWCNT ink at varying CNT concentrations. Samples exposed to probe sonication for 15 and 30 minutes are shown.

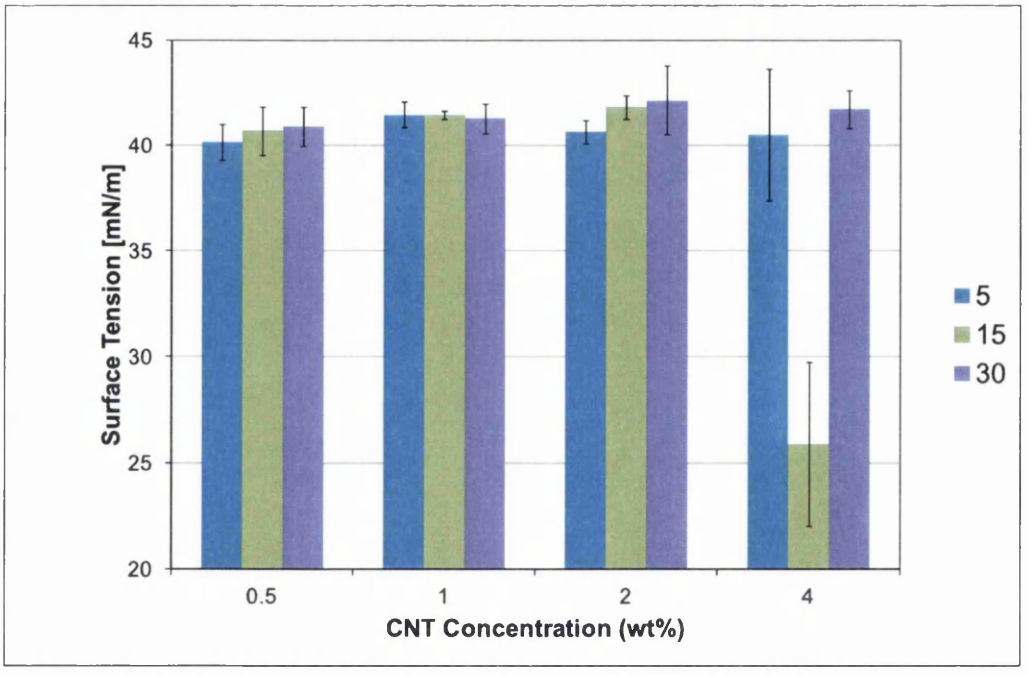

Figure 5.4.20: Surface tension of NH3 MWCNT ink at varying CNT concentrations. Samples exposed to probe sonication for 15 and 30 minutes are shown.

5.4.2.4 Ink Surface Tension Discussion

Initial analysis focussed on the effect of ultrasonic exposure time upon the average surface tension of the inks (section 5.4.2.1). No dependence on sonication time is observed, however higher mixing times appear to stabilise surface tension results but the data is not conclusive. This implies improved dispersion homogeneity.

Further analysis focussed on the effect of CNT functionality upon the average surface tension of the inks (section 5.4.2.2). No significant dependence on CNT functionality is observed, indicating that the covalent functionalisation does not affect the surface tension of dispersions. NH3 suspensions appear to show improved stability with respect to surface tension magnitude which may be indicative of improved dispersion homogeneity.

Final analysis focussed on the effect of CNT concentration upon the average surface tension of the inks (section 5.4.2.3). No significant dependence upon CNT concentration is observed. An increase in surface tension variability with increasing CNT concentration is observed, especially at lower mixing times indicating that increasing CNT concentration requires a corresponding increase in mixing time for homogeneous dispersion.

5.4.3 Printed Film Transparency

5.4.3.1 Effect of Ultrasonic Exposure Time With Varying CNT Functionality

Figures 5.4.21 to 5.4.24 show the percentage light transmission through the coated film samples after varying ultrasonic probe exposure times and CNT functionality.

At 0.5wt% CNT concentration (Figure 5.4.21) a trend of decreasing transmission with increasing ultrasonic exposure time is visible for all CNT functionalities, but the effect is small. All CNT types show similar transmission magnitudes.

The effect of decreasing transmission with increasing mixing time becomes more pronounced at 1wt% CNT concentration (Figure 5.4.22). CNT type still has no significant effect upon the transmission of the printed film.

At 2wt% (Figure 5.4.23) the effect of decreasing transmission with increasing mixing time increases, with NH3 samples showing the lowest transmission values of the CNT types at each mixing time. Transmission variability is increased compared to lower concentrations.

At 4wt% concentration (Figure 5.4.24) the trend of decreasing film transmission with respect to time continues for the O2 and NH3 samples, with the latter showing

lower transmission magnitudes than the O2 samples. However the AsRec samples do not follow this trend, with the 5min mix time samples showing similar transmission to the 15min samples.

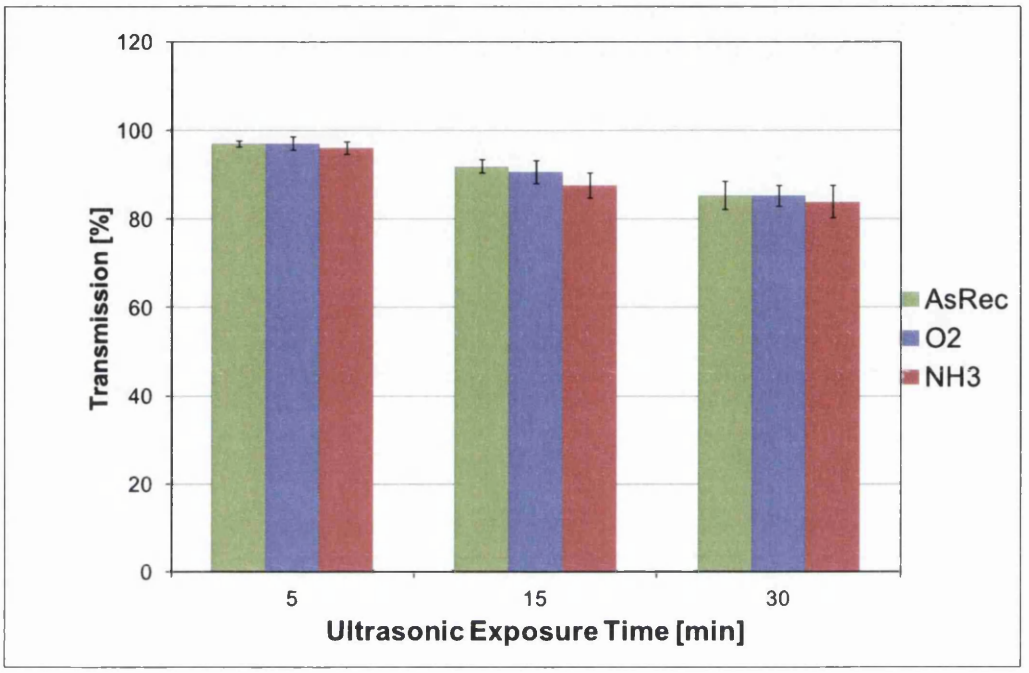

Figure 5.4.21: Transparency of 0.5wt% MWCNT ink after different probe sonication exposure times. Control sample and functionalised CNTs are shown.

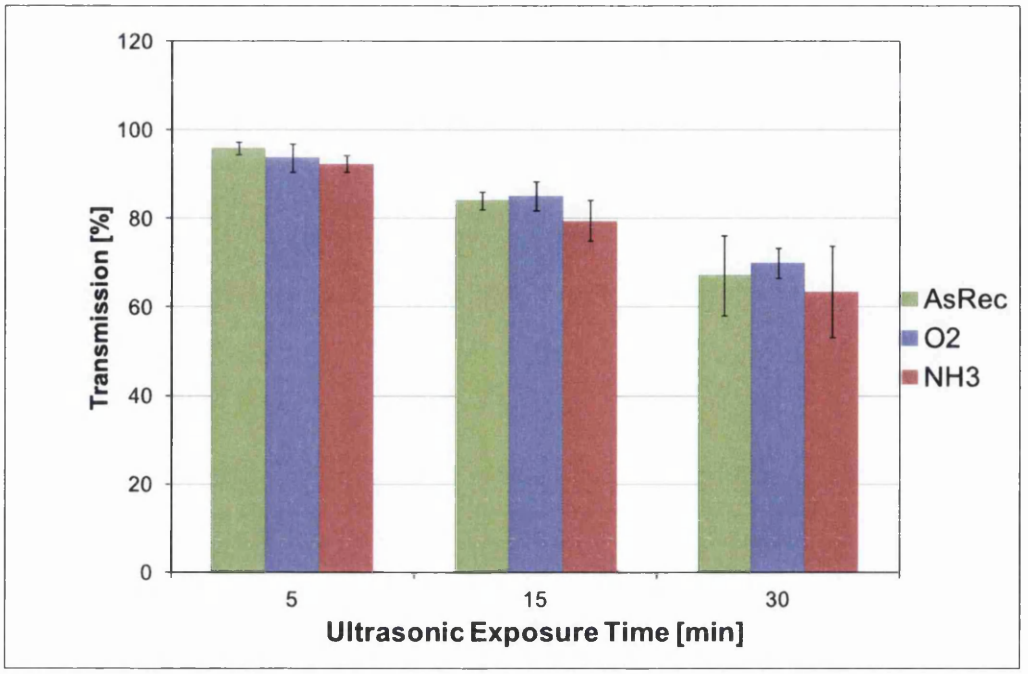

Figure 5.4.22: Transparency of 1wt% MWCNT ink after different probe sonication exposure times. Control sample and functionalised CNTs are shown.

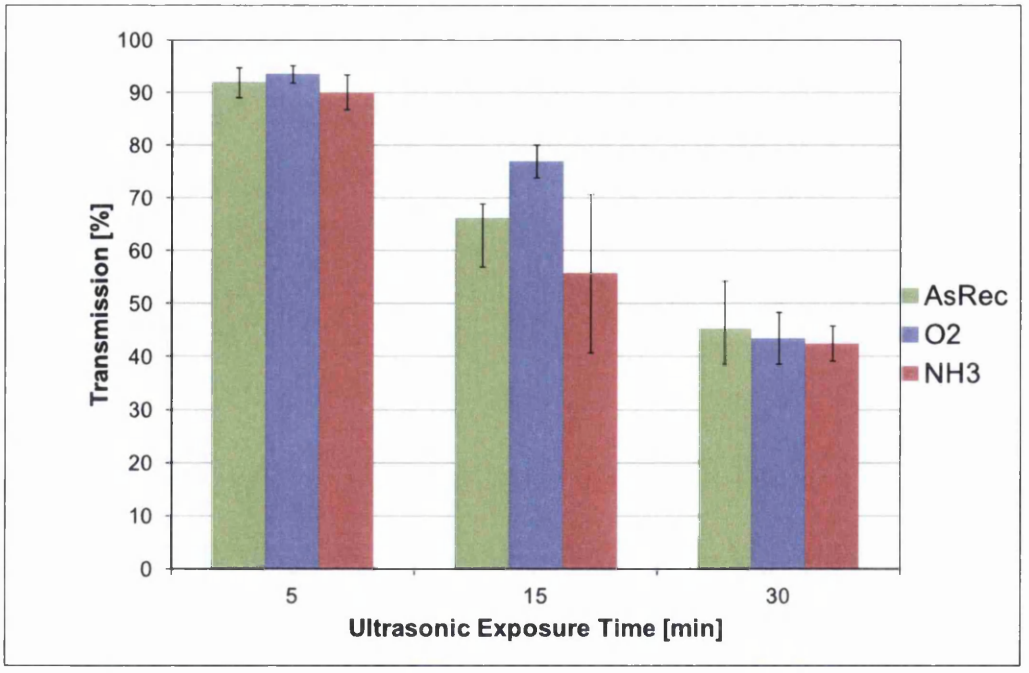

Figure 5.4.23: Transparency of 2wt% MWCNT ink after different probe sonication exposure times. Control sample and functionalised CNTs are shown.

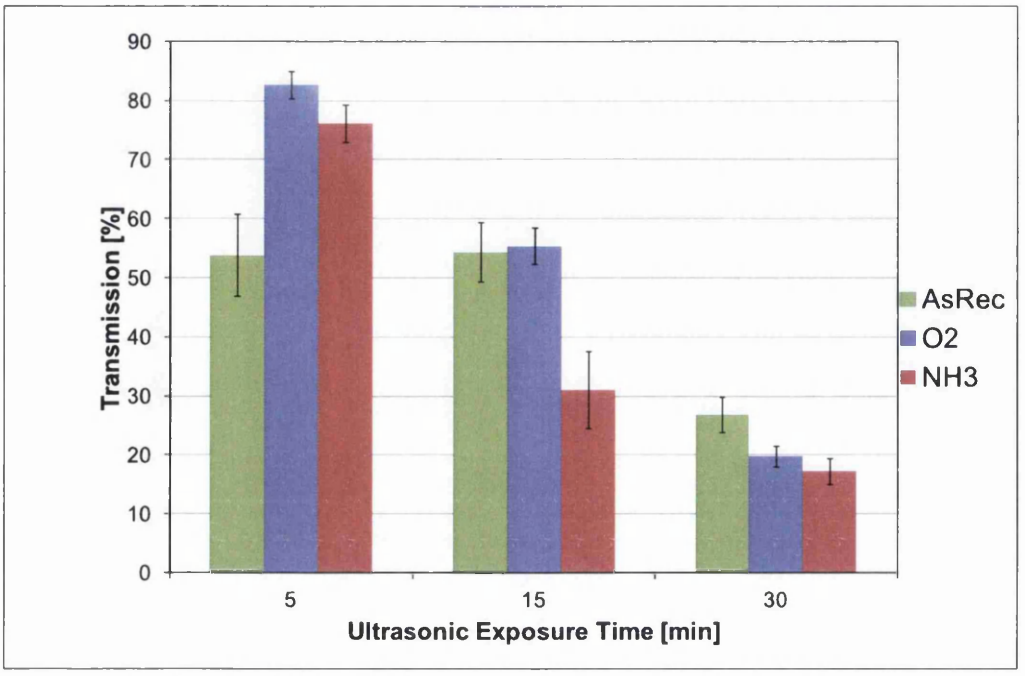

Figure 5.4.24: Transparency of 4wt% MWCNT ink after different probe sonication exposure times. Control sample and functionalised CNTs are shown.

5.4.3.2 Effect of CNT Functionality at Varying Concentrations

Figures 5.4.25 to 5.4.27 show the percentage light transmission through the coated film samples after varying CNT functionality and concentration. After 5min mixing time all CNT concentrations and functionalities show similar transmission percentages except at 4% concentration, where the AsRec sample shows significantly lower transmission.

After longer mixing, this time for 15min in total (Figure 5.4.26), the effect of CNT concentration become more pronounced with higher concentrations causing a bigger drop in percentage transmission compared to after only 5min (Figure 5.4.25). Of all the three CNT functionalities NH3 shows the most significant effect, with the lowest transmission magnitudes at every concentration.

After 30min of mixing (5.4.27) the transmission magnitudes seem to be consistent with respect to CNT type at 0.5, 1 and 2wt%, with AsRec showing higher transmission than the O2 and NH3 samples.

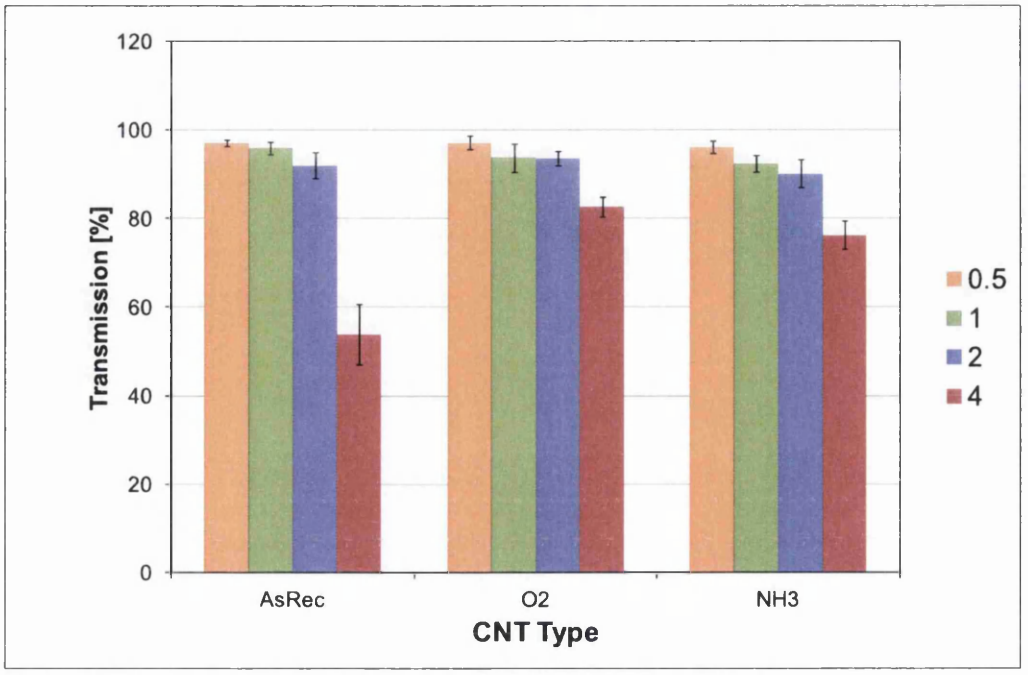

Figure 5.4.25: Transparency of MWCNT ink after probe sonication for 5 minutes at varying CNT functionalities. CNT concentrations of 0.5, 1, 2 and 4wt% are shown.

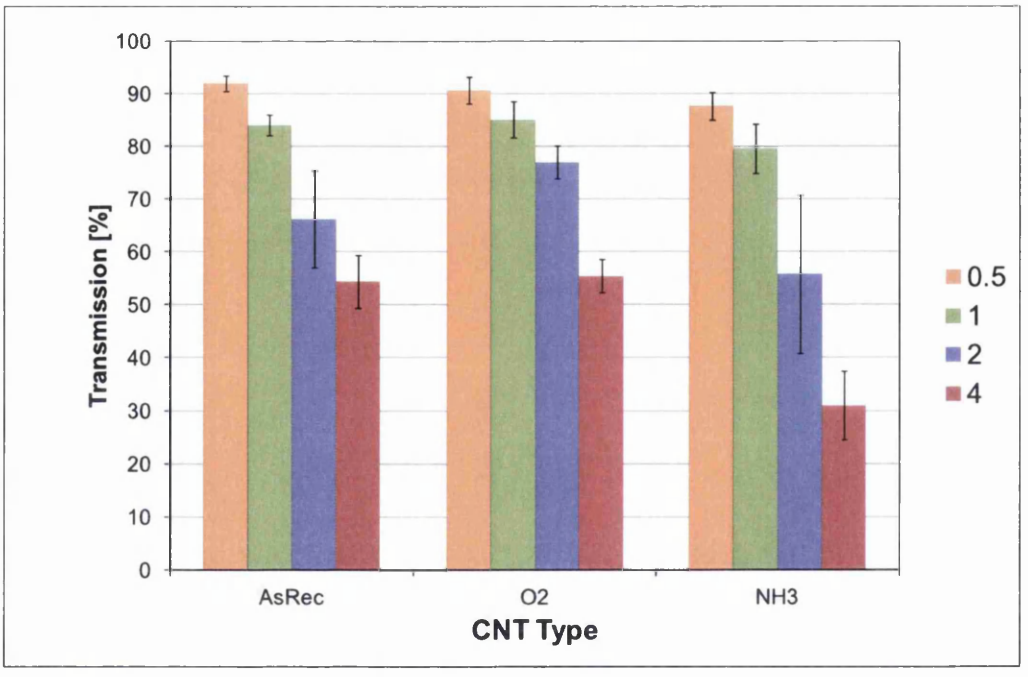

Figure 5.4.26: Transparency of MWCNT ink after probe sonication for 15 minutes at varying CNT functionalities. CNT concentrations of 0.5, 1, 2 and 4wt% are shown.

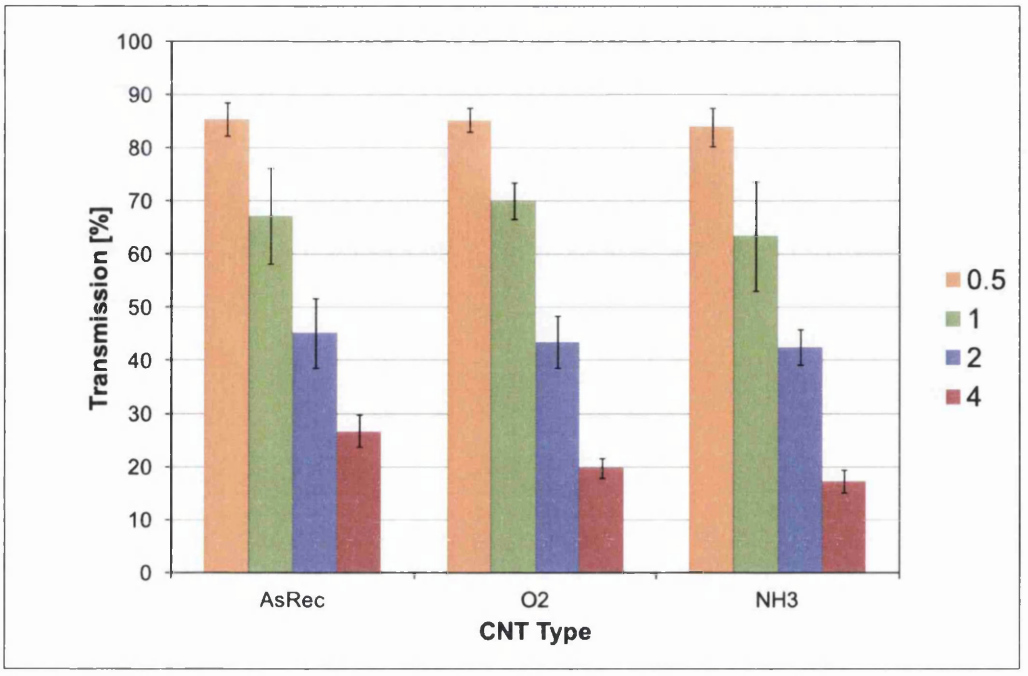

Figure 5.4.27: Transparency of MWCNT ink after probe sonication for 30 minutes at varying CNT functionalities. CNT concentrations of 0.5, 1, 2 and 4wt% are shown.

5.4.3.3 Effect of CNT Concentration at Varying Ultrasonic Exposure Times

Figures 5.4.28 to 5.4.30 show the percentage light transmission through the coated film samples after varying CNT concentration and functionality.

For the AsRec sample (Figure5.4.28) it is clear that ink film transmission decreases with increasing CNT concentration and increasing mixing time. This trend is replicated with the O2 (Figure 5.4.29) and NH3 (Figure 5.4.30) samples, but it can also be noticed that the consistency of the O2 samples appears greatest with respect to the standard deviations shown.

The gradient of the decrease in transmission with respect to mix time appears to increase at higher concentrations for all samples apart from the AsRec sample at 4wt%, where the film samples after 5min mixing show low transmission.

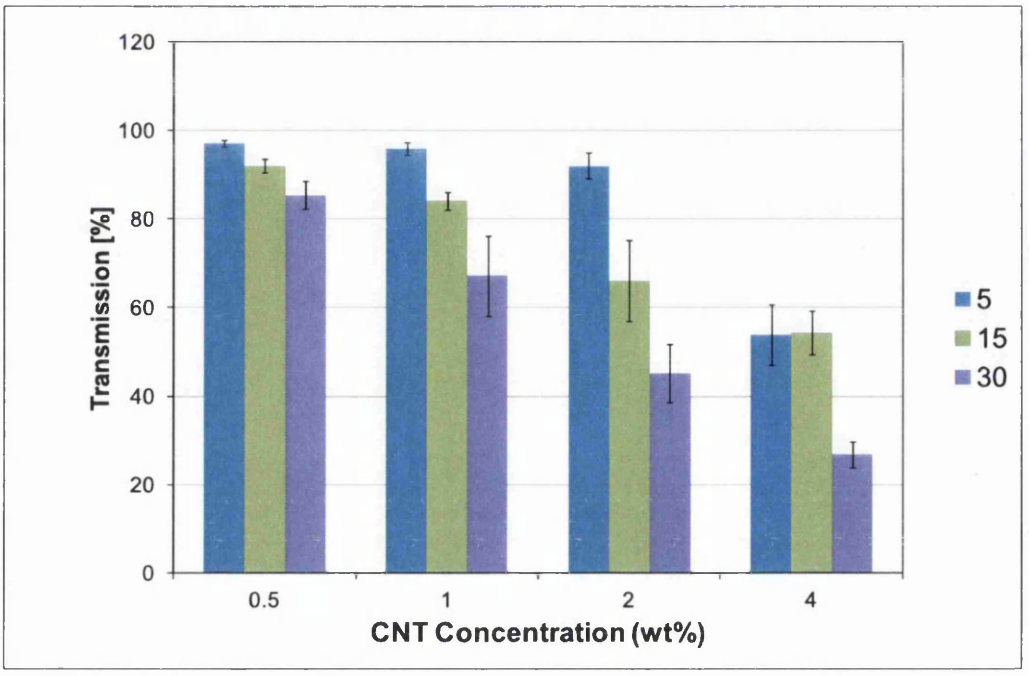

Figure 5.4.28: Transparency of AsRec MWCNT ink at varying CNT concentrations. Samples exposed to probe sonication for 15 and 30 minutes are shown.

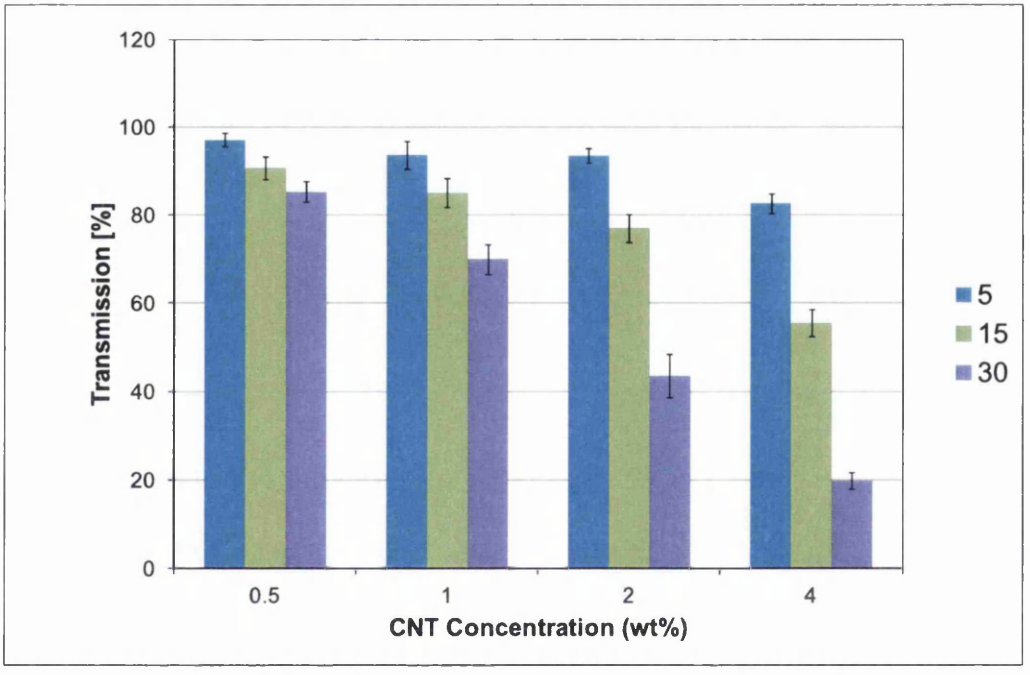

Figure 5.4.29: Transparency of O2 MWCNT ink at varying CNT concentrations. Samples exposed to probe sonication for 15 and 30 minutes are shown.

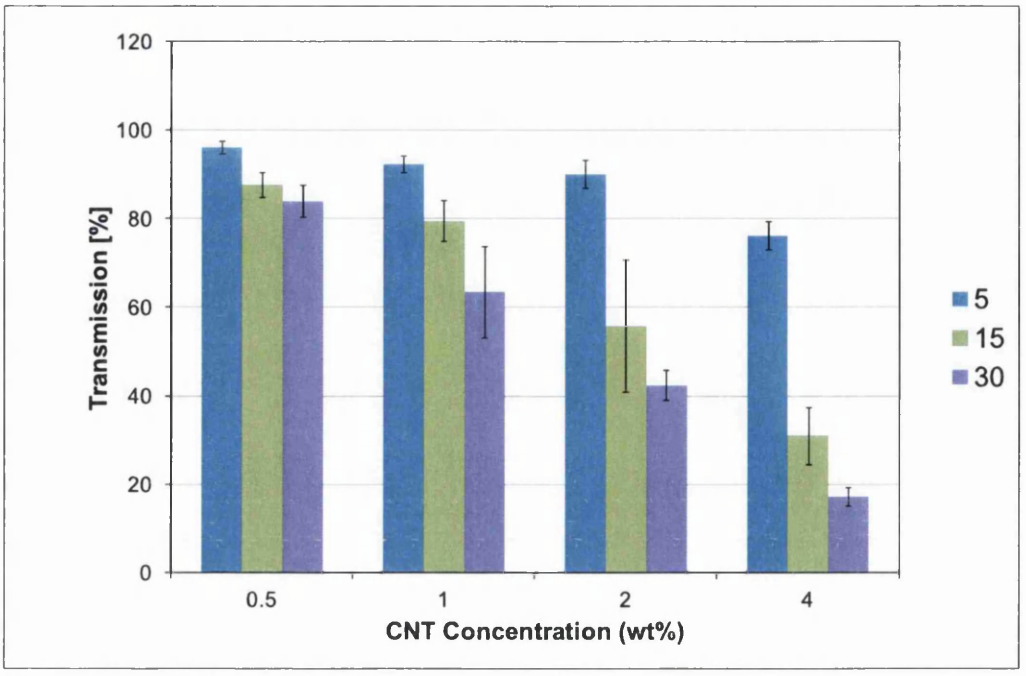

Figure 5.4.30: Transparency of NH3 MWCNT ink at varying CNT concentrations. Samples exposed to probe sonication for 15 and 30 minutes are shown.

5.4.3.4 Printed Film Transparency Discussion

Initial analysis focussed on the effect of ultrasonic exposure time upon the average optical transmission of the coated films (section 5.4.2.1). Increasing sonication time was seen to decrease the transmission through the printed film. This is due to the decrease in agglomerate size caused by the increase in energy applied to the ink. The decrease in agglomerate size results in a more consistent area coverage of CNTs, an effect also proposed in the discussion in section 5.4.1.4. These results appear to verify each other as it is shown in the literature (see section 2.2.1) that sonication results in a decrease in CNT agglomeration size.

Further analysis focussed on the effect of CNT functionality upon the average optical transmission of the coated films (section 5.4.2.2). At low mixing times the CNT functionality has no significant effect upon transmission apart from at high concentrations where the AsRec sample shows low transmission. This result is counter intuitive, and may be due to the poor quality of the film as a result of the inhomogeneity of the ink after insufficient mixing. After further mixing to 15 and 30min the transmission through films made from AsRec and O2 CNT samples remains similar, while the NH3 samples show lower transparency. This may be due to the improved dispersion and corresponding smaller agglomerate size, however the NH3 samples show significantly

lower transmission magnitudes after 30min than 15min. This is likely to be due to the damage to the NH3 CNTs that was theorised from the viscosity data, resulting in amorphous carbon and/or shorter CNTs giving greater area coverage of the film.

Final analysis focussed on the effect of CNT concentration upon the average optical transmission of the coated films (section 5.4.2.3). The higher the CNT concentration the lower the transmission, as a result of the higher density of the CNT films causing an increase in optical absorbance. The rate of decrease in transmission with respect to mixing time increases with respect to CNT concentration. This could be due to the increased number of agglomerates being present in the higher concentration samples, resulting in an increase in deagglomerated structures in the solution at higher mixing times.

5.4.4 Printed Film Sheet Resistivity

5.4.4.1 Effect of Ultrasonic Exposure Time With Varying CNT Functionality

Figures 5.4.31 to 5.4.33 show the average sheet resistivity of the coated film samples after varying ultrasonic probe exposure times and CNT functionality. No data is available for the 0.5wt% concentration or 5 minute ultrasonic agitation time samples due to sheet resistivities being out of the measurable range of the equipment used (>900MΩ/□).

At 1wt% CNT concentration (Figure 5.4.31) sheet resistivities are similar for all CNT functionalities after 15min, with standard deviations high for the AsRec and NH3 samples (note no lower error bar implies deviation above the mean value which cannot be shown on a logarithmic scale). After 30 minutes data still shows high variability in the AsRec sample but O2 and NH3 show higher consistency. The NH3 samples show the lowest sheet resistivity.

At 2wt% concentration (Figure 5.4.32) sheet resistivities are similar for all CNT functionalities after 15 and 30min, with AsRec samples showing high variability. O2 and NH3 samples show lowest sheet resistivities after 30min mixing.

At 4wt% concentration (Figure 5.4.33) the same trends seen at 2wt% are visible, with lower variability for all samples. O2 samples show the highest sheet resistivity after 15min mixing, but AsRec samples are the highest after 30min. NH3 samples consistently show the lowest sheet resistivity.

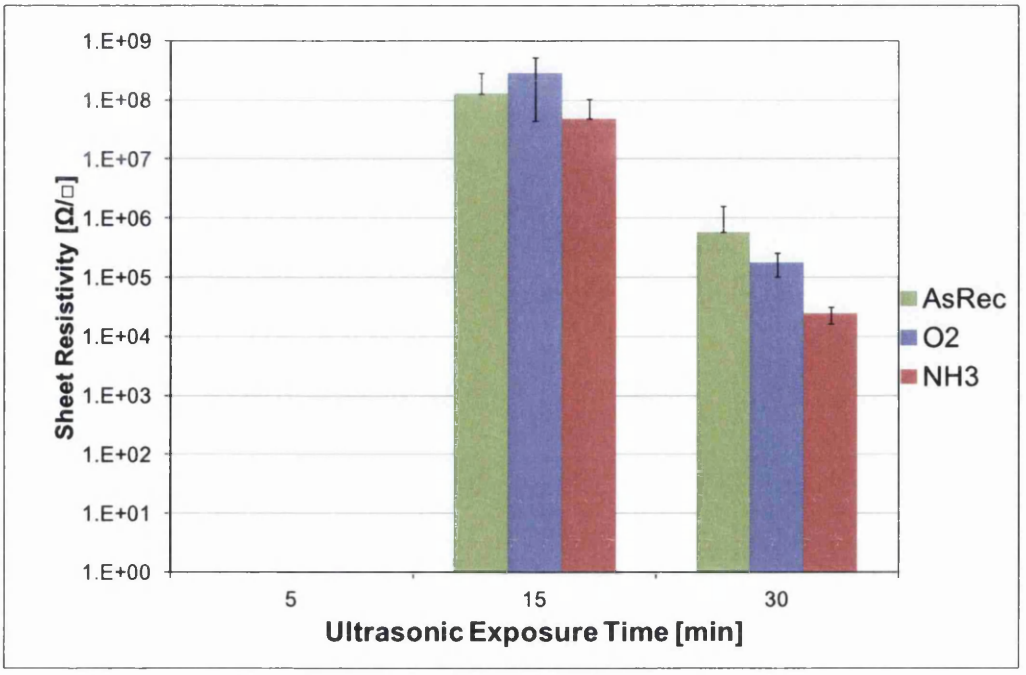

Figure 5.4.31: Sheet resistivity of 1wt% MWCNT ink after different probe sonication exposure times. Control sample and functionalised CNTs are shown.

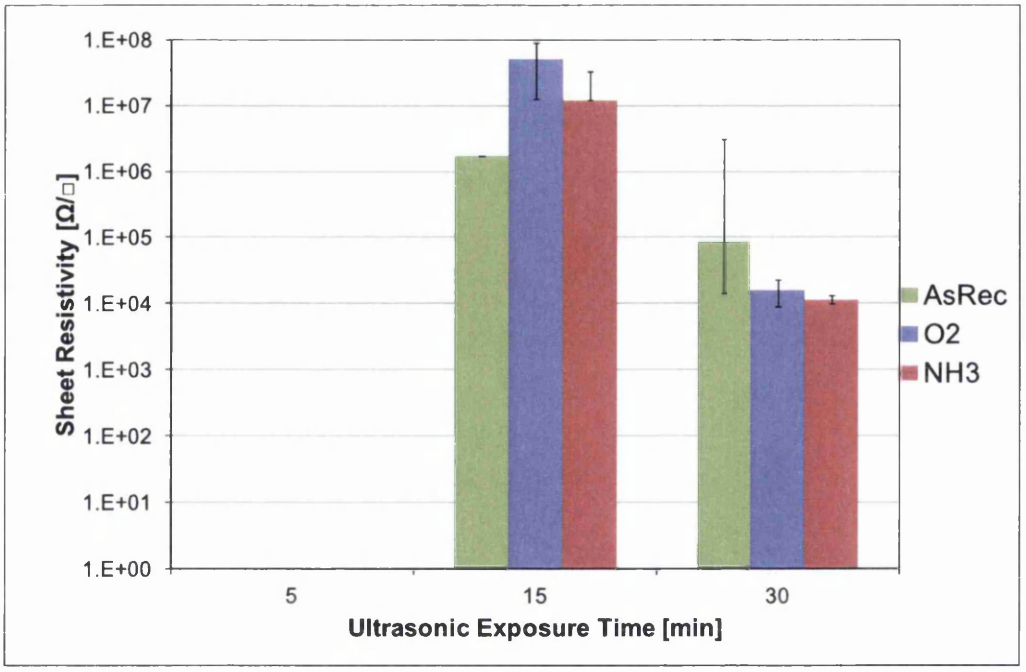

Figure 5.4.32: Sheet resistivity of 2wt% MWCNT ink after different probe sonication exposure times. Control sample and functionalised CNTs are shown.

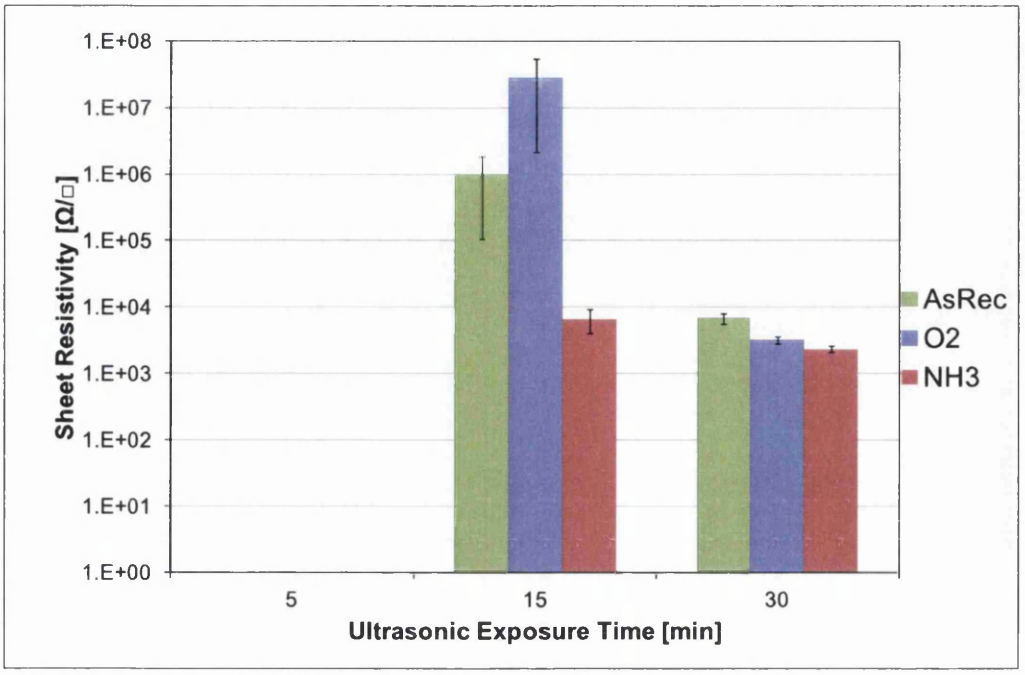

Figure 5.4.33: Sheet resistivity of 4wt% MWCNT ink after different probe sonication exposure times. Control sample and functionalised CNTs are shown.

5.4.4.2 Effect of CNT Functionality at Varying Concentrations

Figures 5.4.34 and 5.4.35 show the average sheet resistivity of the coated film samples after varying CNT functionality and concentration. No data for samples mixed for 5min is available for reasons described above.

After 15min mixing time (Figure 5.4.34) all samples show reduction in sheet resistivity with respect to CNT concentration. Standard deviations are lowest for the O2 functionalised samples.

After 30min mixing time (Figure 5.4.35) all samples show reduction in sheet resistivity with respect to CNT concentration. Standard deviations also decrease with respect to CNT concentration. NH3 samples show the lowest sheet resistivities and standard deviations.

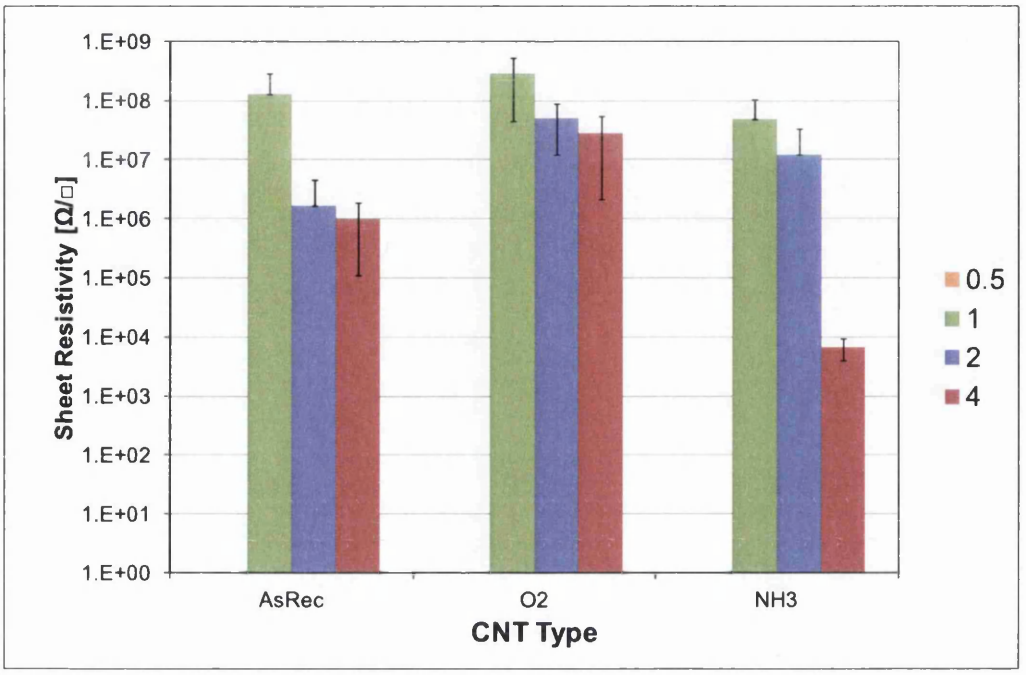

Figure 5.4.34: Sheet resistivity of MWCNT ink after probe sonication for 15 minutes at varying CNT functionalities. CNT concentrations of 0.5, 1, 2 and 4wt% are plotted. No data is available for the 0.5wt% due to values being above measurable range of the equipment.

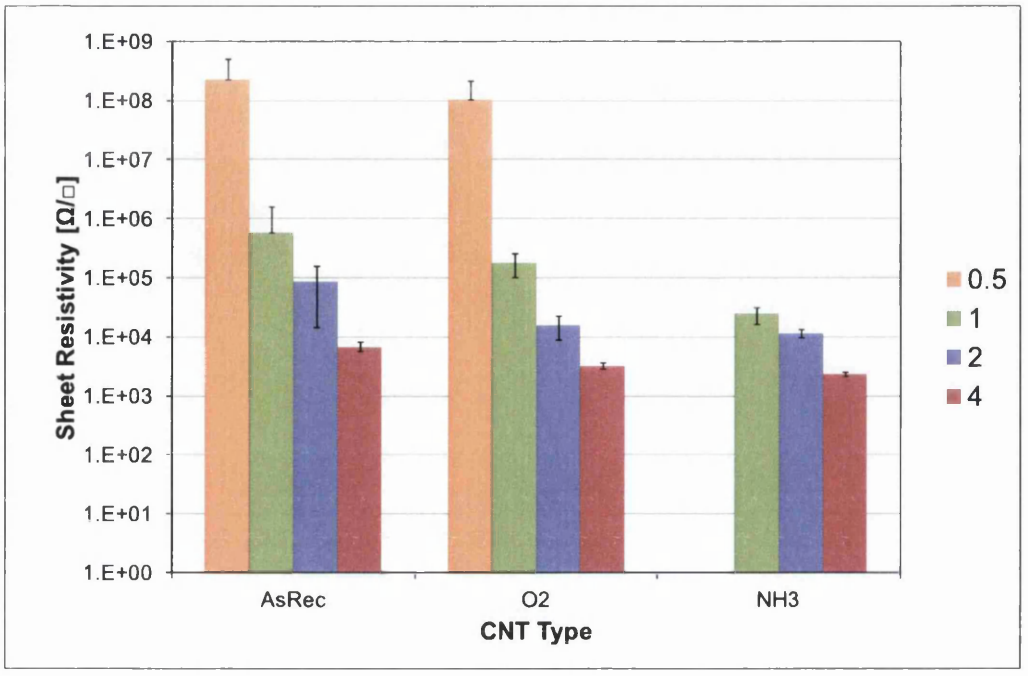

Figure 5.4.35: Sheet resistivity of MWCNT ink after probe sonication for 30 minutes at varying CNT functionalities. CNT concentrations of 0.5, 1, 2 and 4wt% are shown.

5.4.4.3 Effect of CNT Concentration at Varying Ultrasonic Exposure Times

Figures 5.4.36 to 5.4.38 show the average sheet resistivity of the coated film samples after varying CNT concentration and functionality.

The AsRec samples (Figure 5.4.36) only give consistent results for 4wt% concentration at 15min mixing time and 2 and 4wt% at 30min mixing time. Sheet resistivity decreases with increasing CNT concentration and increasing mixing time. Standard deviation of all data points decrease with increasing mixing time.

The O2 samples (Figure 5.4.37) show consistent results for 1, 2 and 4wt% at 15and 30min mixing time. Sheet resistivity decreases with increasing CNT concentration and increasing mixing time. Standard deviation of all data points decrease with increasing mixing time.

The NH3 samples (Figure 5.4.38) show consistent results for 1, 2 and 4wt% at 15and 30min mixing time. Sheet resistivity decreases with increasing CNT concentration and increasing mixing time. Standard deviation of all data points decrease with increasing mixing time. However the rate of decrease in sheet resistivity with respect to CNT concentration after 30min mixture time is relatively low. Also there

is a significant decrease in sheet resistivity for samples mixed for 15min at 4wt%, with little difference between 1 and 2wt%.

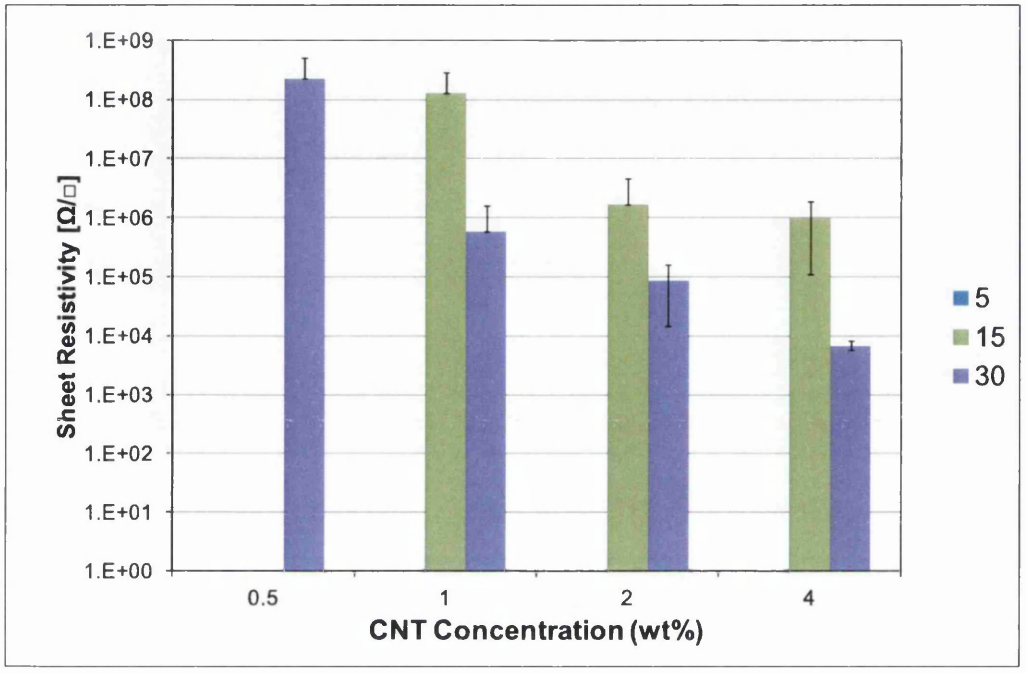

Figure 5.4.36: Sheet resistivity of AsRec MWCNT ink at varying CNT concentrations. Samples exposed to probe sonication for 15 and 30 minutes are shown.

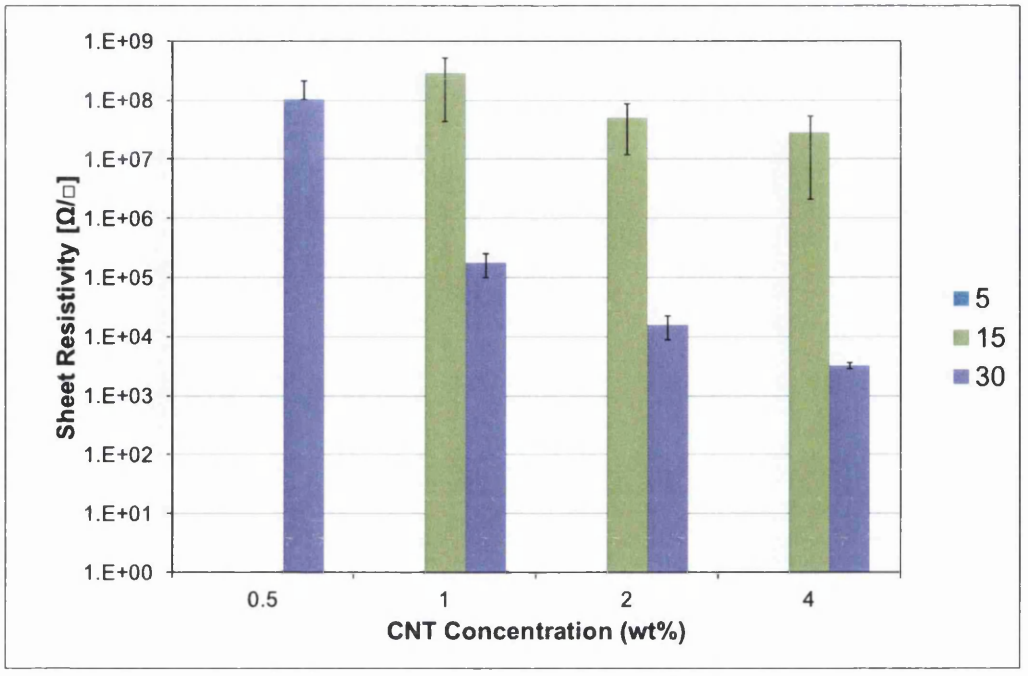

Figure 5.4.37: Sheet resistivity of O2 MWCNT ink at varying CNT concentrations. Samples exposed to probe sonication for 15 and 30 minutes are shown.

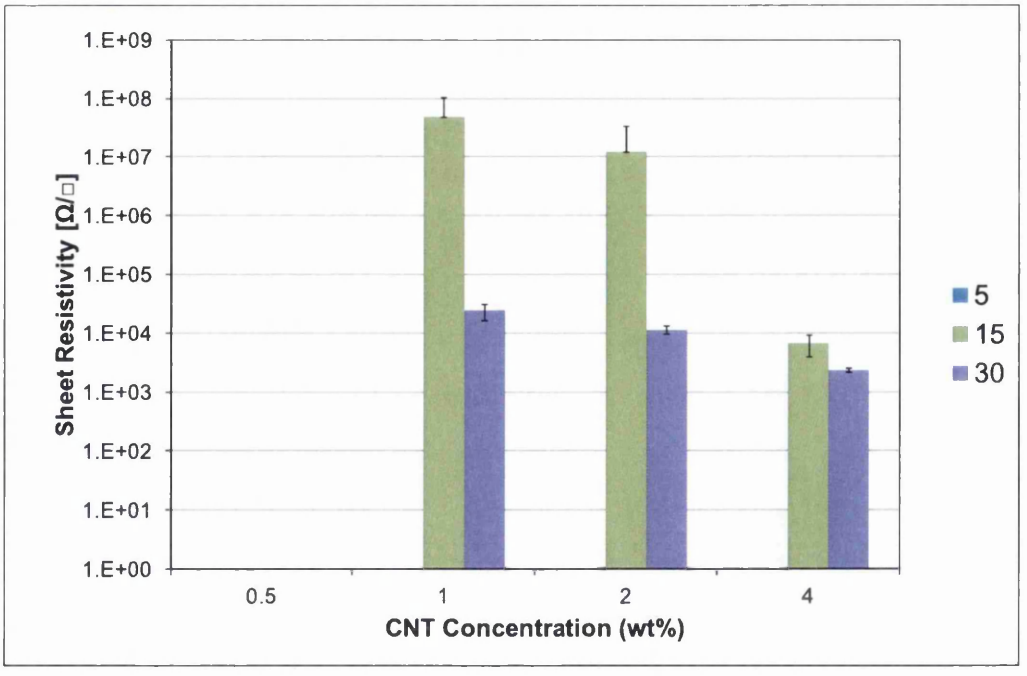

Figure 5.4.38: Sheet resistivity of NH3 MWCNT ink at varying CNT concentrations. Samples exposed to probe sonication for 15 and 30 minutes are shown.

5.4.4.4 Printed Film Sheet Resistivity Discussion

Initial analysis focussed on the effect of ultrasonic exposure time upon the average sheet resistivity of the coated films (section 5.4.2.1). 5min exposure times were insufficient to provide a homogeneous dispersion to form a conductive network, an indication that this is below the critical mixing time proposed by Huang *et al.*[12]. This concurs partially with the viscosity data which was unmeasurable for the AsRec sample after 5min. Increased ultrasonic mixing always resulted in a decrease in sheet resistivity, due to deagglomeration resulting in a higher density and more consistent network forming in the printed film. Data deviation was high for AsRec and NH3 samples after 15min suggesting that the critical mixing time had not been achieved. From the standard deviation data it appears that the critical mixing time has been achieved at 15min for the O2 samples. This indicates higher solubility of the O2 samples, which is in agreement with the conclusions drawn from the viscosity data. After 30min mixing time standard deviations of all samples were reduced, verifying that increased mixing improves film consistency and 30min is above the critical mixing time.

Further analysis focussed on the effect of CNT functionality upon the average sheet resistivity of the coated films (section 5.4.2.2). NH3 samples showed the lowest sheet resistivities at all mixing times and concentrations. This must be due to decreased junction resistance as a result of the functionalisation (see Nirmalraj *et al.*[6]). At 30min when samples appear to have reached the critical mixing time O2 samples show a reduction in sheet resistivity compared to AsRec but higher than the NH3. This suggests that the decrease in junction resistance and improvement in network homogeneity still outweighs the increase in scattering from the defects compared to the unfunctionalised sample, however with respect to the NH3 sample the increase in defects results in an increase in net sheet restivity. As mentioned above, data deviation was low for the O2 sample at 15min mixing, however the significant decrease after further mixing implies that although a consistent network has started to form to allow conduction further sonication is necessary, suggesting that 15min is close to the critical mixing time rather than above. No evidence of CNT damage is visible from the resistivity results, though this may be due to defects lowering junction resistance if CNT damage is not yet severe enough to reduce the percolation threshold significantly.

Final analysis focussed on the effect of CNT concentration upon the average sheet resistivity of the coated films (section 5.4.2.3). No data was available for the 0.5wt% samples indicating that this is below the percolation threshold for these samples to achieve resistances within the measurable range of the equipment. Increasing CNT concentration results in a decrease in sheet resistivity due to the higher densities of

the CNT films produced. Sheet resistivity magnitudes are similar to that seen in literature for MWCNT based inks[90]. The rate of decrease in sheet resistance with respect to concentration appears to be independent of mixing time.

5.5 Conclusions

This chapter has discussed the effect of CNT concentration, CNT functionality and ink mixing time upon the properties of a MWCNT based conductive ink and coated film. The three variables are expected to be dependent, and understanding this dependence is the key to optimisation of CNT based inks.

With respect to CNT concentration it has been seen that an increase in CNT concentration results in an increase in viscosity and a decrease in the optical light transmission and sheet resistivity of the printed film. The linear increase in viscosity is only seen until concentrations of 2wt%, as observed in literature [70]. Increasing CNT concentration has no effect upon surface tension, however the results did highlight the requirement for increased mixing energy to homogenise higher concentration inks. This result, along with others, imply that the critical mixing time proposed by Huang *et al.*[12] is dependent on CNT concentration. Increasing CNT concentration also decreases the optical transparency of printed films, as expected. The results also showed that optical transparency decreases with increasing mix time, and that the rate of this decrease is proportional to the CNT concentration.

With respect to CNT functionalisation it has been seen from the viscosity results that functionalisation decreases the energy required to create a homogeneous dispersion. Results indicate a lower mechanical percolation threshold for the NH3 samples compared to the O2, this could be due to the O2 sample having been over functionalised, resulting in tube shortening, an issue highlighted by Shoda *et al.*[42]. Functionalisation has also been observed to result in a decrease in percolation thresholds in composites by Sung *et al.*[71]. This decrease in percolation is not directly visible in the sheet resistivity results. Sonication for 30min appears to cause damage to the NH3 CNTs, visible from the viscosity and transmission results, a common effect of sonication[58]. Functionalisation only seems to have a significant affect upon net viscosity at higher concentrations where the NH3 samples showed the highest viscosities. This appears counter to the results of Sung *et al.*[71] who observed a decrease in the viscosity of MWCNT composites after oxygen functionalisation, implying that it may be a chemical effect, though the results cannot be conclusive on this point. Surface tension appears to be unaffected by covalently functionalised CNTs. Of the functionalised

samples tested, the NH3 sample showed the lowest sheet resistivities at all concentrations and mixing times. This is due to improved dispersion homogeneity and reduced junction resistance as a result of the functionalisation, as reported by Nirmalraj *et al.*[6]. The standard deviation of the data indicates consistent sheet resistivities of the O2 samples after 15min mixing, whereas this is not seen until the 30min mixing results for AsRec and NH3 samples. This indicates less energy is required to form a suitable dispersion, a result of the high degree of functionalisation of the sample.

With respect to mixing time it has been seen that higher mixing times, and hence higher energy applied to the system, results in increased deagglomeration, and depending on the sample CNT damage can occur. Viscosities of the ink samples tend to increase to a maximum with mixing time, however the NH3 sample viscosity decreases after 30min sonication, an effect which has been attributed in the literature to CNT damage[11;74]. This means that the mixing energy needs to be optimised to the ink formulation to ensure sufficient dispersion with minimal CNT damage. The surface tension of the ink is not affected by the mixing time, suggesting that the formation of a CNT network in the solution, or the integrity of the CNT structure does not impact on the surface tension of the net fluid under these conditions. Increasing mixing time decreases film transparency as a result of increased CNT deagglomeration. Also sheet resistivity magnitude and variability is reduced by increased mixing, though this effect is not linear.

It must be noted that, despite careful sourcing of materials and sample preparation significant deviations are seen in ink and film properties. The variability in CNT quality, even within the same production batch, has been reported in literature[75], and is only highlighted further by these results.

To conclude the formulation of a CNT ink requires careful optimisation of all dependent parameters to achieve application requirements. The covalent functionalisation of CNTs is of significant benefit to the ink properties, with less energy required to achieve dispersion, and corresponding improvement in the film properties. Functionalisation allows improved conductivity at lower CNT concentrations due to the improved CNT solubility. However, care must be taken not to over-functionalise, where damage to the CNT structure will negatively impact functional properties.

Chapter 6

CNT Ink Formulation - Conclusions

6.1 Initial Aims and Approach

As stated in section 1, the initial aims of this first section of work were to:

- explore the potential for formulating a CNT based ink by studying potential resins, solvents and formulation techniques, and
- optimise this ink by improvement of CNT dispersion, with emphasis on mixing and CNT modification.

These targets were approached in a systematic fashion. Initially key parameters for measurement for characterisation of the ink and film were identified. Experiments were then designed to investigate key variables, which were selected from observations made in scoping experiments and a comprehensive review of available literature.

The parameters measured for the ink and film characterisation were:

- ink viscosity,
- ink surface tension,
- film transparency, and
- film sheet resistivity.

In addition selected experiments were also characterised by the adhesion and microscopy of the printed film where relevant.

These parameters were investigated in a series of experiments designed to achieve the above aims. Initial investigations focussed on determination of a suitable ink formulation for further analysis. Once this was achieved further optimisation was performed. The variables investigated during this study were:

- resin material,
- resin to CNT concentration ratio,
- processing temperature during mixing,
- CNT concentration,
- CNT functionality, and
- energy applied during mixing.

6.2 Overall Results and Conclusions

The experiments described in chapter 4.1 focussed on the development of a suitable ink and manufacturing process. Firstly a number of different materials (PA, PLA, NC and PVA) were compared to assess their suitability as a resin for use in further experiments. To the best of the author's knowledge this the first time these materials had been assessed for this application. Given the processing conditions used, the PA and PVA based systems showed the most promise. The NC based system showed the highest viscosity, within the recommended range for flexographic printing, but sheet resistivity was poor in comparison to the alternative systems. The PLA based system was expected to show the lowest sheet resistivity, however this was not the case and the poor printability of the system precluded any further investigations. The PA and PVA based systems showed the lowest viscosities and transparencies but also the lowest sheet resistivity. The PVA system was selected for further investigations due to the relative chemical simplicity of the system compared to the commercial PA based resin, however the potential of the PA based system must be noted.

The PVA content as a ratio of the CNT mass in the ink was varied to optimise the properties of the ink. As expected, increasing the PVA content increased the viscosity and sheet resistivity. To improve the sheet resistivity, reduction in the concentration of PVA in the formulation is desirable. However the resulting decrease in viscosity was not suitable for further printed applications, therefore the ratio was selected as 1:1 for further experiments.

Due to reported instability of CNT solutions at higher temperatures and the need to maintain the ink mass through the mixing process the temperature of the ink during ultrasonic mixing was assessed. The only factor influenced by the temperatures within the selected range was the sheet resistivity, which was found to reduce at higher mixing

temperatures. Therefore further experiments were performed at a bath temperature of 15^oC.

Once the basic ink constituents and processing parameters were selected, a factorial experiment studying the interdependence of the CNT concentration, CNT functionality and sonication energy applied to the system was performed, which is discussed in detail in chapter 5. It was found that increasing CNT concentration had a corresponding effect upon the viscosity and decreased the sheet resistivity and transmission of the printed films. Higher energy was also required to disperse the higher concentration inks to a suitable degree, with the effect of the 'critical mixing time' reported in literature observed.

The covalent functionalisation of the CNT samples was of interest to improve dispersability without the use of surfactants and similar non covalent functionalisation. It was shown that the covalent functionalisation was a promising technique, with the NH3 sample showing improved dispersion resulting in corresponding reduction in sheet resistivity despite the structural damage to the CNTs inherent in the technique. The O2 sample appeared to have been over functionalised, with higher sheet resistivities and lower viscosities observed which are likely due to excess damage to the CNT structure rather than the alternative chemistry. Optimal functionalisation appears to potentially reduce the mechanical and electrical percolation thresholds. No significant effect upon the surface tension of the inks was observed.

Increasing mixing time (and hence applied energy) has the effect of reducing the sheet resistivity and transparency and increasing the viscosity. However excess sonication results in damage and eventual shortening of the CNT structures, leading to a decrease in viscosity and increase in sheet resistivity. This correlates with results observed in literature.

6.3 Final Comments

To conclude this part of the thesis a CNT ink has been formulated and various parameters assessed to identify optimal formulation and processing. To the best of the author's knowledge this is the first such study published with the explicit aim of developing a printing ink, though analogous results have been discussed for CNT solutions and composites.

The use of CNTs in conductive coatings is only one potential application for CNTs in the printed electronics field. As discussed in section 1.2.4, the semiconducting nature of particular CNT chiralities enables the use of CNTs in printed digital

electronics. The following part of this thesis concerns the application of the developed ink within the first reported flexographic printing of a CNT based transistor.

Part III

Flexographically Printed CNT Based TFT Structures

Chapter 7

Introduction and Literature Review

The semiconducting nature of certain chiralities of CNTs (as described in section 1.2.4) enables a number of potential applications, such as the semiconducting component in a transistor. A transistor is a device which can switch or amplify electrical currents. By applying a voltage across one pair of contacts on a transistor the current flow across another pair can be controlled. Transistors are used in a number of applications, commonly being combined to produce digital logic circuits for computational devices.

One of the most common types of transistor is the field-effect transistor (FET). Furthermore, there are a number of different types of FET. In printed electronics applications the dominant FET type is the thin film transistor (TFT). TFT devices are ideal for printed devices due to the fact that the substrate does not need to be an active layer, unlike in many other established transistor architectures where the substrate material is also the active layer. This chapter will discuss the structure and operation of TFT, highlighting the key issues for printed TFTs. This will be followed by a literature review of available research in the field of organic and CNT based TFTs. This literature review will focus on the effect of production methods, device architecture and materials upon TFT devices. The key areas for further work will be identified and further experimental chapters introduced.

7.1 Thin Film Transistors

TFTs were first proposed in the 1930s[106], and the research field has matured steadily since, with the advent of new materials and applications. The use of polymeric semiconductors became common in the 1980s, which allowed the fabrication of TFTs using solution processing methods such as printing. It must be noted that compared to other FET structures such as MOSFETs, most TFTs perform poorly. However,

for many applications the performance is adequate. The combination of flexible production and architectures means that TFT devices are commonplace in numerous electronic sectors, especially displays.

Much of the theory behind the structure and operation of TFTs is well understood and accessible from numerous sources [1;107;108], a brief overview of which is presented below.

7.1.1 Structure

A thin film transistor consists of three contacts known as the source (S), drain (D) and gate (G). The source and drain electrodes are connected to the active semiconductor layer, which is insulated from the gate electrode. A cross section of a typical TFT structure is shown in Figure 7.1.1a.

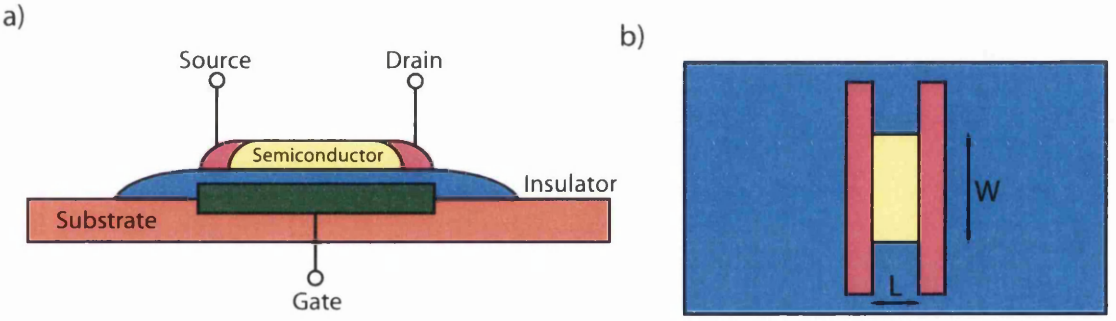

Figure 7.1.1: TFT structure schematic. a) Cross section of a typical TFT structure. b) Overhead cross section of the source and drain electrodes, W and L are channel width and channel length respectively.

Several configurations are available, the choice of which depends on application and material requirements. Figure 7.1.1 shows a bottom gate top contact structure (often referred to as BGTC, a common abbreviation format in the field). This means that the gate electrode is at the bottom of the structure and the source and drain electrodes are above the semiconductor layer. The source and gate electrodes can also be either staggered or coplanar with respect to the semiconductor, the choice of which depends on performance and manufacturing requirements.

The dimensions of the semiconductor channel between the source and drain electrodes are critical to device performance. The channel length (L, distance between the source and drain electrodes) and width (W, contacted semiconductor distance along electrode structure) are both required for calculation of device parameters. Narrower

channel lengths allow faster switching speeds to be obtained at the cost of manufacturing complexity, especially if depositing with printing methods where ink spreading is often an issue. Figure 7.1.1b shows a top down view of the TFT structure highlighting the channel dimensions. Note that the channel width is the width of the area where the semiconductor and electrodes overlap.

The insulator (or dielectric) layer thickness is also a critical factor in device performance. The thickness of the dielectric is a major factor in the capacitance per unit area of the dielectric layer, which is used in calculating the device mobility (a concept introduced in 7.1.2). The dielectric thickness should also be large enough to avoid any potential short circuits between the gate and the source/drain/semiconductor which would destroy device functionality. When considering printed devices this means that the layer may need to be repeatedly printed to ensure insulation, and production must be optimised to produce a suitable thickness layer.

7.1.2 Operation

A FET such as a TFT works by modulating the charge carrier density within a conducting channel in the semiconductor. Application of a potential difference between the gate and source/drain electrodes causes an electric field to develop across the dielectric. This capacitive effect causes charge accumulation, resulting in the ability to modulate the charge carrier density and hence the resistance of the source to drain channel. The number of available charge carriers in the semiconducting layer can be either accumulated, usually in a thin layer at the surface, or depleted. This modulation of the charge carrier density controls the current flow between the source and drain electrodes. TFTs generally operate as accumulation mode devices.

Semiconductors are classified as either p or n type, which refers to the charge of the available charge carriers. P-type semiconductors have an excess of positive charge carriers (known as holes) whereas n-type semiconductors have an excess of negative charge carriers (electrons). For a p-type device a negative voltage is applied to the gate electrode to induce charge carrier accumulation, whereas a positive voltage is applied in the case of n-type devices. Semiconductors can be modified, known as doping, which introduces more available charge carriers to the system. Doping can improve a semiconductor performance or change its type.

A critical parameter to define device performance is the carrier mobility (μ, cm^2/Vs). This describes the ability for the movement of charge carriers to be induced by an electric field, and is defined as the ratio between the drift velocity of the charge carriers and the applied electric field. The higher the mobility the better the

device performance due to the charge carriers being able to be accumulated in less time due to the increased drift velocity induced by the electric field. The mobility of the carriers in a device is largely dependent upon the carrier mobility of the semiconductor material, though they are not equal due to imperfections such as charge traps caused by impurities and surface effects. As stated in 1.2.4, CNTs have shown very high mobilities, which is one of the key motivations of the work reported in the following chapters. The mobility of a device can be calculated empirically, details of which are described in section 8.4.1.

Another commonly used indicator of device performance is the on/off ratio of the device. This is the ratio between the maximum and minimum current observed during device operation, and is usually reported in orders of magnitude. For conventional transistors this parameter is of little significance as off currents should be notionally zero. However for printed TFT devices this is generally not the case, and the on/off ratio is a significant indicator of the potential of the device to work as a switch, and hence digital circuitry. Further discussion of the calculation of the on/off ratio is described in section 8.4.1.

7.1.3 Materials

Many materials are available for the construction of TFT devices, the choice of which depends on required performance, desired manufacturing process and layer compatibility. The semiconductor layer is usually an organic polymer in solution processed TFTs. Some common organic semiconductors are based upon polythiophene or pentacene. It has been observed that although good on/off ratios are achievable with organic semiconductors, mobility and stability is poor with performance degradation caused by light, air and moisture exposure [109]. Carbon nanotubes have the potential to exceed organic semiconductor performance and stability. Further details of device performances are discussed in the following literature review.

Contact material choice is also a factor in device performance. An ohmic contact between the electrodes and active layer is desirable, as this allows more efficient charge transfer between the layers than a non-ohmic (rectifying or Schottky) contact. Efficient charge carrier transfer then relies on the work function of the electrode to match the conduction level of the active layer. This means that the energy required to remove a charge carrier from the solid electrode (the work function) should be lower than the conduction energy (energy of of the conduction band where charge carriers are available).

Factors influencing dielectric material choice are insulating ability, layer compatibility and deposition methods. The dielectric layer must successfully insulate the gate from the active layer and source/drain electrodes. The resulting capacitance per unit area is a factor in calculation of the device mobility (described further in section 8.4.1). Gate leakage can be tolerated if modest in magnitude, this concept is discussed further in section 8.4.3. The layer thickness must be more than the underlying roughness of the substrate and deposited layers to ensure insulation. In conventional electronics SiO_2 is a common dielectric, however this is unsuitable for printed and flexible applications. Common dielectric materials are polyimide, polyvinyl alcohol or poly(methyl methacrylate).

7.2 Printed CNT Based TFTs Literature Review

This literature review is focussed on the development of CNT based TFTs produced using solution processing methods. To this end an overview of the field of printed organic TFT devices is presented as an introduction to the subject, as most of the developments printing organic semiconductor devices are directly applicable to CNT based devices. Likewise, many CNT based TFT devices are not produced using printing methods, but many results are still applicable and a review of such devices is presented. Finally, research into printed CNT based devices is discussed, with the unique issues this brings highlighted.

7.2.1 Printed Organic TFT Devices.

TFT devices have commonly been produced using conventional lithography techniques, however, as previosly mentioned, the combination of the substrate not being an active layer and the solution processability of many organic semiconducting materials allows printing methods to be employed in their manufacture. Reportedly, the first fully printed TFT results were published by Bao *et al.*[110] who used a commercial ITO coated PET as the gate electrode with a screen printed polyimide film as the dielectric. Regioregular poly(3-hexylthiophene) (P3HT) was then deposited as the semiconductor layer and the electrodes screen printed above using a silver ink producing a channel length of $100\mu m$ and a channel width of 4mm. These devices showed mobilities of $0.02cm^2/Vs$ but did not report on/off ratios.

Paul *et al.*[111] also produced TFTs where the semiconducting layer was deposited using spin coating or inkjet printing. The organic polymer printed was either poly(9,9'-dioctyl fluorene-cobithiophene) (F8T2) or regioregular poly(thiophene) (XPT),

printed on a Si substrate with an SiO_2 dielectric layer. Au was used for source and drain electrodes. Mobilities of $0.1cm^2/Vs$ and on off ratios of 10^6 were observed. Printed characteristics were comparable to the spin coated devices.

Printed organic TFTs were also demonstrated by Knobloch *et al.*[112] who produced integrated circuits using a combination of pad printing and blade coating. Issues with registration and layer roughness were discussed, with significant gate thicknesses required to ensure no leakage current, hence the use of blade coating. Devices were printed onto PET, with polyaniline used for the source and drain electrodes and carbon used for the gate electrode. Poly(3-hexylthiophene) (P3HT) or poly(3,3"-dihexyl-2,2':5',2"-terthio-phene) (PDHTT) were used for the semiconducting layer. Channel lengths of $40\mu m$ were achieved and on/off ratios of 10^2 were seen with mobilities of ~$3x10^{-3}cm^2/Vs$. Ring oscillators were then produced but performed poorly compared to conventionally produced control samples, mainly due to the semiconductor mobility and design compromises forced by the poor registration capability.

Tobjörk *et al.*[113] demonstrated all printed flexible transistors using a hygroscopic insulator FET (HIFET) architecture. This type of FET operates at lower voltages than conventional TFTs, however switching speeds tend to be comparatively poor. The device structure is the same as that for TFTs, however a hygroscopic insulator (in this case poly(4-vinyl phenol) (PVP)) is used as the dielectric. This layer absorbs water which causes doping at the semiconductor interface, resulting in the slow transistor behaviour. Source, drain (Au, S/D length of $30\mu m$) and gate (PEDOT) electrodes were inkjet printed whilst the insulator and semiconducting polymer (regioregular poly(3-hexylthiophene) (P3HT)) were reverse gravure printed. On/off ratios of 10^2 were observed measured at a relative humidity of 32%. They have also shown that the HIFET architecture shows higher stability with respect to surface roughness [114], which is potentially a major advantage for printed electronics applications if the performance is not an issue.

Although inkjet is a common printing method for printed electronics, it is limited with respect to speed and feature uniformity. The use of high speed roll-to-roll techniques to print organic TFTs was explored by Voigt *et al.*[115] who used reverse gravure to print the semiconductor, dielectric and gate layers. These were deposited onto photolithographically patterned ITO source and drain contacts on a polyethersulphone substrate. The gravure process was shown to be suitable for application, but multiple layers of dielectric were required to ensure no gate leakage. Ink formulations had to be optimised to minimise surface roughness, and tiger striping or viscous fingering

effects were seen in many prints. Although they did not print the source and drain electrodes, it was noted that this is possible.

Yan *et al.*[13] produced organic TFTs using a number of different deposition methods for the semiconducting layer using a staggered TGBC architecture due to the superior carrier injection performance it provides. Devices were produced on PET and glass. Ag source, drain and gate electrodes were evaporated on and a polymer dielectric was spin or gravure coated. Inkjet, gravure, flexography or spin coating was used for the semiconducting layer using poly{[N,N9-bis(2-octyldodecyl)-naphthalene-1,4,5,8-bis(dicarboximide)-2,6-diyl]-alt-5,59-(2,29-bithiophene)} (P(NDI2OD-T2). The highest performing devices used gravure or spin coating, with mobilities of $0.65 cm^2/Vs$ and on/off ratios of 10^7 achieved. Inkjet deposited layers showed higher surface roughness than the alternative methods, requiring thicker dielectric layers as a result. Further printing optimisation was stated as required for all methods, due to the formation of viscous fingering features after gravure processing and cells being visible on the print for the flexographic prints. AFM images of the semiconductor layer printed using each technique are shown in Figure 7.2.1. Note the relatively large magnitude of the surface roughness of the inkjetted sample. The cell pattern observed upon the flexographic print surface may be due to non optimal printing settings.

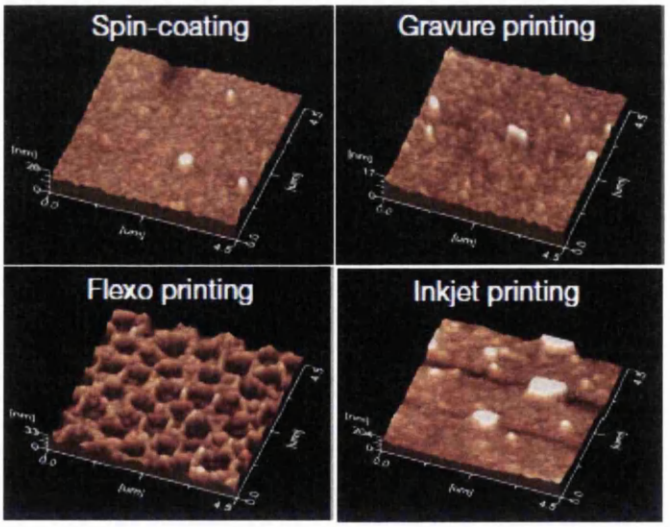

Figure 7.2.1: AFM images showing surface topology of semiconductor layers printed by various methods. Z scale axis maxima are 26nm for spin coating, 17nm for gravure, 33nm for flexography and 204nm for inkjet. Image reproduced from 'A high-mobility electron-transporting polymer for printed transistors'[13].

Fully high speed roll-to-roll printed transistors were produced by Schmidt *et al.*[116]

using gravure for the semiconductor and dielectric and flexography for the gate electrode. A combination of gravure and flexography was used to overcome the limited channel length issues inherent in printed structures. By flexographically printing patterned areas of amorphous perfluorinated poly(alkenyl vinyl ether) the surface energy of the PET film was selectively reduced, allowing the gravure printed PEDOT to form channel lengths of $10\mu m$. These short channel lengths resulting in an increase in operating frequency of the printed devices and would be difficult to achieve using conventional direct printing.

The problem of limited feature resolution can also be improved by using inkjet printing with small nozzle sizes. Sekitani *et al.*[117] developed an inkjet system that could produce sub-picolitre droplets. This allowed channel lengths as low as $1\mu m$ to be printed, and organic transistors produced with the source and drain electrodes printed using this system showed excellent properties. However the speed of inkjet is still limited compared to high speed roll-to-roll techniques such as gravure and flexography.

Increased resolution is not only important to reduce channel lengths. Device switching speeds are also hindered by parasitic capacitance, where the gate electrode overlaps the source and drain electrodes[118;119]. The avoidance of this capacitance is dependent on the interlayer registration capability of the printing process and the process resolution.

One other common concern about printing as a method for mass production of TFTs is device uniformity. All high throughput printing techniques are designed for consistency over long print runs, however small variations in operating parameters can be tolerated in graphics printing. Functional printing is less tolerant of such variations. Hambsch *et al.*[119] printed 50000 TFTs using gravure printing, with random tests of 450 TFTs showing a 75% functional yield. A functional device was defined as one showing an on/off ratio of higher than 10. Printing was performed on a prototype gravure press which the authors admit has issues with ink feed instability and impression cylinder concentricity, therefore yields would be expected to improve on an optimised press design. TFTs were also produced using spin coating to compare device functionality. Spin coated devices performed similarly to the printed samples.

Wen *et al.*[120] have reviewed fabrication methods for organic TFTs and discussed the potential for use of mass printing technologies for TFT production. The issues with registration and feature size were noted, but the potential advantages of high throughput and flexible, varied, substrates give the techniques promise.

Although gravure appears to dominate the printing of TFT devices, work has been done using flexography. Mäkelä *et al.*[121] used flexography to print interdigited source and drain electrodes using a polyaniline based ink. Successful devices were printed, with spin coating used for the active and dielectric layers and the gate electrode drop cast. The importance of ink optimisation to improve print homogeneity was emphasised. Further adoption of flexography as a TFT printing method has been hindered by the film inhomogeneity inherent in the process when printing solid areas and limited resolution compared to gravure[119]. To date no device has been reported using flexography as the primary method for the majority of layers.

7.2.2 CNT TFT Devices

As previously mentioned, CNTs have been discussed as a potential alternative for organic semiconductors in many thin film transistor applications. The mobility of individual CNTs far exceeds that of any organic semiconductor, though the realisation of that value in a production device is unlikely. The on/off ratio of CNT devices are potentially comparable and the stability of CNTs should be excellent due to their chemical inertness. This has been a popular research topic for which an overview of published results is presented below.

7.2.2.1 CNT TFT Devices Produced Using Dry Methods

The concept of the percolating CNT network is introduced in section 1.2.5. For TFT applications using CNTs produced with a typical distribution of 2:1 semiconducting:metallic chiralities the desire is to produce a percolating network that is below the metallic threshold but above the semiconducting threshold. This removes any metallic short circuits between the source and drain electrode.

The first reported study of the use of these random networks in TFT structures was communicated by Snow *et al.*[122]. CNTs were grown on a Si wafer and Ti was evaporated for use as source and drain electrodes. A p-type behaviour was observed, with mobilities of $10cm^2/Vs$. Increasing mobility was observed by increasing CNT density at the expense of higher off state currents.

One of the early CNT based flexible TFT structures was produced by Bradley *et al.*[123] who grew CNTs on an Si substrate using conventional CVD techniques, deposited metal contacts and coated the structure with polyimide. This polyimide encapsulated structure was then removed from the silicon substrate. The polyimide then acted as the dielectric as well as the supporting substrate. The devices has a

channel length of $50\mu m$ and showed a mobility of $12cm^2/Vs$ with no on/off ratio reported. It was also shown that these devices could act as ammonia sensors, as a demonstration of possible post production functionalisation with the aim of producing n-type devices. A significant and reversible decrease in S/D resistance was visible when exposed to ammonia atmospheres.

Sun *et al.*[14] demonstrated flexible CNT based TFTs using random CNT networks produced directly from CVD growth and transferred onto a flexible substrate. Selective removal of unwanted CNTs can be performed to allow for patterned networks. When produced on flexible PEN substrates Al_2O_3 was deposited using atomic layer deposition as the dielectric and Ti/Au was deposited for the gate, source and drain electrodes. Channel length and width was $100\mu m$. After network optimisation these devices showed typical performance of $20cm^2/Vs$ and on/off ratios of 10^6, which is high for a random network. This is thought to be caused by the network morphology differing from solution processed networks due to the manufacturing process, with junction resistances appearing to be minimised. Logic circuits were fabricated using the CNT TFTs. The relationship between mobility and on/off ratio was also investigated using results from available literature and produced devices. A strong correlation between the two is observed, as shown in Figure 7.2.2. This trend is also highlighted as a feature of non chirality controlled networks by Rouhi *et al.*[109] who state that increasing network density results in higher mobility and lower on/off ratios. This highlights the importance of density control in SWCNT networks. Timmermans *et al.*[124] also showed CNT deposition direct from the CVD reactor, using shadow masks to pattern the CNT deposition. Similar electrical performance was seen.

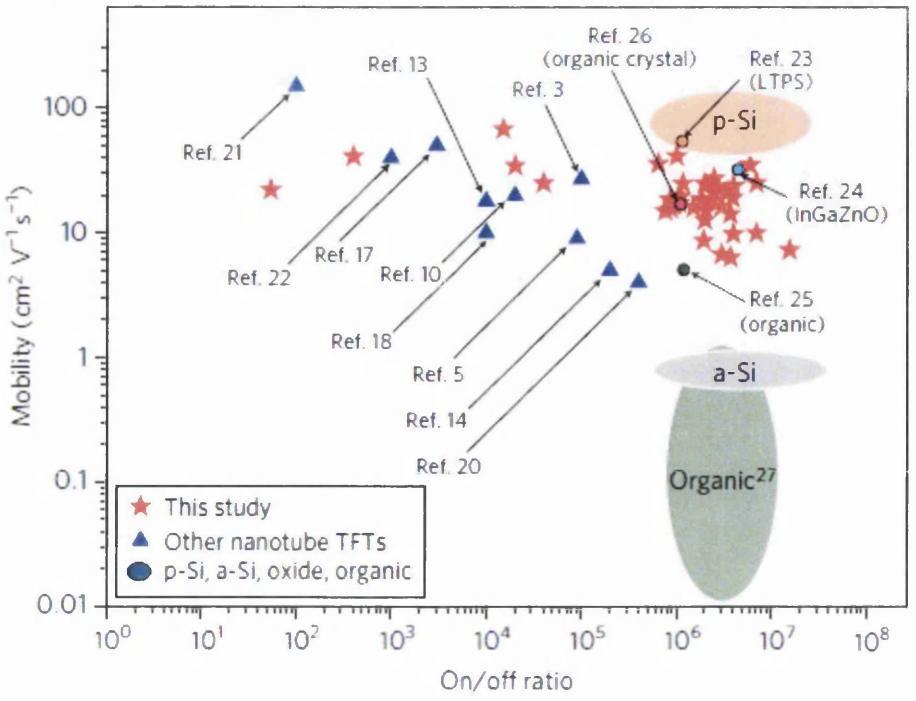

Figure 7.2.2: Relationship between on/off ratio and mobility for CNT TFTs, with other FET types shown for comparison. Image reproduced from 'Flexible high-performance carbon nanotube integrated circuits'[14], to which all references refer.

The on/off ratio can also be affected by the channel width, with Cao *et al.*[125] noting that longer channel widths result in lower on/off ratios in random CVD grown CNT network based TFTs. This is due to an increase in the off current caused by increased probability of metallic pathways. They also produced medium scale integrated circuits using these CNTs, with promising results.

The concept of transparent CNT TFTs, useful for display applications, was explored by Unalan *et al.*[126] who investigated the design criteria to obtain suitable CNT networks. They saw that pristine SWCNT solutions of 0.1 mg/L were needed to reach this point. This was demonstrated by Cao *et al.*[127] who produced transparent, flexible CNT TFTs using CNT networks of varying density for particular layers. The source and drain electrodes used high density CNT networks significantly above the percolation threshold whilst the semiconducting layer was a network tuned to be between the metallic and semiconducting percolation threshold. The CNTs were CVD grown and transferred to the flexible substrate using an elastomeric stamp. Patterns were etched into the transferred networks, with a S/D gaps of 30-300μm

achieved. Poly(dimethylsiloxane) (PDMS) was used for the dielectric layer. Mobilities of $\tilde{}28cm^2/Vs$ were achieved at on off ratios of $\sim 10^2$. Devices showed good stability under bending, highlighting the mechanical properties of the CNT networks. High density CNT networks have also been used for the source and drain electrodes in partially printed organic TFTs[128].

The sensitivity of CNT TFTs to network density means that purification of CNTs to increase the percentage concentration of semiconducting chiralities is appealing. A higher semiconducting CNT concentration will simplify production and improve performance. The decrease in metallic CNTs results in a higher percolation threshold for metallic conduction and improves the device on/off ratio. Methods for CNT chirality purification were discussed in section 2.1.4. Chandra *et al.*[129] demonstrated this by producing TFT structures using CNTs with a semiconducting fraction of >95%. The TFTs were produced on flexible films using photolithography techniques, with the CNTs applied from solution using dip coating. Mobilities of $35cm^2/Vs$ and on/off ratios of 10^6 were observed, significantly better than reported for non-purified CNT devices. It was also observed that mobility decreased with respect to channel length, caused by an increase in channel resistance. Models suggested that at higher CNT densities an increase in channel length or semiconducting CNT fraction will be required to maintain a significant on/off ratio.

7.2.2.2 CNT TFT Devices Produced Using Printing Methods

As investigated earlier in this thesis, inks can be produced using CNTs as the functional component. This development allows for the production of CNT based TFT devices by printing methods.

A comprehensive review of the progress of CNT inks was published by Rouhi *et al.*[109] which emphasised that the key challenges facing CNT ink development were density and chirality control. As previously discussed, excess metallic CNTs within a network significantly increases the off current of the device, lowering the on/off ratio and making the devices unsuitable for many applications such as displays. The prospect of CNT semiconducting inks exceeding current commercial alternatives is clearly possible but it was stated that this is hindered by a lack of fundamental understanding of the effect of various parameters. These parameters include performance scaling with the source drain channel length and the effect of CNT network morphology upon device parameter extraction, such as mobility and capacitance. These issues are not unique to printed devices, but may be exaggerated due to the limited feature sizes possible using conventional printing technologies. The effects of CNT alignment in the

source-drain channel are discussed, with random networks being close to optimal for large (with respect to CNT length) channel lengths. The use of printing technologies to deposit these inks is also discussed in this review, with gravure and inkjet being shown as promising but impeded due to difficulties in reducing metallic CNT content in the inks, resulting in low on/off ratios (a problem explored by Cao *et al.*[125]). It was suggested that this effect can be minimised by introducing CNT stripes into the CNT channel perpendicular to the electrodes, effectively reducing the channel width and hence reducing the off current. The issue with solution deposited networks of CNTs to form a 'coffee-ring' effect when drying due to convection currents caused by solvent evaporation is also discussed. It was proposed that the CNTs align along the edge of these ring effects, which could be used to improve device characteristics in small channel length structures. The difficulties in ink optimisation with low CNT content are highlighted, with emphasis on the lack of fundamental research in this area.

Beecher *et al.*[130] were one of the first groups to produce printed CNT TFTs. By careful solution production to remove all agglomerates that could cause nozzle clogging they were able to inkjet CNT solutions. These were printed onto prefabricated Ag electrodes with $4\mu m$ channel lengths that had been evaporated onto Si wafters with a 150nm oxide thickness. Mobilities of $0.07 cm^2/Vs$ and on/off ratios of 10^3 were observed. The importance of CNT density optimisation was emphasised.

Vaillancourt *et al.*[131] have produced fully printed CNT TFTs on a flexible substrate using an aerosol printing system. Ag was used for source and drain electrodes, with channel lengths of $100\mu m$ achieved. A commercial CNT solution was used for the CNT layer, this was repeatedly overprinted until a S/D resistance of $200 k\Omega$ was achieved. An ion gel was printed as the dielectric and PEDOT was used for the gate electrode. Kapton®, a commercial polyimide film, was used as the substrate. The ion gel and the CNT layer appeared to interact in the final device, lowering the S/D resistance to $72k\Omega$. On/off ratios of 10^2 were reported, but no mobility data was provided. However, operating frequencies as high as 5GHz were demonstrated in a circuit containing printed resistors.

Similar results were achieved by Ha *et al.*[132] who also used aerosol printing to produce digital circuits (inverters, NAND gates and ring oscillators). Purified semiconducting CNTs stabilised in water were sprayed on prepatterned source and drain electrodes (not printed). PEDOT was used for the gate electrode and ion gel for the dielectric. As previously seen, mobility and on/off ratio were dependent on film density, with printed high density films showing mobilities of $31 cm^2/Vs$ and on/off

ratios of 10^3, and low density films showing mobilities of $9cm^2/Vs$ and on/off ratios of 10^5.

By preparing suitable solution concentrations, inkjet printing has been shown as a viable process to tune CNT TFT properties by Okimoto *et al.*[15]. Source and drain electrodes were produced by repeated overprinting to form a high density network, whilst the semiconductor layer was formed using the same ink with fewer printing repetitions. The resulting architecture is similar to that produced by Unlan *et al.*[126]. The devices are shown schematically and optically in Figure 7.2.3. Device mobilities varied from 4.2 to $49cm^2/Vs$ with corresponding on/off ratios of approximately 10^5 to 1.5 observed for the varying CNT densities. The channel length dependence was also investigated, with a clear dependence of mobility and on/off ratio upon the length observed, as shown in Figure 7.2.4. The increase in length reduces the metallic percolation across the channel resulting in the higher on/off ratio, as also observed with other deposition techniques. It was also noticed that as the CNT network density decreases, so does the linearity of the source-drain IV characteristics, as can be observed in Figure 7.2.5a and b. The sharp increase in on/off ratio below the threshold CNT network density and reduction in mobility with reducing network density was also noted, and can be seen in Figure 7.2.5d. The corresponding effect upon the transfer characteristics is clear in Figure 7.2.5c, with devices above the percolation threshold showing little gate voltage dependence.

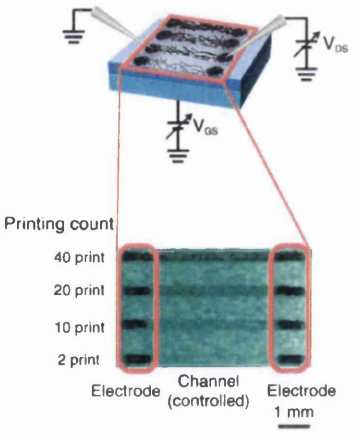

Figure 7.2.3: Visualisation and optical image of CNT TFT devices. The use of repeated overprinting to control the network density is clear. Image reproduced from 'Tunable Carbon Nanotube Thin-Film Transistors Produced Exclusively via Inkjet Printing'.[15]

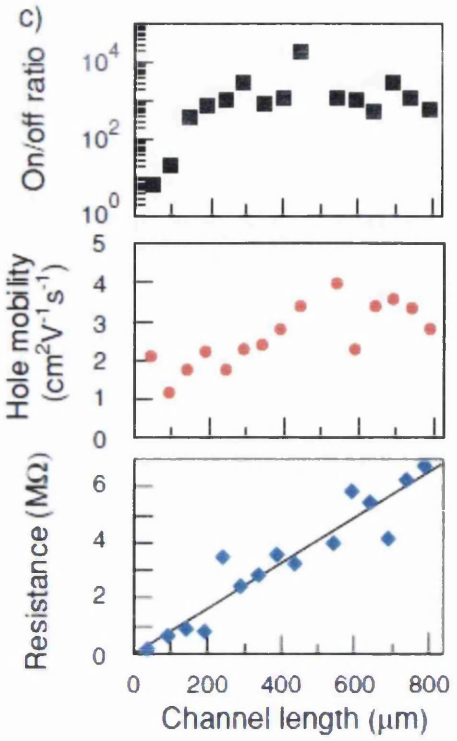

Figure 7.2.4: Channel length dependence of the on/off ratio, mobility and S/D resistance of fully inkjet printed CNT TFTs. Image reproduced from 'Tunable Carbon Nanotube Thin-Film Transistors Produced Exclusively via Inkjet Printing' [15].

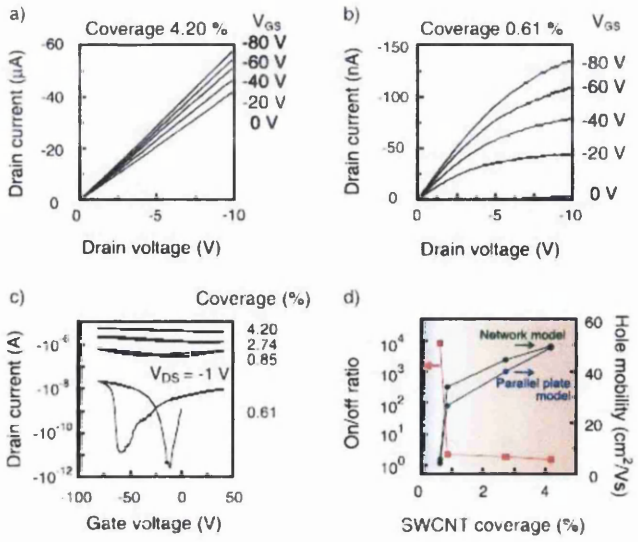

Figure 7.2.5: The effect of CNT network density upon the properties of an inkjet printed CNT TFT. (a) shows the IV output of a high density device, (b) a low density device. (c) shows the transfer characteristics of various density devices. (d) shows the effect upon on/off ratio (red squares) and mobility (blue and green circles). Image reproduced from 'Tunable Carbon Nanotube Thin-Film Transistors Produced Exclusively via Inkjet Printing'[15].

A number of devices have been reported as printed using gravure by Noh *et al.*[81;82]. Functional logic circuits were produced using gravure for all device layers. Ag nanoparticle inks were used for all electrode and BaTiO3 nanopowder (50 nm) hybrid poly(methylmethacrylate) inks for the dielectric. Both were printed using conventional roll-to-roll gravure. SWCNT solutions were deposited using roll-to-plate gravure. The reasons for changing from a continuous to a batch printing method were not clarified, however it may be due to the low concentration CNT solutions having viscosities too low for roll-to-roll gravure ink feed systems. The limitations of gravure for electrode printing was also visible, with edge defects visible on the electrodes. This caused variation in TFT performance, with fluctuations of 500% seen in device characteristics in the worst case. By process optimisation to reduce the line inhomogenity the device variance was reduced to 30-100%. Channel lengths of $170\mu m$ were printed at channel widths of 3mm. Different TFT characteristics required for device functionality were produced by varying the CNT concentration deposited. Mobilities of $0.2cm^2/Vs$ and on/off ratios of 10^4 were seen for the lower concentration 'drive' TFTs, and mobilities of $0.5cm^2/Vs$ and on/off ratios of 10^2 were seen for higher concentration 'load' TFTs.

7.3 Conclusions

This chapter has introduced the concept of field effect devices, in particular TFTs. The structure and operation of TFT devices has been outlined and important device parameters highlighted. Common materials and material requirements have been discussed.

A literature review has been presented highlighting many major developments in the field of printed organic TFTs. It is clear that device performance is limited by the poor mobility and stability of organic semiconductors, areas in which CNTs should excel. The use of printing as a method for producing organic TFTs is well established, with inkjet being popular. In term of high speed roll to roll processes gravure is commonly used, however flexography has been proven to be capable of printing electrode and semiconductor layers. The key barriers to printed TFTs are layer homogeneity, feature size and overprinting registration.

Many results have been published using CNTs in TFT devices produced using 'dry' processes. The effect of using a network structure with metallic content is clearly a compromise between device performance and architecture. Results show that network density is crucial to mobility and on/off ratio. CNT devices tend to be p-type in nature, with mobilities exceeding organic semiconductors regularly observed. However, optimisation is required to achieve similar on/off ratios. This is still true if the CNT layers are deposited using solution processing methods. CNT based inks have been deposited using inkjet, aerosol printing and gravure. The optimisation of what is often referred to as the 'CNT ink' is crucial to device performance, however these are often not inks in the printing sense of the word, merely CNT dispersions with no binder present. Device architectures tend to be larger than those produced using photolithography or similar methods, emphasising the issue of channel dimension dependent mobility and on/off ratios.

Reported TFT properties vary considerably, however it is clear from the literature that characteristically semiconducting polymer based printed TFTs have low mobility but good on/off ratios, whilst CNT based devices show higher mobility but lower on/off ratios. In the literature for printed devices above organic based devices reported mobilities between 0.02 and $3cm^2/Vs$, whilst CNT based devices reported between 0.07 and $49cm^2/Vs$. With regards to on/off ratio organic devices ranged between 10^2 to 10^7 and CNT based devices between 1.5 and 10^7. A wider range of examples is shown graphically in Figure 7.2.2.

It is clear that CNT based devices show significant advantages to equivalent organic polymer based systems, however the use of high speed, roll to roll techniques with both types of devices is still at an early stage. Much research seems to focus on inkjet and gravure, however both have limitations which have been discussed above. This thesis has previously presented the development of a CNT based ink suitable for flexography or gravure printing. Flexography could eliminate the electrode edge defects reported in the literature due to the continuous image carrier, and is therefore a promising candidate for further investigation into the production of CNT based TFTs printed using entirely high speed, roll to roll techniques. Also, as reported in Chapter 2, flexography has not been reported as a method for deposition for CNT networks, therefore this is an area for further study.

Chapter 8

Experimental Techniques and Equipment

8.1 Introduction

This chapter introduces the theories, equipment and experimental methods utilised in the production, optimisation and characterisation of CNT based TFT structures. Functional TFT structures were produced using the CNT based inks introduced in the previous sections of this thesis as the active semiconductor layer. All layers were manufactured using high speed, roll-to-roll capable techniques which are suitable for upscale to industrial production.

All devices were characterised in accordance with the IEEE Standard for Test Methods for the Characterisation of Organic Transistors and Materials (IEEE Std 1620-2008)[133]. This specifies that the following sample characteristics that are required to be reported:

- Transfer (I_{DS} vs. V_{GS}) curves, including the on/off ratio, mobility and threshold voltage (V_T) which can be empirically derived from the data.
- IV (I_{DS} vs. V_{DS}) output.
- Gate leakage (I_{GS} vs. V_{GS}).

Also the following sample characteristics are recommended to be reported:

- Stray capacitance (C_{GS} and C_{GD}).
- Device parameters:
  - Geometric:

    * Gate structure configuration.
    * Source and drain electrode configuration.
    * Channel length and width.
    * Dielectric thickness.
  - Fabrication:
    * Substrate composition.
    * Deposition processes used for all layers.

- Sample population.

All required and recommended characteristics will be reported for samples described in this thesis.

8.2 Device Production

8.2.1 Flexographic Printing

8.2.1.1 Theory

The principles of flexographic printing are described in section 1.1.1.1.

8.2.1.2 Equipment

All flexographic printing was performed using an IGT F1 flexographic printability tester, an image of which is shown in Figure 8.2.1. The F1 is a pressure driven system, in which only the plate cylinder is driven. The substrate, impression cylinder and anilox cylinder are driven by contact pressure from the plate cylinder. This results in engagement pressures between the printing plate and substrate being significantly higher than in conventional independently driven substrate web systems. This reduces the printing resolution and causes feature deformity due to ink spreading. However, results from the printability tester are still applicable to industrial scale flexography presses which is key for potential manufacturing scale-up.

To print, ink is manually deposited directly onto the anilox cylinder which is brought into contact with the plate cylinder. The plate cylinder is then rotated during which time the ink is doctored into the anilox cells and deposited onto the relief image areas of the plate. The substrate is then brought into contact between the printing and impression cylinder and drawn through, patterning the ink onto the substrate. The point of contact between the printing plate, substrate and impression

cylinder is shown in Figure 8.2.2. The anilox-to-plate and plate-to-substrate pressure can be specified in steps of 25N. Other system variables available are the printing speed and the number of revolutions for which the anilox and plate cylinders are in contact prior to substrate engagement (known as inking revolutions). Anilox cylinders are available in nominal volumes of 2.7, 8.0, 12.0 and 24.0cm^3/m^2.

Figure 8.2.1: Photograph of the IGT F1 flexographic printability tester used for device production.

F1 plates measure 52.5cm by 5.0cm. Solid areas (known as bearer bars) are required to be placed on either side of the printing image to support the relief structure and avoid deposition from non imaged areas of the plate during printing. This constrains the available image area to a maximum width of 4.0cm. The plate is mounted onto the cylinder using conventional flexographic mounting tape. The plate mounted on the impression cylinder can clearly be seen in Figure 8.2.2.

Figure 8.2.2: Close up view of the point of contact between the printing plate, substrate, substrate holder and impression cylinder. Note how the substrate is driven by pressure between the two cylinders.

Substrates are usually mounted onto a rigid substrate carrier which is drawn between the plate and impression cylinder, as seen in Figure 8.2.2. The system

was not designed with accurate overprinting in mind, however by careful placement of the substrate carrier within the track (shown clearly in Figure 8.2.1) adequate overprinting registration can be achieved. This is due to the fact that the plate cylinder always rotates to the same location before pressure is applied to the substrate between the impression and plate cylinders.

8.2.1.3 Method

When printing multilayered devices on the F1 care must be taken at each step to ensure accurate overprinting. Plates were mounted using a hard tape to improve solid area printing. Manual mounting allowed plates to be mounted with an accuracy of approximately $\pm 5mm$ to the previous plates position in the print direction and $\pm 1mm$ across the print direction. Substrates were cut to fit the substrate carrier width and fixed in position using adhesive tape. Substrate mounting position was achieved with a repeatability of approximately $\pm 1mm$ in the print direction and approximately $\pm 0.5mm$ across the print direction. The substrate carrier must then be mounted into the F1 as shown in Figure 8.2.2. This could be achieved with a repeatability of approximately $\pm 0.1mm$ in both axis due to the limits of the printing track.

Optimal print settings and anilox volumes were chosen for each layer printed, the details of which are discussed in the relevant chapters. Printing pressures had to be high enough to avoid slipping between the anilox or substrate and the printing plate whilst being low enough to minimise plate deformation and ink spreading effects. During printing ink was applied to the anilox as necessary to maintain cell flooding.

All samples were oven dried as per ink specifications discussed in the relevant chapter.

8.3 Printed Feature Characterisation

8.3.1 Surface Profile Analysis

8.3.1.1 Theory

Surface profiles were analysed using white light interferometry (WLI). WLI is a non contact measurement technique that is based on the analysis of the interference effects between light reflected from a sample surface and light reflected from a reference surface. The constructive or destructive interference between the two waves results in interference fringes in a combined image. There are a number of WLI techniques

available, however all data presented in this thesis was collected using vertical scanning interferometry (VSI). It must be noted that this technique relies on reflected light from the sample, and therefore cannot be used on non reflective samples such as CNT prints. Further details on the white light technique and its applicability to printed feature measurement are available from a number of sources [134;135].

8.3.1.2 Equipment

All surface profile data presented in this thesis was obtained using a Veeco Instruments Wyko NT9800 wide area white light interferometer, as shown in Figure 8.3.1. Data is processed using proprietary instrument software.

Figure 8.3.1: Photograph of Veeco 9800 wide area white light interferometer.

8.3.1.3 Method

Samples were imaged in VSI mode using suitable optical magnification.

8.4 Device Characterisation

The required parameters for device characterisation were outlined in section 8.1. The specific methods for measurement and calculation of these parameters are outlined below. As an aside on notation, within the field voltages and currents between electrodes are usually identified by the respective symbol followed by two letters in subscript that identify the electrodes being measured between (S, D and G for source, drain and gate respectively). For example I_{DS} is the current between the source and drain electrodes. This notation is used throughout the following chapters.

8.4.1 Transfer Characteristics

8.4.1.1 Theory

Transfer (I_{DS} vs. V_{GS}) measurements are used for calculation of the field effect mobility, threshold voltage and on/off ratio of devices. When sweeping the gate voltage between two values in discrete steps, the resistance between the source and drain electrodes should change. By application of a small constant potential difference across the two electrodes, the change in current can be measured. The slope of this curve is known as the transconductance (g_m) and is expressed as

$$g_m = \frac{\delta I_{DS}}{\delta V_{GS}} \tag{8.4.1}$$

IEEE Std. 1620-2008 states that the carrier mobility can be calculated using the transconductance. A number of methods are available to calculate this, with the most common being the linear regime method. This assume that the TFT is a linearly variable resistor, with the resistance between the source and gate voltages being directly proportional to the gate voltage. This assumption is usually valid between certain ranges of V_G. To calculate this value from the empirical transconductance data the relationship between I_{DS} and V_{DS} must be derived. I_{DS} is defined as the rate of flow of charge through the semiconductor channel of width W and length L, and can therefore be expressed as,

$$I_{DS} = \frac{Q_i W L}{t_i} \tag{8.4.2}$$

where Q_i is the electric charge transferred through a unit area in a time t_i . The charge density is governed by the capacitance per unit area (C_i) across the channel such that

$$C_i = \frac{Q_i}{V_{GS}}. \tag{8.4.3}$$

The time taken for the current to flow across the length of the semiconducting channel is proportional to the velocity (v) of the charge carriers such that

$$t_i = \frac{L}{v}. \tag{8.4.4}$$

This velocity is known to be proportional to the electric field such that

$$v = \mu E \tag{8.4.5}$$

where μ is the carrier mobility and E is the electric field along the channel, established by the potential difference between the source and drain electrodes such that

$$E = \frac{V_{DS}}{L}. \tag{8.4.6}$$

By substitution of Equations 8.4.3, 8.4.4, 8.4.5 and 8.4.6 into Equation 8.4.2 it can be seen that

$$I_{DS} = \frac{W}{L} C_i \mu V_{DS} V_{GS}. \tag{8.4.7}$$

Differentiating with respect to V_{GS} to find the transconductance in Equation 8.4.1 gives

$$\frac{\delta I_{DS}}{\delta V_{GS}} = \frac{W}{L} C_i \mu V_{DS}. \tag{8.4.8}$$

Which rearranged for μ gives

$$\mu = \frac{\delta I_{DS}}{\delta V_{GS}} \frac{L}{W C_i V_{DS}} \tag{8.4.9}$$

It must be noted that this derivation assumes the threshold voltage (V_T) is zero and is only valid if $V_{DS} \ll V_{GS}$ (assuming the device is p-type). If the threshold voltage is more than zero then this needs to be taken into account by substitution of V_{GS} by (V_{GS}-V_T) to account for carrier accumulation up to the relevant conduction level. Also it must be noted that this method is not ideal when considering CNT networks (for reasons discussed by Rouhi *et al.*[109]), however it is still commonly applied in literature.

The threshold voltage can also be derived from the transfer curve. The threshold voltage is defined as the minimum V_{GS} at which the drain current starts to increase, indicating that the transistor is 'on'.

Finally, the on/off ratio is also a critical property of all transistors. It is defined at the ratio between the maximum and minimum drain currents measured on the transfer curve. This may be dependent on V_{DS}, and the largest ratio observed is usually reported.

8.4.1.2 Equipment

All TFT characterisation was performed using an Agilent E5262A 2-channel source monitor unit. Sample contact was performed using a Signatone S-116O four point probe station, using $5\mu m$ titanium tips which allowed for consistent contact placement

and pressure. Instrument control and data collection was performed remotely using the Agilent EasyDesktop software. A photograph of the equipment used is shown in Figure 8.4.1. Data was collected in an environmentally controlled laboratory. The E5262A can reportedly force and measure voltages to a worst case of ±0.04% and can force and measure currents to a worst case of ±0.12%[136]. Measurement of the IV characteristics of a calibrated ohmic sample of ITO coated glass was performed to validate equipment accuracy. Analysis of results was performed in OriginLab Origin 7.

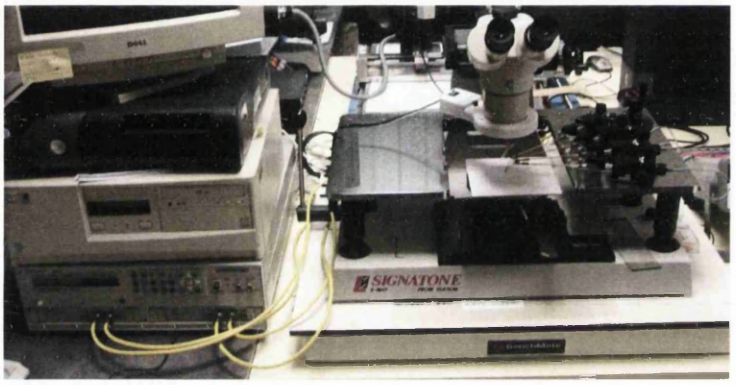

Figure 8.4.1: Photograph showing Agilent E5262A plus Signatone S-116O probe station.

8.4.1.3 Method

The TFT was connected into the circuit shown in Figure 8.4.2, in accordance with established techniques[137]. V_{GS} was swept from 0 to -80V in steps of 100mV whilst V_{DS} was held constant at 1V. These values were chosen as the operating range of the device after a number of scoping experiments. V_{GS} steps were made at suitable intervals. A Faraday cage was not used for these experiments.

Transconductance was derived from the transfer data for use in determining the effective mobility by means of the linear regime method. This was performed by fitting a linear line of best fit to the area where the resistance between the source and drain electrodes is seen to change in a linear fashion. In the results presented a gate voltage range of 5V was used when approximating the gradient to provide a suitable average from which to fit. An example transfer curve of a MWCNT device presented in this thesis and the linear fit are shown in Figure 8.4.3.

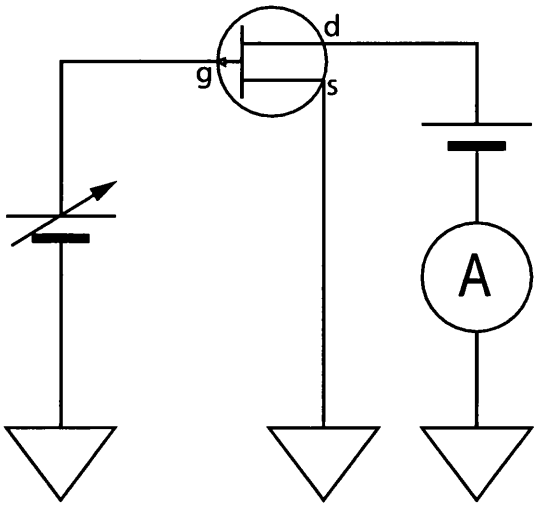

Figure 8.4.2: Circuit diagram for measuring transfer characteristics.

8.4.2 IV Output

8.4.2.1 Theory

The dependence of I_{DS} upon V_{DS} is dependent upon V_{GS}, as stated in Equation 8.4.7. By holding V_{GS} constant and sweeping V_{DS} the IV characteristics of the semiconductor layer can be measured and compared to that at varying values of V_{GS}. By comparison of IV output characteristics at values of V_{GS} above and below V_T the FET behaviour of the device can be observed. IEEE Std. 1620-2008 recommends that a minimum of three V_{GS} values that reflect the operating range of the TFT are tested.

8.4.2.2 Equipment

See Section 8.4.1.2 for details of equipment used.

8.4.2.3 Method

The TFT was connected into the circuit shown in Figure 8.4.4, in accordance with established techniques[137]. V_{DS} was swept from 0 to 20V in steps of 100mV whilst V_{GS} was held constant at values of 0, 40 and -40V. V_{DS} steps were made at 100ms intervals. RF interference was minimised.

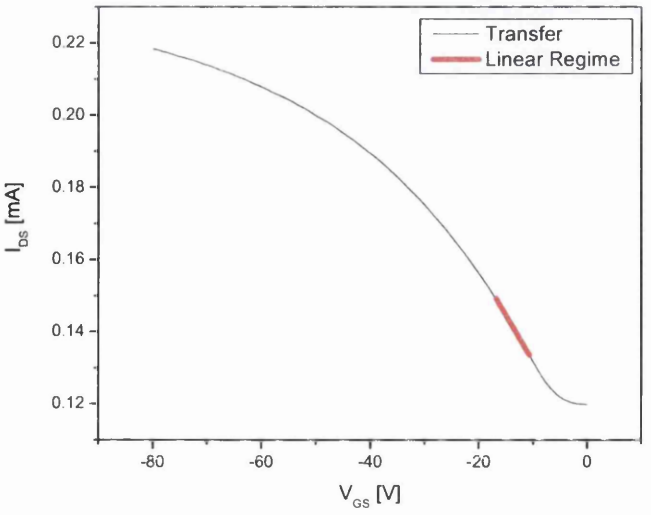

Figure 8.4.3: Transfer characteristics of a MWCNT based TFT device. Linear regime is highlighted and a best fit approximation has been made.

8.4.3 Gate Leakage

8.4.3.1 Theory

Gate leakage is the flow of current from the gate electrode to the source and drain electrode, through the dielectric layer. This is undesirable and should be avoided. Dielectric breakdown may occur at high voltages, therefore voltages should be applied across the operational range of the transistor and any leakage current measured. Leakage current may be observed at all voltages, however if $I_{GS} < 0.001 I_{DS}$ during application of a potential across to the gate electrode then the leak is considered acceptable. If significant gate leakage is observed then this indicates that the dielectric layer is not insulating. In printed TFTs this is often due to print defects causing short circuits or inadequate material deposited resulting in insufficient layer thickness.

8.4.3.2 Equipment

See Section 8.4.1.2 for details of equipment used.

8.4.3.3 Method

The TFT was connected into the circuit shown in Figure 8.4.5, in accordance with established techniques[137]. V_{GS} was swept from 0 to 20V in steps of 100mV. V_{GS}

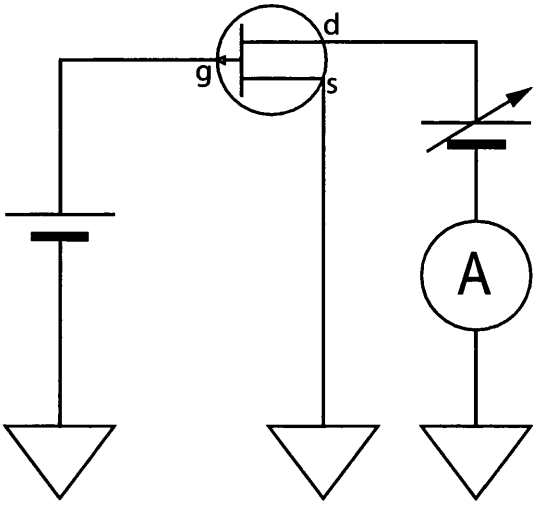

Figure 8.4.4: Circuit diagram for measuring IV characteristics.

steps were made at 100ms intervals. RF interference was minimised.

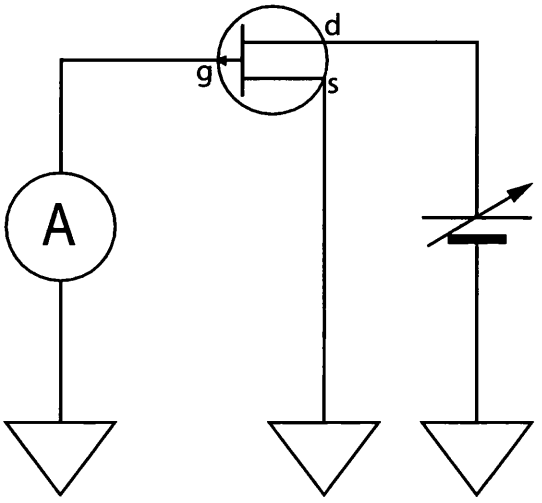

Figure 8.4.5: Circuit diagram for measurement of gate leakage.

8.4.4 Stray Capacitance

8.4.4.1 Theory

Stray (or parasitic) capacitance is the interlayer capacitance between the source and drain electrodes and the gate electrode. This capacitance will limit device speed and should be minimised. Minimising the electrode overlap and careful dielectric layer design will reduce the stray capacitance.

8.4.4.2 Equipment

Capacitance was measured using an AIM LCR Databridge 401, as shown in Figure 8.4.6.

Figure 8.4.6: Photograph of AIM LCR Databridge 401.

8.4.4.3 Method

Capacitance was characterised at a frequency of 1kHz, in accordance with IEEE Std. 1620-2008. C_{GS} and C_{GD} were both recorded.

8.5 Conclusions

This chapter has focused on the experimental techniques and equipment used to prepare and characterise the CNT based TFTs. The precise details of device fabrication differs depending on the generation of device, and will be outlined in the relevant results section. All samples are characterised in accordance with IEEE Std. 1620-2008.

The next chapter will detail the first generation devices, which were designed as proof of concept and used MWCNTs. Further device design optimisation was performed, and SWCNTs inks were employed for the semiconducting layer in subsequent devices. The optimisation, preparation and characterisation of these second generation devices is discussed in further chapters.

Chapter 9

Proof of Concept - MWCNT Based Field Effect Devices

9.1 Introduction

The aim of the work described in this chapter was to print and characterise MWCNT based TFT devices produced using roll-to-roll capable techniques. The ultimate aim of this work is to use flexography for all device layers. To achieve this two TFT structures were designed to be printed using an IGT F1 flexographic printability tester (the details of which are discussed in section 8.2.1). The devices were then produced, with each layer characterised individually to determine the parameter values required for reporting in IEEE Std. 1620-2008 and assess the suitability of the production methods used. The devices were then characterised electrically and comparisons made.

To minimise the effect of CNT network density dependence upon the resulting device performance all devices were constructed using a MWCNT ink based on the parameters defined as a result of the previous work described in this thesis. MWCNTs tend to show semimetal behaviour (see section 1.2.4) therefore network density is not a critical factor. The CNT concentration was 2wt% in all inks used in this chapter.

The target was to produce a device that showed field effect behaviour and investigate the ability of the IGT F1 to produce TFT device structures. These structures can then be optimised and a SWCNT ink used for semiconducting properties in further study.

9.2 Device Design

TFT device design is by necessity a compromise between material and manufacturing process limitations. In the case of the devices presented in this chapter flexography was chosen as the manufacturing method for all layers. Flexography has a number of advantages that are of particular benefit to TFT structures. Firstly the ability to produce a continuous, uniform feature is ideal for electrode production as line inhomogeneity has been shown to affect device performance [81]. The independence of the ink metering system from the image master may also be of benefit to CNT based TFTs as the electrical behaviour of the CNT network has been shown to be dependent upon network density, a factor which is directly proportional to the ink volume deposited. The wide range of printable rheologies allows flexibility in ink development, key when using developmental CNT inks and with varying layer requirements. The roll-to-roll capability of the technique is appealing from an industrial relevance point of view, and the low cost of image masters compared to similar technologies such as gravure is attractive for experimental design optimisation. Although flexography has been reported to be used for printing individual layers [13;121], no work has been reported which uses flexography for every individual layer.

9.2.1 Materials

When considering the materials to be used for device production, priority must be given to functionality. Layers must also be compatible for overprinting, where components of inks used in upper layers of the device must not negatively affect the layers beneath. Material stability must also be a consideration if longer device lifetimes are desirable. Further discussion on materials choice is presented below.

9.2.1.1 Semiconductor Layer

One of the motivating factors behind the development of the CNT based inks presented in this thesis was the potential for use in printed electronics applications. One application where CNTs show significant potential is TFT devices, as presented in chapter 7. Therefore the work presented in this chapter will use the CNT based inks formulation optimised previously in this thesis.

As stated in section 1.2.4, MWCNTs show a semimetal behaviour and therefore will not be suitable for use in transistor applications where low off currents are required. However for variable resistance applications and proof-of-concept TFT devices MWCNTs are a viable material. The semimetal behaviour also means that device

characteristics are less dependent upon CNT network density, hence high concentration inks can be used which will provide viscosity appropriate for flexography and result in networks that are significantly above the percolation threshold density. The ink used in the devices are based on the research presented in part II. The ink contained 2wt% CNTs (Baytube C150P, used without modification), and was mixed for 30min using an ultrasonic probe at the same settings described in section 3.2. This concentration was selected because the ink characteristics were well defined in previous work, and it was known to give a homogeneous network. NMP was used as the solvent and PVA was used as the resin at a 1:1 ratio. The ink formulation contents are shown in Table 9.2.1.

Constituent	Target Mass [g]
CNT	0.4
NMP	17.8
PVA	4
Total Mass	20

Table 9.2.1: Target ink constituent mass for 2wt% MWCNT based ink for use in TFT structures.

9.2.1.2 Source and Drain Electrodes

The key property of the source and drain electrodes is to provide a low resistance ohmic contact to the active semiconductor layer. Ag has been shown to be a suitable material, having been used for CNT based TFT devices by a number of groups[81;82;130;131]. A commercial nanosilver based ink (Inktec PR-030) formulated for flexographic printing was used. This ink was selected due to the low resistivity obtainable and the excellent printability. This ink contains silver particles of an average diameter of approximately 30nm which when deposited need to be sintered to cause the particles to coalesce and achieve maximum macroscopic conductivity. This generally requires high temperatures and long drying times, with drying conditions of $130°C$ for 5 minutes recommended by the manufacturer. These drying conditions are not ideal for further roll-to-roll upscaling, however advances in rapid ink curing technologies have been made[138]. The manufacturer claims sheet resistivities of approximately $45m\Omega/\square$ are achievable.

9.2.1.3 Dielectric Layer

The ink used for the dielectric layer was a commercial dielectric ink produced by Gwent Electronic Materials (D2090130P5 Pink Dielectric Ink). Suggested drying conditions are 130^oC for 10 minutes. The ink is based upon a thermosetting polymer and scoping experiments showed it to have suitable adhesion and insulating properties.

9.2.1.4 Gate Electrode

The ink used for the gate electrode was a commercial silver ink produced by Gwent Electronic Materials (C2090210P12 silver ink). This ink is based upon a micro-particle formulation and the manufacturer claims sheet resistivities of approximately $200m\Omega/\square$ are achievable. Suggested drying conditions are 130^oC for 10 minutes. This ink was chosen due to the fact that it is formulated to be compatible with the dielectric ink described above. This layer compatibility is critical as damage to the insulating layer will result in significant gate leakage which will prohibit device functionality.

9.2.1.5 Substrate

The substrate chosen for this work was a polyester based film. Substrate thickness was specified as $350\mu m$, with the average surface roughness measured using white light interferometry as 138nm. This substrate was chosen due to the rigidity providing good device support and the suitable printability in terms of adhesion and wetting observed in preliminary experiments.

9.2.2 Structure

The basic structure of a TFT is well defined and described in detail in section 7.1.1. A top gate top contact (TGTC) architecture (shown in Figure 9.2.1) was chosen to ensure layer compatibility. Preliminary tests indicated that the NMP used as the solvent in the CNT inks may be incompatible with the nanosilver ink used for the electrodes. As a result the MWCNT layer was required to be the initial layer deposited. This constrained the design to the TGTC structure. Two electrode structures were chosen, the details of which are described in section 9.2.2.2. Both structures were defined on a single printing plate to ensure consistency in print conditions. Layer dimensions were defined to compensate for the poor registration capabilities of the F1 (discussed in section 8.2.1), and are discussed in the relevant sections below.

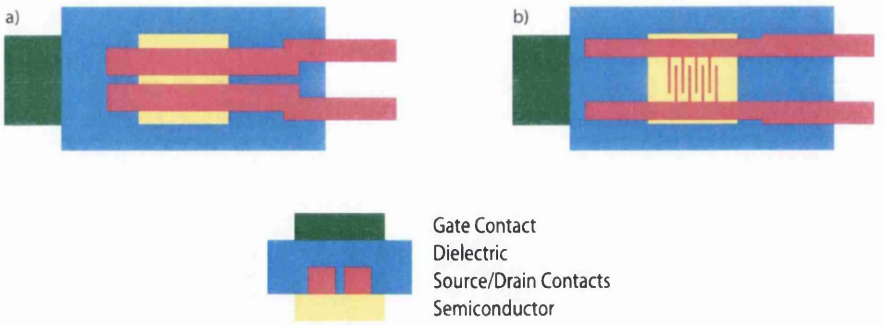

Figure 9.2.1: Top gate, top contact TFT structure shown schematically from a top down and cross section view. Devices were printed from left to right as viewed. (a) shows the parallel electrode structure design, (b) the interdigited electrode structure design.

9.2.2.1 Semiconductor Layer

The master image for the semiconductor layer is shown in Figure 9.2.2. This was defined as a 20mm solid square. The size was dictated by the registration capability of the F1, as the source and drain electrodes will need to be overprinted to ensure a semiconducting channel between the electrodes.

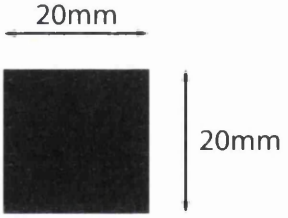

Figure 9.2.2: Semiconductor layer master image used in the production of MWCNT devices.

9.2.2.2 Source and Drain Electrodes

Two electrode structures were chosen, the image masters for which are shown in Figure 9.2.3. One structure (Figure 9.2.3a) consists of the source and drain electrodes parallel to each other, with a 2mm channel length defined. Assuming accurate overprinting this structure provides a nominal channel length of 2mm and channel width of 20mm. The second electrode structure was an interdigited design with a nominal channel length of 1mm and width of 42mm, assuming the channel exists between the overlapped electrodes only and the channel width is a summation of the overlapped section widths. Both electrode structures featured large contact areas defined to simplify contact during characterisation.

The parallel electrode structure offers a number of advantages, including structure simplicity (especially important for further miniaturisation). However registration requirements are equal to the channel length. The interdigited structure provides greater margin for registration error at the expense of structure complexity and overall device size. Channel lengths and widths are not a critical factor at this scale when considering semimetal MWCNTs at network density used. The key factor is to ensure no contact between electrodes which prohibit device functionality.

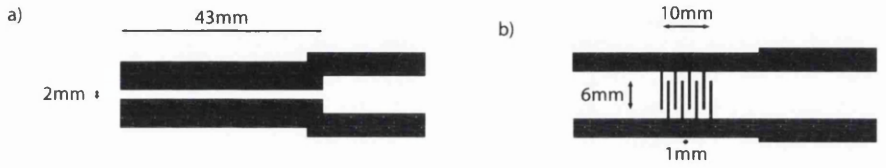

Figure 9.2.3: Parallel and interdigited source and drain electrode image masters used in the production of MWCNT devices.

9.2.2.3 Dielectric Layer

Figure 9.2.4 shows the image master defined for the dielectric layer printing. This is defined to cover the entire electrode and active layers including significant margin for registration error, taking into account the fact that the gate electrode layer to be deposited above cannot contact the source and drain electrodes.

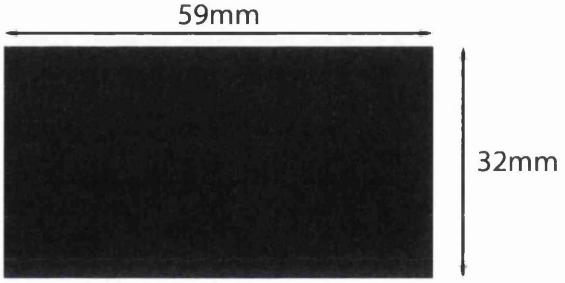

Figure 9.2.4: Dielectric layer master image used in the production of MWCNT devices.

9.2.2.4 Gate Electrode

Figure 9.2.5 shows the image master for the gate electrode. For simplicity of production the design was kept as a solid area. This minimised the potential for poor contact at the substrate to dielectric layer step at the expense of introducing high parasitic capacitance. The large area of the source and drain electrodes which will be overlapped by the gate electrode (assuming ideal registration) will cause a significant

parasitic capacitance which will reduce device speed. However for the development of a proof of concept device this was considered acceptable.

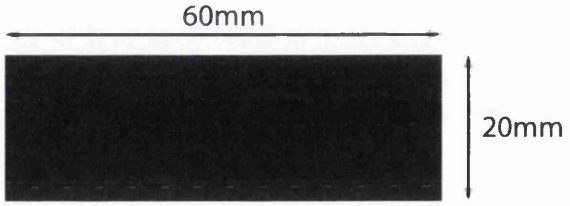

Figure 9.2.5: Gate electrode layer master image used in the production of MWCNT devices.

9.2.3 Design Summary

The overall device structure was defined by the limitations of the CNT ink with respect to layer compatibility. Further design requirements were specified by the equipment limitations in this initial trial. This results in relatively large structures in TFT terms, however as the initial aim is to observe field effect behaviour the simplicity of production takes precedence over device performance. Further design optimisation can be performed after the concept is proven viable.

Although flexography is a roll-to-roll capable technique, as previously mentioned the F1 is a batch printing device. To ensure printing consistency each printing batch would produce two devices, one of each architecture. The complete printing plate master images are shown in Figure 9.2.6. Solid areas were included for layer characterisation and registration lines were provided as an optical guide in the print direction.

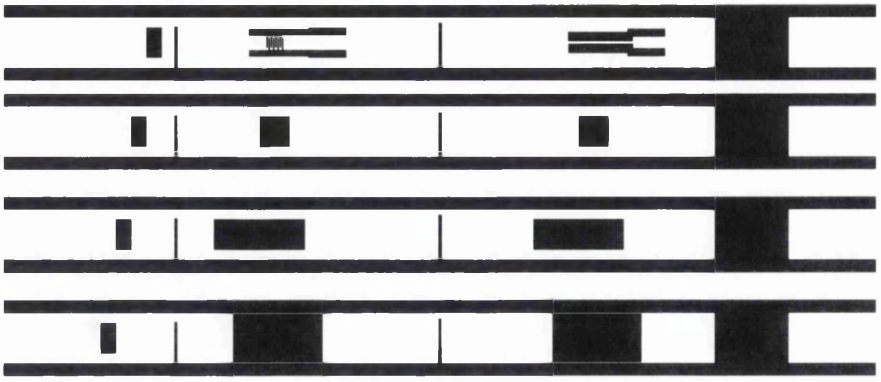

Figure 9.2.6: Image masters for the four printing plates used in the device production of MWCNT based TFT structures.

9.3 Device Production and Structural Characterisation

Each layer was produced sequentially, with devices imaged and characterised as necessary at each step. Each step required specific processing parameters due to the design and materials used, the details of which are defined in each relevant section.

9.3.1 Semiconductor Layer

The semiconductor layer was printed using an anilox-to-plate pressure of 100N and a plate-to-substrate pressure of 200N. These pressures were chosen after visual analysis of prints produced in preliminary trials. The anilox used had a nominal cell volume of $8.0cm^3/m^2$. Assuming this is the correct anilox cell volume and an ink release rate of approximately 40%[135] this should result in a theoretical ink film thickness of $0.13\mu m$.

Figure 9.3.1 shows a digital scan of a representative MWCNT layer print. Average spread in the print direction from the nominal specified size was $76\pm10\mu m$ and across the print direction was $43\pm10\mu m$. This size increase is likely due to ink spreading during the printing process. The inhomogeneity of the feature can be observed in the optical image. This consists of two dominant features. The first is the excess deposits at the feature boundaries. This is due to ink spreading during the printing process, an effect which is increased when using systems where the substrate is driven by plate-to-substrate pressure such as the F1 due to the high engagement pressures required. This effect also manifests itself in ink build-up along the print direction. This ink flow is caused by hydrodynamic pressures at the nip contact, and can also be reduced by decreasing the printing pressure. However a minimum pressure is required by the F1 system to accurately engage and move the substrate. The second feature is a stripe pattern along the print direction. This pattern is a known phenomenon when printing solid areas and is often referred to as 'viscous fingering' or 'tiger striping'. Is has been observed with gravure[13;139] and flexographic[140;141] printing and the causes are still unclear. Bornemann *et al.*[139] suggest that it is due to either hydrodynamic instabilities, dewetting or drying (specifically Marangoni) effects. Further device production will require optimisation to reduce this effect, as it may be detrimental to device performance.

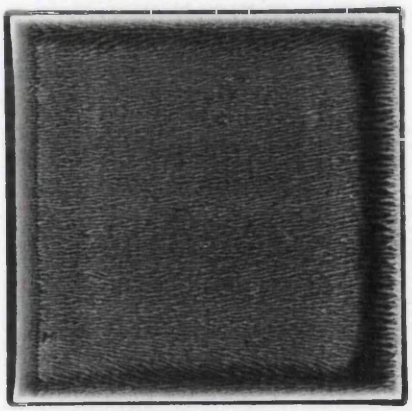

Figure 9.3.1: Optical scan of representative print of 2wt% MWCNT ink. Printing direction was left to right.

9.3.2 Source and Drain Electrodes

The source and drain electrode layer was printed using an anilox-to-plate pressure of 100N, a plate-to-substrate pressure of 150N and an anilox volume of $8.0 cm^3/m^2$. These pressures were chosen after visual analysis of prints produced in preliminary trials.

Figure 9.3.2 shows a digital scan of representative prints of parallel and interdigited electrode structures. Channel lengths and widths can be measured using white light interferometry (for details on this technique see section 8.3.1). For the parallel electrode structure the average channel length was measured to be 1.85±0.02mm at a channel width of 20.43±0.02mm (width of MWCNT layer) assuming accurate registration. For the interdigited electrode structure the channel length was measured to be 0.91±0.02mm at a channel width of 43.33±0.6mm, again assuming accurate registration. The reduction in channel lengths and increase in channel widths is due to the spreading of printed features. This may need to be compensated for in further designs if devices require minimum printable channel widths.

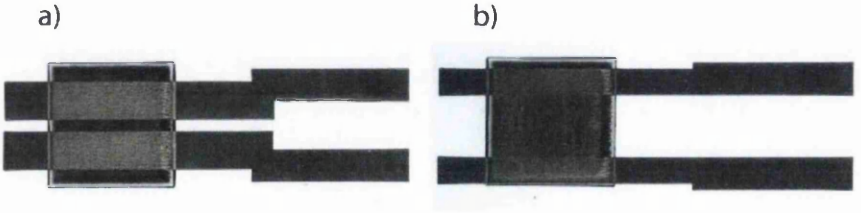

Figure 9.3.2: Optical scans of representative prints of (a) parallel and (b) interdigited electrode structures printed above the CNT layer. Printing direction was left to right.

9.3.3 Dielectric Layer

Initial trials showed poor printability of the chosen dielectric ink resulting in gate leakage and resulting non-functionality of the device. Further devices were produced using the meyer bar coating system (see section 3.4.1 for details) for this layer as the design allowed sufficient registration margin for this to be viable. Repeated overprints were performed till repeatable insulation was achieved. Final devices were produced using a total of 4 coatings alternating between bar US20 and US8 to minimise layer inhomogeneity caused by the bar structure. This resulted in a dielectric layer thickness of $24.1 \pm 3.2\mu m$. Capacitance per unit area was measured by construction of a test parallel plate capacitors with a plate area of $1 cm^2$. This was measured to be $292 \pm 103 pF/cm^2$.

9.3.4 Gate Electrode

Because the device substrates had to be altered to bar-coat the dielectric layer registration for flexographic printing of the gate electrode would prove to be difficult. As a result of this the gate electrode was also bar-coated. This was coated using a US20 bar (see Table 3.4.1 for details).

9.3.5 Summary

A representative image of the completed device is shown in Figure 9.3.3. Printing of the CNT and source/drain electrode layers was successful. Further design optimisation must concentrate on reducing feature sizes whilst compensating for ink spread and improving CNT layer homogeneity. Further research into available dielectric inks is required to obtain a suitable ink with improved printability. There is no reason why the gate electrode cannot be flexographically printed in further devices. Registration achieved was of higher accuracy than initially expected which provides further scope for feature miniaturisation. It must be noted that the magnitude of many issues observed from this printing will be reduced when performed on a conventional driven web press where impression pressures can be reduced. An example of the resolution achievable by an industrial scale flexographic press is given by Deganello *et al.*[142] who achieved reliable and repeatable printing of silver grids with line widths of 74.6 µm.

Figure 9.3.3: Representative image of a completed interdigited electrode device.

9.4 Electrical Characterisation

All devices were characterised in accordance with IEEE Std. 1620-2008, using the methods outlined in section 8.4. Data shown is from a representative sample unless otherwise stated.

9.4.1 Gate Leakage and Capacitance

The first experiment performed on every device produced was to test the IV characteristics between the gate and source/drain electrodes within the selected range of -80 to 80V. Any devices which showed a significant gate current leakage to this test was discarded, in line with the rules discussed in section 8.4.3. Capacitance between the gate and source/drain electrodes was also measured in accordance with the method outlined in section 8.4.4. The measured values are shown in Table 9.4.1. These results are not significantly different, which is unsurprising given the similar surface areas of the electrode structures which form the plate area of the equivalent parallel plate capacitor. Differences in observed capacitance can be assigned to variability in the electrode areas coated when using the draw down method for the gate electrode.

Sample Electrode Type	Capacitance [nF]
Interdigited	1.7±0.84
Parallel	0.88

Table 9.4.1: Average device capacitance magnitudes of the two electrode structures investigated in this chapter. No errors are reported for the parallel electrodes due to the lack of samples tested.

9.4.1.1 Device Hysteresis

Device reaction is slow and significant hysteresis is observed. This is likely due to a number of reasons. High parasitic capacitance caused by the electrode overlap will have a small effect, but polarisation of the dielectric is likely to be the main cause. For example Figure 9.4.1 shows the result of three transfer sweeps performed on the same sample under identical conditions. The second test was performed approximately 11 hours after the first. The third was performed approximately 50 hours after the first. The final I_{ON} current is similar for all sweeps, however the I_{OFF} current is not, suggesting insufficient relaxation time between the first and second sweep. This affects the measurement of the transconductance as well as the measurement of the on/off ratio. Due to this all tests are performed with large timescales between test times where possible to allow initial conditions to be restored. Comparison of I_{ON} currents measured using the same settings is not affected.

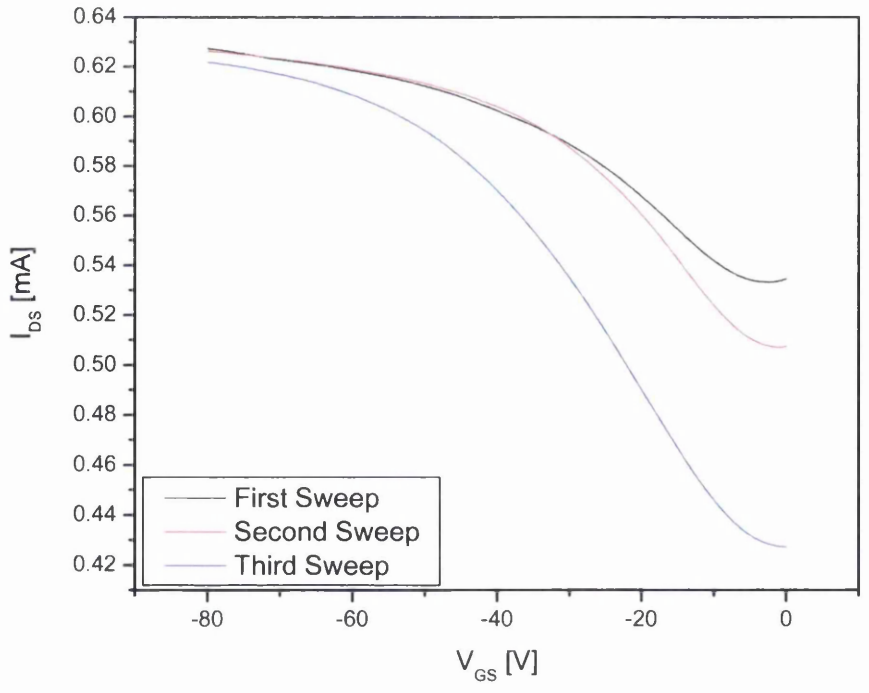

Figure 9.4.1: Transfer characteristics of an interdigited sample from -80 to 80V. Measurements were performed under identical conditions, with a time delay of 11 hours, 11 minutes and 22 seconds between first and second test and 50 hours, 32 minutes and 4 seconds between the third and first. V_{DS} was 0.5V.

9.4.2 Response Time

As stated above, response time of the devices was observed to be slow compared to conventional devices. To investigate this time delay the source drain current was monitored after a rapid increase of gate voltage from 0 to -80V in 100ms, which was then held for 12000s. Due to the limitations of the controlling software the fixed voltage of -80V applied was actually a slow voltage sweep, immediately applying -79.8V and sweeping to -80.2V in 0.001V steps at 30s delays. The results of this experiment are shown in Figure 9.4.2. This indicates an inverse negative exponential increase in source drain current that reaches a maximum of approximately 1.25mA. It takes approximately 9000 seconds for the trend to reach a state that appears linear and as such is likely due to the slow gate voltage sweep applied. Further testing to this magnitude of gate voltage must be performed over this timescale. This timescale suggests polarisation of the dielectric is occurring.

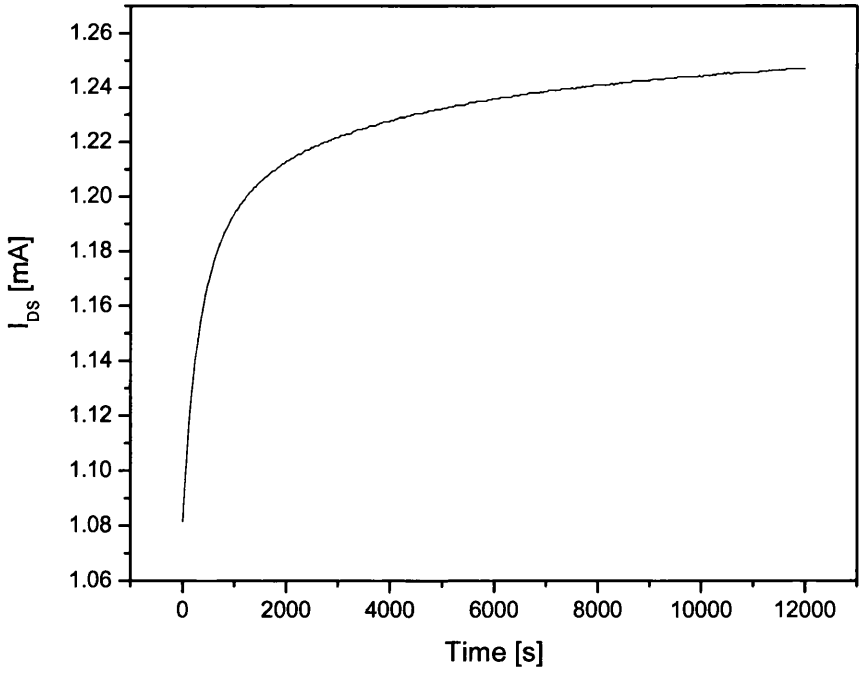

Figure 9.4.2: I_{DS} dependence with time after V_{GS} of -80V was applied. V_{DS} was 1V.

As a result of this response time care must be taken when performing transfer measurements. Figure 9.4.3 shows the maximum current measured during transfer

measurements performed over the same gate voltage range but over different times as a result of varying the sweep step delay. Sufficient time delays between sweep steps must be made to ensure maximum device performance can be reached. Notice the I_{ON} current reached using 0.1 and 1s step delays is below the minimum current observed in Figure 9.4.2, indicating that these are not indicative of the potential of the device.

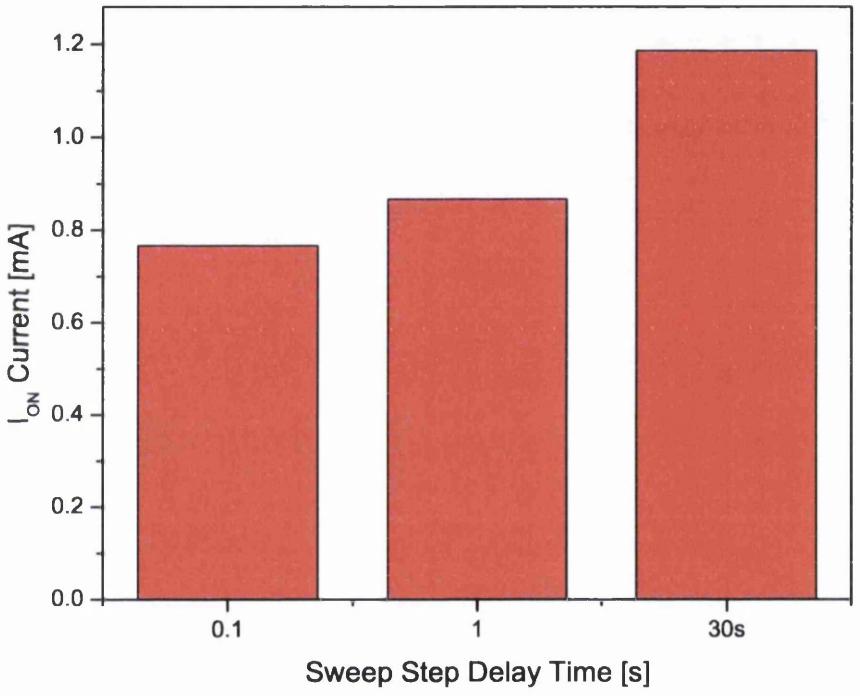

Figure 9.4.3: Maximum current measured during transfer measurements from 0 to -80V in 100mV steps at varying time delays between steps. V_{DS} was 1V.

9.4.3 IV Output

Figure 9.4.4 shows the IV characteristics of the semiconductor channel of a representative interdigited electrode sample at gate voltages of -40, 0 and 40V. Note the dependence of the gradient upon the gate voltage, an indicator of FET-like behaviour. The increase in change of gradient at negative gate voltages compared to positive gate voltages is indicative of p-type devices.

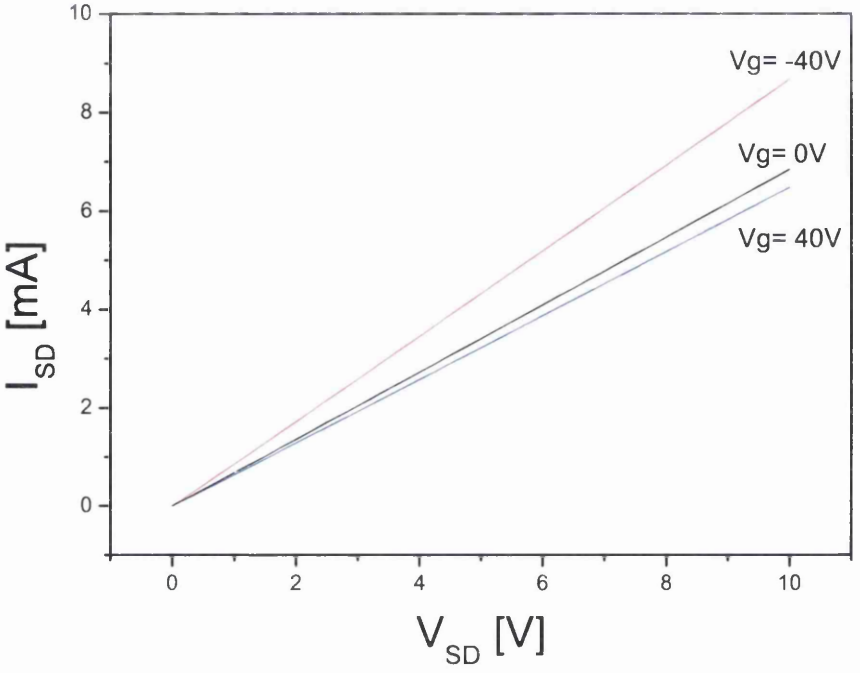

Figure 9.4.4: IV characteristics of an interdigited electrode sample at gate voltages of -40, 0 and 40V.

9.4.4 Transfer Characteristics

Figure 9.4.5 shows the positive and negative gate voltage characteristics of a representative interdigited electrode sample. Hysteresis is apparent from the 0V Vg values, see above for discussion on this point. The sweeps had to be performed independently due to software limitations, however the negative sweep was performed when the device was time stabilised, and as such the initial current is considered correct. The transfer characteristics are indicative of p-type behaviour, in line with other CNT based devices reported in the literature (see section 7.2.2).

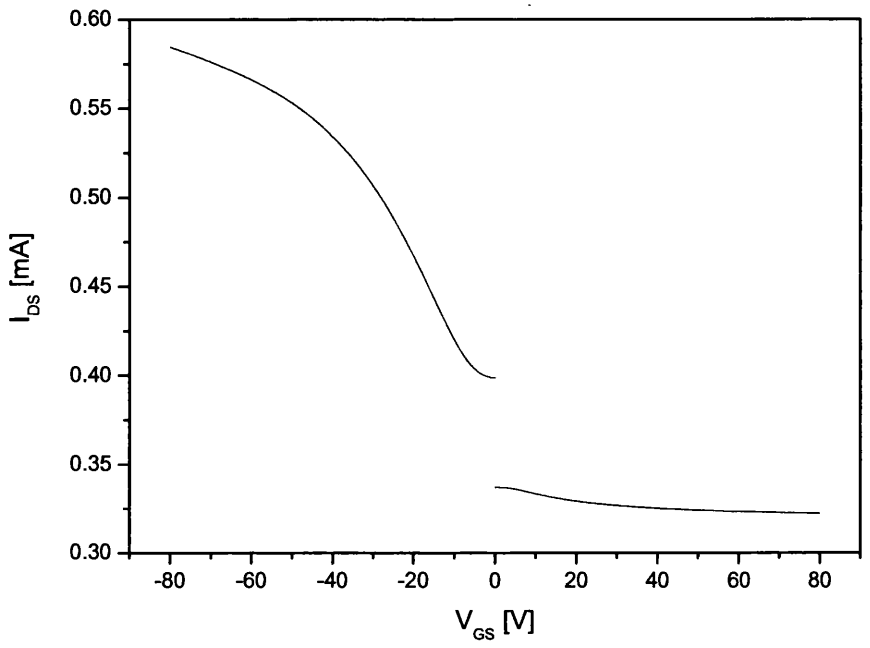

Figure 9.4.5: Transfer characteristics of an interdigited sample from -80 to 80V. Positive and negative sweeps were performed independently. V_{DS} was 0.5V.

9.4.4.1 Electrode Type Comparison

The transfer characteristics of the two electrode types are shown in Figure 9.4.6. Both show similar characteristics and on/off ratios. The interdigited electrode shown has an on/off ratio of 1.46, the parallel has a ratio of 1.77. Current magnitudes are different due to the shorter channel length of the interdigited electrode resulting in a smaller source-drain resistance.

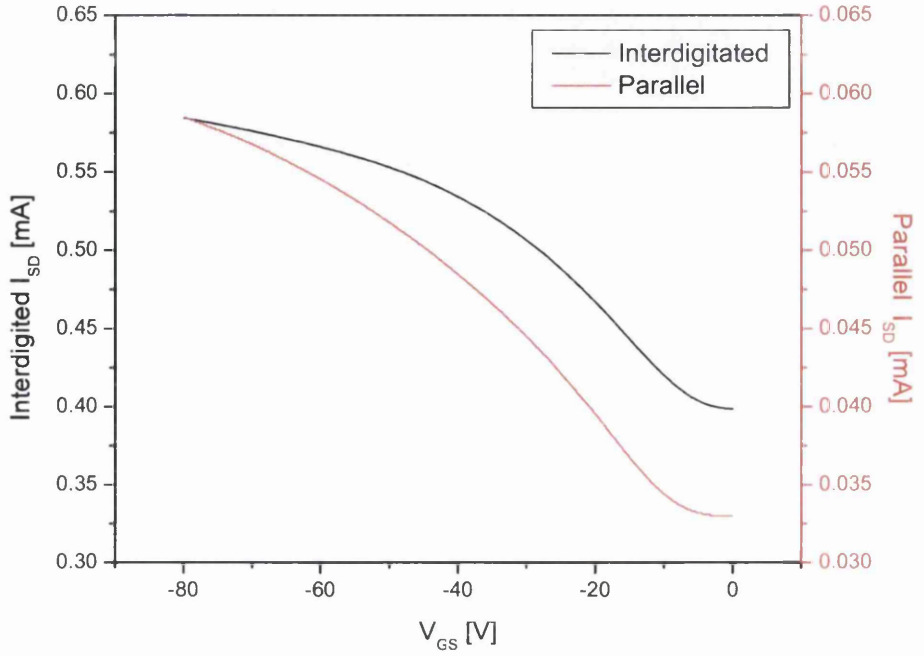

Figure 9.4.6: Comparison of interdigited (black, left axis) and parallel (red, right axis) transfer characteristics. Both electrodes were measured at a V_{DS} of 0.5V and at a sweep delay of 30s. Note that the Y scales are different in magnitude, but not proportion.

9.4.4.2 Mobility and On/Off Ratio

From the linear regime of the transfer characteristics the mobility can be calculated, in line with the method outlined in section 8.4.1. The ratio of the maximum on and off currents can also be calculated from the same results. The summary of these results is shown in Table 9.4.2. Interdigited electrode structures appear to show a higher mobility than the parallel, with a similar on/off ratio. This is counter to the results of Cao *et al.*[128], who state that the on/off ratio decreases at larger channel widths due to the higher off current. However the off and on currents observed were similar for both electrode structures, resulting in the similar ratios, as seen in Figure 9.4.6.

Sample Electrode Type	Average Mobility $[cm^2/Vs]$	Average On/Off Ratio
Interdigited	756.9±407.2	1.75±0.26
Parallel	338.5	1.77

Table 9.4.2: Average mobility and on/off ratio of the two electrode structures investigated in this chapter. No errors are reported for the parallel electrodes due to the lack of samples tested.

9.4.5 Stability Over Time

Figure 9.4.7 shows two transfer measurements made of an interdigited sample made using the same test parameters. The two tests were performed 17 months apart. During this time the devices were stored without environmental protection at room temperature and humidity. The characteristics appear similar, with an overall decrease in semiconductor channel resistance visible, the cause of which may be due to minor temperature variations in the test environment. Mobility and on/off ratio appear unchanged.

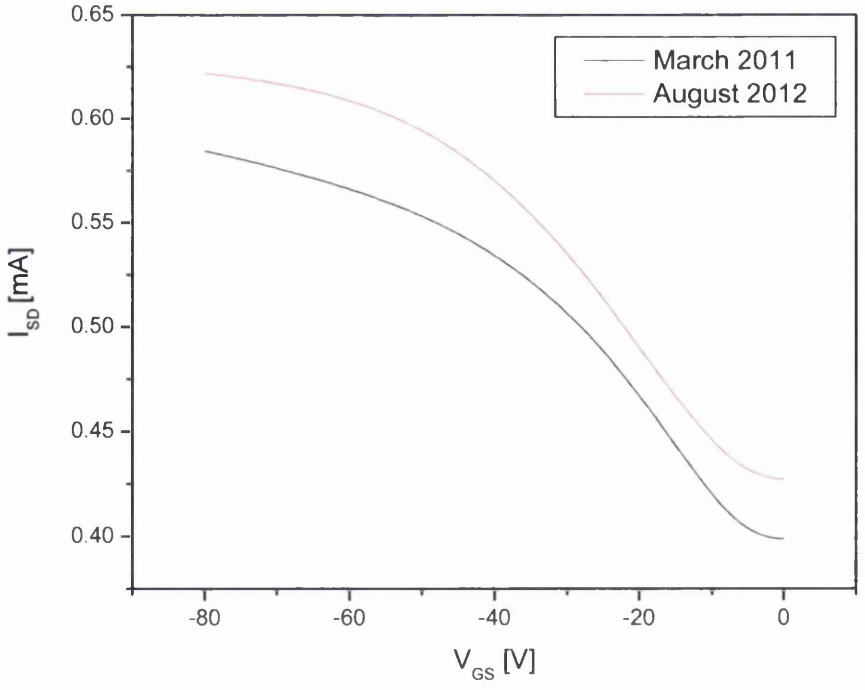

Figure 9.4.7: Transfer characteristics of an interdigited sample from 0 to -80V performed 17 months apart. V_{DS} was 0.5V.

9.4.6 Discussion

The electrical characterisation of the MWCNT based TFT structures proved that the devices show FET like behaviour. The current between the source and drain electrodes could be controlled by the application of a potential difference bias between the gate electrode and active layer. The magnitude of this effect was small, however this was expected as MWCNTs were used for the active layer, which are known to display semimetal properties (see section 1.2.4), resulting in high off currents. The devices showed p-type behaviour consistent with results from the literature [122]. It was also observed that device response was slow with large hysterisis, this is likely due to a combination of factors. The dimensions of the device are large with a high parasitic capacitance caused by the electrode overlap, although this is not likely to affect the device performance over the time periods observed. The timescale of the effects suggests gate dielectric polarisation. This caused hysteresis in the source/drain resistance, resulting in care having to be taken when selecting measurement parameters and when repeatedly testing devices. The two electrode structures selected performed similarly in terms of device attributes. The reduction in on/off ratio due to the increased channel length of the interdigited electrode structure was not observed, this may be due to the high network density minimising this effect. Device mobilities were high compared to many reported organic TFTs [13;110;111], however on/off ratios were considerably lower due to reasons already discussed. The high mobility is due to the semi metal nature of the MWCNT devices, as highlighted by the low on/off ratio, and is in line with the trends observed for CNT based TFT devices reported by Sun *et al.* [14]. Devices showed excellent stability over time, with FET like behaviour of similar magnitudes still observed after 17 months, with no special precautions taken when storing samples. A decrease in the channel resistance over time was observed, the cause of which may be due to channel doping, though the origin of this is unknown.

9.5 Conclusions

To conclude this chapter, the concept of using flexography to print the key layers of a CNT-based TFT device has been proven. The devices cannot be said to be transistors in the true sense of the word due to the high off currents observed, however they can be considered as variable resistors.

Flexography proved capable of patterning the CNT based ink, however print defects such as ink spread and viscous fingering were observed. The ink spreading is exaggerated by the printing method used, when upscaling to a driven substrate

web device the effect will be minimised. Viscous fingering is a common issue when printing solid areas. Further design optimisation is required to ensure efficient network percolation along the channel length, minimising detrimental effects caused by this inhomogeneity. Flexography also proved suitable for electrode production, with minimal edge defects observed compared to alternative printing methods.

Device performance was characterised and compared to suitable literature. Mobilities were high compared to organic TFT devices, however on/off ratios and device response speeds were poor in comparison. This was caused by material and design compromises. One key improvement in device performance compared to organic structures was in the long term stability, which proved to be excellent. This is due to the chemical stability of CNTs compared to commonly used organic semiconductors [109]. The two electrode structures tested did not have a significant effect upon device performance at this scale.

It must be noted that these initial devices are compromised in a number of aspects, primarily in the aspect of channel length and electrode overlap. These were initially thought to be close to the limits of what the printing equipment used could achieve, and not representative of the flexographic process. However during device production it was seen that the safety margins applied to the device design were conservative, and significant improvements could be made whilst still using the same equipment. Further investigation into the limits of the F1 is required to optimise the design. The use of bar coating for the printing of the gate dielectric and electrode was due to material selection, further optimisation in this area should allow the overall aim of using flexography to print every layer of the device to be achieved. The final limiting factor performance of the TFTs described in this chapter was the use of a high density MWCNT network as the active layer. This was suitable for proof of the concept, however further devices should use SWCNT networks of suitable densities to improve the on/off ratio.

Chapter 10

Flexographically Printed SWCNT Based Field Effect Devices

10.1 Introduction

The aim of the work described in this chapter is to further develop the MWCNT TFT devices produced in the previous chapter, working towards the aim of producing the first fully flexographically printed CNT based TFTs. To achieve this, firstly the key issues highlighted by the previous work must be addressed. These include minimising the parasitic capacitance of the device, reducing the channel length and optimising the materials to achieve flexographic printed TFTs.

To achieve this preliminary experiments were performed to quantify the limits of the IGT F1 in terms of registration and feature size. This allowed optimisation of the device design. In terms of materials a suitable dielectric ink was be selected to allow the layer to be flexographically printed. SWCNTs were used instead of the MWCNTs that were used in the previous study. This was expected to reduce the off current resulting in a corresponding increase in the on/off ratio. However the use of SWCNTs does increase the complexity of the device production as for optimal results the network density needs to be close to but above the percolation threshold. From the printed MWCNT results described in chapter 9 it appears that the percolation threshold is between 0.5 to 1wt% for the bar coated samples. This corresponds with the percolation threshold observed in many publications [51;62;70]. Inks should be formulated in this concentration range. It was also seen that the reduction in CNT concentration will have the corresponding effect of reducing the ink viscosity, which may increase the magnitude of the layer inhomogeneity observed in the MWCNT prints (see section 9.3.1). Steps will need to be taken to reduce the impact of this effect upon device performance.

An optimised TFT structure design was produced, with each layer characterised individually to determine the parameters required for reporting in IEEE Std 1620-2008. The devices were then characterised electrically, again in accordance with the aforementioned standards, and the performance assessed in relation to previous devices and devices reported in relevant literature.

10.2 IGT F1 Registration Capability

During the printing of the devices reported in the previous chapter it was apparent that the device design was excessively conservative in terms of the safety margin for overprinting registration. This resulted in a large dimension device with high channel lengths and parasitic capacitance. This caused slow device response times and high hysteresis in the source/drain resistance. To reduce this a study was performed to accurately assess the registration capabilities of the IGT F1. Two layers were printed, with crosses used as registration marks. The machine was reset between prints, with the plate removed from the plate cylinder and remounted to simulate the printing of different layers. A SWCNT based ink (1wt%, 1:1 PVA:CNT, NMP solvent) was used for the lower layer and a nanosilver ink (InkTec PR-030) for the upper layer to simulate further device production, as errors have been seen to occur due to slipping between the plate and substrate, the effect of which may be dependent upon the ink used. Print settings used were identical to those used in the previous device production chapter for the relevant layers (see section 9.3). The prints were digitised and the deviation in and across the print direction measured. In total 16 samples were produced, with two sets of registration marks measured on each print at opposite corners of the printing area to account for skew in the print.

The results of this study are shown in Table 10.2.1. It can be seen that the deviation across the print direction is smaller than in the print direction. This is unsurprising due to substrate movement being constrained by the F1 across the print direction (see figure 8.2.2). Standard deviation is high for both directions, therefore when considering device design the margin for registration error should be a minimum of twice the reported deviation. Skew was observed in the overprinted images resulting in differing registration depending on the image position. This is due to plate and substrate mounting errors, and can only be minimised by careful preparation during production.

	Magnitude Deviation [mm]
Across Print Direction	0.8 ± 0.7
In Print Direction	1.8 ± 1.7

Table 10.2.1: Average deviation of position of overprinted features printed using the IGT F1

10.3 IGT F1 Track and Gap Capability

To further reduce the parasitic capacitance of the device design the planar area of the source and drain electrodes should be reduced. Device speed will also be increased by reducing the channel length. This reduction in electrode size and separation must be achieved whilst still maintaining a conductive track to suitable contact points and not causing conduction between the source and drain electrodes. Significant ink spreading was also observed in the prints described in the previous chapter, resulting in a difference between the dimensions of the final structure and the specified dimensions. This phenomena should also be investigated.

To investigate this, two electrode structures were printed on the IGT F1 and the profiles measured using white light interferometry. Both structures had a 0.5mm gap separating the two electrodes. One structure had an electrode thickness of 1mm, the other 0.5mm. Devices were printed using the lowest engagement pressure printable (50N) and the lowest anilox volume available of $2.7cm^3/m^2$. The same nanosilver ink used for device electrode production (InkTec PR-030) was used.

The results of the trial are summarised in Table 10.3.1. Significant spreading can be seen on all printed lines. Significant decrease in the printed gap size is observed as a result, which can be used to minimise the channel length in printed devices though care must be taken not to cause shorting between the electrodes. A nominal $250\mu m$ gap is printable using the F1 with $500\mu m$ electrode widths.

The spreading tends to increase at the end of the lines in relation to the print direction, as shown in the white light profile image in Figure 10.3.1. This spreading caused by the separation of the relief area of the image master from the deposited ink film should be compensated for in the design. A similar effect, but not as severe in magnitude, is seen at the initial contact points.

10.4 Device Design

The compromises made in the design used in chapter 9 detrimentally affected the performance of the resulting devices. As previously discussed, the design of a TFT

	Electrode Width [μm]	Gap Width [μm]
500μm Electrodes, 500μm Gap		
Polymer Plate	471.0	501.5
Print Average	730.0±41.7	268.9±39.4
Percentage Change	55.0%	-46.4%
500μm Electrodes, 500μm Gap		
Polymer Plate	469.4	274.0
Print Average	702.5±12.4	80.4±5.2
Percentage Change	49.7%	-70.7%

Table 10.3.1: Table summarising the results of the track and gap study performed on the IGT F1 for electrode optimisation.

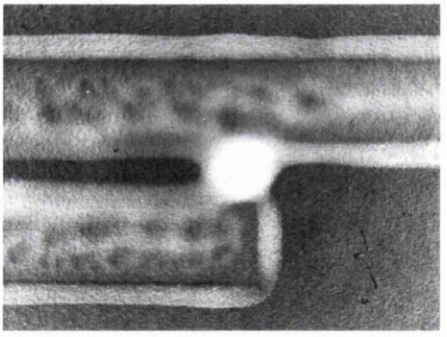

Figure 10.3.1: Grayscale representation of profile data from electrode tip showing shorting across the channel length. Lighter areas indicate raised points.

structure is determined by the materials and manufacturing process used. By optimising the manufacturing process and using more suitable materials the performance is expected to improve with respect to on/off ratio, mobility and device response. In terms of the manufacturing process flexography is used for the production of all layers, for reasons described previously (see section 9.2). The use of flexography has now been proven to be suitable for the electrode and active layers, and its suitability for manufacturing the dielectric and gate insulator is to be investigated in this chapter.

10.4.1 Materials

In terms of materials selection the previous work showed that MWCNTs provided device functionality, but were limited in performance. The Ag inks used for the electrodes was seen to be suitable. The dielectric ink used was not suitable for flexographic printing. Optimisation of the active and dielectric layer is required to improve performance.

10.4.1.1 Semiconductor Layer

As stated above, MWCNTs were seen to provide device functionality but at the expense of high off current due to their semimetal properties. Although a SWCNT network will show semimetal properties at high densities, as the density is reduced towards the percolation threshold the on/off ratio should increase, as seen in the literature (see section 7.2.2). All the research concerning CNT based inks presented so far in this thesis has used MWCNTs for cost reasons. However the substitution of MWCNTs with SWCNTs is possible, though it has been shown that SWCNTs are harder to disperse due to the higher quality of the CNT structure resulting in fewer defects. The defects act as functionalisation sites, which affect the solubility of the structure. As a result it is unlikely that the high concentration MWCNT inks can be reproduced with SWCNTs, though lower concentration inks will be required to achieve suitable density networks.

The inks used in the device are based on the research presented in Part II. Two inks were produced containing CNT concentrations of 0.5 and 1wt%. The CNT used were Thomas Swan EliCarb SW and were used without modification. Inks were mixed for 45min using an ultrasonic probe at the same settings described in section 3.2.1.3. NMP was used as the solvent and PVA was used as the resin at a 1:1 ratio. The ink formulation contents are shown in Table 10.4.1.

Constituent	Target Mass [g]	Target Mass [g]
	1wt% Concentration	0.5wt% Concentration
CNT	0.2	0.1
NMP	19.6	19.8
PVA	0.2	0.1
Total Mass	20	20

Table 10.4.1: Target ink constituent mass for 0.5 and 1wt% SWCNT based ink for use in TFT structures.

10.4.1.2 Source and Drain Electrodes

A commercial nanosilver based ink (Inktec PR-030) was used due the suitability shown in previous devices and optimisation tests. The properties of this ink were discussed in section 9.2.1.2.

10.4.1.3 Dielectric Layer

The ink used for the dielectric layer was a commercial dielectric ink produced by Gwent Electronic Materials (D2071120D1 Polymer Dielectric). Scoping experiments showed it to have suitable adhesion and insulating properties. These experiments also indicated improved flexographic printability in comparison to the D2090130P5 ink used in the previous experiments, a major consideration as device production by flexography was a key target for the work. Suggested drying conditions are 130^{o}C for 10 to 15 minutes.

10.4.1.4 Gate Electrode

A commercial silver based ink (Gwent Electronic Materials C2090210P12 silver ink) was used due the layer compatibility shown in previous devices. The properties of this ink were discussed in section 9.2.1.4.

10.4.1.5 Substrate

The polyester based film used for previous devices was used. For further details see section 9.2.1.5.

10.4.2 Structure

The experimental determination of the layer registration and feature size capabilities of the IGT F1 system (see sections 10.2 and 10.3) allows the optimisation of the

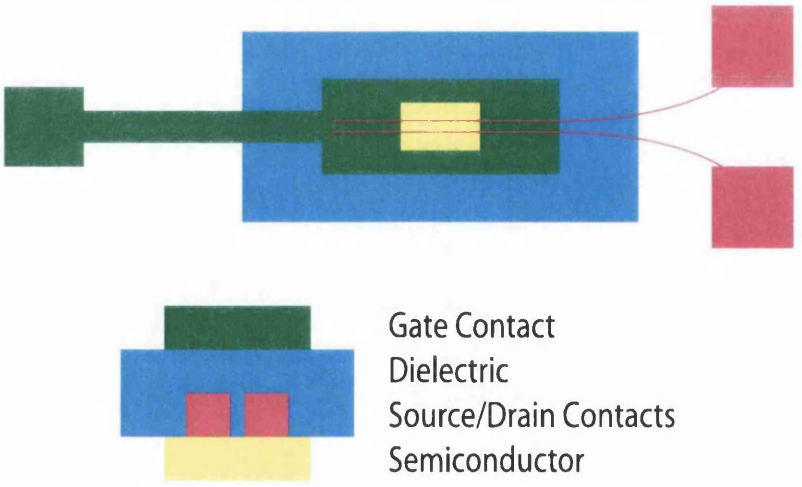

Figure 10.4.1: Top gate, top contact TFT structure shown schematically from a top down and cross section view. Devices were printed from left to right as viewed.

design by reduction of feature dimensions. The TGTC structure was maintained due to the previously discussed layer compatibility issues. The overall device layout is shown in Figure 10.4.1.

10.4.2.1 Semiconductor Layer

The semiconductor layer master image is shown in Figure 10.4.2. The image consists of repeated 0.1mm lines placed perpendicular to the electrode direction separated by 0.1mm spacings. The lines are used to separate the image to avoid inhomogeneities forming parallel to the print direction, a technique similar to that proposed by Rouhi *et al.*[109] to reduce the effective channel width and by Hamblyn *et al.*[143] to reduce viscous fingering effects. The striping results in a nominal channel width of 2.5mm (5mm including gaps), though ink spreading will increase this value significantly.

The dimensions of the CNT layer were selected with regards to the registration limit of the F1 investigated in section 10.2, with the channel length direction dimension of 3mm being twice the average registration accuracy observed.

10.4.2.2 Source and Drain Electrodes

The image master for the source and drain electrodes is shown in Figure 10.4.3. The electrodes are $200\mu m$ wide with a source to drain gap of $250\mu m$, values that were selected as the minimum that can be reliably printed based on the results of scoping experiments including those described in section 10.3. The contact areas were positioned so that they are the final areas to be printed and the electrode tracks

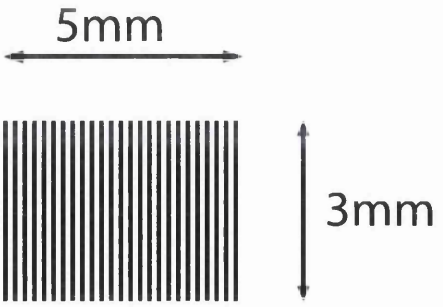

Figure 10.4.2: Semiconductor layer master image used in the production of SWCNT devices. Lines are 0.1mm repeated at 0.1mm spacings.

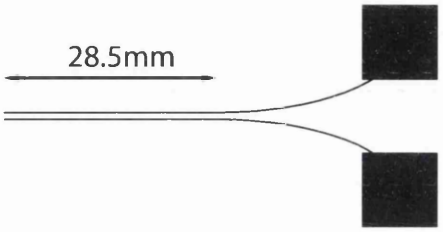

Figure 10.4.3: Source and drain electrode image masters used in the production of SWCNT devices.

diverge to avoid shorting due to spreading at the point of disengagement of the imaged area of the plate and substrate, a phenomenon noted in earlier trials. The electrode tips at the start of the print direction were also rounded to minimise this phenomenon. The minimisation of the electrode widths serves to decrease the conductive area of the layer, hence reducing the parasitic capacitance.

10.4.2.3 Dielectric Layer

The dielectric layer master image is shown in Figure 10.4.4. The dimensions of this layer do not affect the device performance, and as a result are made arbitrarily large to minimise the possibility of poor registration.

10.4.2.4 Gate Electrode

The gate electrode layer master image is shown in Figure 10.4.5. Minimisation of the parasitic capacitance of the device is achieved by the reduction in the surface area of the source and drain electrode, hence the dimensions of the gate electrode not being of critical importance to device performance.

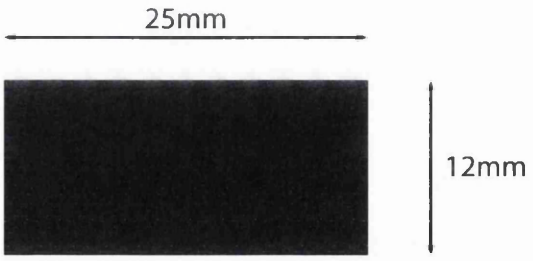

Figure 10.4.4: Dielectric layer master image used in the production of SWCNT devices.

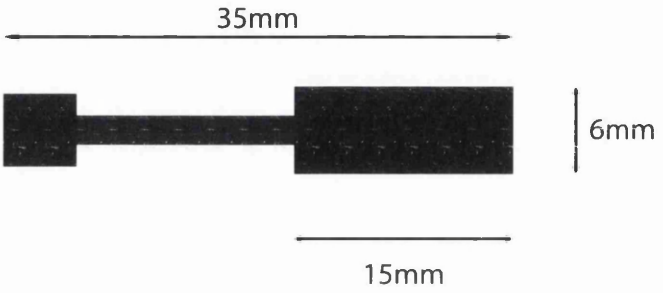

Figure 10.4.5: Gate electrode layer master image used in the production of SWCNT devices.

10.4.3 Design Summary

The device structure for the TFTs produced in this chapter was an evolution of the structure produced in chapter 9. The key improvements made were the use of SWCNTs and the minimisation of the electrode size and channel length. This was expected to reduce parasitic capacitance, increase device response speed and improve mobility and on/off ratio.

The final printing plate master images are shown in Figure 10.4.6. Two devices are produced in each batch. Crosses were included to improve visualisation of layer registration.

10.5 Device Production and Structural Characterisation

10.5.1 Semiconductor Layer

The CNT layer was produced using a specified engagement pressure of 75N using an anilox volume of $8.0cm^3/m^2$. These settings were selected after scoping experiments in which prints were characterised by electrical and visual properties. Assuming the

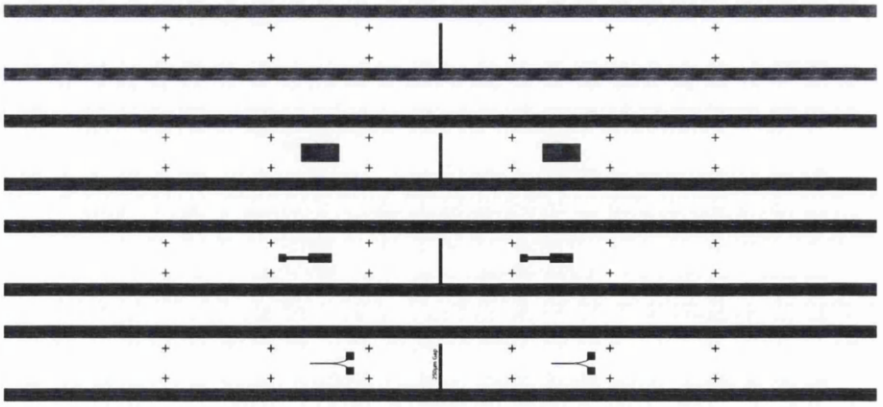

Figure 10.4.6: Image masters for the four printing plates used in the device production of SWCNT based TFT structures.

Figure 10.5.1: Optical scan of representative print of 1wt% SWCNT ink. Printing direction was left to right.

nominal anilox cell volume and an ink release rate of approximately 40% [135] this should result in a theoretical ink film thickness of 64nm for the 1wt% concentration ink and 32nm for the 0.5wt% concentration.

The use of plate patterning to minimise the effect of layer inhomogeneities perpendicular to the channel length has had a significant effect, with no viscous fingering and minimal ink spreading visible despite the non-ideal viscoelastic properties of the ink for flexographic printing. The line spacing is of sufficient magnitude to still be visible in the print despite the line spread, which occurs in isolated areas. Inhomogeneous areas are still apparent where ink spread causes coalescing of the lines. This appears to lead to higher density areas, as visible in the lower right portion of the print.

10.5.2 Source and Drain Electrodes

The source and drain electrode layer was printed using an anilox-to-plate pressure of 60N, a plate-to-substrate pressure of 60N and an anilox volume of $2.7 cm^3/m^2$. These

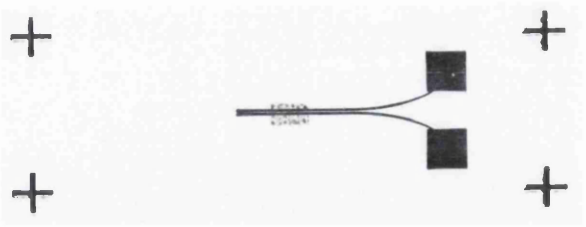

Figure 10.5.2: Optical scan of representative print of electrode structure printed above the CNT layer. Printing direction was left to right.

settings were based upon the settings used in the track and gap trial discussed in section 10.3.

Figure 10.5.2 shows an optical scan of a representative device. The average channel length was measured using WLI techniques, from which a value of $120 \pm 15\mu m$ was obtained, a drop of 52% from the nominal value. The divergence of the electrode to the contact points ensures no shorting between the electrodes occurs, however the rounding of the tips at the point of contact between the imaged area of the plate and the substrate did not remove spreading at this point. This resulted in some devices shorting, though the majority of prints were suitable. Any reduction in channel length in this area is irrelevant to device performance due to it being outside the active layer overlap.

10.5.3 Dielectric Layer

The dielectric layer was printed using an anilox-to-plate pressure of 100N, a plate-to-substrate pressure of 150N and an anilox volume of $12cm^3/m^2$. These settings were optimised in a series of preliminary printability trials. Initial tests indicated that repeated overprinting was necessary to ensure no gate leakage current occurred. Initial trials printed upon solid areas indicated that four overprints were necessary to ensure an insulating layer was formed, however devices produced using four layers showed significant leakage current, rendering them unusable. This was because the source and drain electrode layer was rougher than the lower layer used in the earlier trial. All further devices used five overprints of the dielectric layer. This resulted in an average layer thickness of $49.2 \pm 4.6\mu m$.

10.5.4 Gate Electrode

The gate electrode was printed using an anilox-to-plate pressure of 100N, a plate-to-substrate pressure of 150N and an anilox volume of $24cm^3/m^2$. These settings were

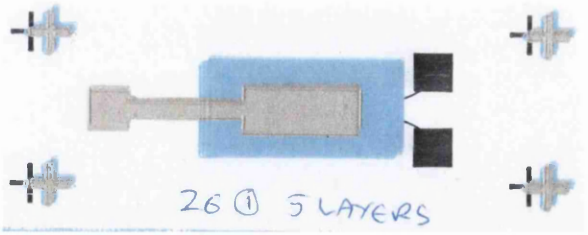

Figure 10.5.3: Representative image of a complete, fully flexographically printed, SWCNT based, TFT device.

optimised in a series of preliminary printability trials. Two overprints were required to ensure conductivity along the entire electrode due to the step at the edge of the dielectric layer. Average device capacitance was $51 \pm 16pF$, a significant decrease from the previous generation of devices reported in chapter 9. Assuming nominal device area, this results in an average capacitance per unit area of $386.9pF/cm^2$.

10.5.5 Summary

A representative image of the completed device is shown in Figure 10.5.3. This is the first reported example of a CNT based TFT structure printed entirely using flexographic methods. In terms of channel length and parasitic capacitance this device structure is near to optimal for a TFT designed with the aim of minimum response time printed using the IGT F1 printability tester. An indicative visual representation of the registration capabilities of the equipment can be seen from the registration marks shown. Further device optimisation will only be obtained by material improvements, or by manufacture using flexographic presses with independently driven substrates, accurate plate-to-substrate engagement control and accurate registration capabilities.

10.6 Electrical Characterisation

All devices were characterised in accordance with IEEE Std. 1620-2008, using the methods outlined in section 8.4. Data shown is from a representative sample unless otherwise stated.

10.6.1 Gate Leakage and Capacitance

Initial devices produced using four overprints for the dielectric layer were seen to have significant gate leakage, as reported in section 10.5.3. Another factor observed

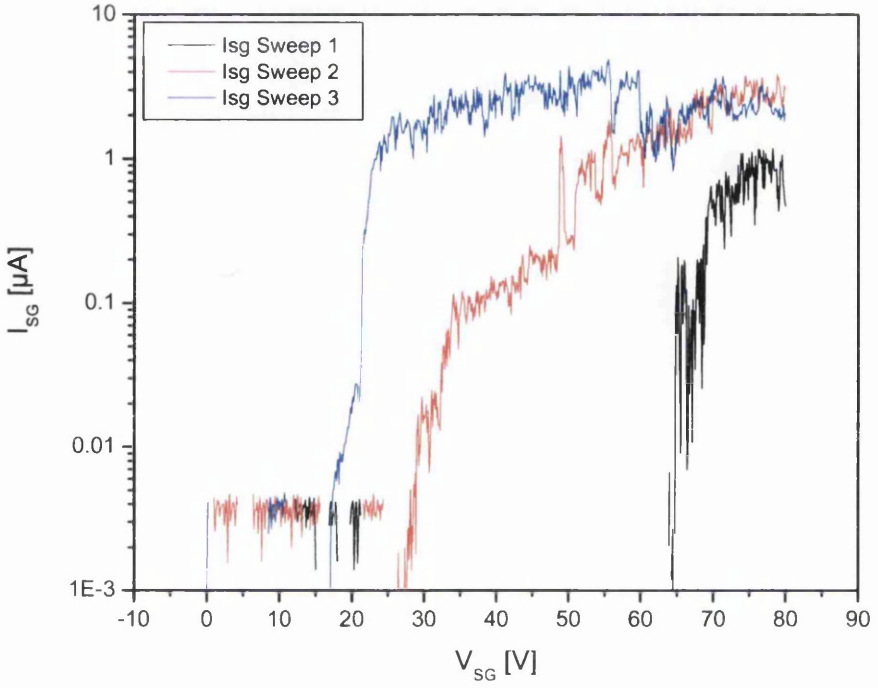

Figure 10.6.1: Repeated IV sweeps between source and gate electrode of a sample printed with 4 overprints of dielectric.

during the experiments to characterise the gate leakage was that there was a threshold leakage voltage (known as the dielectric breakdown voltage) above which the leakage current was observed, and that this breakdown voltage appeared to become lower after repeated tests. This can be observed in Figure 10.6.1, where three IV curves of the source to gate electrodes are plotted, which were taken one after the other. Note the breakdown voltage for leakage dropping from approximately 65V to 20V. All further devices were repeatedly tested for gate leakage in this manner before subsequent characterisation. Gate leakage was not observed to be significant, with no breakdown voltage observed within the measured range in samples printed with five overprints for the dielectric layer.

Capacitance between the the gate and source/drain electrodes was also measured in accordance with the method outlined in section 8.4.4. The measured values are shown in Table 10.6.1. The 0.5wt% SWCNT devices show lower capacitance than the 1wt% devices, as both were prepared identically it can only be assumed that this

SWCNT Concentration [wt%]	Capacitance [pF]
1	53.40 ±17.33
0.5	26.90 ±3.57

Table 10.6.1: Average device capacitance magnitudes of the two SWCNT concentrations investigated in this chapter.

is due to the higher S/D resistance. The capacitance is multiple orders of magnitude lower than the MWCNT devices previously reported. This is due to a combination of the reduction in electrode area and the change in dielectric material. The new material and reduced electrode overlap has led to a reduction in parasitic capacitance and dielectric polarisation leading to a corresponding improvement in device response. However any drop in capacitance due to the dielectric material is not necessarily advantageous. It has been observed by Kim *et al.*[144] that a reduction in dielectric thickness (and hence an increase in device capacitance) causes an increase in on/off ratio. As reported above, the number of layers printed was the minimum to obtain suitable insulation, therefore any further increase in capacitance would require a higher dielectric constant material at this layer thickness.

10.6.1.1 Noise

Due to the high S-D resistance of the samples and the requirement for the S-D voltage to be significantly lower than the gate voltage for calculation of the mobility (see section 8.4.1) many transfer measurements were observed to show significant random noise. To minimise the effect of this data was smoothed by the adjacent averaging method, with a sample size of 10 points. Unless otherwise stated, all transfer data presented in this chapter has been smoothed, and smoothed data was used for all mobility and on/off ratio calculations.

10.6.1.2 Device Hysteresis

Figure 10.6.2 shows the results of two transfer measurements, with the second measurement started 4s after the end of the first. No significant hysteresis is observed, indicating that the sample relaxation time is suitable for repeated measurements with minimal delay, unlike the devices discussed in section 9.4.1.

10.6.2 IV Output

Initial IV characteristics of devices commonly showed non-ohmic tendencies. This is highlighted in Figure 10.6.3. This has been observed at low temperatures by Kim *et*

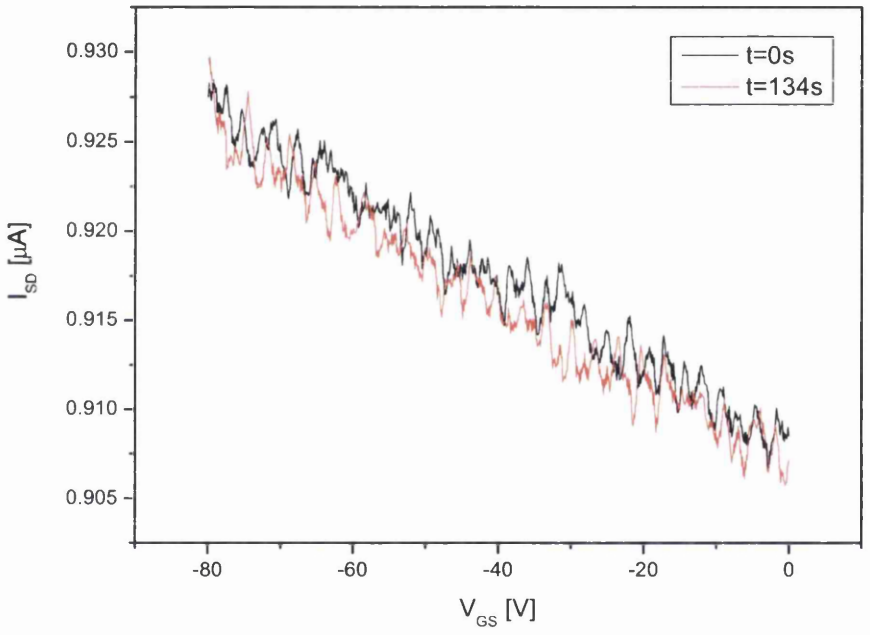

Figure 10.6.2: Two sets of transfer characterisation data of a representative sample. The time (t) refers to the start of the measurement sweep, and total time for the sweep was 130s, meaning that the second sweep was performed 4s after the end of the first.

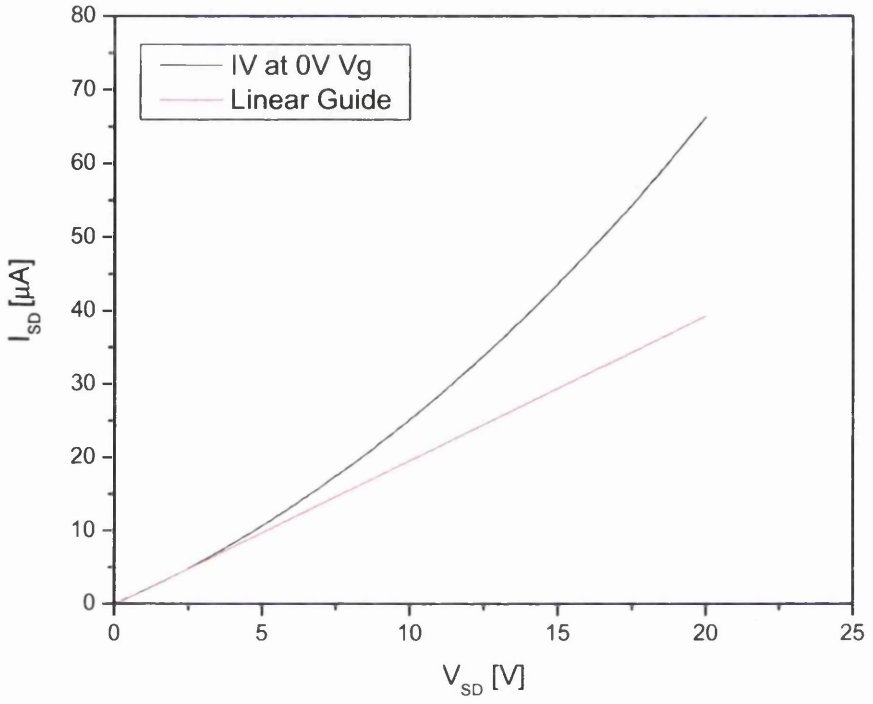

Figure 10.6.3: Source-drain IV characteristics of a representative 0.5wt% CNT concentration device. To highlight the non linearity of the sample a linear approximation of the 0 to 2.5V range has been projected to 20V.

al.[44] who attributed it to the potential barrier formed at tube contact points. It is also reported to be visible at room temperature in printed networks[47] and SWCNT based printed TFTs[15;130]. The results of Okimoto *et al.*[15] show the IV characteristics being linear at higher CNT densities and non-linear when below the percolation threshold, therefore this non-linearity may be an indicator that the solutions are approaching the percolation threshold. It may also be due to poor S/D contact with the CNT layer, however Ag is a common electrode material and no non-linearity was observed with the high density MWCNT networks. The 0.5wt% device IV characteristics appear to show more pronounced non-ohmic characteristics compared to the 1wt% devices.

The IV output characteristics of representative 1wt% and 0.5wt% samples are shown in Figures 10.6.4 and 10.6.5 respectively. Field effect behaviour is observed, however the effect is small. Both devices show a more significant effect at negative gate voltages, an indicator of p-type behaviour.

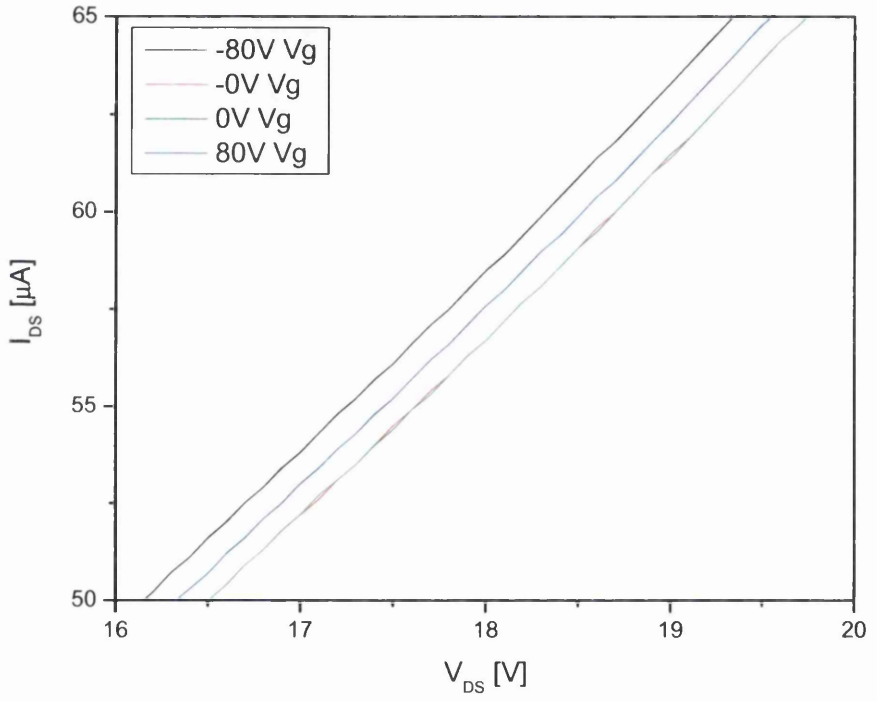

Figure 10.6.4: IV characteristics of a 1wt% SWCNT based sample at gate voltages of -80, 0 and 80V. The two 0V datasets were measured before measuring the +80V and -80V characteristics to ensure device was in a stable state.

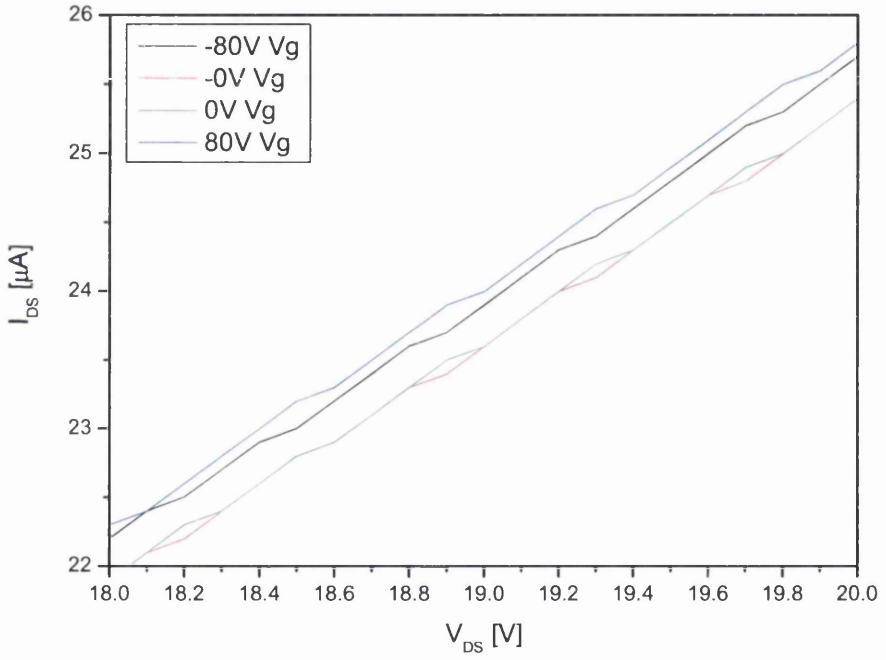

Figure 10.6.5: IV characteristics of a 0.5wt% SWCNT based sample at gate voltages of -80, 0 and 80V. The two 0V datasets were measured before measuring the +80V and -80V characteristics to ensure device was in a stable state.

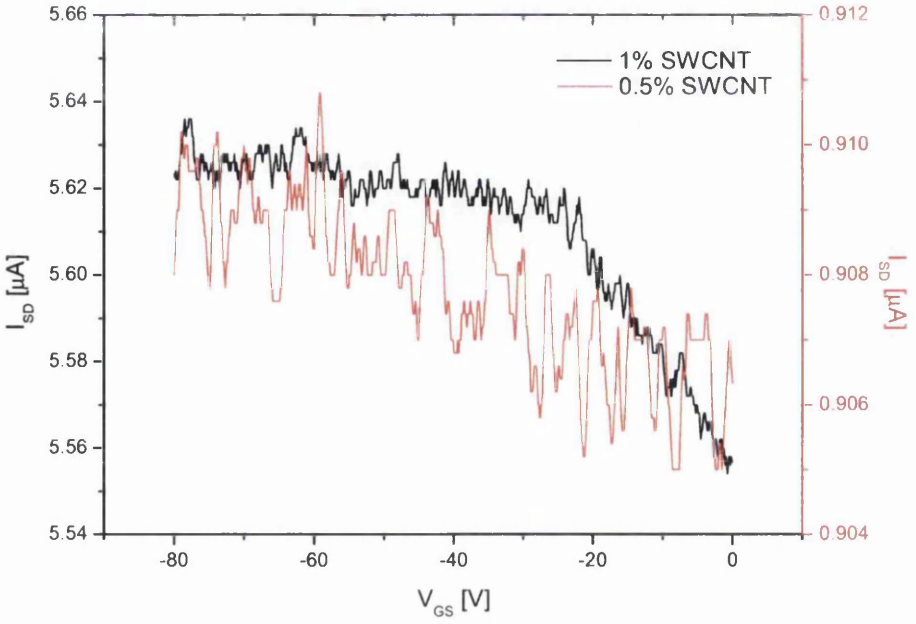

Figure 10.6.6: Comparison of 1wt% (black, left axis) and 0.5wt% (red, right axis) concentration transfer characteristics. Devices were measured at a V_{DS} of 1V and at a sweep delay of 1s at 1V steps.

10.6.3 Transfer Characteristics

The transfer characteristics of both CNT concentration devices are shown in Figure 10.6.6. The increase in noise in the 0.5wt% sample may be due to the lower drain currents seen at the applied drain voltage due to the higher channel resistance. Both devices show similar characteristics, with p-type behaviour observed.

10.6.3.1 Mobility and On/Off Ratio

From the transfer data mobility and on/off ratio can be calculated using the method described in section 8.4.1. The average mobility and on/off ratio for the 1 and 0.5wt% devices is summarised in Table 10.6.2. Mobility is reduced when the CNT network density is reduced.

10.6.4 Stability Over Time

Figure 10.6.7 compares two transfer measurements taken 10 months apart of a 1% SWCNT based sample. Devices were stored without environmental protection at

SWCNT Concentration [wt%]	Average Mobility $[cm^2/Vs]$	Average On/Off Ratio
1	0.14 ±0.05	1.12 ±0.21
0.5	0.002±0.001	1.02±0.02

Table 10.6.2: Average mobility and on/off ratio of the two CNT concentrations investigated in this chapter.

room temperature and humidity. Although the magnitude of the source-drain current has changed, the transfer characteristics have not. The magnitude change may be due to small temperature differences in the test environment between the two tests.

10.6.5 Discussion

The electrical characterisation of the SWCNT based devices showed field effect behaviour, however this is reduced compared to the MWCNT based devices described in the previous chapter (Chapter 9). The small magnitude of this effect is likely to be caused by the CNT networks being of a density higher than the metallic percolation threshold. The results compare favourably with those of Okimoto *et al.*[15] shown in Figure 7.2.5. Okimoto observed that at network densities higher than the percolation threshold linear transfer characteristics are observed, similar to those seen in Figure 10.6.6. The paper also shows that as network densities decrease the IV output characteristics become increasingly non-linear, an effect observed in Figure 10.6.3. Finally the reduction in mobility and stable on/off ratio with decreasing network density are also consistent with literature. These results strongly indicate that the devices are functioning correctly but the CNT concentration in the inks was too high, resulting in network densities that appear comparable to the 4 to 2% regime seen in Figure 7.2.5. The non-ohmic IV behaviour further implies that the devices are approaching the percolation threshold. Mobility and on/off ratio may have also been impeded by the low S/D gap, as $100\mu m$ is shown in Figure 7.2.4 to show the lowest values.

The devices showed significant improvement in response and hysteresis compared to previous generations. Stability over time was also observed to be excellent, with a change in S/D resistance attributable to unavoidable variance in temperature.

10.7 Conclusions

To conclude this chapter, the use of flexography to print CNT based TFT devices has been proven. Devices with practical architecture have been produced using only

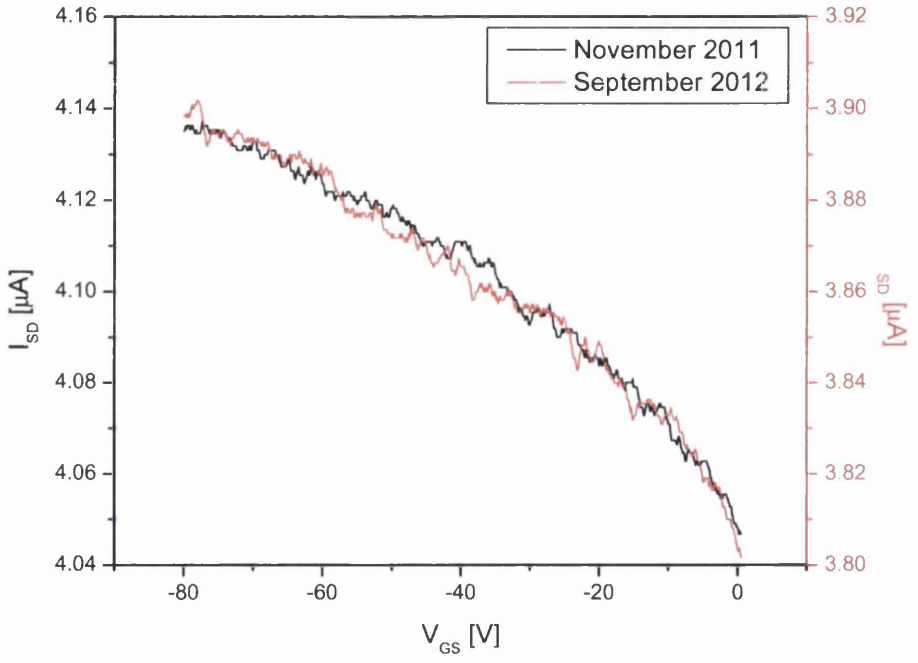

Figure 10.6.7: Transfer characteristics of a 1wt% SWCNT sample from 0 to -80V performed 10 months apart. V_{DS} was 2V. Note that the Y scales are different in magnitude, but not scale.

flexography and although electrical performance is poor results are comparable to those of high density devices in the literature.

By optimisation and characterisation of the printing capabilities of the IGT F1 equipment devices with S/D gaps of the order of $100\mu m$ were fully printed. As suggested by Hamblyn *et al.*[143] plate patterning can be used to minimise the effects of print inhomogeneities which are common in the flexographic printing process and exaggerated by the reduced viscosity of the low concentration SWCNT inks. The dielectric layer required multiple overprints, which would not be ideal if production were to be upscaled. Further materials development in this area is required.

Device performance was characterised and compared to suitable literature. Overall performance was poor, however was comparable to high CNT density devices reported by Okimoto *et al.*[15]. The change of dielectric material, reduction in channel length and reduction in parasitic capacitance has resulted in devices that show little of the hysteresis and slow response time observed in previous results (Chapter 9). IV output showed non-ohmic behaviour, as observed in CNT networks approaching the percolation threshold[15;44;130]. Transfer characteristics for the two CNT concentrations tested showed behaviour consistent with that of devices with CNT networks in the density range of 4-2%[15]. The reduction in mobility observed at lower densities reinforces this observation. Device stability was excellent over the timescale tested.

The optimisation of the design by thorough characterisation of the printing method used resulted in efficient architectures that were fully printable by roll to roll methods. Poor device performance has been observed to be directly due to the CNT concentration, therefore further investigation should concentrate on reducing this whilst maintaining a printable CNT layer. The use of lower anilox volumes may be a potential method to achieve this without reducing ink viscosity further by reducing CNT concentration. Investigation into the effects of channel length would also be advantageous, especially if thorough analysis of device response can be performed. The only remaining barrier to upscaling device production onto a true roll-to-roll production line is the drying of the layers, a common issue in printed electronics and an active area of research.

Chapter 11

Flexographically Printed CNT Based TFT Structures - Conclusions

11.1 Initial Aims and Approach

As stated in Chapter 1, the initial aim of this section of work was to:

- develop a CNT based TFT manufactured entirely using processes that can be scaled for high speed, roll to roll printing techniques.

To this end, an experimental outline consisting of initial proof of concept followed by incremental optimisation was planned and performed. To achieve the aim of using roll to roll techniques flexography was chosen to produce all layers. Two generations of devices were presented in this thesis, the first being the initial proof of concept devices. These devices were produced using a combination of flexography and bar coating, with a high concentration MWCNT based ink used for the active layer. The results of this study were then used to highlight key areas for optimisation, and further study was then performed to investigate the capability of the flexographic printability tester used for device production. Once this capability was known, devices were redesigned to maximise potential performance. These generation devices were then produced using 1 and 0.5wt% SWCNT based inks using only flexography for all layers. All devices were electrically characterised in accordance with established standards.

11.2 Overall Results and Conclusions

The experiments described in chapter 9 describe the initial device design and production for the proof of the concept that CNT based TFT devices could be produced using flexography. The device design was constrained by the a combination of the

compatibility of the ink systems used and the assumed limitations of the flexographic printability tester used for production. These limitations resulted in a TGTC structure with a large source drain gap and high parasitic capacitance. Two electrode structures were investigated, parallel and interdigited.

Device production was partially successful. The CNT ink was printable using flexography, but the print inhomogeneities were visible. These were spreading due to the engagement pressure required for printing and viscous fingering, common with solid area printing. The source and drain electrodes were printed, with ohmic contact observed between the CNT and electrode layers. The dielectric and gate electrode layer were coated using the Meyer bar method due to the dielectric material selection. Bar coating is a roll-to-roll capable technique, however it is not possible to pattern in a single step in a production environment.

The electrical performance of the devices was examined, with field effect behaviour observed, proving the concept of flexographically printed CNT based TFT structures. Device capacitance was high due to the electrode area overlap of the design. Slow device response and significant hysteresis during measurement was observed, the timescales of which suggest that the dielectric is susceptible to polarisation, though further experiments are required to investigate this phenomena fully. The two electrode structures showed similar performance, with average on/off ratios of 1.76 and mobilities of $651 cm^2/Vs$. The mobility is significantly higher than commonly reported organic TFT devices, however the on/off ratio is significantly lower. The high mobility and off current caused by the use of a high density MWCNT network as the active layer means that the devices cannot be considered to act as transistors, however they can be considered as variable resistors. The devices were observed to show p-type behaviour, which is in agreement with literature on undoped CNT based field effect devices. The stability of the electrical performance over a 17 month timescale was assessed with excellent results, despite no particular precautions being taken during storage.

The high parasitic capacitance of the devices led to experiments being performed to establish the maximum capabilities of the IGT F1 flexographic proofing device used for device production. The registration capabilities were assessed to establish required margins for overprinting of layers, leading to required minimum margins of 0.8mm across the print direction and 1.8 mm in the print direction being required. Minimum feature sizes were also assessed to minimise electrode areas to reduce parasitic capacitance and channel lengths to improve device response times. It was seen that

nominal track sizes of $500\mu m$ were consistently achievable with $250\mu m$ gaps achievable with care. Key areas of ink spreading during plate and substrate engagement were highlighted, which were factored into further designs.

The final generation of device design reported took the results of the capability studies into account and reduced nominal source/drain electrode widths to $200\,\mu m$ with a $250\mu m$ specified channel length. The CNT layer design was modified to reduce unintentional inhomogeneity. The TGTC structure was maintained due to ink compatibility requirements. A parallel source/drain electrode structure was used for device simplicity as no significant advantage to the interdigited electrode structure was seen. The dielectric material was substituted for one with improved flexographic printability, which also proved to be less susceptible to polarisation. SWCNTs were used in inks based on the same formulation developed in part II at concentrations of 0.5 and 1wt% to examine the CNT density required to reduce the high off current with the high density MWCNT network.

Device production was successful. All layers were printed using flexography. The patterning of the CNT layer reduced inhomogenities parallel to the electrode direction. Average channel length was $120 \pm 15\mu m$. A minimum of 5 overprints of the dielectric layer was required to obtain insulation between the electrode layers. Flexography shows a number of advantages over comparable printing techniques, namely the homogeneity of the electrode structures and flexibility of ink rheologies. The low image master cost is also a significant advantage for R&D purposes.

The performance of the devices was poor, with mobilities in the range of 0.002 to $0.14cm^2/Vs$ and on/off ratios in the range of 1.12 to 1.02 observed. This was not due to the design optimisation, which was a success with the aims of reducing parasitic capacitance and improving device response achieved. The electrical performance was compared to literature and was seen to be comparable to reported high network density devices. The reduction in mobility and non-ohmic IV characteristics reinforced the conclusion that the network densities printed were approaching the percolation threshold but too high for adequate device performance. Device stability was again excellent over a 10 month period.

11.3 Summary

In summary, the first ever reported printed TFT devices produced using solely flexography, and the first ever use of flexography to deposit CNT networks has been shown. Flexography is a viable method for TFT device production, and shows a number of

advantages, particularly in the printing of source and drain electrodes. CNTs have been shown in the literature to be a potential material for use in the active layer of TFTs, and this study has reinforced this view, whilst using novel methods for CNT deposition. Despite poor device performance, the aims of this section of the thesis have been achieved, however further investigations into CNT network density are ongoing.

Part IV

Thesis Conclusions

Chapter 12

Conclusions and Further Work

12.1 Initial Aims and Approach

This work has described a comprehensive study to explore the possibility of formulating an ink containing CNTs and the potential use of these inks in functional devices. The initial aims, as stated in Chapter 1 were to:

- explore the potential for formulating a CNT based ink by studying potential resins, solvents and formulation techniques,
- optimise this ink by improvement of CNT dispersion, with emphasis on mixing and CNT modification, and
- develop a CNT based TFT manufactured entirely using processes that can be scaled for high speed, roll to roll printing techniques.

To this end two experimental directions were researched. The first was designed to investigate the first two aims. Following a comprehensive literature review potential suitable materials, ink formulations and film characterisation parameters were chosen and experimental techniques to investigate these developed in scoping studies. A basic ink formulation was defined after consideration of the challenges identified from the literature and scoping experiments. These challenges include but were not limited to the solubility of CNTs, the formation of a suitable conductive network, CNT handling and ink deposition. Several variables were then investigated. Initially these included the resin material, resin:CNT ratio and processing temperature. Following these studies a factorial experiment investigating CNT concentration, sonication energy and CNT functionalisation was performed.

The second experimental direction was designed to achieve the third objective. A second literature review was performed to investigate the state of printed TFT

research for both organic and CNT based devices. Experiments were performed in a systematic fashion, with initial experiments focussing on proving the fundamental viability of the devices by using a simple design and a MWCNT ink based on the results of the previous research. Flexography was chosen as the roll-to-roll manufacturing technique. This design could then be optimised by characterisation of the manufacturing equipment and the active material changed to SWCNTs for comparison with contemporary reported devices.

12.2 CNT Ink Formulation

- Of the resin materials tested, the PA and PVA based systems showed the most promise for further investigation under the tested conditions. In particular these systems showed the lowest sheet resistivity and transparency of the printed films, whilst ink properties were within the ranges specified for major roll-to-roll printing methods specified in Table 1.1.1. Two mechanisms for this improvement in sheet resistivity and lower transmission could be concluded, with a combination of the two likely. The results show that the dispersion of the CNTs is more homogeneous in the PVA and PA polymer matrix under the conditions tested. It may also be caused by the PA and PVA resin systems having a lower detrimental effect on the contact resistance within the CNT network than the alternatives. It was also noticed that the PLA system, despite being marketed as a conductive polymer, did not improve the sheet resistivity of the CNT network. This may be due to high contact resistance between the polymer and CNTs, or the poor quality of the dispersion. In summary:

  - NC based inks showed the highest viscosity, with PA and PVA based systems the lowest,
  - PVA based inks showed the highest surface tension, with all others being similar,
  - PA and PVA based systems shows the lowest film transparency,
  - PA based inks showed the lowest sheet resistivity, with the NC and PLA systems the highest, and
  - PA based inks showed the highest adhesion, with the NC based systems being the worst.

- The ratio between the CNT and resin, in this case PVA, should be optimised to control ink characteristics. It is intuitive to expect that an increase in polymer content results in an increase in the viscosity of the continuous phase of the dispersion, as observed. It can also be concluded that the resin base coats the CNTs within the ink system, impeding CNT contact within the final network. Therefore an increase in PVA content results in higher junction resistances within the network, resulting in a higher sheet resistivity of the macro-scale film. In summary:
  - Increasing PVA content increases ink viscosity.
  - PVA content has no significant effect upon the surface tension of the ink.
  - PVA content has no significant effect upon the transmission of the film.
  - Increasing PVA content increases the sheet resistivity of the film.
  - Increasing PVA content above the lowest ratio tested improves film adhesion, though results are inconclusive.
- When using sonication for ink preparation the sample temperature must be controlled, as literature suggests CNT dispersion instability occurs above $40\,^{o}C$. However higher temperature may be preferable during dispersion as it results in an increase in energy in the system, resulting in improved dispersion. Lower sheet resistivities are observed for films mixed at higher temperatures, therefore it can be concluded that the increase in temperature results in a more homogeneous network. In summary:
  - Sample temperature during ink preparation has no significant effect upon the viscosity of the final ink.
  - Sample temperature during ink preparation has no significant effect upon the surface tension of the final ink.
  - Sample temperature during ink preparation has no significant effect upon the transparency of the resulting film.
  - Increasing sample temperature during ink preparation decreases the sheet resistivity of the resulting film.
- CNT concentration, CNT functionalisation and sonication time are dependent variables, with optimisation required for application.

- Increasing CNT concentration increases the critical mixing energy (and hence sonication time) required to obtain a suitable dispersion, this is due to the increase in agglomerate density. The deagglomeration of CNT bundles results in an increase in viscosity as the particle shape tends from spherical to rod like and an elastic network forms. Increasing CNT network density intuitively results in a decrease in film transmission and sheet resistivity. In summary:
  - Increasing CNT concentration increases the viscosity of the final ink.
  - Increasing CNT concentration has no significant effect upon the surface tension of the final ink.
  - Increasing CNT concentration decreases the transparency of the resulting film.
  - Increasing CNT concentration decreases the sheet resistivity of the resulting film.
- Sonication time must be optimised to the CNT type and concentration to achieve a suitable dispersion without excess damage to the CNT structure. Sonication is understood to damage the CNT structure, introducing defects, stretching and eventually cutting the CNTs. With regards to the properties of a printing ink this manifests itself as a decrease in viscosity, which is known to be dependent on the aspect ratio of particles in suspension. A concurrent effect is not observed with the sheet resistivity, though it is possible that the damage reduced the junction resistance which is known to be the dominant factor in network conduction properties. The deagglomeration caused by increased sonication reduces the transparency of the printed film due to more consistent coverage, no effect of CNT damage is apparent. In summary:
  - Increasing sonication time increases the viscosity of the final ink to a maximum, after which a decrease is observed.
  - Increasing sonication time has no significant effect upon the surface tension of the final ink.
  - Increasing sonication time decreases the transparency of the resulting film.
  - Increasing sonication time decreases the sheet resistivity of the resulting film.

- Covalent CNT functionalisation results in a significant change in ink and film properties. Functionalisation results in an overall decrease in sheet resistivity of the printed films. From this it can be concluded that the improvement in dispersion homogeneity and reduction in junction resistance outweighs the decrease in the resistance of the CNTs caused by the reduction in mean free path length of the charge carriers caused by scattering as a result of defects. Ink viscosity magnitude shows little effect upon functionalisation,it can be seen that functionalisation reduces the critical mixing energy required to create a homogeneous dispersion. Film transmission is also reduced by the use of functionalised CNTs due to the more consistent film. However, it must be noted that the degree of functionalisation is a significant factor. Functionalisation results in CNTs which may initially result in improved dispersion but damage from sonication is visible from the rheology in lower time scales than samples which are not functionalised. Excess functionalisation is visible in the sheet resistivity results, where the O2 samples showed significantly higher sheet resistivities than the NH3, which is likely to be due to the decrease in tube conductance. The functionalisation chemistry is also likely to have an effect upon the properties of the printed film, however no conclusions are possible from the results of this work. Although two functionality products were used, the majority of effects seen are more likely to be due to the varying degrees of functionalisation of the samples. In summary:

  - Appropriate CNT functionalisation has minimal effect upon the viscosity of the final ink.
  - Appropriate CNT functionalisation has no significant effect upon the surface tension of the final ink.
  - Appropriate CNT functionalisation decreases the transparency of the resulting film.
  - Appropriate CNT functionalisation decreases the sheet resistivity of the resulting film.
  - Appropriate CNT functionalisation decreases the critical mixing energy required to obtain a suitable dispersion.
  - Lower concentrations of appropriately functionalised CNTs are required to achieve similar properties to that of non-functionalised CNTs.

- This work has also highlighted the inconsistency in CNT batch properties. Although care was taken to source materials from consistent batches and samples were prepared in a controlled environment significant variation in ink and film properties were observed. This is not just an issue for printed electronics applications; it is an issue that needs addressing before the use of CNTs in any application becomes viable.

12.3 Flexographically Printed CNT Based TFT Structures

- Flexography can be used to produce every layer of a CNT based TFT structure. Flexography provides significant advantages to alternative techniques, especially with regards to electrode edge consistency and controlling layer thickness. Although print inhomogeneities are common in solid areas, especially when depositing low density inks, the effect of these can be minimised by careful design. Basic proofing equipment is capable of producing devices with S/D gaps of as low as $120\mu m$, however progress is limited by layer registration requiring large dimension devices. The capability of production scale equipment will increase print accuracy resulting in significant reduction in device dimensions

- MWCNTs can be used as the active layer in flexographically printed TFT devices. The on/off ratio of devices is limited by the semi-metal properties of the MWCNTs, with average ratios of 1.6 observed. The semi-metal CNT network also resulted in device mobilities of $651cm^2/Vs$. These mobilities are high compared to that of reported organic devices, however the on/off ratio is significantly lower. This is due to the semi-metal nature of the MWCNTs used as the active layer. Two electrode structures (parallel and interdigited) were assessed with no significant difference in device performance observed. Device response speed was very poor, likely due to dielectric polarisation, device scale, the high density MWCNT network and large channel lengths (1.85 and 0.91mm). Devices showed excellent stability over time, with no change in device performance observed over 17 months.

- SWCNT based devices were produced. Device design was refined following the MWCNT based results and improvement in the understanding of the capabilities of the printing equipment. S/D gaps were reduced to $120\mu m$ and two concentration (1 and 0.5wt%) SWCNT inks were printed for the active layer. Low

on/off ratios (average of 1.12 and 1.02 for the 1 and 0.5wt% respectively) and mobilities ($0.14cm^2/Vs$ and $0.002cm^2/Vs$ respectively) were observed. When comparing to literature it was seen that device performance was consistent with films that were still significantly above the network percolation threshold, hence the poor performance. The reduction in performance for the lower CNT concentration is consistent with observed trends as the devices approach the percolation threshold. The reduction in parasitic capacitance and channel length significantly improved response times. Devices showed excellent stability over time, with no change in device performance observed over 10 months. Optimisation of the CNT network density whist maintaining the printability of the ink is key to further device development.

12.4 Further Work

This thesis has presented the development of a CNT based ink and proposed and proven the viability of a potential application whilst employing a novel deposition technique for the device production. This work opens a number of avenues for further exploration. In particular the author considers that the following areas should be prioritised for further investigation:

- Further investigate the use of functionalised CNT structures to reduce requirements for undesirable additives in potential commercial ink products. In particular the type and degree of functionality must be optimised for a particular ink system and production. This should include investigation into the interaction between the ink base and the functionalisation. The desirable properties observed with the PA based resin system may be further explored.

- Investigate alternative solvents. NMP was used for all inks in this thesis, for reasons previously discussed. However it is not desirable from an industrial point of view. Many printing inks are migrating to water based systems, this poses a number of challenges for CNT dispersion, especially if additives are to be minimised. Further work in this area is essential.

- Optimisation of the CNT ink and flexographic printing process for TFT production. Flexography offers a number of advantages for TFT printing, not least for accurate and consistent S/D electrode production and finer control of layer thickness which may prove key when depositing CNT networks for particular

applications. However several challenges remain, including minimising print inhomogeneities for the low solid concentration inks which are required for the CNT layer, drying of layers in a production environment and identification of suitable dielectric materials which can be deposited in a minimum of prints. The production of functional CNT based TFTs on a continuous, roll-to-roll production line should be the ultimate aim of this work.

- Investigate alternative carbon nanostructures. It has now been shown in literature that graphene can be produced in solution and printed using inkjet methods, the investigation of this in an industrial roll to roll environment is of great interest due to the limitations of the inkjet process.

- Improve CNT production consistency. Apart from the widely reported toxicology issues the variation in CNT batch properties is the reason that CNTs have not yet been employed in commercial applications. This requires a number of improvements throughout the production process, but it is the author's opinion that the key issue is a lack of repeatable, rapid characterisation that can be performed in line with the production process hindering production improvement.

Finally, it must be realised that further ink optimisation research must be performed with respect to a particular application. The use of CNTs in printed electronics has long been touted as a potential solution to virtually any problem. This is not the case, and specific applications require specific ink development. As a result, and as a direct consequence of this work, a number of new funded projects have been initiated investigating the characterisation and use of solution processed carbon nanostructures for photovoltaics, RFID and sensors.

12.5 Final Comments

To summarise, this thesis is the first reported work to study the use of CNTs in a conventional printing ink formulation with the aim of roll-to-roll deposition. The effects of various ink production and formulation parameters have been studied and areas for optimisation identified and investigated. This ink was then employed in the production of fully printed TFT devices using a novel deposition method which has not been reported to have been used to produce entire TFT structures or for CNT network deposition before. It is the author's hope that this work acts as a stimulus to further research into the use of CNTs in printed electronics, as it is clear that CNTs

offer significant advantages over many currently available materials employed in this field.

12.5.1 Publications

- N. Graddage. Plasma Functionalised Carbon Nanotubes for use in Functional Inks. In *LOPE-C Conference Proceedings*, 2011.
- N. Graddage. Carbon Nanotubes as a Material for Functional Printing. In *Printing Future Days Conference Proceedings*, 2009.

References

[1] D.R. Gamota, P. Brazis, K. Kalyanasundaram, and J. Zhang, editors. *Printed Organic and Molecular Electronics*. Kluwer Academic Publishers, 2004.

[2] A. K. Geim. Graphene: Status and prospects. *Science*, 324(5934):1530–1534, 2009.

[3] Philippe Poncharal, Z. L. Wang, Daniel Ugarte, and Walt A. de Heer. Electrostatic deflections and electromechanical resonances of carbon nanotubes. *Science*, 283(5407):1513–1516, 1999.

[4] Sumio Iijima. Helical microtubules of graphitic carbon. *Nature*, 354:56–58, 1991.

[5] R. Saito, M. Fujita, G. Dresselhaus, and M. S Dresselhaus. Electronic structure of chiral graphene tubules. *Applied Physics Letters*, 60(18):2204–2206, 1992.

[6] Peter N. Nirmalraj, Philip E. Lyons, Sukanta De, Jonathan N. Coleman, and John J. Boland. Electrical connectivity in single-walled carbon nanotube networks. *Nano Letters*, 9(11):3890–3895, 2009. PMID: 19775126.

[7] Philip G. Collins, Michael S. Arnold, and Phaedon Avouris. Engineering carbon nanotubes and nanotube circuits using electrical breakdown. *Science*, 292(5517):706–709, 2001.

[8] Paritosh Garg, Jorge L. Alvarado, Charles Marsh, Thomas A. Carlson, David A. Kessler, and Kalyan Annamalai. An experimental study on the effect of ultrasonication on viscosity and heat transfer performance of multi-wall carbon nanotube-based aqueous nanofluids. *International Journal of Heat and Mass Transfer*, 52(21-22):5090 – 5101, 2009.

[9] Jenny Hilding, Eric A. Grulke, Z. George Zhang, and Fran Lockwood. Dispersion of carbon nanotubes in liquids. *Journal of Dispersion Science and Technology*, 24(1):1–41, 2003.

[10] Young Seok Song and Jae Ryoun Youn. Influence of dispersion states of carbon nanotubes on physical properties of epoxy nanocomposites. *Carbon*, 43(7):1378 – 1385, 2005.

[11] Irina Cotiuga, Francesco Picchioni, Uday S. Agarwal, Daan Wouters, Joachim Loos, and Piet J. Lemstra. Block-copolymer-assisted solubilization of carbon nanotubes and exfoliation monitoring through viscosity. *Macromolecular Rapid Communications*, 27(13):1073–1078, 2006.

[12] Y. Y. Huang, S. V. Ahir, and E. M. Terentjev. Dispersion rheology of carbon nanotubes in a polymer matrix. *Physical Review B (Condensed Matter and Materials Physics)*, 73(12):125422, 2006.

[13] He Yan, Zhihua Chen, Yan Zheng, Christopher Newman, Jordan R. Quinn, Florian Dotz, Marcel Kastler, and Antonio Facchetti. A high-mobility electron-transporting polymer for printed transistors. *Nature*, 457(7230):679–686, 2009.

[14] Dong-ming Sun, Marina Y. Timmermans, Ying Tian, Albert G. Nasibulin, Esko I. Kauppinen, Shigeru Kishimoto, Takashi Mizutani, and Yutaka Ohno. Flexible high-performance carbon nanotube integrated circuits. *Nat Nano*, 6(3):156–161, March 2011.

[15] H. Okimoto, T. Takenobu, K. Yanagi, Y. Miyata, H. Shimotani, H. Kataura, and Y. Iwasa. Tunable carbon nanotube thin-film transistors produced exclusively via inkjet printing. *Advanced Materials*, 22(36):3981–3986, 2010.

[16] H. Kipphan, editor. *Handbook of Print Media.* Springer, 2001.

[17] J.P. Crouch. *Flexography Primer.* GATF, 1998.

[18] J.P. Crouch. *Gravure Primer.* GATF, 1998.

[19] FUJIFILM Dimatix. *FUJIFILM Dimatix Materials Printer DMP-2800 Series User Manual.*

[20] D. Deganello. *Organic Light-Emitting Diodes (OLEDs): Materials, Devices and Applications.* Woodhead Publishing, Preprint.

[21] Guido Pagani, Micah J. Green, Philippe Poulin, and Matteo Pasquali. Competing mechanisms and scaling laws for carbon nanotube scission by ultrasonication. *Proceedings of the National Academy of Sciences*, 109(29):11599–11604, 2012.

[22] Hugo Miguel Santos, Carlos Lodeiro, and José-Luis Capelo-Martínez. *The Power of Ultrasound*, pages 1–16. Wiley-VCH Verlag GmbH & Co. KGaA, 2009.

[23] K. S. Novoselov, A. K. Geim, S. V. Morozov, D. Jiang, Y. Zhang, S. V. Dubonos, I. V. Grigorieva, and A. A. Firsov. Electric field effect in atomically thin carbon films. *Science*, 306(5696):666–669, 2004.

[24] P.J.F. Harris. *Carbon Nanotube Science*. Cambridge, 2008.

[25] M. Daenen, R.D. de Fouw, B. Hamers, P.G.A. Janssen, K. Schouteden, and M.A.J. Veld. The wondrous world of carbon nanotubes. Technical report, Eindhoven University of Technology, 2003.

[26] M.S. Dresselhaus, G. Dresselhaus, and R. Saito. Physics of carbon nanotubes. *Carbon*, 33(7):883 - 891, 1995.

[27] P. Delaney, M. Di Ventra, and S. T. Pantelides. Quantized conductance of multiwalled carbon nanotubes. *Applied Physics Letters*, 75(24):3787–3789, 1999.

[28] A. Bachtold, M. S. Fuhrer, S. Plyasunov, M. Forero, Erik H. Anderson, A. Zettl, and Paul L. McEuen. Scanned probe microscopy of electronic transport in carbon nanotubes. *Phys. Rev. Lett.*, 84:6082–6085, Jun 2000.

[29] T. Ando. Theory of electronic states and transport in carbon nanotubes. *Journal of the Physical Society of Japan*, 74(3):777–817, 2005.

[30] B. Q. Wei, R. Vajtai, and P. M. Ajayan. Reliability and current carrying capacity of carbon nanotubes. *Applied Physics Letters*, 79(8):1172–1174, 2001.

[31] L T Singh and K K Nanda. General theories for the electrical transport properties of carbon nanotubes. *Nanotechnology*, 22(31):315705, 2011.

[32] E. Hernández, C. Goze, P. Bernier, and A. Rubio. Elastic properties of c and $B_xC_yN_z$ composite nanotubes. *Phys. Rev. Lett.*, 80:4502–4505, May 1998.

[33] A. Krishnan, E. Dujardin, T. W. Ebbesen, P. N. Yianilos, and M. M. J. Treacy. Young's modulus of single-walled nanotubes. *Phys. Rev. B*, 58:14013–14019, Nov 1998.

[34] Min-Feng Yu, Bradley S. Files, Sivaram Arepalli, and Rodney S. Ruoff. Tensile loading of ropes of single wall carbon nanotubes and their mechanical properties. *Phys. Rev. Lett.*, 84:5552–5555, Jun 2000.

[35] A.G. Rinzler, J. Liu, H. Dai, P. Nikolaev, C.B. Huffman, F.J. Rodríguez-Macías, P.J. Boul, A.H. Lu, D. Heymann, D.T. Colbert, R.S. Lee, J.E. Fischer, A.M. Rao, P.C. Eklund, and R.E. Smalley. Large-scale purification of single-wall carbon nanotubes: process, product, and characterization. *Applied Physics A: Materials Science & Processing*, 67:29–37, 1998. 10.1007/s003390050734.

[36] P.G. Collins and P. Avouris. Nanotubes for electronics. *Scientific American*, 283:62–69, 2000.

[37] A. Peigney, Ch. Laurent, E. Flahaut, R.R. Bacsa, and A. Rousset. Specific surface area of carbon nanotubes and bundles of carbon nanotubes. *Carbon*, 39(4):507 – 514, 2001.

[38] Ya-Ping Sun, Kefu Fu, Yi Lin, and Weijie Huang. Functionalized carbon nanotubes: Properties and applications. *Accounts of Chemical Research*, 35(12):1096–1104, 2002. PMID: 12484798.

[39] Kannan Balasubramanian and Marko Burghard. Chemically functionalized carbon nanotubes. *Small*, 1(2):180–192, 2005.

[40] A. Felten, C. Bittencourt, J. J. Pireaux, G. Van Lier, and J. C. Charlier. Radio-frequency plasma functionalization of carbon nanotubes surface o_2, nh_3, and cf_4 treatments. *Journal of Applied Physics*, 98(7):074308, 2005.

[41] Changlun Chen, Bo Liang, Akihisa Ogino, Xiangke Wang, and Masaaki Nagatsu. Oxygen functionalization of multiwall carbon nanotubes by microwave-excited surface-wave plasma treatment. *The Journal of Physical Chemistry C*, 113(18):7659–7665, May 2009.

[42] Kaoru Shoda and Seiji Takeda. Systematic characterization of carbon nanotubes functionalized in cf_4 plasma. *Japanese Journal of Applied Physics*, 46(12):7977–7982, 2007.

[43] Chun-Hao Tseng, Cheng-Chien Wang, and Chuh-Yung Chen. Functionalizing carbon nanotubes by plasma modification for the preparation of covalent-integrated epoxy composites. *Chemistry of Materials*, 19(2):308–315, 2006.

[44] G. T. Kim, S. H. Jhang, J. G. Park, Y. W. Park, and S. Roth. Non-ohmic current-voltage characteristics in single-wall carbon nanotube network. *Synthetic Metals*, 117(1-3):123–126, 2001.

[45] A. B. Kaiser, K. J. Challis, G. C. McIntosh, G. T. Kim, H. Y. Yu, J. G. Park, S. H. Jhang, and Y. W. Park. Frequency and field dependent conductivity of carbon nanotube networks. *Current Applied Physics*, 2(2):163–166, 2002.

[46] L. Hu, D. S. Hecht, and G. Grüner. Percolation in transparent and conducting carbon nanotube networks. *Nano Letters*, 4(12):2513–2517, 2004.

[47] Elena Bekyarova, Mikhail E. Itkis, Nelson Cabrera, Bin Zhao, Aiping Yu, Junbo Gao, and Robert C. Haddon. Electronic properties of single-walled carbon nanotube networks. *Journal of the American Chemical Society*, 127(16):5990–5995, 2005.

[48] Philip E. Lyons, Sukanta De, Fiona Blighe, Valeria Nicolosi, Luiz Felipe C. Pereira, Mauro S. Ferreira, and Jonathan N. Coleman. The relationship between network morphology and conductivity in nanotube films. *J. Appl. Phys.*, 104(4):044302, 2008.

[49] L. F. C. Pereira, C. G. Rocha, A. Latge, J. N. Coleman, and M. S. Ferreira. Upper bound for the conductivity of nanotube networks. *Applied Physics Letters*, 95(12):123106, 2009.

[50] Sukanta De, Paul J. King, Philip E. Lyons, Umar Khan, and Jonathan N. Coleman. Size effects and the problem with percolation in nanostructured transparent conductors. *ACS Nano*, 4(12):7064–7072, 2010.

[51] Andriy V. Kyrylyuk, Marie Claire Hermant, Tanja Schilling, Bert Klumperman, Cor E. Koning, and Paul van der Schoot. Controlling electrical percolation in multicomponent carbon nanotube dispersions. *Nat Nano*, advance online publication:–, April 2011.

[52] Tero Mustonen, Krisztián Kordás, Sami Saukko, Géza Tóth, Jari S. Penttilä, Panu Helistö, Heikki Seppä, and Heli Jantunen. Inkjet printing of transparent and conductive patterns of single-walled carbon nanotubes and pedot-pss composites. *Phys. Stat. Sol. (B)*, 244(11):4336–4340, 2007.

[53] Ralph Krupke, Frank Hennrich, Hilbert v Lohneysen, and Manfred M. Kappes. Separation of metallic from semiconducting single-walled carbon nanotubes. *Science*, 301(5631):344–347, 2003.

[54] Stephane Campidelli, Moreno Meneghetti, and Maurizio Prato. Separation of metallic and semiconducting single-walled carbon nanotubes via covalent functionalization. *Small*, 3(10):1672–1676, 2007.

[55] Zhihong Chen, Xu Du, Mao-Hua Du, C. Daniel Rancken, Hai-Ping Cheng, and Andrew G. Rinzler. Bulk separative enrichment in metallic or semiconducting single-walled carbon nanotubes. *Nano Letters*, 3(9):1245–1249, 2003.

[56] Michael S. Arnold, Alexander A. Green, James F. Hulvat, Samuel I. Stupp, and Mark C. Hersam. Sorting carbon nanotubes by electronic structure using density differentiation. *Nat Nano*, 1(1):60–65, October 2006.

[57] Rajyashree M. Sundaram, Krzysztof K. K. Koziol, and Alan H. Windle. Continuous direct spinning of fibers of single-walled carbon nanotubes with metallic chirality. *Advanced Materials*, 23(43):5064–5068, 2011.

[58] L. Lu, M. Lago, K. Chen, H. Green, F. Harris, and C. Tsang. Mechanical damage of carbon nanotubes by ultrasound. *Carbon*, 34(6):814–816, 1996. Anglais.

[59] Kevin D. Ausman, Richard Piner, Oleg Lourie, Rodney S. Ruoff, and Mikhail Korobov. Organic solvent dispersions of single-walled carbon nanotubes: Toward solutions of pristine nanotubes. *The Journal of Physical Chemistry B*, 104(38):8911–8915, 2000.

[60] Jeffrey L. Bahr, Edward T. Mickelson, Michael J. Bronikowski, Richard E. Smalley, and James M. Tour. Dissolution of small diameter single-wall carbon nanotubes in organic solvents? *Chem. Commun.*, 2:193–194, 2001.

[61] M. F. Islam, E. Rojas, D. M. Bergey, A. T. Johnson, and A. G. Yodh. High weight fraction surfactant solubilization of single-wall carbon nanotubes in water. *Nano Letters*, 3(2):269–273, 2003.

[62] Cheol Park, Zoubeida Ounaies, Kent A. Watson, Roy E. Crooks, Joseph Smith, Sharon E. Lowther, John W. Connell, Emilie J. Siochi, Joycelyn S. Harrison, and Terry L. St Clair. Dispersion of single wall carbon nanotubes by in situ polymerization under sonication. *Chemical Physics Letters*, 364(3-4):303–308, 2002.

[63] Jeongwoo Lee, Myunghun Kim, Chang Kook Hong, and Sang Eun Shim. Measurement of the dispersion stability of pristine and surface-modified multiwalled carbon nanotubes in various nonpolar and polar solvents. *Measurement Science and Technology*, 18(12):3707, 2007.

[64] Shane D. Bergin, Zhenyu Sun, David Rickard, Philip V. Streich, James P. Hamilton, and Jonathan N. Coleman. Multicomponent solubility parameters for single-walled carbon nanotube-solvent mixtures. *ACS Nano*, 3(8):2340–2350, 2009. PMID: 19655724.

[65] Shane D. Bergin, Zhenyu Sun, Philip Streich, James Hamilton, and Jonathan N. Coleman. New solvents for nanotubes: Approaching the dispersibility of surfactants. *The Journal of Physical Chemistry C*, 114(1):231–237, 2010.

[66] Zhenyu Sun, Ian O'Connor, Shane D. Bergin, and Jonathan N. Coleman. Effects of ambient conditions on solvent-nanotube dispersions: Exposure to water and temperature variation. *The Journal of Physical Chemistry C*, 113(4):1260–1266, 2009.

[67] Johnny Amiran, Valeria Nicolosi, Shane D. Bergin, Umar Khan, Philip E. Lyons, and Jonathan N. Coleman. High quality dispersions of functionalized single walled nanotubes at high concentration. *The Journal of Physical Chemistry C*, 112(10):3519–3524, 2008.

[68] Jonathan N. Coleman. Liquid-phase exfoliation of nanotubes and graphene. *Advanced Functional Materials*, 19(23):3680–3695, 2009.

[69] Micah J Green. Analysis and measurement of carbon nanotube dispersions: nanodispersion versus macrodispersion. *Polymer International*, 59(10):1319–1322, 2010.

[70] Petra Pötschke, Mahmoud Abdel-Goad, Ingo Alig, Sergej Dudkin, and Dirk Lellinger. Rheological and dielectrical characterization of melt mixed polycarbonate-multiwalled carbon nanotube composites. *Polymer*, 45(26):8863 – 8870, 2004.

[71] Y. T. Sung, M. S. Han, K. H. Song, J. W. Jung, H. S. Lee, C. K. Kum, J. Joo, and W. N. Kim. Rheological and electrical properties of polycarbonate/multiwalled carbon nanotube composites. *Polymer*, 47(12):4434–4439, 2006.

[72] G. Barthelmes, S. E. Pratsinis, and H. Buggisch. Particle size distributions and viscosity of suspensions undergoing shear-induced coagulation and fragmentation. *Chemical Engineering Science*, 58(13):2893 – 2902, 2003.

[73] Micah J. Green, Natnael Behabtu, Matteo Pasquali, and W. Wade Adams. Nanotubes as polymers. *Polymer*, 50(21):4979 – 4997, 2009.

[74] Brian P. Grady. The use of solution viscosity to characterize single-walled carbon nanotube dispersions. *Macromolecular Chemistry and Physics*, 207(23):2167–2169, 2006.

[75] Sven Pegel, Petra Pötschke, Gudrun Petzold, Ingo Alig, Sergej M. Dudkin, and Dirk Lellinger. Dispersion, agglomeration, and network formation of multiwalled carbon nanotubes in polycarbonate melts. *Polymer*, 49(4):974 – 984, 2008.

[76] Axel Schindler, Jochen Brill, Norbert Fruehauf, James P. Novak, and Zvi Yaniv. Solution-deposited carbon nanotube layers for flexible display applications. *Physica E*, 37:119–123, 2007.

[77] Young Il Song, Cheol-Min Yang, Dong Young Kim, Hirofumi Kanoh, and Katsumi Kaneko. Flexible transparent conducting single-wall carbon nanotube film with network bridging method. *Journal of Colloid and Interface Science*, 318(2):365–371, 2008.

[78] Sungsoo Kim, Jonghyuk Yim, Xuhua Wang, Donal D.C. Bradley, Soonil Lee, and John C. deMello. Spin- and spray-deposited single-walled carbon-nanotube electrodes for organic solar cells. *Advanced Functional Materials*, 20(14):2310–2316, 2010.

[79] Abdelaziz Rahy, Pooja Bajaj, Inga H. Musselman, Soon Hyung Hong, Ya-Ping Sun, and Duck J. Yang. Coating of carbon nanotubes on flexible substrate and its adhesion study. *Applied Surface Science*, In Press, Corrected Proof:7084–7089, 2009.

[80] Vittorio Scardaci, Richard Coull, and Jonathan N. Coleman. Very thin transparent, conductive carbon nanotube films on flexible substrates. *Appl. Phys. Lett.*, 97(2):023114, 2010.

[81] Jinsoo Noh, Sungho Kim, Kyunghwan Jung, Joonseok Kim, Sungho Cho, and Gyoujin Cho. Fully gravure printed half adder on plastic foils. *Electron Device Letters, IEEE*, 32(11):1555 –1557, nov. 2011.

[82] J. Noh, Minhun Jung, Kyunghwan Jung, Gwangyong Lee, Joonseok Kim, Soyeon Lim, Daae Kim, Youngchul Choi, Yoonjin Kim, V. Subramanian, and Gyoujin Cho. Fully gravure-printed d flip-flop on plastic foils using single-walled carbon-nanotube-based tfts. *Electron Device Letters, IEEE*, 32(5):638 –640, may 2011.

[83] D.J. Arthur and P.J. Glatkowski. Method for patterning carbon nanotube coating and carbon nanotube wiring, 2006.

[84] P.J. Glatkowski, N. Landrau, D.H. Landis, J.W. Piche, and J.L. Conroy. Conformal coatings comprising carbon nanotubes, 2004.

[85] Juntao Li, Wei Lei, Xiaobing Zhang, Xuedong Zhou, Qilong Wang, Yuning Zhang, and Baoping Wang. Field emission characteristic of screen-printed carbon nanotube cathode. *Applied Surface Science*, 220(14):96–104, 2003.

[86] Hyeon Jae Lee, Yang Doo Lee, Seung Il Moon, Woo Sung Cho, Yun-Hi Lee, Jai Kyeong Kim, Sung Woo Hwang, and Byeong Kwon Ju. Enhanced surface morphologies of screen-printed carbon nanotube films by heat treatment and their field-emission properties. *Carbon*, 44(13):2625 – 2630, 2006.

[87] W. B. Choi, D. S. Chung, J. H. Kang, H. Y. Kim, Y. W. Jin, I. T. Han, Y. H. Lee, J. E. Jung, N. S. Lee, G. S. Park, and J. M. Kim. Fully sealed, high-brightness carbon-nanotube field-emission display. *Applied Physics Letters*, 75(20):3129–3131, 1999.

[88] Yao Wang, Fei Wei, Guangsheng Gu, and Hao Yu. Agglomerated carbon nanotubes and its mass production in a fluidized-bed reactor. *Physica B: Condensed Matter*, 323(1-4):327–329, 2002.

[89] Zhuanghun Fan, Tong Wei, Guohua Luo, and Fei Wei. Fabrication and characterization of multi-walled carbon nanotubes-based ink. *Journal of Materials Science*, 40(18):5075–5077, 2005.

[90] Tong Wei, Jun Ruan, Zhuangjun Fan, Guohua Luo, and Fei Wei. Preparation of a carbon nanotube film by ink-jet printing. *Carbon*, 45(13):2712–2716, 2007.

[91] A. Denneulin, J. Bras, A. Blayo, B. Khelifi, F. Roussel-Dherbey, and C. Neuman. The influence of carbon nanotubes in inkjet printing of conductive polymer suspensions. *Nanotechnology*, 20(38):385701, 2009.

[92] B. Kumar, H. S. Tan, N. Ramalingam, and S. G. Mhaisalkar. Integration of ink jet and transfer printing for device fabrication using nanostructured materials. *Carbon*, 47(1):321–324, 2009.

[93] Hiroki Ago, Kazuhiro Murata, Motoo Yumura, Junko Yotani, and Sashiro Uemurac. Ink-jet printing of nanoparticle catalyst for site-selective carbon nanotube growth. *Applied Physics Letters*, 82(5):811–813, 2002.

[94] R.G. Larson. *The Structure and Rheology of Complex Fluids*. Oxford University Press, 1999.

[95] H.A. Barnes. *A Handbook of Elementary Rheology*. University of Wales, 2000.

[96] T.C. Patton. *Paint Flow and Pigment Dispersion*. Wiley, 1979.

[97] Malvern Instruments Ltd. *Bohlin Gemini HR Nano rheometer User's Manual*.

[98] A.W. Adamson. *Physical Chemistry of Surfaces*. Wiley Interscience, 1982.

[99] Fibro System AB. *Fibro DAT 1100 User's Manual*.

[100] Kaye & Laby. Tables of physical & chemical constants (16th edition 1995). version 1.0. Online, 2005.

[101] Craig E. Murphy, Li Yang, Santanu Ray, Liyang Yu, Steven Knox, and Natalie Stingelin. Wire-bar coating of semiconducting polythiophene/insulating polyethylene blend thin films for organic transistors. *Journal of Applied Physics*, 110(9):093523, 2011.

[102] FAG-VRG S. *FAG VIPDENS 620 Instruction manual*.

[103] F.M. Smits. Measurement of sheet resistivities with the four-point probe. *The Bell System Technical Journal*, 1:711–718, 1958.

[104] Keithley Instruments, Inc. *Kiethley Model 2400 SourceMeter User's Manual*, g edition, 2012.

[105] Ta-Jo Liu, Wen-bing Chu, Jia-wei Yang, Yu-chin Wang, Carlos Tiu, and Jian Guo. Effect of inorganic particles on slot die coating of poly(vinyl alcohol) solutions. *Journal of Central South University of Technology*, 14:386–388, 2007. 10.1007/s11771-007-0288-5.

[106] Cherie Kagan and Paul Andry, editors. *Thin-Film Transistors*. Marcel Dekker, Inc., 2003.

[107] H. Sirringhaus. Device physics of solution-processed organic field-effect transistors. *Advanced Materials*, 17(20):2411–2425, 2005.

[108] P.K. Weimer. The tft a new thin-film transistor. *Proceedings of the IRE*, 50(6):1462 –1469, june 1962.

[109] Nima Rouhi, Dheeraj Jain, and Peter John Burke. High-performance semiconducting nanotube inks: Progress and prospects. *ACS Nano*, 5(11):8471–8487, 2011.

[110] Zhenan Bao, Yi Feng, Ananth Dodabalapur, V. R. Raju, and Andrew J. Lovinger. High-performance plastic transistors fabricated by printing techniques. *Chemistry of Materials*, 9(6):1299–1301, 1997.

[111] Kateri E. Paul, William S. Wong, Steven E. Ready, and Robert A. Street. Additive jet printing of polymer thin-film transistors. *Applied Physics Letters*, 83(10):2070–2072, 2003.

[112] A. Knobloch, A. Manuelli, A. Bernds, and W. Clemens. Fully printed integrated circuits from solution processable polymers. *Journal of Applied Physics*, 96(4):2286–2291, 2004.

[113] D. Tobjörk, N.J. Kaihovirta, T. Mäkelä, F.S. Pettersson, and R. Österbacka. All-printed low-voltage organic transistors. *Organic Electronics*, 9(6):931 – 935, 2008.

[114] Nikolai J. Kaihovirta, Daniel Tobjörk, Tapio Mäkelä, and Ronald Österbacka. Absence of substrate roughness effects on an all-printed organic transistor operating at one volt. *Appl. Phys. Lett.*, 93(5):053302, 2008.

[115] Monika M. Voigt, Alexander Guite, Dae-Young Chung, Rizwan U. A. Khan, Alasdair J. Campbell, Donal D. C. Bradley, Fanshun Meng, Joachim H. G. Steinke, Steve Tierney, Iain McCulloch, Huguette Penxten, Laurence Lutsen,

Olivier Douheret, Jean Manca, Ulrike Brokmann, Karin Sönnichsen, Dagmar Hülsenberg, Wolfgang Bock, Cecile Barron, Nicolas Blanckaert, Simon Springer, Joachim Grupp, and Alan Mosley. Polymer field-effect transistors fabricated by the sequential gravure printing of polythiophene, two insulator layers, and a metal ink gate. *Advanced Functional Materials*, 20(2):239–246, 2010.

[116] G.C. Schmidt, M. Bellmann, B. Meier, M. Hambsch, K. Reuter, H. Kempa, and A.C. Hübler. Modified mass printing technique for the realization of source/drain electrodes with high resolution. *Organic Electronics*, 11(10):1683 – 1687, 2010.

[117] Tsuyoshi Sekitani, Yoshiaki Noguchi, Ute Zschieschang, Hagen Klauk, and Takao Someya. Organic transistors manufactured using inkjet technology with subfemtoliter accuracy. *Proceedings of the National Academy of Sciences*, 105(13):4976–4980, 2008.

[118] M.L. Chabinyc, W.S. Wong, A.C. Arias, S. Ready, R.A. Lujan, J.H. Daniel, B. Krusor, R.B. Apte, A. Salleo, and R.A. Street. Printing methods and materials for large-area electronic devices. *Proceedings of the IEEE*, 93(8):1491 –1499, aug. 2005.

[119] M. Hambsch, K. Reuter, M. Stanel, G. Schmidt, H. Kempa, U. Fügmann, U. Hahn, and A. C. Hübler. Uniformity of fully gravure printed organic field-effect transistors. *Materials Science and Engineering: B*, 170(1-3):93–98, 2010.

[120] Yugeng Wen, Yunqi Liu, Yunlong Guo, Gui Yu, and Wenping Hu. Experimental techniques for the fabrication and characterization of organic thin films for field-effect transistors. *Chemical Reviews*, 111(5):3358–3406, 2011.

[121] T. Mäkelä, S. Jussila, H. Kosonen, T. G. Bäcklund, H. G. O. Sandberg, and H. Stubb. Utilizing roll-to-roll techniques for manufacturing source-drain electrodes for all-polymer transistors. *Synthetic Metals*, 153(1-3):285–288, 2005.

[122] E. S. Snow, J. P. Novak, P. M. Campbell, and D. Park. Random networks of carbon nanotubes as an electronic material. *Applied Physics Letters*, 82(13):2145–2147, 2003.

[123] Keith Bradley, Jean-Christophe P. Gabriel, and George Gruner. Flexible nanotube electronics. *Nano Letters*, 3(10):1353–1355, 2003.

[124] Marina Y Timmermans, Kestutis Grigoras, Albert G Nasibulin, Ville Hurskainen, Sami Franssila, Vladimir Ermolov, and Esko I Kauppinen. Lithography-free fabrication of carbon nanotube network transistors. *Nanotechnology*, 22(6):065303, 2011.

[125] Qing Cao, Hoon-sik Kim, Ninad Pimparkar, Jaydeep P. Kulkarni, Congjun Wang, Moonsub Shim, Kaushik Roy, Muhammad A. Alam, and John A. Rogers. Medium-scale carbon nanotube thin-film integrated circuits on flexible plastic substrates. *Nature*, 454(7203):495–500, July 2008.

[126] Husnu Emrah Unalan, Giovanni Fanchini, Alokik Kanwal, Aurelien Du Pasquier, and Manish Chhowalla. Design criteria for transparent single-wall carbon nanotube thin-film transistors. *Nano Letters*, 6(4):677–682, 2006.

[127] Qing Cao, Seung-Hyun Hur, Zheng-Tao Zhu, Yugang Sun, Congjun Wang, Matthew A. Meitl, Moonsub Shim, and John A. Rogers. Highly bendable, transparent thin-film transistors that use carbon-nanotube-based conductors and semiconductors with elastomeric dielectrics. *Adv. Mater.*, 18:304–309, 2006.

[128] Qing Cao, Zheng-Tao Zhu, Maxime G. Lemaitre, Ming-Gang Xia, Moonsub Shim, and John A. Rogers. Transparent flexible organic thin-film transistors that use printed single-walled carbon nanotube electrodes. *Applied Physics Letters*, 88(11):113511, 2006.

[129] Bhupesh Chandra, Hongsik Park, Ahmed Maarouf, Glenn J. Martyna, and George S. Tulevski. Carbon nanotube thin film transistors on flexible substrates. *Appl. Phys. Lett.*, 99(7):072110, 2011.

[130] P. Beecher, P. Servati, A. Rozhin, A. Colli, V. Scardaci, S. Pisana, T. Hasan, A. J. Flewitt, J. Robertson, G. W. Hsieh, F. M. Li, A. Nathan, A. C. Ferrari, and W. I. Milne. Ink-jet printing of carbon nanotube thin film transistors. *Journal of Applied Physics*, 102(4):043710, 2007.

[131] Jarrod Vaillancourt, Haiyan Zhang, Puminun Vasinajindakaw, Haitao Xia, Xuejun Lu, Xuliang Han, Daniel C. Janzen, Wu-Sheng Shih, Carissa S. Jones, Mike Stroder, Maggie Y. Chen, Harish Subbaraman, Ray T. Chen, Urs Berger, and Mike Renn. All ink-jet-printed carbon nanotube thin-film transistor on a polyimide substrate with an ultrahigh operating frequency of over 5 ghz. *Applied Physics Letters*, 93(24):243301, 2008.

[132] Mingjing Ha, Yu Xia, Alexander A. Green, Wei Zhang, Mike J. Renn, Chris H. Kim, Mark C. Hersam, and C. Daniel Frisbie. Printed, sub-3v digital circuits on plastic from aqueous carbon nanotube inks. *ACS Nano*, 4(8):4388–4395, 2010.

[133] Standard for test methods for the characterization of organic transistors and materials, 2008.

[134] Veeco Instruments Inc. *Veeco Wyko NT9800 Optical Profiler User Manual.*

[135] J.A. Cherry. *Ink Release Characteristics of Anilox Rolls*. PhD thesis, Swansea University, 2007.

[136] Agilent Technologies. *Agilent E5262A User's Manual.*

[137] Motorola inc. Field effect transistors in theory and practice. Technical report, Freescale Inc., 1993.

[138] Martyn Cherrington, Tim C. Claypole, Davide Deganello, Ian Mabbett, Trystan Watson, and David Worsley. Ultrafast near-infrared sintering of a slot-die coated nano-silver conducting ink. *J. Mater. Chem.*, 21:7562–7564, 2011.

[139] N. Bornemann and E. Sauer, H.M.and Dorsam. Gravure printed ultrathin layers of small-molecule semiconductors on glass. *Journal of Imaging Science and Technology*, 55(4):040201–1:040201–8, 2011.

[140] Christian Voß. *Analytische Modellierung, experimentelle Untersuchungen und dreidimensionale Gitter-Boltzmann Simulation der quasistatischen und instabilen Farbspaltung.* PhD thesis, Bergische Universität Wuppertal, 2007.

[141] H. M. Sauer. Viscous fingering in functional flexo printing: an inevitable bug? In *LOPE-C Conference Proceedings*, 2011.

[142] D. Deganello, J.A. Cherry, D.T. Gethin, and T.C. Claypole. Patterning of micro-scale conductive networks using reel-to-reel flexographic printing. *Thin Solid Films*, 518(21):6113 – 6116, 2010.

[143] A. Hamblyn, D. Deganello, and T. C. Claypole. Surface patterning of flexo plates for improved ink transfer. In *IARIGAI Advances in Printing and Media Technology Conference Proceedings*, 2012.

[144] Chang Su Kim, Sung Jin Jo, Sung Won Lee, Woo Jin Kim, Hong Koo Baik, and Se Jong Lee. Thickness dependence of gate dielectric layer on structural and electrical characteristics in the pentacene thin-film transistors. *Journal of The Electrochemical Society*, 154(2):H102–H104, 2007.